Investigating candidate genes for amyloid-β accumulation and toxicity in Alzheimer's disease-Down syndrome

Katharina Wenz

A Thesis submitted in partial fulfilment of the requirements for the degree of Doctor of Philosophy from University College London

March 2025

UK Dementia Research Institute at UCL

Declaration

I, Katharina Wenz, confirm that the work presented in this thesis is my own. Where information and data have been derived from collaborators and other sources, I confirm that this has been indicated in the thesis.

Abstract

Down Syndrome (DS), caused by trisomy of chromosome 21 (Hsa21), is the most common genetic cause of early-onset Alzheimer's disease (termed Alzheimer's disease-Down Syndrome, AD-DS). Early AD pathology is characterised by extracellular amyloid-β (Aβ) deposition generated through sequential cleavage of the Hsa21 encoded amyloid precursor protein (APP). Triplication of *APP* has been causally implicated in early-onset AD (EOAD). However, pre-clinical studies in mice have demonstrated that an additional copy of Hsa21 genes other than *APP* is sufficient to increase Aβ deposition and exacerbate cognitive decline but which gene(s) mediate this effect has not been elucidated.

In this study, I used a *Drosophila melanogaster* model of amyloid accumulation to assess whether pan-neuronal overexpression of single Hsa21 orthologues can modulate Aβ toxicity and accumulation. I screened thirty-five genes and identified seven potential modifiers, though not all findings could be replicated, indicating that overexpression of single Hsa21 orthologues may not be sufficient to modify amyloid pathology. Subsequently, I selected two genes of interest, *Usp47* (*USP25*) and *ATPsynCF6* (*ATP5J*), for further characterisation. To determine whether USP25 and ATP5J could impact Aβ pathology in AD-DS, I used human post-mortem brain tissue from individuals with AD-DS, EOAD and healthy ageing controls to assess whether these genes are dosage sensitive in DS. I found a trend towards reduction of USP25 with AD but no difference in ATP5J at the protein level and a significant upregulation of gene expression in neuronal populations.

Additionally, differential gene expression analysed from a single-nuclear RNA sequencing (snRNAseq) dataset revealed a signature of dysregulated pathways related to impaired synaptic function and neuronal polarisation in AD-DS. Lastly, combining information from the literature and our snRNAseq dataset, I explored additional Hsa21 candidate modifiers of Aβ toxicity/accumulation, highlighting a potential role of *TTC3*.

Impact statement

Down syndrome (DS) is caused by an extra copy of chromosome 21 (Hsa21). This chromosomal aneuploidy predisposes individuals with DS to a variety of developmental and age-related conditions, including early-onset Alzheimer's disease (EOAD). Hsa21 encodes the gene *APP,* which is processed to produce amyloid-β (Aβ) that aggregates into amyloid plaques, a hallmark pathology of AD. Triplication of *APP* is necessary and sufficient for the development of AD-DS. However, how three copies of the other over 230 protein coding genes encoded on Hsa21 contribute to AD risk in individuals with DS is not well understood.

Therefore, I investigated the effects of increased Hsa21 gene dosage on Aβ toxicity and accumulation in a genetic screen using a *Drosophila melanogaster* model of AD. For this, I assessed whether overexpression of single Hsa21 fly orthologues was sufficient to modify phenotypic readouts of the response to Aβ toxicity and accumulation of Aβ in the brain. An initial screen identified potential modifiers of amyloid toxicity, although repeat experiments indicated that single Hsa21 orthologues are insufficient to exert this effect. To determine whether their human orthologues may exert the same effect in individuals with AD-DS, I wanted to investigate whether an increase in their copy number causes an increase at the transcript and protein level of the gene product in the human brain (i.e. whether these genes are dosage sensitive).

Firstly, I selected *USP25*, whose orthologue acted as a suppressor of Aβ toxicity in the fly screen, as overexpression of this gene was previously found to interact with APP, exacerbating Aβ accumulation in a mouse model of AD. I found *USP25* transcript was raised in neuronal cell populations from individuals who had AD-DS compared with those who had EOAD and matched healthy ageing (HA) controls. However, at the protein level, USP25 abundance was decreased in post-mortem brain tissue from individuals with AD-DS and EOAD. My results indicated that this was likely due to neuronal loss as a result of late-stage AD brain atrophy.

Secondly, I investigated the dosage sensitivity of *ATP5J*, whose orthologue was identified as an enhancer of amyloid toxicity in my *Drosophila* screen. I found that ATP5J was not dosage sensitive at the transcript and protein level in post-mortem brain tissue from individuals with AD-DS compared with EOAD and HA controls. Taken together, my results indicate that USP25 and ATP5J are unlikely candidate modifiers of Aβ pathology in AD-DS (at least in late-stage disease) due to a lack of increased protein dosage caused by trisomy 21.

This work has demonstrated that *Drosophila* are a suitable model system for large-scale screens relating to AD-DS, though translational limitations highlight the importance of validating findings. Furthermore, my results demonstrate the importance of assessing Hsa21 dosage sensitivity at both the transcript and protein level to understand whether three copies of the gene may have functional consequences in AD-DS.

More broadly, furthering our understanding of the genetics of AD-DS and how it differs from other forms of AD is crucial for the development of safe and effective disease modifying therapies for AD-DS.

Acknowledgements

Thank you to my supervisors, Dr Teresa Niccoli and Dr Frances Wiseman for giving me the opportunity to do this PhD. Your great support throughout the years has been so generous. Teresa, thank you for your support with all my fly work, always being available for questions, guidance and feedback. Frances, thank you for supporting me throughout my project and, in particular, with all the human tissue work and for accommodating me in your lab. Thank you to Professor Elizabeth Fisher for stepping in to supervise my thesis writing process and sharing your wisdom on the field of Down Syndrome research.

This work was made possible through the funding from the NC3Rs. Thank you for supporting this 3Rs project.

Thank you to the people who generously donated their brain for research. This project would not have been possible without the generosity of these individuals, their families as well as the South West Dementia Brain Bank and Newcastle Brain Tissue Resource for providing access to these samples.

Thank you to my thesis committee, Dr Nathan Woodling, Dr Christina Toomey, Professor Elizabeth Fisher and Professor Nazif Alić, for your feedback and support throughout my PhD. With special thanks to Nazif, you have been a continuous source of scientific and personal wisdom to me over the years.

My gratitude goes to members of the Partridge and Wiseman labs for their contribution to my project. Nathan, thank you for sharing your knowledge and skills about ELISAs. Yixing and Clíona, thank you for giving your time to help with my western blot work, taking on the steps I was not able to carry out.

Working in the IHA was a great experience because of its wonderful members across the different research groups, creating a welcoming and supportive environment. Chats over lunch and Friday morning coffee are some of my fondest memories.

Although I only joined the Wiseman lab for a couple of months, I was made to feel warmly welcome in the group at Queen Square House, thank you.

Thank you to my wonderful friends in London and beyond for providing the balance and fun I needed during this PhD. Thank you to my in-laws who have been so hands on and supportive over the years. Thank you to my parents for always believing that I could do this.

Mama, you may not be here to watch me complete this project but I know no one would be prouder than you. You are the reason I am the person I am today and there are no words to capture how grateful I am for everything you have done for me.

Last but certainly not least, thank you to my amazing family. My boys, Felix and Henry, who joined us during my PhD journey. You show me how to find joy in the little things every day and make me so proud. Thank you for bringing so much happiness into my life – getting to raise you is my greatest privilege. And to my husband, Danny, you have been with me through all the ups and downs, my constant, my absolute rock. Thank you for everything.

TABLE OF CONTENTS

List of Tables

Appendix

List of Figures

Appendix

List of Abbreviations

aa	Amino acid
AD	Alzheimer's disease
AD-DS	Alzheimer's disease-Down Syndrome
AICD	Amyloid precursor protein intracellular domain
ANOVA	Analysis of variance
APOE	Apolipoprotein E
APP	Amyloid precursor protein (human)
App	Amyloid precursor protein (mouse)
APPL	Beta amyloid protein precursor-like (*Drosophila*)
ARRIVE	Animal Research: Reporting of In Vivo Experiments
ATP5J/ATP5PF	ATP synthase coupling factor 6/ATP synthase peripheral stalk subunit 6 (human)
ATPsynCF6	ATP synthase coupling factor 6 (*Drosophila*)
Aβ	Amyloid beta
BA	Brodmann area
BSA	Bovine serum albumin
CAA	Cerebral amyloid angiopathy
CNS	Central nervous system
CSF	Cerebrospinal fluid
CTFα/C83	C-terminal fragment alpha
CTFβ/C99	C-terminal fragment beta
DEA	Diethanolamine
DEGs	Differentially expressed genes
DIOPT	DSRC integrative orthologue prediction tool
DS	Down Syndrome
DUBs	deuquitinating enzymes
dupAPP	Duplication of the APP locus
DYRK1A	Dual specificity tyrosine-phosphorylation-regulated kinase 1A
elavGS	Elav Gene-switch
ELISA	Enzyme-linked immunosorbent assay

EOAD	Early-onset Alzheimer's disease
eQTL	Expression quantitative trait loci
ERAD	Endoplasmic-reticulum-associated degradation pathway
ETC	Electron transport chain
FDR	False discovery rate
flAPP	Full-length amyloid precurser protein
FPKM	Fragments Per Kilobase per Million mapped fragments
GO	Gene ontology
GWAS	Genome wide association study
HA	Healthy ageing
HEPES	4-(2-hydroxyethyl)-1-piperazineethanesulfonic acid
Hsa21	*Homo sapiens* chromosome 21
HTA	Human Tissue Act
ID	Intellectual disability
iNs	Induced neurons
iPSCs	Induced pluripotent stem cells
LOAD	Late-onset Alzheimer's disease
logFC	$\log_2$ fold-change
MCI	Mild cognitive impairment
Mmu	*Mus musculus* chromosome
mnb	minibrain
MW	Molecular weight
NBTR	Newcastle Brain Tissue Resource
NC3Rs	National Centre for the Replacement, Refinement and Reduction of Animals in Research
NEMGs	Nuclear encoded mitochondrial genes
NFT	Neurofibrillary tangles
NPCs	Neuronal precursor cells
nTPM	Normalised transcripts per million
OXPHOS	Oxidative phosphorylation
PET	Positron emission tomography
PMI	Post-mortem interval

PSEN1/2	Presenilin 1/2
RT-qPCR	Real-time quantitative polymerase chain reaction
RU	RU-486, mifepristone
sAPPα	Soluble amyloid precursor protein alpha
sAPPβ	Soluble amyloid precursor protein beta
SEM	Standard error of the mean
snRNA-seq	Single-nuclei RNA-sequencing
SWDBB	South West Dementia Brain Bank
SYA	Sugar yeast agar (*Drosophila* media)
THB	Tissue homogenisation buffer
TTC3	Tetratricopeptide Repeat Domain 3
UAS	Upstream activation sequence
UPS	Ubiquitin protease system
USP25	Ubiquitin specific peptidase 25
Usp47	Ubiquitin specific protease 47
USPs	Ubiquitin specific peptidases

Chapter 1: Introduction

1.1 Introduction to Down syndrome

1.1.1 History and prevalence

Down syndrome (DS) is the most frequent genetic cause of intellectual disability (ID) and was first described by British physician John Langdon Down in 1866 (Down, 1866). However, the underlying chromosomal aberration, the triplication of *Homo sapiens* chromosome 21 (Hsa21), was discovered almost a century later by Martha Gautier working with Jerome LeJeune (LeJeune, Gautier and Turpin, 1959). DS has the highest survival rate of all autosomal human trisomies, accounting for approximately 1 in 800 live births. Notably, prevalence varies considerably across countries, averaging 5.7 per 10,000 between 2011 and 2015 in Europe and 6.7 per 10,000 live births in the US in a similar period (De Graaf, Buckley and Skotko, 2017; de Graaf, Buckley and Skotko, 2020). The regional DS birth rate is dependent on several factors, including average maternal age, availability of prenatal screening, pregnancy termination laws, and socioeconomic and cultural factors.

In recent decades, the balance between advanced maternal age and an increase in pregnancy terminations has kept birth rates relatively stable, with selective terminations estimated to have reduced DS population prevalence by 27% and 21% in Europe and the US, respectively (Morris and Alberman, 2009; de Graaf, Buckley and Skotko, 2020). However, overall population prevalence of DS has increased significantly since the middle of the last century, particularly in countries with a higher socio-demographic index (SDI) where the highest mortality rate is in the over 50s compared with under 5s in middle and low SDI countries (Chen *et al.*, 2022). This is due to improvements in medical care for trisomy 21 associated conditions as well as better social care and disability rights, resulting in a major increase in life expectancy

of individuals with DS. In 1950, median lifespan was just 4 years in the US, rising to 58 years in 2010 (De Graaf, Buckley and Skotko, 2017). However, this has also led to a higher percentage of individuals with DS being affected by diseases of ageing, particularly Alzheimer's Disease (AD) (Fortea *et al.*, 2021).

1.1.2 Genetics and clinical features

Euploid individuals carry an even number of chromosomes, with every cell containing 22 autosome pairs and a pair of sex chromosomes. However, chromosomal mis-segregation (non-disjunction) can lead to daughter cells obtaining an uneven number of chromosomes that can be inherited by the next generation when it occurs during meiosis (Hassold and Hunt, 2001). This aneuploidy can result from the loss of a chromosome (monosomy) or gain of an extra chromosome (trisomy). Studies have found that DS, which arises from trisomy of Hsa21, is most commonly caused by non-disjunction of homologous chromosomes during maternal meiosis I and non-disjunction of sister chromatids during maternal meiosis II, with paternal meiosis errors accounting for around 8% of DS cases (Antonarakis *et al.*, 2020). Additionally, in around 5% of cases post conception mitotic errors can result in trisomy 21 (Antonarakis *et al.*, 1993). Alternatively, aneuploidy may arise from Robertsonian translocations, where the long arm of a chromosome fuses with another, most commonly between Hsa21 and Hsa14. This age-independent chromosomal abnormality can be heritable or arise spontaneously and is the cause of DS in 3-4% of cases (Figure 1.1) (Antonarakis *et al.*, 1993; Mutton, Alberman and Hook, 1996; Gerton, 2024). Notably, while 95% of DS individuals carry an additional complete freely segregating copy of Hsa21 in every cell, around two percent are mosaic for trisomy 21, with only some cells affected by the aneuploidy in the affected individual (Papavassiliou *et al.*, 2015). Rarely, DS can also be caused by a partial extra copy of Hsa21 where only some genes are present in three copies (Pelleri *et al.*, 2019, 2022). Complete trisomy 21 results in an extra copy of over 230 protein coding genes, over 400 non-coding genes and over 180 pseudogenes.

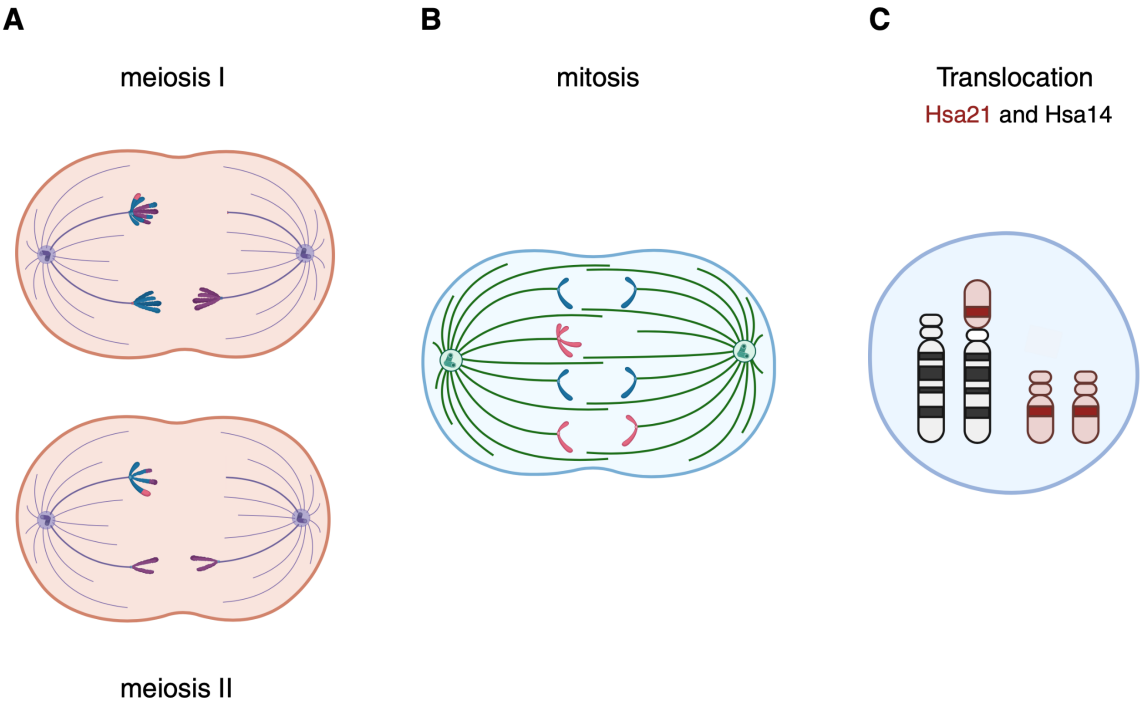

Figure 1.1 Genetic causes of trisomy 21.

(A) Chromosomal non-disjunction is the most common cause of DS, with maternal meiosis I and II accounting for two-thirds of cases. (B) Chromosomal non-disjunction may also occur during mitosis, posing a post-conception cause of DS. (C) Robertsonian translocations between the long arms of Hsa21 (red) and another acrocentric chromosome (most commonly Hsa14, black) also result in three copies of Hsa21. Figure created with BioRender.com.

Investigating the genotype-phenotype relationship in DS can provide insight into how triplication of Hsa21 encoded genes causes the observed differences in individuals with DS with the possibility of developing treatments for pathologies that occur more frequently in this population. Two major theories have been proposed to explain the phenotypic characteristics of DS. Firstly, the gene-dosage hypothesis suggests that the 1.5-fold increase in Hsa21 genes results in increased abundance of gene products with direct and downstream consequences on biological function. Secondly, the presence of an extra chromosome itself may influence the nuclear environment,

resulting in a globally altered chromatin landscape although it is not clear whether this is a contributing factor (Antonarakis *et al.*, 2020).

DS is characterised by phenotypes that affect multiple organ systems. Importantly, the penetrance of these phenotypes varies considerably between individuals. Aside from short stature and craniofacial features such as a more flattened nasal bridge and upward slanting eyes, most phenotypic differences are not visible. This includes musculoskeletal weakness, an increased risk of congenital heart defects, autoimmune conditions, immune system dysregulation and sensory impairments (Antonarakis *et al.*, 2020). Interestingly, DS appears to be protective against certain conditions with people experiencing lower rates of hypertension, hypercholesterolaemia and solid tumours (Baksh *et al.*, 2023). Additionally, the neurological system is impaired in DS throughout life with all individuals experiencing some degree of ID.

Neurological differences are present from fetal stages but the underlying molecular mechanisms are not well understood. Anatomically, brain volumetric differences have been observed, including a thinner cortical layer and reduction in overall brain volume, particularly of the frontal and occipital lobes associated with memory, executive function, movement and language, and sensory processing, all of which are impaired in DS (Pinter *et al.*, 2001; Fukami-Gartner *et al.*, 2023). Interestingly, some areas of the brain also show an increase in volume, including regions of the temporal lobe (Yun *et al.*, 2021). At the cellular level, lower brain volume has been attributed to reduced neurogenesis in the fetal brain and, to a lesser extent, increased neuronal apoptosis compared with euploid controls (Guidi *et al.*, 2008, 2011). Mechanistically, animal and in vitro studies suggest that impaired neurogenesis stems from a reduction in neuronal progenitor cells (NPCs) as well as a bias towards preferential differentiation into glial (astrocytes and oligodendrocytes) over neuronal phenotype caused by altered timing in the differentiation process (Guidi *et al.*, 2011; Zdaniuk *et al.*, 2011; Baburamani *et al.*, 2020; Giffin-Rao *et al.*, 2022; Qiu *et al.*, 2023).

Several Hsa21 genes have been proposed to mediate these differences. Firstly, overexpression of Dual specificity tyrosine-phosphorylation-regulated kinase 1A

(*DYRK1A*) or amyloid precursor protein (*APP*) has been shown to impair cellular proliferation through alteration of cell cycle regulating proteins (Chen *et al.*, 2013; Wu *et al.*, 2016). Inhibition of DYRK1A restored normal cell cycle length and neuronal differentiation (Hibaoui *et al.*, 2014). Secondly, oligodendrocyte transcription factor *OLIG2* activates oligodendrocyte specific promotors and its overexpression has been associated with inhibition of NPC proliferation (Lu *et al.*, 2012). Lastly, increased dosage of regulator of calcineurin, *RCAN1,* resulted in delayed NPC differentiation in the developing neocortex in a mouse model of DS (Kurabayashi and Sanada, 2013). These candidate genes have also been implicated in increased apoptotic cell death, which may exacerbate reduced neurogenesis in the brain of individuals with DS (Park *et al.*, 2010; Lu *et al.*, 2011; Sun *et al.*, 2011; Patel *et al.*, 2015). This DS specific increase in cellular apoptosis has been supported by a recent single cell transcriptomic analysis that identified overexpression of genes linked to apoptotic processes in proliferating cells (Y. Chen *et al.*, 2023). Additionally, evidence from DS post-mortem brain tissue has found dysregulation of genes involved in processes related to myelination and gliogenesis, indicating a white matter and oligodendrocyte differentiation defect that results in reduced signal transmission in the developing brain of individuals with trisomy 21 (Olmos-Serrano *et al.*, 2016). These studies provide insight into potential underlying mechanisms that may contribute to ID in DS. Notably, epigenetic mechanisms such as altered brain methylation patterns have also been proposed to influence DS associated ID and may account for some of the considerable inter-person variability in cognitive impairment (Laufer *et al.*, 2019).

Individuals with DS not only present with clinical phenotypes during development but also show differences during the ageing process. DS has been described as a form of progeroid syndrome based on several markers of accelerated ageing, some of which can be detected at the fetal stage and remain advanced throughout the lifespan (Borelli *et al.*, 2015; Cole *et al.*, 2017; Franceschi *et al.*, 2019; Xu *et al.*, 2022). Phenotypically, this is characterised by accelerated immunosenescence, sensory impairments and early-onset menopause (Schupf *et al.*, 1997; Meuwese-Jongejeugd *et al.*, 2006; Franceschi *et al.*, 2019). Diseases of ageing also impact the brain in individuals with DS, leading to a marked increased risk of early onset AD (EOAD)

compared with the general population, with dementia now being the leading cause of death in individuals with DS over the age of 35 (Hithersay *et al.*, 2019). This highlights the importance of furthering our understanding of AD in DS (AD-DS) to alleviate the burden of dementia in this population.

1.2 Introduction to Alzheimer's disease

1.2.1 History and prevalence

Alzheimer's disease is a progressive neurodegenerative condition and the most common cause of dementia that leads to progressive cognitive impairment and eventually death. It is named after German physician Alois Alzheimer who, in 1907, first published a case report describing brain pathology that had been discovered in a woman who had experienced memory loss during the last few years of her life (Alzheimer, 1907). Several decades later, the protein components of plaques and neurofibrillary tangles (NFTs) were determined to be amyloid-β (Aβ) and tau, respectively, establishing a causal link between this cerebral peptide build up and disease symptoms (Glenner and Wong, 1984a; Brion *et al.*, 1985). The presence of these two hallmark pathologies is used to define AD.

With global population growth and ageing, prevalence of all-cause dementia has been on the rise for many decades globally, with an estimated 55 million people currently living with the condition (WHO, 2022). By 2050, this has been estimated to increase to over 150 million people despite a slight recent decline in some high SDI countries, including the UK (Wu *et al.*, 2017; Wolters *et al.*, 2020; Nichols *et al.*, 2022). AD is estimated to account for 60-80% of dementia cases with a lifetime risk of 10% and 20% for males and females, respectively (Chêne *et al.*, 2015; Raskin *et al.*, 2015). This disproportional effect of AD in women can only in part be explained by differences in longevity between the two sexes (Gauthier *et al.*, 2021). However, disentangling the

incidence of AD from other forms of dementia is challenging as symptoms and biomarkers are not unique to this disease and it can only be definitively diagnosed by post-mortem examination and is frequently accompanied by additional pathologies (Karanth *et al.*, 2020).

1.2.2 Pathophysiology and genetic risk factors

Extracellular amyloid plaques and intracellular NFTs constitute the hallmark pathologies of AD. Importantly, disease aetiology encompasses several additional pathophysiological changes that develop many years before symptom onset, including endolysosomal dysfunction and neuroinflammation (Van Acker, Bretou and Annaert, 2019; Leng and Edison, 2020). Additional co-morbid pathologies, including α-synuclein and/or TDP43, are also present in many cases (Karanth *et al.*, 2020). The early, asymptomatic stages of the disease are characterised by an accumulation of soluble Aβ that aggregates into oligomers and fibrils and eventually forms insoluble neuritic plaques (Ono and Watanabe-Nakayama, 2021). Accumulated Aβ becomes distributed throughout the cortex where it has been proposed to exert neurotoxic effects, including through activation of proinflammatory processes and synaptic dysfunction (Ripoli *et al.*, 2014; LaRocca *et al.*, 2021). Temporally, amyloid pathology is followed by the appearance of NFTs consisting of hyperphosphorylated tau protein that mis-localises and accumulates intracellularly in cell bodies and dendrites (Yin *et al.*, 2021). Hyperphosphorylated tau oligomers have been shown to propagate in a specific spatial pattern through synaptic transmission, resulting in further tau aggregation, though the mechanisms determining this spread are not fully understood (Vogel *et al.*, 2020; Zhang *et al.*, 2021). The extent of tau NFT pathology has been employed to determine the severity of AD through Braak staging. This method divides Braak stages into categories I-VI, with 0 indicating a lack of NFT pathology. Stages I-II represent mild to severe NFTs in the entorhinal region, stages III-IV equates to severe pathology in cortex and limbic regions (e.g. hippocampus) and brains with late

stage disease V-VI exhibit moderate to severe pathology that also includes the neocortex (Braak and Braak, 1991).

In most cases, following a prolonged asymptomatic latency phase, the combined impact of these pathologies results in synaptic dysfunction, neuronal loss and brain atrophy that is reflected in symptoms of progressive memory, language and executive function decline (Vermunt *et al.*, 2019). Symptoms are initially classed as mild cognitive impairment (MCI) that frequently progresses to a clinical dementia diagnosis.

AD can be categorised into two main types: sporadic or late-onset AD (LOAD) and familial or early-onset AD (EOAD). LOAD accounts for 95% of AD cases, with age being the greatest risk factor. Aside from environmental risk factors such as low educational attainment, tobacco smoke and air pollution, a growing number of genetic risk factors for LOAD have been identified, indicating that the cause of sporadic AD is complex and multifactorial (Zhao *et al.*, 2021). Genome-wide association (GWAS) studies have identified at least 75 LOAD risk loci that each confer a small increase in disease risk and may impact progression of different stages of AD development (Bellenguez *et al.*, 2022; Altmann *et al.*, 2024). The *APOE ε4* allele confers the greatest risk and homozygosity of this allele has recently been proposed to constitute a genetic form of AD with almost all carriers exhibiting amyloid pathology by 65 years of age (Fortea *et al.*, 2024). The rarer EOAD cases are caused by heritable mutations in the *APP* gene (including duplication), presenilin genes *PSEN1* or *PSEN2*, with *PSEN1* mutations accounting for the most severe and earliest onset cases (Cacace, Sleegers and Van Broeckhoven, 2016; Bagaria, Bagyinszky and An, 2022). The encoded APP protein is a precursor of Aβ and mutations of the gene lead to increased production of more aggregation prone versions of amyloid (e.g. $A\beta_{42}$). *PSEN1/2* encode subunits of the γ-secretase that cleaves APP protein products, resulting in an overproduction of Aβ (Lanoiselée *et al.*, 2017). These mutations lead to dementia symptom onset before the age of 65, suggesting that increased Aβ pathology plays a key role in EOAD pathogenesis.

1.2.3 The role of amyloid in AD

All forms of AD are characterised by cerebral accumulation of Aβ which led to the amyloid cascade hypothesis that places amyloid at the centre of disease development and progression and makes it a target for interventions (Hardy and Higgins, 1992; Cummings, 2023). This hypothesis proposes that accumulation of Aβ initiates AD pathology, triggering tau accumulation and eventually synaptic dysfunction and neuronal loss and accompanying cognitive decline. Generation of Aβ involves the sequential cleavage of APP. APP is a type I transmembrane protein that is highly expressed in neurons. Its physiological functions include dendritic spine development and synaptic transmission (Lee *et al.*, 2010; Rice *et al.*, 2019). Processing of APP can occur via two distinct pathways (Figure 1.2). Firstly, the non-amyloidogenic pathway involves central cleavage by α-secretase, creating extracellular sAPPα which is neuroprotective by promoting neuronal survival and neurite outgrowth as well as membrane bound CTFα (C83) (Dar and Glazner, 2020). Subsequent cleavage of CTFα by γ-secretase releases APP Intracellular Domain fragment (AICD) from the remaining P3 membrane bound fragment into the cytoplasm. Secondly, the amyloidogenic pathway consists of a multi-step cascade that begins with the cleavage of full-length APP (flAPP) by β-secretase BACE1, resulting in a soluble N-terminus of APP (sAPPβ) and membrane bound C-terminal fragment (CTF-β/C99). Subsequently, cleavage of the CTF-β fragment by γ-secretase (including PSEN1/2 subunits) produces cytoplasmic AICD and Aβ that is cleaved at varying sites to release species of differing lengths into the extracellular space (Hampel *et al.*, 2021). Peptides with fewer residues tend to be less aggregate prone than longer versions such as $A\beta_{42}$, the most common constituent of amyloid plaques. Assembly of Aβ monomers occurs in a step wise manner from dimers to oligomers to fibrils that accumulate into extracellular plaques (Chen *et al.*, 2017).

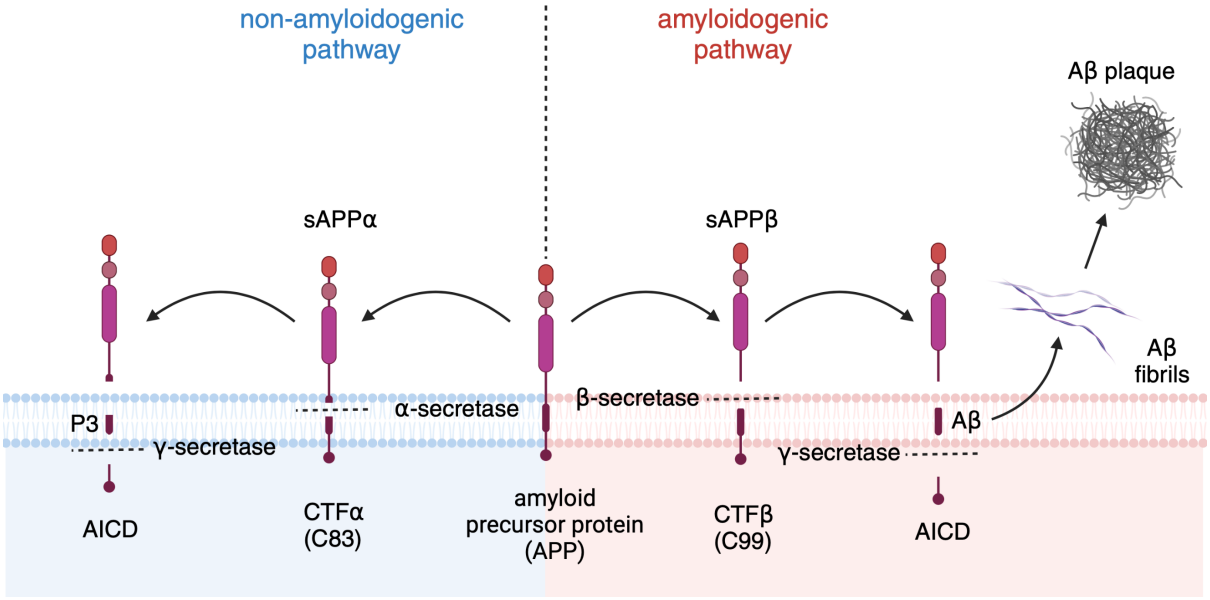

Figure 1.2 APP processing via the non-amyloidogenic and amyloidogenic pathways.

Non-amyloidogenic processing of APP (blue, left) involved cleavage by α-secretase creating sAPPα and membrane bound CTFα/C83 which is subsequently cleaved by γ-secretase releasing AICD from membrane bound P3 into the cytoplasm. The amyloidogenic pathway (red, right) involved sequential cleavage of APP by β-secretase into extracellular sAPPβ and membrane bound CTF-β/C99. Subsequent cleavage of CTF-β by γ-secretase liberates the Aβ peptide into the extracellular space and AICD into the cytoplasm. Extracellularly, Aβ peptides assemble into oligomers, fibrils and eventually plaques. Created with BioRender.com.

Sequential cleavage of APP to release Aβ peptides takes place in the brains of healthy adults but the physiological function of these peptides is still not fully understood (Bateman *et al.*, 2006). In its monomeric form, Aβ has been implicated in synaptic vesicle release and plasticity through regulation of hippocampal neurogenesis, indicating a neuroprotective role (Abramov *et al.*, 2009; Zimbone *et al.*, 2018). However, when the balance of Aβ production and clearance becomes perturbed, the peptides can assemble into misfolded aggregates. Clearance of Aβ takes place via several different routes. Non-enzymatic clearance of soluble Aβ is mediated by endothelial cells of the blood brain barrier into the bloodstream or drainage of the

interstitial fluid into the cerebrospinal fluid (CSF) via the glial-lymphatic (glymphatic) pathway (Mawuenyega *et al.*, 2010; Cockerill *et al.*, 2018). Additionally, evidence from mouse models suggests that Aβ can be eliminated by Aβ-degrading enzymes via the neprilysin–mediated or UPS pathways (Iwata *et al.*, 2001). Notably, some of these degradation pathways are mediated by microglia (Ries and Sastre, 2016). Impaired clearance of Aβ is a major driver of amyloid accumulation in the brain, particularly in LOAD (Zou *et al.*, 2006; Sweeney, Sagare and Zlokovic, 2018; Reeves *et al.*, 2020).

More than three decades after the formulation of the amyloid cascade hypothesis, the role of Aβ in AD pathogenesis remains to be fully elucidated. One of the key research questions has been whether and how amyloid and tau pathology and their potential interaction are related to AD progression. The strongest support for Aβ being the driver of AD comes from familial cases of the disease where increased production of Aβ (e.g. through duplication of the *APP* locus as seen in DS) results in a significantly earlier onset of the disease compared with the general population (Fortea *et al.*, 2021). Similarly, in a *PSEN1* mutation kindred, tau levels measured by positron emission tomography (PET) showed a positive correlation with Aβ plaque load (Quiroz *et al.*, 2018). This temporal disease progression from Aβ to tau pathology has also been observed in LOAD cases (Jacobs *et al.*, 2018; Hanseeuw *et al.*, 2019; Jack *et al.*, 2019). In vitro and animal model studies have also provided support for this hypothesis. In induced pluripotent stem cells (iPSCs) derived from fibroblasts with familial AD mutations, a direct relationship between APP processing and tau was observed, with γ-secretase inhibition reducing tau levels. Additionally, some APP mouse models exhibit tau hyperphosphorylation even in the absence of humanised tau (Maia *et al.*, 2013).

The mechanistic link between the two hallmark AD pathologies has not been fully elucidated. Recent evidence suggests that the two may be synergistically linked. The presence of Aβ may create a permissive environment for tau aggregation by inducing conformational changes that stabilise tau proteins and promoting its hyperphosphorylation thus accelerating tau propagation (De Felice *et al.*, 2008; Pooler *et al.*, 2015; DeVos *et al.*, 2018). Aside from impacting tau, Aβ has also been shown

to exacerbate neuroinflammation in AD by promoting proinflammatory cytokine release by microglia and astrocytes as well as blocking anti-inflammatory cytokines such as TGF- β1 (Olabarria *et al.*, 2010; Chen *et al.*, 2015).

Notably, clinical translation of findings supporting the toxic role of Aβ in AD does not appear to be as straightforward. Amyloid on its own is a poor predictor of cognitive impairment with tau showing a stronger correlation (Bejanin *et al.*, 2017). In cognitively normal individuals, amyloid plaque prevalence reaches over 40% by age 90, suggesting a disconnect between amyloid pathology and clinical dementia (Jansen *et al.*, 2015). Furthermore, an implicit consequence of Aβ driving disease development would be that its reduction will alleviate or at least slow symptom progression. However, despite the recent approval of anti-amyloid therapies, clinical benefit of reducing cerebral amyloid deposits appears marginal (Avgerinos *et al.*, 2024). There are several reasons that could explain a lack of significant benefit, including that treatment administration may be taking place too late in the disease process. Moreover, it appears that AD pathogenesis is more complex than the linear progression of events posited by the amyloid cascade hypothesis. Instead, these pathologies are co-occurring and potentially synergistically interacting to promote neuronal death and brain atrophy that is related to clinical symptoms of the disease.

1.3 Introduction to Alzheimer's disease in Down syndrome

1.3.1 Epidemiology and Diagnosis

The link between DS and AD was first discovered in the 1940s (Jervis, 1948). In the 1980s, the isolation of the amyloid protein from the brain of an individual with DS established a genetic relationship between DS and AD (Glenner and Wong, 1984). DS results from the triplication of Hsa21 genes, including *APP,* which has been found to be sufficient to cause EOAD (Sleegers *et al.*, 2006). An additional copy of *APP* also

appears to be necessary for the development of AD-DS, as individuals with a rare partial trisomy 21 that precludes the triplication of the *APP* locus do not develop EOAD (Prasher *et al.*, 1998; Doran *et al.*, 2017). Therefore, most individuals with DS are at increased risk of developing AD compared to the general population. Individuals with DS carry a lifetime risk of over 90%, making DS the greatest genetic cause of AD (McCarron *et al.*, 2017; Shimizu *et al.*, 2024).

The considerable increase in life expectancy of individuals with DS has led to a rise in AD-DS prevalence, with the mean age of AD dementia diagnosis in individuals with DS of 56 years of age and a disease duration of less than 5 years from diagnosis (Iulita *et al.*, 2023; Shimizu *et al.*, 2024). Unlike in the general population where females are disproportionally affected by dementia, AD-DS appears to affect both sexes at similar rates, although disease duration may be longer in females (Lai *et al.*, 2020). Interestingly, some recent studies suggest that females may be more susceptible to the adverse effects of carrying the *APOE* ε4 allele than males, although others did not find a significant association between sex and *APOE* allele effects on AD risk (Lai *et al.*, 2020; Iulita *et al.*, 2023; Silverman *et al.*, 2023). Although AD has been recognised as the leading cause of death from the mid-thirties in DS, incidence may still be underreported, as DS itself is frequently quoted on death certificates as the causal condition leading to an underestimation of the burden of AD in this population (Landes, Finan and Turk, 2023). An additional challenge of estimating AD-DS incidence is the lack of standardised criteria for AD diagnosis in this population. Underlying ID varies between individuals, rendering tests developed for cognitively typical patients unreliable. Modification of diagnostic tests, including the 'Cued Recall Test' have improved the detection of cognitive impairment in individuals with DS with recent analysis suggesting that stratification by ID level may be sufficient for diagnosing prodromal AD and AD dementia in individuals with mild to moderate ID (Benejam *et al.*, 2020; Krinsky-McHale *et al.*, 2022). Longitudinal assessment of cognition has indicated that trajectories of progressive cognitive decline are similar between mild and moderate ID, beginning with episodic memory decline from the 4th decade of life (Videla *et al.*, 2022). These findings support that testing for dementia in DS through

both modified cognitive and biomarker assessments should be undertaken by this age to identify those most vulnerable to EOAD development (Carmona-Iragui *et al.*, 2024).

1.3.2 Differences and similarities between AD-DS and other forms of AD

Neuropathological changes in genetically determined forms of AD follow a sequential pattern, with the earliest observed changes of enlarged endosomes being present from the fetal stage in DS (Figure 1.3) (Cataldo *et al.*, 2000). The hallmark pathologies emerge as intraneuronal accumulation of amyloid before the age of 10, followed by diffuse plaques by adolescence condensing into neuritic plaques accompanied by the appearance of intracellular NFTs, amyloid deposition in the walls of cerebral arteries (cerebral amyloid angiopathy, CAA) and neuroinflammation by the fourth decade of life. This period marks the transition from the preclinical to the symptomatic phase of AD-DS, with dementia increasing exponentially, affecting two-thirds of individuals with complete trisomy 21 by the age of 65 (Fortea *et al.*, 2021). Interestingly, despite the presence of AD neuropathology, some individuals with DS do not develop clinical dementia symptoms, indicating that disease progression is governed by a complex interaction of genetic and environmental factors (Liou *et al.*, 2025).

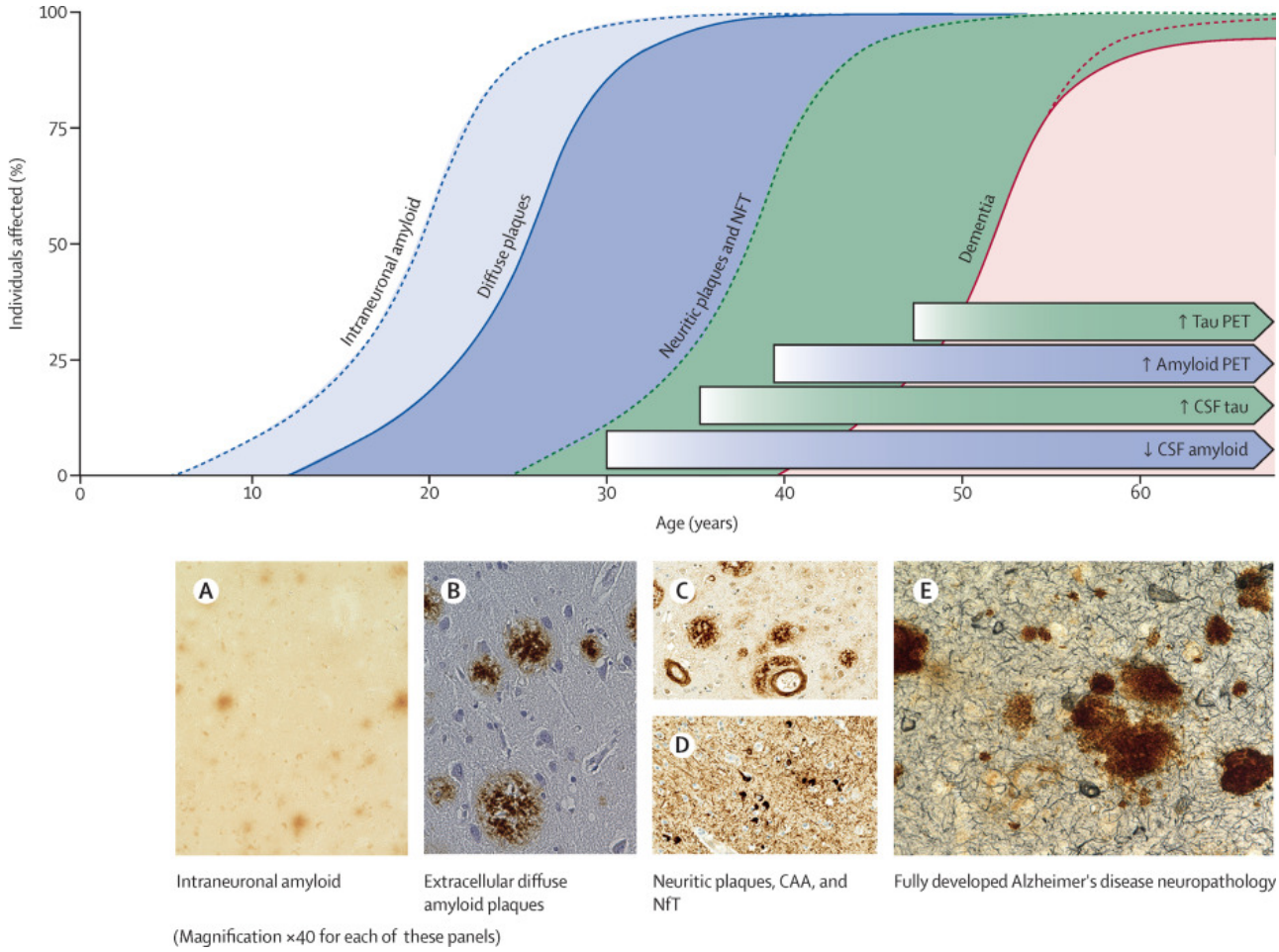

Figure 1.3 Neuropathology along the AD-DS continuum.

In individuals with DS, early amyloid pathology begins with intraneuronal accumulation in the first decade of life (light blue, [A]), progressing to extracellular diffuse plaque formation (dark blue, [B]). Aggregation of amyloid results in neuritic plaques accompanied by NFT and CAA pathologies from the middle of the third decade of life, becoming more severe with age (green, [C-E]). These hallmark pathologies result in clinical symptoms of dementia that begin to emerge from around age 40, increasing exponentially and reaching a lifetime prevalence of over 90% (red). Detection of amyloid and tau in CSF precedes their respective PET positivity by around 10 years. Figure reprinted from (Fortea *et al.*, 2021), copyright (2025), with permission from Elsevier.

Clinical biomarkers offer important insight into the progression of AD pathology prior to symptom onset. As part of the assessment, CSF and plasma Aβ concentration, as well as PET amyloid burden, are used as early biomarkers to determine the extent of Aβ deposition in the brain, with fluid biomarkers revealing signs of disease almost a decade earlier than imaging biomarkers (Fortea *et al.*, 2020). However, although the sequence of AD neuropathological progression is similar in genetic and sporadic AD, staging differs between these two forms of the disease. This is because autosomal dominant mutation carriers and individuals with DS show signs of disease pathology from an early age and are considered to be on the AD pathological continuum from birth (Jack *et al.*, 2024). The *APP* dosage effect is reflected in elevated plasma Aβ40 and 42 levels throughout adulthood in individuals with DS, making the plasma Aβ42/40 ratio an unreliable predictor of disease risk in this population (Alhajraf *et al.*, 2019). In contrast, longitudinal changes in plasma neurofilament light (NfL) levels, a marker for neuronal damage, have been determined to be a good diagnostic predictor of symptomatic AD-DS (Carmona-Iragui *et al.*, 2021). Similarly to sporadic AD, combined amyloid and tau positivity has been found to be more closely associated with dementia symptoms than amyloid alone (Grigorova *et al.*, 2022; Hartley *et al.*, 2024).

A notable phenotypic difference between AD-DS and other forms of AD is the high rate of co-occurring epileptic seizures in individuals with trisomy 21, present in over 60% of AD-DS cases (Gholipour *et al.*, 2017; Altuna, Giménez and Fortea, 2021). An increased risk of seizures is present in early childhood in individuals with DS and subsequently exhibits a second peak in prevalence from the age of 40 (termed late-onset myoclonic epilepsy), coinciding with the onset of symptomatic AD (Fortea *et al.*, 2021).

Recent studies have pointed to several distinct differences in the development and progression of AD pathological hallmarks and accompanying co-morbidities. Overproduction of Aβ in familial AD and AD-DS has been associated with increased early striatal, thalamic and parenchymal deposition compared with LOAD (Cohen *et al.*, 2018). Brain tissue samples from individuals with AD-DS also exhibited increased plaque size in the temporal lobe (Ichimata *et al.*, 2023). Furthermore, a greater level

of tau and faster accumulation of pathological tau for the same amount of deposited Aβ has been observed in AD-DS compared with EOAD, indicating that trisomy 21 may modify AD progression compared with other genetically deterministic forms of the disease (Boerwinkle *et al.*, 2023; Ichimata *et al.*, 2023).

At the structural level, subtle differences have recently been identified. While AD associated tau fibril structure appears to be identical in individuals with DS and euploid individuals, structural differences in amyloid filaments have been observed (Fernandez *et al.*, 2024). Furthermore, amyloid plaques in AD-DS frequently take on a dense fibrillar structure with a distinct border termed 'bird nest' plaque which contains a higher Aβ40:Aβ42 ratio compared with LOAD cases (Ghosh *et al.*,2024). Bird nest plaques were found to be surrounded by microglia and associated with CAA, suggesting that this unique plaque structure may be driven by neuroinflammation known to be increased in AD-DS (Ichimata *et al.*, 2022). Individuals with AD-DS are disproportionally affected by CAA pathology compared to individuals who have EOAD caused by mutations in *APP* (Kasri *et al.*, 2024). However, in comparison with a rare genetic form of AD caused by the duplication of the *APP* locus (dupAPP), the CAA load is observed to be lower in AD-DS (Kasri *et al.*, 2024). Recent evidence suggests a possible link between higher levels of CAA in AD-DS and dupAPP compared with other forms of AD and a truncated version of Aβ42 found in these cases (Mann *et al.*, 2018; Kasri *et al.*, 2024). Anti-amyloid immunotherapies have been shown to associate with CAA, increasing the risk for brain swelling and bleeding events. This raises concerns over the safety of its use in DS and underlines the importance of including this population in clinical trials for anti-amyloid therapies (Liu *et al.*, 2024; Söderberg *et al.*, 2024).

Furthermore, longitudinal PET and magnetic resonance imaging (MRI) evidence suggests that the period between amyloid accumulation and the emergence of tau positivity is halved in AD-DS compared with sporadic AD (Zammit *et al.*, 2024). These studies illustrate that, despite the relatively subtle differences in neuropathology between the different forms of AD, they may be of clinical relevance by impacting treatment options and timing for individuals with AD-DS (Liu *et al.*, 2024).

1.3.3 Hsa21 candidate genes that may influence amyloid load and toxicity

Triplication of the *APP* locus is known to be causal for AD in individuals with trisomy 21 (Rovelet-Lecrux *et al.*, 2006; Sleegers *et al.*, 2006). However, how an additional copy of other Hsa21 genes may modify disease risk is not well understood. While increased dosage of certain Hsa21 genes may favour the development of AD neuropathology, a later onset of amyloid accumulation in AD-DS compared with some forms of EOAD suggests that others may confer a protective effect (Boerwinkle *et al.*, 2023). This hypothesis is supported by studies in AD-DS mouse models that have demonstrated that triplication of Hsa21 genes (and their mouse orthologues) other than *APP* is sufficient to modify amyloid accumulation and cognitive decline (Wiseman *et al.*, 2018; Tosh *et al.*, 2021; Mumford *et al.*, 2022). In recent years, overexpression of several Hsa21 genes has been proposed to mediate this effect.

Exacerbation of amyloid pathology has been linked to overexpression of several Hsa21 genes. The kinase DYRK1A directly interacts with APP, resulting in its phosphorylation, leading to increased production of Aβ when overexpressed (Ryoo *et al.*, 2008; García-Cerro *et al.*, 2017). In contrast, dosage correction or inhibition of DYRK1A reduces levels of Aβ and neurotoxicity in animal models (Lowe, Usowicz and Hodge, 2019; Zhu, Parsons, Foley, *et al.*, 2022). These findings have recently informed a phase 1 clinical trial of a DYRK1A inhibitor for the treatment of AD-DS (Meijer, Chrétien and Ravel, 2024). The small ubiquitin-like modifier *SUMO3* has been suggested as another candidate gene whose overexpression exacerbates secretion of Aβ although this does not appear to be dependent on its sumoylation activity and the underlying mechanism has not been determined (Dorval *et al.*, 2007). In a mouse model of AD, post-translational modification of APP and BACE1 by deubiquitinase USP25 has been shown to stabilise APP, decreasing its proteasomal degradation and resulting in elevated levels of Aβ in these animals which was rescued by genetic deletion of the gene (Zheng *et al.*, 2022).

A potential protective effect against amyloid accumulation has been attributed to Hsa21 encoded β-secretase *BACE2. BACE2* polymorphisms have been shown to be associated with age of onset of AD-DS (Mok *et al.*, 2014). Furthermore, an in vitro study found that T21 organoids exhibited increased levels of Aβ degeneration products compared with those dosage corrected for *BACE2,* suggesting that this gene may act as an AD suppressor when overexpressed in DS (Alić *et al.*, 2020).

In addition to protein coding genes, increased dosage of non-coding miRNA *miR-155* may further modulate the development and progression of AD neuropathology in individuals with DS by promoting neuroinflammation (Y. Y. Li *et al.*, 2012; Sun *et al.*, 2019). These studies demonstrate that, while having three copies of *APP* is crucial for the development of AD-DS, other Hsa21 encoded genes can modify disease pathology and symptoms. Investigating which genes modulate certain aspects of disease pathology and whether their effects require the interaction with other genes will improve our understanding of the aetiology of AD-DS.

1.4. Modelling AD-DS: in vitro and ex vivo approaches

1.4.1 Human post-mortem brain tissue to study AD-DS

Human post-mortem brain tissue can be employed in a variety of ways, including in histology, transcriptomic and proteomics studies. Histological examination of post-mortem brain tissue from individuals with DS, with and without AD, offers crucial insight into how AD neuropathology develops across the lifespan in this population. Many decades ago, neuropathological studies revealed that amyloid plaque and NFT density significantly increased after age 40 in individuals with trisomy 21, consistent with more recent PET imaging studies (Motte and Williams, 1989; LeVine *et al.*, 2017; Fortea *et al.*, 2021).

Isolation of RNA from human post-mortem brain tissue allows for the measurement of transcripts to assess which genes are differentially expressed in AD-DS compared with other forms of AD and healthy controls. Differential gene expression analyses have revealed that a 1.5-fold increase in gene dosage due to trisomy of Hsa21 does not necessarily predict a matched increase in transcript level and is variable between brain regions and cell types (Olmos-Serrano *et al.*, 2016; Palmer *et al.*, 2021; Miyoshi *et al.*, 2024). Several Hsa21 genes have shown consistent upregulation at the transcript level in the adult brain of individuals with DS, including candidate modifiers of AD-DS, *DYRK1A* and *BACE2* (Lockstone *et al.*, 2007; Olmos-Serrano *et al.*, 2016; Palmer *et al.*, 2021). Proteomic analyses of post-mortem brain tissue samples are an important complement to transcriptomic studies as post-translational regulation of transcripts frequently results in altered protein abundance for some genes while others, including DYRK1A and APP remain dosage sensitive at the protein level (i.e. a third copy of the gene causes an increase in protein level) (Dowjat *et al.*, 2007; Cheon *et al.*, 2008; Wegiel *et al.*, 2008; Carlyle *et al.*, 2017). This discrepancy between transcript and protein abundance has recently been demonstrated in a multi-omics study of trisomy 21 brains that found a low correlation between RNA and protein levels (Rastogi *et al.*, 2024).

Notably, analysis of human post-mortem brain tissue has several limitations. While test and control samples can be matched for certain confounding factors, including age, sex and post-mortem interval (PMI), many other environmental factors known to impact AD risk cannot be accounted for. Additionally, due to ethical and technical difficulties around banking brain tissue from individuals with DS, obtaining sufficient samples can be challenging. Nonetheless, elucidating Hsa21 genes that exhibit an increase in transcript and protein abundance as a result of an additional gene copy (are dosage sensitive) in post-mortem brain tissue from individuals who had AD-DS and determining their associated pathways can be used to generate hypotheses of potential disease mechanisms to be tested in cell and animal models.

1.4.2 Cell Models of AD-DS

Human cellular models offer a biologically relevant environment to test mechanistic hypothesis without the need for animals. Several different types of cell models have been implemented to study aspects of AD-DS pathology. Immortalised cell lines such as human neuroblastoma cells (SHSY-5Y, SK-N-MC) are of neuronal origin and retain many of their functional properties. These cells have been used to study the impacts of amyloid accumulation. Overexpression of *APP* in SHSY-5Y cells was found to increase susceptibility to oxidative stress, while Aβ fibrils were found to have an apoptotic effect on cells (Matsumoto *et al.*, 2006; Krishtal *et al.*, 2017). Notably, although immortalised cell lines can be used to study the effects of overexpressing single genes, they have limited translational use for DS research as they are not trisomic for Hsa21. Therefore, the lack of an additional copy of all Hsa21 genes means that they cannot recapitulate the consequences of trisomy 21 on AD pathology. To circumvent this limitation, cell cultures can also be derived from DS tissues, including neurons and NPCs which have the added advantage of differentiating into desired neuronal subtypes. DS derived neurons display intracellular accumulation of insoluble Aβ42 and mitochondrial dysfunction (Busciglio *et al.*, 2002).

Human iPSCs offer additional advantages for disease research owed to their potential to differentiate into almost any cell type, including all major brain cell types. For modelling AD pathology, iPSCs were first derived from fibroblasts obtained from familial AD patients and exhibited increased secretion of Aβ (Yagi *et al.*, 2011). Since then, iPSCs have been derived from different forms of AD and used to probe disease mechanisms and test potential therapeutics (Sullivan and Young-Pearse, 2017). To study AD in the context of DS, trisomy 21 iPSCs differentiated into neurons have been shown to reproduce certain properties of those derived from AD patients, including extracellular accumulation of Aβ although this is not sufficient for plaque formation (Shi *et al.*, 2012; Dashinimaev *et al.*, 2017; Slanzi *et al.*, 2020). Additionally, normalisation of *APP* copy number in iPSC-derived cortical neurons that were otherwise trisomic for

Hsa21 genes reduced Aβ levels, confirming the crucial role of *APP* overexpression in the development of AD pathology (Ovchinnikov *et al.*, 2018). Isogenic euploid cells can be used as controls for trisomy 21 cells. Alternatively, to reduce heterogeneity in the genetic background, disomic controls can be created by introducing and subsequently selecting against a transgene, creating cells with spontaneous loss of the triplicated Hsa21 (L. B. Li *et al.*, 2012). Alternatively, one copy of Hsa21 can be silenced epigenetically in control cells using XIST RNA (Gupta, Czerminski and Lawrence, 2024). Notably, cells derived from iPSCs remain immature and only represent one cell type once differentiated which does not recapitulate the cellular diversity present in the brain environment.

To avoid the limitations of immature iPSC-derived neurons resulting from differentiating via the NPC stage, iPSCs can be directly differentiated into induced neurons (iNs), bypassing the NPC stage (Yang *et al.*, 2011; Mertens *et al.*, 2018). During this process, cell type specific transcription factors determine the resulting neuronal subtype while maintaining their original genetic background (Pang *et al.*, 2011). Trisomy 21 derived iNs have been shown to present with impaired axonal transport, a pathology observed in AD-DS (C. I. Wu *et al.*, 2022). However, iN cultures used for AD-DS research are still in their infancy and currently lack isogenic controls, confounding findings. Furthermore, these types of cell cultures are also restricted to one cell type and thus do not recapitulate the complexity of cell-cell interactions.

The development of cerebral organoids has provided a 3D in vitro system comprised of multiple cell types that can better model the complex brain environment (Lancaster and Knoblich, 2014). Organoids originate from PSCs and, when obtained from familial AD mutation carriers, accumulate Aβ plaques and phosphorylated tau (Choi *et al.*, 2014). Similarly to monolayer iPSC-derived neuronal cultures, trisomy 21 derived cerebral organoids display several features of AD neuropathology, including an increased Aβ42:40 ratio and the accumulation of amyloid plaques and neuroinflammatory markers (Alić *et al.*, 2021; Zhao and Haddad, 2022; Campbell *et al.*, 2023; Johnson *et al.*, 2023). Interestingly, temporal progression of AD neuropathology can be observed in these models (Fertan *et al.*, 2024). Although the

cerebral organoids used in these studies are comprised of multiple cell types, they lack the vasculature that is the site of CAA frequently observed in AD-DS and involved in many aspects of AD neuropathology. It has recently been demonstrated that vascularised brain organoids can be generated and include microglia and blood brain barrier structures, offering the opportunity for the development of improved 3D in vitro systems for studying AD-DS (Sun *et al.*, 2022).

Mouse – iPSC chimeric models offer a novel approach that permits long-term growth of human cell lines engrafted in mouse models. Transplantation of human iPSC derived NPCs that differentiate inside the mouse brain have been used to study the response of neurons and microglia to Aβ and for specific mechanistic studies of DS (Espuny-Camacho *et al.*, 2017; Real *et al.*, 2018; Hasselmann *et al.*, 2019; Jin *et al.*, 2022).

1.5. Animal Models for studying AD-DS

1.5.1 Mouse Models

Mouse models have made crucial contributions to our understanding of genetic and sporadic AD biology (Zhong *et al.*, 2024). Transgenic models of amyloid accumulation have been engineered to encode a human version of *APP* containing one or more causal mutations of familial AD under the control of an artificial promotor (Murrell *et al.*, 1991; Schellenberg *et al.*, 1991; Mullan *et al.*, 1992). This results in the expression of humanised Aβ that is significantly more aggregate prone than its mouse orthologue (Lv *et al.*, 2013). These animals, such as the J20 or 5XFAD (which contains additional familial AD mutations in the *PSEN1* gene), accumulate Aβ plaques and show memory defects with age (Mucke *et al.*, 2000; Oakley *et al.*, 2006). Importantly, *APP* expression in these AD mouse models substantially exceeds physiological levels in AD patients, resulting in particularly high levels of CTF-α/β fragments that may affect observed

phenotypes (Wiseman *et al.*, 2018). Alternatively, knock-in models have been developed to model amyloid accumulation by substituting 3 amino acids in mouse *App* to humanise the gene (Saito *et al.*, 2014). Because *App* remains under the control of the endogenous promotor, its expression occurs at physiological levels in these models. In the context of studying the effects of trisomy 21 on AD pathology, mouse models of amyloid accumulation can be crossed to mouse models of DS.

Recapitulating trisomy 21 presents a challenge, as orthologous genes are divided over three regions on mouse chromosomes (Mmu) 10, 16 and 17 (Figure 1.4). This has led to the development of DS models of aneuploidy that carry a freely segregating additional chromosome such as the Ts65Dn (triplicated region of Mmu16) and Tc1 (mice that carry a copy of Hsa21) mice, where trisomy covers around 55% and 75% of Hsa21 genes, respectively (Reeves *et al.*, 1995; O'Doherty *et al.*, 2005). The Ts65Dn model accumulates Aβ in an age-dependent manner, suggesting that an extra copy of genes that are triplicated in this model are sufficient to cause this pathology (Tallino *et al.*, 2022). However, this mouse encodes an additional copy of several Mmu17 protein-coding genes non-orthologous to Hsa21 genes, which may confound results.

Interestingly, resulting from structural rearrangements and deletions in the additional copy of Hsa21 in the Tc1 mouse, this DS model lacks a third functional copy of *APP* as well as aneuploidy only being present in around two-thirds of cells. Despite this, a Tc1xJ20 cross develops exacerbated accumulation of Aβ42, plaque deposition and cognitive deficits, suggesting that triplication of Hsa21 genes other than *APP* is sufficient to promote amyloid pathology (Gribble *et al.*, 2013; Wiseman *et al.*, 2018). The most complete aneuploid mouse model of trisomy 21 to date is the TcMAC21 mouse with complete penetrance of around 95% of Hsa21 protein coding genes and exhibits raised fl-APP and Aβ levels providing a promising model for studying AD-DS (Kazuki *et al.*, 2020).

Segmental duplication models present an alternative to models of aneuploidy. These animals have genetic duplications of different sections of genes syntenic to Hsa21

such as the Dp1Tyb/Dp1Yey, Dp2Tyb and Dp3Tyb mice encoding three copies of Mmu16 genes, the Dp10Yey, and Dp17Yey carrying three copies of Mmn10 and Mmu17 sections, respectively (Yu *et al.*, 2010; Lana-Elola *et al.*, 2016). When crossed to a J20 mouse, an additional copy of a subset of Hsa21 orthologues (excluding *App*) was sufficient to exacerbate insoluble levels of Aβ42, while other regions were found to have no significant effect (Tosh *et al.*, 2021). Furthermore, triplication of an Hsa21 syntenic region on Mmu16 (Dp3Tyb) was found to have a protective effect, reducing amyloid burden in a mouse model of AD (Mumford *et al.*, 2022). This is consistent with a later onset of AD in individuals with DS compared with EOAD caused by triplication of the *APP* locus in euploid individuals (Wiseman *et al.*, 2015), However, although segmental duplication models of DS can be used to narrow down which genes, when present in three copies result in a particular phenotype, they fail to capture the full extent of the multigenic nature of DS. Furthermore, these models do not encompass the effects of aneuploidy itself as they are euploid animals and do not reflect all aspects of human biology.

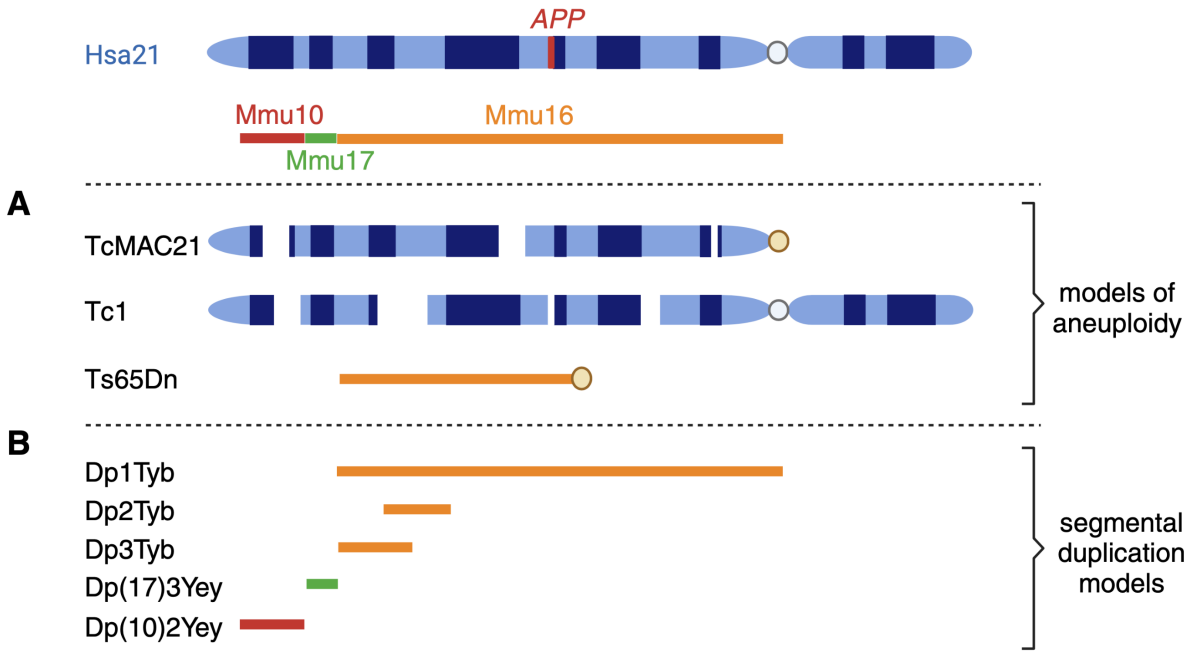

Figure 1.4 Syntenic regions between Hsa21 and Mmu10, 16 and 17 and associated models of trisomy 21.

Hsa21 has syntenic regions of homology on Mmu10 (red), Mmu17 (green), Mmu16 (yellow). (A) Examples of DS models of aneuploidy: TcMAC21, Tc1 and Ts65Dn

containing structural rearrangements and deletions. (B) Examples of DS segmental duplication models: Dp1Tyb, Dp2Tyb, Dp3Tyb (duplications of Mmu16), Dp(17)3Yey (duplication of Mmu17) and Dp(10)2Yey (duplication of Mmu10). Created with Biorender.com based on (Y. Wu *et al.*, 2022).

1.5.2 *Drosophila* Models

The fruit fly *Drosophila melanogaster* is a model organism that has been key to furthering our understanding of diseases, owed to its relatively short lifespan and easily modifiable genetics that allow large populations to be generated, resulting in high statistical power (Piper and Partridge, 2018). Across four pairs of fully sequenced chromosomes, *Drosophila* carry around 14,000 protein-coding genes (Adams *et al.*, 2000). Despite a greater evolutionary distance between *Drosophila* and humans compared with rodent models, around 75% of disease causing genes in humans have functional homologues in *Drosophila* (Chien *et al.*, 2002; Ugur, Chen and Bellen, 2016). Genetic modifications, including knockdown/knockout or overexpression of single genes, allow for large scale genetic screens to identify candidates that can modify disease-related molecular and behavioural phenotypes. Spatiotemporal restriction of these modifications, such as to adult neurons, enables even more precise readouts of cell type specific functions (Osterwalder *et al.*, 2001). Furthermore, assessment of amyloid toxicity can be carried out longitudinally using the same population, providing an insight into disease progression. Importantly for neurodegenerative disease research, *Drosophila* brains are relatively complex with multiple cell types including more than 125,000 neurons comprised of multiple subtypes as well as glial cells, recapitulating many aspects of human cerebral biology (Schlegel *et al.*, 2024).

APP is one of the disease-causing genes that is present as an orthologue in *Drosophila* (Rosen *et al.*, 1989). The APP-like protein (APP-L) plays a role in synaptic function and neuronal survival (Kessissoglou *et al.*, 2020). However, homologous

regions do not include the sequence corresponding to the Aβ42 peptide. Thus, cleavage of APP-L by orthologues of secretases does not result in endogenous production of Aβ42 (Luo, Tully and White, 1992; Prüßing, Voigt and Schulz, 2013). Therefore, to model amyloid toxicity in *Drosophila,* a variety of fly lines have been engineered to neuronally express a combination of human *APP* and human *BACE* genes or, more commonly, directly express human Aβ42. This causes an age-dependent accumulation of soluble and insoluble amyloid in the fly brain as well as a range of behavioural phenotypes including degeneration of photoreceptor neurons (when expressed directly in the eye), locomotor dysfunction, disturbed circadian rhythm and shortened lifespan indicating that Aβ exerts a systemic toxic effect similar to that observed in AD patients (Greeve *et al.*, 2004; Crowther *et al.*, 2005; Casas-Tinto *et al.*, 2011; Niccoli *et al.*, 2016). To increase the aggregation propensity of amyloid in these transgenic models, flies have been engineered to either carry two copies of wild-type Aβ or one copy of Aβ containing the arctic familial AD mutation, resulting in stronger phenotypic modifications (Casas-Tinto *et al.*, 2011; Balamurugan *et al.*, 2017). For modelling AD-DS biology, using flies that express wild-type Aβ more closely recapitulates the genetics of trisomy 21.

Drosophila models of amyloid toxicity have provided mechanistic insight into Aβ biology. Interference with polymerisation and subsequent reduced aggregation of Aβ42 resulted in a partial rescue of multiple phenotypic readouts of neurotoxicity as well as reduced memory impairment, indicating that aggregated forms of Aβ42 contribute to its toxicity (Nerelius *et al.*, 2009; Martín-Peña, Rincón-Limas and Fernandez-Fúnez, 2018). Accumulation of Aβ can result from both the overproduction and impaired clearance of the peptide. A protective role of human Aβ degrading enzymes has been found in transgenic *Drosophila.* Neuronal expression of insulin degrading enzyme reduced levels of secreted Aβ while expression of human neprilysin rescued Aβ induced neuronal loss (Qiu *et al.*, 1998; Iijima-Ando *et al.*, 2008). Models of amyloid toxicity have further provided mechanistic insight into genes previously identified as sporadic AD risk loci in human GWAS studies, such as *APOE* and *PICALM* (Haddadi *et al.*, 2016; Yu *et al.*, 2020). Additionally, forward genetic screens have uncovered naturally occurring variants as modifiers of Aβ42 toxicity,

some of which had not been previously linked to AD risk (Cao *et al.*, 2008; Tan *et al.*, 2008; Belfiori-Carrasco *et al.*, 2017; Yang *et al.*, 2023).

Trisomy of Hsa21 cannot be easily modelled in *Drosophila*, as orthologous genes are distributed over chromosomes 2, 3 and X. However, they are a powerful screening tool for characterising the effects of single genes or the interaction between a small set of genes when overexpressed to mimic their trisomy. Overexpression of the *DYRK1A* orthologue *minibrain* (*mnb*) has been found to shorten *Drosophila* lifespan. In contrast, inhibition of *mnb* decreased photoreceptor neuron degeneration and rescued lifespan and locomotor impairment induced by neuronal expression of Aβ42 (Zhu, Parsons, Foley, *et al.*, 2022; Zhu, Parsons, Stensen, *et al.*, 2022). Overexpression of Down syndrome cell adhesion molecule (*Dscam1*), an orthologue of Hsa21 gene *DSCAM* involved in alternative splicing events, has been shown to modify glutaminergic synaptic transmission in *Drosophila* larvae and impaired locomotor coordination in adult flies (Lowe, Hodge and Usowicz, 2018a). Furthermore, in *Drosophila* cell culture, APP-L was found to increase Dscam1 protein level during development to promote axon terminal growth, demonstrating a functional interaction between the two Hsa21 orthologues (Pizzano *et al.*, 2023). These studies demonstrate the potential of using *Drosophila* to study the interaction between overexpression of Aβ42 and Hsa21 orthologues. This Aβ42 x Hsa21 orthologue cross can be used to model the effects of overexpressing single Hsa21 genes on readouts of Aβ accumulation and toxicity, isolating the role of Aβ itself from the effects of APP processing.

1.6 Outstanding questions from current knowledge & aims of this study

Preclinical and clinical studies of AD-DS neuropathology have established the central role of *APP* triplication in the development of AD in this population (Fortea *et al.*, 2021). However, evidence from AD-DS mouse models also supports a role of Hsa21 genes

other than *APP* in disease pathology (Wiseman *et al.*, 2018; Tosh *et al.*, 2021). Consistent with these findings, studies have identified several additional Hsa21 gene candidates that, when present in three copies, modify amyloid toxicity and accumulation, although the extent of their contribution is not fully understood (Ryoo *et al.*, 2008; García-Cerro *et al.*, 2017; Alić *et al.*, 2020). Previous pre-clinical investigations have used models that either overexpress many Hsa21 genes/orthologues within the same animal or focused on the effect of a small subset of single gene candidates. Thus, it has not been determined whether and how triplication of each individual Hsa21 protein-coding gene in DS may impact the development and progression of AD-DS through modification of amyloid pathology. Genetic screens offer an opportunity to investigate this research question. However, although much of the current knowledge has been gained from AD-DS mouse models, these animals are not best suited to large scale screens as generating the required number of genetically engineered populations would require long experimental timelines and high costs as well as posing ethical challenges. In contrast, *Drosophila* offer an opportunity to design studies with high statistical power to investigate the impact of increased Hsa21 gene dosage on amyloid toxicity and accumulation through co-overexpression of Aβ and Hsa21 orthologues in disease relevant tissues (neurons).

Therefore, the aims of my thesis were to investigate the following research questions:

1. Does pan-neuronal overexpression of single Hsa21 orthologues modify amyloid toxicity and accumulation in adult flies (Chapter 3)?

2. Are the Hsa21 candidate genes identified in the *Drosophila* screen dosage sensitive at the protein level in human post-mortem brain tissue from individuals with AD-DS compared with EOAD and age-matched healthy controls (Chapters 4 & 5)?

3. What are the differential gene expression patterns and associated pathways dysregulated in neuronal cell populations in AD-DS and how do they differ

from those dysregulated in EOAD compared with age-matched healthy controls (Chapter 6)?

4. Which Hsa21 genes are differentially expressed in AD-DS post-mortem brain tissue at the transcript level, including candidate genes identified in the *Drosophila* screen as well as those that could not be included? This may identify further genes of interest as potential modifiers of Aβ toxicity and accumulation in AD-DS (Chapter 6).

Chapter 2: Materials and Methods

Drosophila Materials and Methods

2.1 *Drosophila* media recipes and preparation

2.1.1 SYA medium

Agar was added to 700 mL of distilled water and brought to a boil until fully dissolved. To this, 100 g of autolysed yeast powder and 50 g of beet sugar were added while stirring. Heat was reduced, and the remaining 170 mL of distilled water added. Once the mixture had reached 60 °C 30 mL of nipagin (10 % in ethanol) and 3 mL of propionic acid were added. Food was dispensed into bottles or vials, depending on the experiment. For experiments with RU-486 (Sigma), 2 mL of the drug was added to the liquid media at a final concentration of 200 µM (from a 500X stock solution dissolved in ethanol) for +RU or 2 mL ethanol for -RU (vehicle control) media. Food was stored at 4 °C and used within 4-6 weeks of cooking.

Table 2.1 *Drosophila* Sugar Yeast Agar medium recipe (per 1 L).

Reagent	Amount	Supplier
Autolysed yeast powder	100 g	Brian Drewitt
Agar	15 g	Merck
Beet sugar	50 g	Lidl supermarket/Tate & Lyle
Nipagen	30 mL	Fisher scientific
Propionic acid	3 mL	Fisher scientific
dH_2O	870 mL	-

2.1.2 Grape plates

25 g of agar was added to 500 mL of distilled water and brought to a boil. Once fully dissolved, 300 mL of red grape juice (Young's definitive) was added to the mixture and briefly brought to a boil. The mixture was removed from the heat and an additional 50 mL of water was added. Once the media had reached 60 °C, 21 mL of nipagin (10% in ethanol) was added. The liquid media was poured into small plastic plates and left to solidify. Grape plates were stored at 4 °C until use.

Table 2.2 *Drosophila* grape plate recipe (per 1 L).

Reagent	Amount	Supplier
dH_2O	550 mL	-
Agar	25 g	Merck
Red grape juice	300 mL	Magnum (Brian Drewitt)
Nipagin	21 mL	Fisher scientific

2.2 *Drosophila* stocks and husbandry

Drosophila melanogaster used in this work carry the w^{1118} mutation. The elavGS line was derived from the original elavGS 301.2 line and obtained as a generous gift from Dr H. Tricoire (CNRS, France) (Osterwalder *et al.*, 2001). The UAS-Aβx2 stock was a gift from Pedro Fernandez Funez (University of Minnesota) (Casas-Tinto *et al.*, 2011). Overexpression lines were obtained from either Bloomington Drosophila Stock Centre (https://bdsc.indiana.edu) or FlyORF (https://flyorf.ch) and are listed in table 2.3. All fly lines were backcrossed at least six times into the *w1118* genetic background. Stocks were maintained in glass bottles on SYA media at 25 °C and constant humidity on a 12-hour light:dark cycle. All stocks used in this thesis are listed in table 2.3.

Table 2.3 Genotypes of *Drosophila* stocks used in this thesis.

Stock	Genotype
w1118	w[1118]
$A\beta_{1-42}$	w[1118]; P{UAS-Aβ42}
elavGS	w[1118]; P{elavGSGAL4}

achi	w[1118]; M{UAS-achi.ORF-CC}ZH-21F
Agpat3	w[1118]; P{y[+mDint2] w[+mC]=EPgy2}Agpat3[EY02120]
Art8	w[1118]; M{UAS-Art8.ORF.3xHA}attP-86Fb
ATPsynCF6	w[1118]; M{UAS-ATPsynCF6.ORF}ZH-86Fb
Cbs	w[1118]; P{y[+mDint2]w[+mC]=EPgy2}Cbs[EY04457]
CG11454	w[1118]; P{y[+mDint2] w[+mC]=EPgy2}CG11454[EY07354]
CG12325	w[1118; P{y[+mDint2]w[+mC]=EPgy2}CG12343[EY04947]
CG17646	w[1118]; P{EPgy2}CG17646[EY03935]
CG4266	w[1118]; P{w[+mC]=EP}Isha[G7664]
CG42709	w[1118]; P{y[+mDint2]w[+mC]=EPgy2}Atg1[EY09216]
clumsy	w[1118]; P{y[+mDint2]w[+mC]=EPgy2}EY07947, P{ry[+t7.2]=sevRas1.V12}FK1
DIP1	w[1118]; P{y[+mDint2] w[+mC]=EPgy2}DIP1[EY02625]
Dscam4	w[1118]; P{w[+mC]=EP}Dscam4[EP3362]
Ets97D	w[1118]; M{UAS-Ets97D.ORF.3xHA.GW}ZH-86Fb
Hcs	w[1118]; P{y[+mDint2]w[+mC]= EPgy2}Hcs[EY14537]
Ltn1	w[1118]; P{w[+mC]=EP}Ltn1[G9156]
mnb	w[1118]; P{y[+mDint2]w[+mC]=EPgy2}mnb[EY14320]CG12985[EY14320]
mRpL39	w[1118]; P{y[+mDint2] w[+mC]=EPgy2}EY07826
mys	w[1118]; P{ry[+t7.2]=neoFRT}19A; P{w[+mC]=UAS-mys.L}3
Nnp-1	w[1118]; P{w[+mC]=EP}Nnp-1[G3622]/CyO
O-fut2	w[1118]; M{UAS-O-fut2.ORF.3xHA}ZH-86Fb
Pfk	w[1118]; P{w[+mC]=UAS-Pfk.T}3
Plp	w[1118]; P{y[+mDint2] w[+mC]=EPgy2}sstn[EY06542]Plp[EY06542]
pnt	w[1118]; M{UAS-pnt.ORF}ZH-86Fb
Pten	w[1118]; P{w[+mC]=UAS-Pten.H}3
Sb	w[1118]; P{w[+mC]=EP}CG5916[G13766
shi	w[1118]; P{w[+mC]=UAS-shi[ts1].K}3
SIDL	w[1118]; P{w[+mC]=EP}SIDL[G3994]

sif	w[1118]; P{w[+mC]=UAS-sif.S}M3.1
Sik2	w[1118]; P{y[+t7.7] w[+mC]=UAS-Sik2.F}attP2
sim	w[1118]; P{w[+mC]=UAS-sim.X}2
SKIP	w[1118]; P{y[+mDint2] w[+mC]=EPgy2}EY04643
Sod1	w[1118]; P{w[+mC]=UAS-Sod1.A}B37
Usp16-45	w[1118]; P{y[+mDint2] w[+mC]=EPgy2}Usp16-45[EY19835]
Usp47	w[1118]; P{y[+mDint2] w[+mC]=EPgy2}Usp47[EY11769]
wuho	w[1118]; P{y[+mDint2] w[+mC]=EPgy2}wuho[EY06844]

Fly crosses for experiments were set up in cages with grape plates containing grape juice agar and a small amount of freshly prepared Brewer's yeast paste (1:1 ratio of dry yeast granules (Saf-Leuvre) to distilled water). Cages contained ~ 100 virgin females and 30 males (ratio of 3:1). Grape plates were changed, and fresh yeast added every ~24 hours for two consecutive days. On day three, eggs were suspended in 1X PBS (pH 7.4), collected, and dispensed into SYA food containing bottles at a volume of 20 μl per bottle for standard density fly rearing. After ten days, eclosed flies were given 48 hours to mate before being anesthetised with CO_2 and sorted as required for experiments.

2.3 Behavioural Assays

2.3.1 Lifespan assay

Mated females of the desired genotype were selected after eclosion and split into plastic vials with SYA food at a density of 15 flies per vial for experiments. Flies were maintained in drosoflippers (www.drosoflipper.com). Approximately 150 flies (15 flies x 10 vials) per condition were tipped into new vials with fresh food every 2-3 days and deaths and censors were scored. Log-rank test was used to compare survival rate of different conditions within the same experiment in Microsoft Excel (template by (Piper and Partridge, 2016)). Cox proportional hazards test was used to check for an interaction between genotype and RU media which was performed using the 'survival' package in Rstudio (version 1.3.1093). Each fly was treated as a biological replicate.

Data are presented as lifespan curves of cumulative survival that were plotted using GraphPad Prism 10 (version 10.1.1).

2.3.2 Negative geotaxis assay

Flies were raised in 200 mL glass bottles, females of the appropriate genotype were selected, split into 15 flies per vial (total of 75 flies per condition) and maintained in drosoflippers. Experimental flies were kept in vials containing SYA media with either 2 mL/L 100% ethanol (-RU vehicle control) or 200 µM RU-486 (+RU). At regular intervals, flies were transferred to empty vials arranged so that they could climb two vial heights in the drosopflippers. Flies were allowed to acclimatise for 10 minutes before being gently tapped to the bottom of the vials. A video was recorded for 30 seconds. For analysis, a screenshot was taken at 15 seconds after the flies had been tapped to the bottom of the vials (this is the time point at which young flies reach maximum height). The same cohort of flies was assayed per experiment throughout. Y-coordinates of flies in the screenshots were analysed in Image J (version 1.53a). Statistical analysis (linear model) of mean fly height per condition and timepoint was carried out. Simple linear regression Y-coordinates from negative geotaxis data was analysed using the 'ordinal' package in Rstudio (version 1.3.1093). Graphs were plotted in GraphPad Prism (version 10.1.1).

2.4 RNA extraction

Experimental flies (set up as described in 2.3.1) were snap frozen in liquid nitrogen and stored at -80 °C. Keeping flies frozen at all times, fly heads were separated from bodies by vigorously shaking the Eppendorf tubes. Heads were isolated using a fine sieve over dry ice. Frozen heads were placed into screw cap tubes at 10 heads/tube, containing acid-washed glass beads (Merck) and 1 mL of cold TRIzol Reagent (Ambion). Fly heads were homogenised in a ribolyser at maximum speed for 30 seconds. Following a 5-minute incubation at room temperature, 200 µL of chloroform (Fluka) was added and tubes were vortexed for 15 seconds and left to incubate for a

further 2 minutes. Subsequently, samples were centrifuged at 13,400 rcf for 15 minutes at 4 °C, creating a chloroform layer at the bottom, an interphase and a colourless aqueous phase at the top of the tubes. Up to 500 µL of the aqueous layer was removed and placed into new RNase-free Eppendorf tubes with the addition of 500 µL of isopropanol. Tubes were briefly mixed and left to incubate for 15 minutes at room temperature. To create an RNA containing pellet, samples were centrifuged at 13,400 rcf for 15 minutes at 4 °C. Samples were washed three times. To do this, supernatant was removed and 500 µL of 70% ethanol (0.7 100% ethanol + 0.3 RNase free water) was added. Tubes were centrifuged at 13,400 rcf for 2.5 minutes at room temperature. Following the final wash step, the supernatant was removed and pellets were left to air dry in a heat block set to 50 °C. Translucent pellets were reconstituted in 30 µL Nuclease-Free Water (Ambion) and left to dissolve for 10 minutes at 60 °C. Extracted RNA was stored at -80 °C. RNA concentration and quality were measured using a NanoDrop Spectrophotometer 2000c (Thermo Scientific).

2.5 cDNA synthesis

cDNA was synthesised from total RNA extracted as above. RNA from all samples was diluted in Nuclease-Free Water to a final concentration of 100 ng/µL. 3.4 µL of diluted RNA per sample was incubated with TURBO DNase buffer (Invitrogen) at 37 °C for 15 minutes. Subsequently, the reaction was inhibited by adding 2 µL of 24 mM EDTA (pH8, RNase free) and incubated for 5 minutes at 75 °C followed by cooling on ice. 2 µL of 0.5 µg/µL Oligo (dT) (Invitrogen) and 2 µL 10 mM dNTP mix (made up from 100 mM dNTP Set, Invitrogen) were added to each sample and incubated for 5 minutes at 65 °C followed by cooling on ice for at least 1 minute. Samples were centrifuged followed by the addition of 8 µL 5X First-Standard Buffer), 8 µL 25 mM $MgCl_2$, 4 µL 0.1 M DTT, 2 µL RNaseOut Recombinant Ribonuclease Inhibitor and 1 µL SuperScript II RT (Superscript II Reverse Transcriptase Kit, Invitrogen). Following gentle mixing, samples were incubated for 50 minutes at 42 °C and the reaction was terminated by heating to 70 °C for 15 minutes. Samples were stored at -20 °C until being used for RT-qPCR.

2.6 Real-Time qPCR

Real-time quantitative PCR (RT-qPCR) was performed using the QuantStudio 6 Flex Real-Time PCR system (Applied Biosystems). cDNA was diluted 1:4 in Nuclease-Free Water and samples were quantified against a relative standard curve made up of pooled cDNA from all samples used on any given plate. The standard curve consisted of a two-fold serial dilution ranging from 1:1 to 1:64 and Nuclease-Free Water as a non-template control. A master mix was made up consisting of the following: 10 µL SYBR Green Master Mix (Applied Biosystems), 1 µL forward primer, 1 µL reverse primer and 6 µL Nuclease-Free Water per reaction. 2 µL of cDNA diluted 1:4 in nuclease free water, and 18 µL of master mix containing the appropriate primer pair were added to a 96-well PCR plate (STARLAB). The sealed plate was briefly centrifuged before being place in the qPCR machine. Relative mRNA levels were normalised to eIF1A. Primers were obtained from Merck and used at a concentration of 7.5 µM, sequences are listed in table 2.4. One biological replicate was made up of 10 fly heads. Expression level was compared by an unpaired student T-test and graphs plotted as mean ± SEM in GraphPad Prism 10.

Table 2.4 Primer sequences.

Oligomer name	Sequence
ATPsynCF6.fwd	CAGAGGCCCGTCGTAACTTC
ATPsynCF6.rev	GATCGGAGGCCTTGTTCAGG
Usp47.fwd	GCACCGTCTCGGTCTTTGA
Usp47.rev	CCAGCCACTTCGTACATCAGC
Hcs.fwd	GCTGCAAACGCTACACATCAC
Hcs.rev	CTCGGCGGCATAGGAGAAG
Plp.fwd	CTTCAACATGAGCGGGATACG
Plp.rev	GGGTATTCAAGTCTGATGTGCC
SKIP.fwd	AAGAGCATCCGATCGCTGAG
SKIP.rev	AGCGAGTTGGGATCGTTGAG
mnb.fwd	GCACCATCACTCTAGTCCCTCGT
mnb.rev	CGAAAGTGGTTGGGAATC
eIF1A.fwd	AAGAATCGTCGTCGTGGTAAGA
eIF1A.rev	CTGCGCGTACTCCTGTTGG

2.7 Aβ1-42 ELISA

Flies were snap frozen in liquid nitrogen and stored at -80 °C. Heads were separated from bodies as described in 2.4.

2.7.1 Sample preparation total Aβ1-42

5 heads/tube were homogenised in 50µL extraction buffer consisting of 5 M Guanidine Hydrochloride (Merck), 50 mM Hepes (Fisher scientific), 5 mM EDTA (Merck) and 1X cOmplete Mini Protease Inhibitor Cocktail (Roche). Samples were centrifuged at 15870 rcf for 5 minutes at 4 °C.

2.7.2 Sample preparation soluble/insoluble fractions of Aβ1-42

30 heads/tube were homogenised in 50 µL tissue homogenisation buffer (THB) consisting of 250 mM sucrose (Merck), 20 mM Tris-base (Fisher Scientific) and freshly added 1 mM EDTA, 1 mM EGTA (both Merck) and 7X cOmplete Mini Protease Inhibitor Cocktail in distilled water. Subsequently, 50 µL of DEA buffer consisting of 0.4 % Diethanolamine (Merck), 100 mM NaCl (Merck) and freshly added 1X cOmplete Mini Protease Inhibitor Cocktail in distilled water was added to each tube. Samples were centrifuged at 135,000 rcf for 1 hour at 4 °C using the Beckmann Optima Max Benchtop Ultracentrifuge with TLA-120.1 Fixed-Angle Rotor. Following centrifugation, supernatant from each sample was removed as the cytosolic soluble fraction. To obtain the insoluble fraction, pellets were washed with 100 µL/tube THB and 0.4 % DEA buffer at a ratio of 1:1. Pellets were re-suspended in 200 µL/tube of 70 % ice cold formic acid (Merck) and sonicated 4x 15 seconds in ice cold water until pellets were fully broken up. Samples were centrifuged at 135,000 rcf for 1 hour at 4 °C. 50 µL of supernatant was removed from centrifuged samples and diluted in 1 mL formic acid neutralisation buffer (1 M Tris base and 0.5 M sodium phosphate dibasic in distilled water). Samples were aliquoted and stored at -80 °C. This protocol was adapted from previously published methods (Burns *et al.*, 2003; Sofola *et al.*, 2010).

2.7.3 ELISA

96-well plates (Nunc-Immuno MaxiSorp Plate, U-style wells) were coated with Anti-β-Amyloid, 1-16 Antibody (clone 6E10, #803015, BioLegend) primary antibody diluted at 1:400 in coating buffer (15 mM sodium carbonate, 25 mM sodium bicarbonate (Merck) in distilled water, pH 9.6) at 100 µL/well. Plates were incubated overnight at 4 °C with gentle rocking. The following day, plates were washed 3x with 200 µL/well PBST (PBS with 0.05 % Tween-20). 200 µL of 1:4 Block Ace (BioRad) in PBS was added to each well and incubated for at least 2 hours at room temperature with gentle rocking. **i** For total $A\beta_{1-42}$ ELISA, samples were centrifuged for 4 minutes at 15870 rcf. Standards were prepared as a two-fold serial dilution (in 1:50 extraction buffer in diluent buffer) ranging from 2500 pg/mL to 39.1 pg/mL and diluent only as a blank sample. Diluent consisted of 17mM Triton-X 100 (BDH), 1.7mM PSMF (Merck, 30 mg/mL in ethanol), in 49 mL PBS, 7X cOmplete Mini tablet Protease Inhibitor Cocktail, in 1X PBS. Samples were added at 1:50 in diluent buffer. **ii** For soluble $A\beta_{1-42}$ ELISA, samples were mixed prior to loading. The soluble fraction was loaded at 1:10 and the insoluble fraction at 1:5 in diluent buffer. All samples and standard curve were loaded in duplicate.

Plates were incubated overnight at 4 °C with gentle rocking. The following day, plates were washed 3x with PBST. Secondary antibody Biotin anti-β-Amyloid, 1-42 Antibody (clone 12F4, #805504, BioLegend), was added at 1:1000 in 1:10 Block Ace at 100 µL/well and incubated for 2 hours at room temperature. Following 3 washes with PBST, 100 µL/well of NeutrAvidin-HRP (Thermo Scientific) was added at 1:10,000 in 1:10 Block Ace and incubated for 1 hour at room temperature with gentle rocking. Plates were washed 3x with PBST before adding 100 µL/well of KPL TMB Microwell Peroxidase Substrate Solution (1:1 solution A and B, KPL). Plates were incubated at room temperature in the dark for 15-25 minutes with gentle rocking until a blue colour developed. The reaction was terminated by adding 100 µL/well of freshly prepared 1 M HCl resulting in a colour change to yellow. Plates were read at 450 nm using the Tecan Infinite200 Plate Reader. Data are presented as mean ± SEM µg/mL of $A\beta_{1-42}$ normalised to total protein. Each data point represents 10 fly heads (for total $A\beta_{1-42}$) or 50 fly heads for soluble/insoluble $A\beta_{1-42}$. Conditions were compared using one-way

ANOVA with Tukey's multiple comparisons, using w1118 $A\beta_{1-42}$ +RU as the reference condition. Graphs were plotted as mean ± SEM in GraphPad Prism 10.

2.8 BCA Assay

BCA Assay was performed using the Pierce BCA Protein Assay Kit (Thermo Scientific) with 96-well plates. Standards were made up by serial dilution (diluent used as above in ELISA protocol) fo BSA ranging from 2000 µg/mL to 25 µg/mL and diluent only as a blank sample. Samples were diluted 1:4 in diluent buffer before plating. 10 µL of diluted sample was pipetted into each well, followed by 200 µL of Working Reagent (1:50 Reagent A and Reagent B) and mixed well. The plate was covered and incubated at 37 °C for 30 minutes. Samples were read at 562 nm using the Tecan Infinite200 Plate Reader. $A\beta_{1-42}$ ELISA values for each sample were normalised to their respective BCA reading.

2.9 ARRIVE guidelines 2.0

In this thesis, *Drosophila melanogaster* were used as a partial replacement for mice in accordance with the 3Rs (Replacement, Reduction and Refinement) principals.

'Essential 10' regarding fly experiments.

1. Study design: Flies co-overexpressing a Hsa21 orthologue and Aβ42 in adult neurons are compared to flies of the same genotype but where expression is not induced (+RU486 or -RU vehicle control). Each fly is treated as a biological replicate in behavioural assays. For molecular experiments, each sample containing multiple fly heads (number specified in figure legends) is considered a biological replicate.
2. Sample size: for lifespan assays, each condition has n of 150. For negative geotaxis assays, each condition has n of 75. For qPCR, 10 fly heads per replicate were used. 10 or 50 fly heads per sample were used for total or soluble/insoluble Aβ42 ELISA, respectively. Sample sizes are based on published literature.

3. Inclusion and exclusion criteria: For negative geotaxis assays, dead flies were excluded from the analysis. For all other experiments, all data points were included in the analyses.
4. Randomisation: (and minimising potential confounders). For behavioural assays, +RU and -RU vials were alternated during fly sorting. This is to avoid flies which were raised in the same bottle being used for one condition only. Additionally, for negative geotaxis assays, each drosoflipper contained all the different conditions within the experiment. This is to avoid differences in the handling of the flipper as a possible confounder of climbing speed. To account for differences in climbing speed at different points in the circadian rhythm, all negative geotaxis assays were performed during the early afternoon.
5. Blinding/Masking: For behavioural experiments, conditions were marked on vials/drosoflippers (not blinded) but analysis was not carried out until the end of each experiment to avoid bias.
6. Outcome measures: For lifespan assays, the outcome measure was time to death of the animal. For negative geotaxis assays, the outcome measure was height climbed after 15 seconds of being tapped to the bottom of the vial across the lifespan.
7. Statistical methods: For lifespans, a log-rank test was used to compare survival rate of different conditions within the same experiment. Where there was a statistically significant difference between genotypes on control media, Cox proportional hazards model was determined to check for an interaction between genotype and +/-RU media. For negative geotaxis assays, simple linear regression was used to identify statistically significant differences of climbing speed with age between conditions. For molecular experiments, an unpaired Students t-test or one-way ANOVA with Dunnett's multiple comparisons as appropriate was used to compare difference in gene expression or Aβ42 levels.
8. Experimental animals: Mated female adult *Drosophila melanogaster* were used in this thesis.
9. Experimental procedures: The number of flies in the parental generation used to create the experimental flies was estimated based on known egg-laying capacity of females. Notably, for *Drosophila* experiments, n numbers are high

which leads to an inevitable excess of flies being generated that had to be discarded in ethanol. Details of experimental procedures, including frequency and acclimatisation periods, are described in their respective methodology sections.

10. Results: details of statistical outcomes for each experiment are listed in Chapters 3, 4 and 5.

Information about ARRIVE 2.0 Essential 10 can be found at https://arriveguidelines.org/arrive-guidelines/randomisation/4a/explanation.

Human Materials and Methods

2.10 Human Tissue Selection, Sources and Ethics

All use of human post-mortem brain tissue in this thesis was carried out in accordance with the Human Tissue Act (2004). The study design was approved by the research ethics committees of the Newcastle Brain Tissue Resource (NBTR) and South West Dementia Brain Bank (SWDBB). NBTR and SWDBB provided guidance on sample selection of Healthy ageing (CTRL), EOAD and AD-DS cases for the best possible match of sex, age at death, Braak stage and *APOE* genotype across case types and provided research consent for all samples. Samples used in this study were anonymised.

Table 2.5 Case demographics used for Western blots: SWDBB batch 1.

Case	Case type	Braak stage	Sex	Age at death	PMI (h)	APOE	Brain region
1	HA	-	M	63	40	3,3	BA21
2	HA	-	M	64	12	3,4	BA21
3	HA	-	M	58	20	2,3	BA21
4	HA	-	M	64	16	3,3	BA21
5	HA	-	F	73	59	3,3	BA21

6	HA	-	F	72	24	3,3	BA21
7	HA	-	F	68	38.75	2,3	BA21
8	HA	II	F	73	50	3,4	BA21
9	HA	II	F	74	39.5	3,3	BA21
10	EOAD	VI	F	54	24	3,3	BA21
11	EOAD	VI	M	63	43	3,3	BA21
12	EOAD	VI	F	65	22	3,3	BA21
13	EOAD	VI	F	47	54	3,4	BA21
14	EOAD	VI	F	60	5	2,3	BA21
15	EOAD	VI	M	62	24.5	3,4	BA21
16	EOAD	VI	F	67	24.25	3,4	BA21
17	EOAD	VI	M	61	32.5	2,3	BA21
18	AD-DS	n/a	M	63	31	3,3	BA21
19	AD-DS	VI	F	63	51	2,3	BA21
20	AD-DS	VI	F	50	50	3,4	BA21
21	AD-DS	VI	F	59	24	3,3	BA21
22	AD-DS	VI	F	67	17	3,4	BA21
23	AD-DS	VI	F	48	79	2,4	BA21
24	AD-DS	VI	F	64	48	3,3	BA21

Table 2.6 Case demographics used for Western blots: NBTR.

Case	**Case type**	**Braak stage/ pathology**	**Sex**	**Age at death**	**PMI (h)**	**APOE**	**Brain region**
25	HA	No pathology reported	M	46	24	3,4	BA10
26	HA	0	M	53	19	3,3	BA10
27	EOAD	VI	M	59	44	3,3	BA10

28	EOAD	VI	F	63	11	3,4	BA10
29	EOAD	VI	F	58	70	3,3	BA10
30	AD-DS	Severe senile plaques	F	48	24	3,3	BA10
31	AD-DS	Severe AD	F	58	48	3,4	BA10
32	AD-DS	AD pathology	M	53	84	3,3	BA10
33	AD-DS	VI	M	67	4	2,2	BA10
34	AD-DS	VI	F	60	13	*TBC*	BA10

Table 2.7 Case demographics used for Western blots: SWDBB batch 2.

Sample ID	Case type	Braak stage	Sex	Age at death	PMI (h)	APOE	Brain region
4	HA	0	M	64	16	3,3	BA10
35	HA	II	M	69	66	3,3	BA10
6	HA	0	F	72	24	3,3	BA10
7	HA	0	F	68	38.75	2,3	BA10
8	HA	II	F	73	50	4,3	BA10
9	HA	I	F	74	39.5	3,3	BA10
36	HA	0	M	74	57.5	3,3	BA10
37	HA	II	F	74	27.5	2,4	BA10
38	HA	II	F	70	33.25	3,3	BA10
39	HA	0	M	51	68.25	2,3	BA10
10	EOAD	VI	F	54	24	3,3	BA10
11	EOAD	VI	M	63	43	3,3	BA10
40	EOAD	VI	F	68	87	3,4	BA10
41	EOAD	VI	M	65	90	3,3	BA10
12	EOAD	VI	F	65	22	3,3	BA10
13	EOAD	VI	F	47	54	3,4	BA10

14	EOAD	VI	F	60	5	3,2	BA10
15	EOAD	VI	M	62	24.5	3,4	BA10
41	EOAD	VI	F	57	63	2,4	BA10
42	EOAD	VI	M	63	21.25	3,3	BA10
43	AD-DS	VI	M	62	24	3,4	BA10
44	AD-DS	V	M	62	51	3,3	BA10
19	AD-DS	VI	F	63	51	2,3	BA10
20	AD-DS	VI	F	50	43	3,4	BA10
24	AD-DS	VI	F	64	48	3,3	BA10
45	AD-DS	V	M	64	16	3,3	BA10
21	AD-DS	VI	F	59	24	3,3	BA10
22	AD-DS	VI	F	67	17	3,4	BA10
23	AD-DS	IV	F	48	79	2,4	BA10
46	AD-DS	IV	M	71	77.75	3,2	BA10

2.11 Western blot

2.11.1 Homogenisation of human post-mortem brain tissue for Western blot

All the steps in 2.11.1 were carried out by a member of the Wiseman lab.

Frozen brain tissue was chipped over dry ice and homogenised in 50-100 mg/tube in 500 µL T-PER Tissue Protein Extraction Reagent (Thermo Scientific), PhosSTOP phosphatase (Roche) and cOmplete Protease Inhibitor Cocktail (Roche). Homogenisation was carried out in a MSC Class I laminar cabinet using a Tissue Ruptor (Qiagen). Tissue lysate was centrifuged at 10,000 rcf for 30 minutes at 4 °C. Subsequently, supernatants were aliquoted and stored at -70 °C until use. Protein concentration of each sample was determined using the Pierce 660 nm Protein Assay Reagent Kit (Thermo Scientific). Sample total protein concentration was determined against a BSA standard curve. For this, Protein Assay Dye Reagent Concentrate (Bio-

Rad) was added to 5 µL of samples (diluted 1:20 in PBS) or BSA standard (diluted 1:5 in distilled water, Thermo Scientific). Plates were read at 595 nm using a Multimode Microplate Reader (Tecan Spark).

2.11.2 Western Blot

Sample preparation and loading were carried out by Dr Yixing Wu, Wiseman lab. I designed the western blot experiemnts and carried on experimental proceredures from the point of membrane transfer as well as completing data analysis.

Protein samples were denatured by incubating 1 µg/µL with ddH_2O, NuPAGE LDS Sample Buffer (4X) (Invitrogen), and NuPAGE Sample Reducing Agent (10X) (Invitrogen) at 95 °C for 5 minutes.

All Western blots were carried out using 4-12 %, Bis-Tris, 1 mm Mini/Midi Protein Gels (Invitrogen). For each antibody, the limit of detection was determined by a linearity Western blot. For this, 2.5, 5, 10 and 20 µg of protein were loaded into the gel to assess the linear range of the signal. 5 µL SeeBlue Plus2 Pre-stained Protein Standard (Invitrogen) was loaded into gels as a molecular weight marker. Sample order was randomised using RAND() function in excel and (unless otherwise specified in the figure legend) 10 µL sample homogenate was added to each lane. For quantification of large proteins (USP25 and TTC3) and small proteins (ATP5J) 1X NuPAGE MOPS SDS Running Buffer or 1X NuPAGE MES SDS Running Buffer (Invitrogen) respectively was added to the gel tank and samples were electrophoresed at 150V, 400 mA and 120 W for 50-340 minutes until the loading dye had reached the bottom of the gel. Proteins were transferred onto Trans-Blot Turbo Mini/Midi 0.2 µm PVDF or Trans-Blot Turbo Midi 0.2 µm Nitrocellulose membranes (Bio-Rad) using the Transblot Turbo Transfer system (Bio-Rad). For USP25 and ATP5J Western blots, gels were transferred at 25 V and 1.3 A for 7 minutes, whereas for TTC3 Western blot transfer time was increased to 20-30 minutes. Membranes were blocked in Intercept (PBS) Blocking Buffer (LI-COR) for 1 hour at room temperature with gentle rocking. Subsequently, membranes were incubated with primary antibodies (all antibodies listed in table 2.8) diluted in Intercept (PBS) Blocking Buffer overnight at 4 °C with

gentle rocking. The following day, membranes were washed 3x 10 minutes in PBST (0.05% TWEEN-20, Merck) and incubated with secondary antibodies (IRDye 680RD Goat anti-Mouse IgG Secondary Antibody, LI-COR, #926-68070 or IRDye 800CW Goat anti-Rabbit IgG Secondary Antibody LI-COR, #926-32211) diluted at 1:10,000 in Intercept (PBS) Blocking Buffer for 1 hour at room temperature in the dark with gentle rocking. Membranes were washed 3x 10 minutes in PBST before being imaged using the Odyssey DLx Imaging System (LI-COR). For re-blotting, membranes were stripped for 15 minutes in Restore Western Blot Stripping Buffer (Thermo Scientific), blocked for 1 hour before adding primary antibodies and resuming the protocol as above. When checking for successful transfer of protein to the membrane, Revert 700 Stain (LI-COR) was used. After transfer, membranes were airdried for 20-30 minutes. Membranes were rinsed in PBS for 5 minutes with gentle rocking (PVDF membranes were additionally rehydrated in 100 % methanol before rinsing), followed by a brief rinse with distilled water. Membranes were incubated for 5 minutes with 10 mL Revert 700 Total Protein Stain with gentle rocking. Lastly, membranes were washed 2x for 30 seconds with Revert 700 Wash Solution and immediately imaged in the 700 nm channel using the Odyssey DLx Imaging System. Signal was quantified using ImageJ (version 1.53a) and normalised against β-actin (housekeeping gene) and, in some cases, β3-tubulin (neuronal marker). All samples were normalised against the gel average. Western blots for each sample and antibody were repeated at least 2 times.

For human data acquisition and analysis case type was blinded. Each case was treated as a biological replicate. Technical replicates of the same biological replicate were averaged where all samples were above the limit of detection. Sex, age at death, post-mortem interval (PMI), brain region (Brodmann area) and brain bank were included as covariates in univariate ANOVA analyses. Linear regression of covariates, unpaired Student's t-test and ordinary one-way ANOVA with Tukey's multiple comparison of relative protein signal per case type was analysed in GraphPad Prism 10. Co-variate analysis was performed in IBM SPSS statistics.

Table 2.8 List of primary antibodies used for Western blots.

Protein of interest	Clone/ Immunogen	Host species	Type	Dilution	MW (kDA)	Catalogue number
β-actin	Clone: AC-15. Immunogen: slightly modified β-cytoplasmic actin N-terminal peptide, Ac-Asp-Asp-Asp-Ile-Ala-Ala-Leu-Val-Asp-Asn-Gly-Ser-Gly-Lys, conjugated to KLH.	Mouse	Monoclonal	1:10,000	42	Sigma #A5441
β3-tubulin	Immunogen: synthetic peptide corresponding to residues near C-terminus of mouse β3-tubulin	Chicken	Polyclonal	1:1000	55	Synaptic Systems #302 306
USP25	Immunogen: Recombinant fragment corresponding to Human USP25 aa850-1050.	Rabbit	Polyclonal	1:1000 (work up: 1:1000, 1:2000, 1:5000)	125	Abcam #ab246948
USP25	Immunogen: Recombinant fragment	Rabbit	Monoclonal	1:1000 (work up: 1:1000, 1:2000, 1:5000)	125	Abcam #ab187156
ATP5J	Immunogen: Recombinant fragment corresponding to Human ATP5J aa 1 to the C-terminus.	Rabbit	Polyclonal	1:1000, 1:2000, 1:5000	13	Abcam #ab224139

ATP5J	Clone number: AG5263	Rabbit	Polyclonal	1:1000, 1:2000, 1:5000	13	Proteintech #14114-1-AP
ATP5J	Immunogen: Full length human ATP5J Recombinant protein.	Rabbit	Polyclonal	1:500 (workup: 1:500 1:1000 1:2000	13	Invitrogen #PA5-29202
TTC3	Immunogen: Synthetic peptide derived from the N terminal domain of Human TTC3	Rabbit	Polyclonal	1:500, 1:1000	229	Abcam #ab80061

2.12 Single-nucleus RNA sequencing differential gene expression and gene ontology analysis

Processed snRNA sequencing data were generated at UCL Genomics, Yazead Buhidma (Lashley lab) and by Clíona Farrell (Wiseman lab) (Farrell *et al*., in preparation). This dataset comprises gene expression values from frontal cortex (BA10) grey matter samples of f Yazead Buhidma (Lashley lab) our healthy ageing (CTRL), four EOAD and eight AD-DS cases (table 2.9). In my downstream analysis, significant differential gene expression was defined as average log fold change (log2FC) having an FDR <0.05 in AD-DS versus CTRL, AD-DS versus EOAD and EOAD versus CTRL and gene expression being detected in both conditions within a given comparison (i.e. pct 1 and 2 values > 0). I divided differentially expressed genes (DEGs) into upregulated (positive log2FC) and downregulated (negative log2FC) relative to controls in my clusters of interest (neurons). Firstly, I examined overall patterns of differential gene expression of all genes versus Hsa21 genes in AD-DS and EOAD and subsequently selected my genes of interest (modifiers of Aβ toxicity/accumulation identified in my *Drosophila* screen) in eight excitatory and four inhibitory neuronal subclusters.

Gene ontology (GO) pathway analysis was performed in ShinyGO (version 0.80). Lists of significantly differentially expressed genes (FDR<0.05) from eight excitatory and four inhibitory neuron subclusters were combined into 'excitatory neurons' and 'inhibitory neurons' for GO analysis. The genetic background was defined as all genes detected in the snRNA dataset within the analysed clusters. GO categories of biological processes were filtered by smallest FDR value and visualised in ShinyGO 'Chart'. Pathways unique to AD-DS were defined as being associated with significantly up or downregulated genes in AD-DS versus HA cases. Differential gene expression in prefrontal cortex (BA8 and 9) neuronal excitatory and inhibitory clusters published by (Palmer *et al.*, 2021) was used to generate GO categories associated with up and downregulated genes in DS versus healthy ageing and compared to those associated with AD-DS in the Farrell *et al.* dataset. Venn diagrams were plotted in Rstudio (version 2024.04.1+748) using 'grDevices', 'grid', 'futile.logger', 'ggplot2', 'ggVennDiagram' and 'ggvenn' packages.

Table 2.9 Case demographics used for snRNA-sequencing.

Sample ID	Case type	Confirmed dementia	Sex	Age at death	PMI (h)	Brain region	Batch	Batch sample
47	AD-DS	yes	M	55	77	BA10	1	b1s1
27	EOAD	no	M	59	44	BA10	1	b1s2
34	AD-DS	yes	F	60	13	BA10	1	b1s3
32	AD-DS	yes	M	53	84	BA10	1	b1s4
26	HA	no	M	53	19	BA10	1	b1s5
48	AD-DS	yes	F	45	9	BA10	1	b1s6
25	HA	no	M	46	24	BA10	1	b1s7
49	EOAD	no	F	67	47	BA10	1	b1s8

33	AD-DS	yes	M	67	4	BA10	2	b2s1
29	EOAD	no	F	58	70	BA10	2	b2s2
50	AD-DS	yes	M	63	40	BA10	2	b2s3
30	AD-DS	yes	F	48	24	BA10	2	b2s4
51	HA	no	M	47	29	BA10	2	b2s5
31	AD-DS	yes	F	58	48	BA10	2	b2s6
52	HA	no	F	59	19	BA10	2	b2s7
28	EOAD	no	F	63	11	BA10	2	b2s8

2.13 List of Software

Adobe Illustrator 2023 (Adobe, version 27.2), BioRender Scientific Image and Illustration Software (https://www.biorender.com/), Microsoft Excel (version 16.87), GraphPad Prism 10 (version 10.1.1-10.2.3), DSRC integrative ortholog prediction tool (DIOPT, version 8.5 and 9.0, Rstudio (version 1.3.1093-2024.04.1+748), ImageJ (version 15.3a), IBM SPSS statistics (version 29.0.2.0(20)), https://www.flyrnai.org/diopt) , ShinyGO 0.80 (http://bioinformatics.sdstate.edu/go/).

Chapter 3: *Drosophila* screen of human chromosome 21 orthologues

3.1 Introduction

Down syndrome is a multigenic condition that results in a range of phenotypes, including early-onset AD pathology. While triplication of *APP* is understood to be the major genetic cause of AD-DS, more recent studies have furthered our understanding of other Hsa21 genes that may be responsible for altered toxicity and accumulation of Aβ in this population (Wiseman *et al.*, 2018; Sawa *et al.*, 2021; Tosh *et al.*, 2021; Mumford *et al.*, 2022). The Tc1 mouse model has been critical in this investigation. In addition to Hsa21 homologous regions on Mmu16, Mmu17 and Mmu10 present in two copies, these animals carry a freely segregating copy of Hsa21 including more than 75% of its functional genes (Gribble *et al.*, 2013). Crucially, this does not include an additional functional copy of *APP.* Therefore, by using mouse genetic crosses, overexpression of *APP* can be studied on a euploid background and in the context of a DS model. To assess whether trisomy of the 75% of Hsa21 genes affects AD pathology and cognitive symptoms, in a study by Wiseman *et al.* Tc1 mice were crossed to a model of amyloid deposition. This amyloid model was the transgenic 'J20 TgAPP' mouse which overexpresses human mutant *APP* inserted into the *Zbtb20* locus on Mmu16, resulting in the accumulation of Aβ, synaptic loss and cognitive decline in this model (Mucke *et al.*, 2000; Fisher *et al.*, 2017). This cross produces four possible mouse genotypes: wildtype, Tc1, trisomic TgAPP and euploid TgAPP. The trisomic TgAPP offspring showed increased Aβ aggregation and exacerbated cognitive decline compared to euploid TgAPP littermates (Figure 3.1). As the only difference between these two types of progeny was the presence or absence of Hsa21 (without a functional copy of *APP*), this shows that an additional copy of Hsa21 genes other than *APP* is sufficient to mediate this effect (Wiseman *et al.*, 2018). This finding was replicated in another study in which the Dp16(1)Yey DS mouse model was

crossed with the 5XFAD transgenic mouse model of Aβ accumulation (Mumford *et al.*, 2022). In this study, the effect of the Dp16(1)Yey model was proposed to be resultant from an additional copy of *Usp25*; although this was not formally proven in the paper. Additionally, triplication of regions of Hsa21 synteny present in the Dp3Tyb mouse model have been shown to partially rescue Aβ in knock-in AD mice. These data indicate that an extra copy of Hsa21 orthologues other than *APP* can exacerbate and ameliorate Aβ accumulation and/or response. The identity of the Hsa21 genes responsible for these effects is currently unknown.

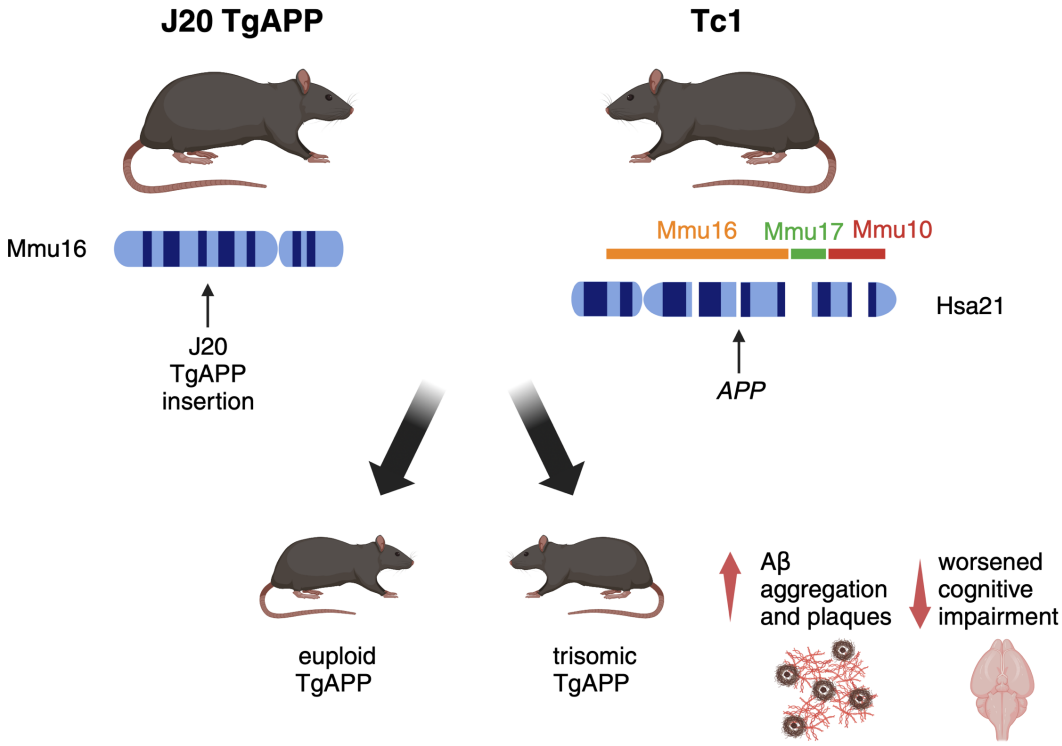

Figure 3.1 J20 TgAPP x Tc1 cross.

An additional copy of Hsa21 genes other than *APP* is sufficient to increase amyloid load and plaques and exacerbate cognitive decline in a mouse model of AD-DS. Adapted from (Herault *et al.*, 2017; Y. Wu *et al.*, 2022). Created with Biorender.com.

Based on these findings, we took a single gene screening approach to narrow down which gene(s) may be mediating this effect. In line with NC3Rs guidelines on reducing

the use of animal models in research, we used *Drosophila melanogaster* as a partial replacement model. *Drosophila* is an established screening tool due to its fully sequenced and easily modifiable genome with low genetic redundancy (Adams *et al.*, 2000; Lenz *et al.*, 2013). Additionally, the GAL4/UAS expression system enables spatial restriction of gene expression in the flies. For this, males that contain a tissue/cell type specific genomic enhancer fused with a yeast-derived GAL4 transcriptional activator (the 'driver' line) are crossed with virgin females that encode a transgene under the control of an upstream activation sequence (UAS) containing GAL4 binding sites (Brand and Perrimon, 1993). In the F_1 progeny, binding of the GAL4 protein to UAS sites results in the transcription of the downstream gene of interest (Brand and Perrimon, 1993). This system was later modified to also allow for temporal restriction of gene expression, e.g. to adulthood. The addition of a Gene-Switch module to GAL4 makes the protein activatable through the progesterone analogue mifepristone (RU-486) which can be added to fly media (Osterwalder *et al.*, 2001). In my study, I utilised this GeneSwitch/UAS system to express the human peptide Aβ1-42 to model amyloid accumulation. Expression was induced in adulthood through the addition of RU-486 to fly media. The upstream enhancer of the *elav* gene results in its expression in post-mitotic neurons and was used as a neuron specific 'driver', termed elavGeneSwitch (*elavGS*) (Figure 3.2) (Robinow and White, 1988).

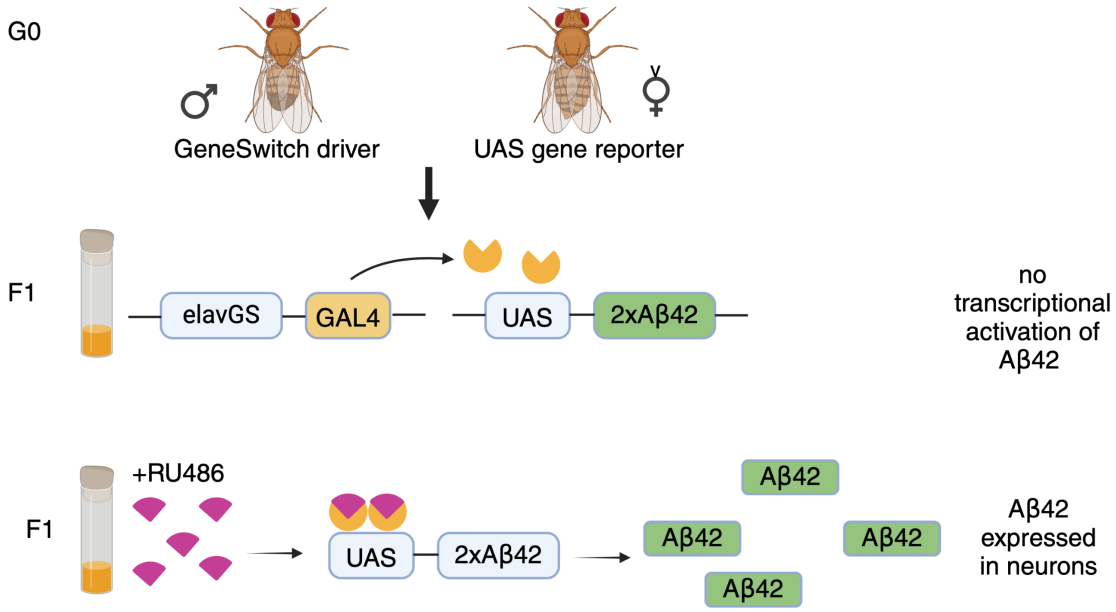

Figure 3.2 RU-486 inducible GeneSwitch/UAS expression system.

The parental generation (G0) consists of a cross between a fly carrying neuronal enhancer *elav* fused to a modified GAL4 with a Gene-Switch module and a fly carrying two tandem copies of Aβ1-42 downstream of an UAS with GAL4 binding sites. (A) In the absence of the progesterone analogue RU-486, the GAL4/Gene-Switch protein is expressed in neurons but remains transcriptionally inactivated, repressing Aβ expression in the F1 generation. (B) When RU-486 is added to fly media, it attaches to the progesterone receptor and the expressed GAL4 protein can bind to the target UAS site, resulting in transcriptional activation of Aβ. Therefore, Aβ expression can be spatially and temporally restricted to adult neurons. Figure adapted from (Osterwalder *et al.*, 2001). Created with BioRender.com

To assess whether toxicity and accumulation of Aβ in this model is modified by a Hsa21 orthologue, *UAS-Aβx2*, *elavGS* flies can then be crossed to lines that contain an Hsa21 orthologue under the control of an UAS. Adult offspring carrying all three constructs are then placed on food containing RU-486 or a vehicle control (ethanol). This results in pan-neuronal co-overexpression of the orthologue and Aβ in the induced condition.

In the field of neurodegeneration, several phenotypic assays can be employed to assess the effects of single gene misexpression in high-throughput screens. These include the rough eye phenotype, negative geotaxis and lifespan assays. In our screen, we focused on the negative geotaxis assay as the primary phenotypic readout. In AD, pathological aggregation of Aβ contributes to neuronal dysfunction which affects both cognition and locomotor ability (Palop and Mucke, 2010; Wisniewski and Masurkar, 2023). Negative geotaxis is an innate escape response that causes flies to climb upwards when knocked down and this locomotor readout can be used as a measure of neuronal function, though it also has a muscular and metabolic component (Gargano *et al.*, 2005; Madabattula *et al.*, 2015). The negative geotaxis response declines with age and the rate of this decline can be altered by certain genetic modifications. Pan-neuronal expression of Aβ42 has been shown to reduce the negative geotaxis response (decrease climbing speed) compared to wild-type flies (Yu *et al.*, 2020; F. H. P. Tan *et al.*, 2023). Previous work has employed the climbing assay to conduct a genetic screen, identifying genes that can modify the Aβ induced neuromotor defect (Belfiori-Carrasco *et al.*, 2017). In addition to assessing the phenotypic effects of Aβ toxicity, the amount of Aβ present in fly brains can also be measured. When transgenic expression of Aβ is induced, the protein accumulates in the brain with age and the amount may be modified by other genes. To measure this, studies have employed immunostaining, western blot or ELISA assays (Ray, Speese and Logan, 2017; Huang *et al.*, 2019). To investigate how overexpression of Hsa21 orthologues modifies Aβ pathology, in our study, we combined the phenotypic negative geotaxis assay with Aβ42 ELISAs as a molecular readout.

The aims of this chapter were:

1. To identify *Drosophila* orthologues of Hsa21 genes that are present as an additional functional copy in the Tc1 mouse. Triplication of these genes has been shown to be sufficient to modify Aβ accumulation and toxicity in this mouse model of AD-DS.

2. Screen the identified orthologues as modifiers of Aβ toxicity and accumulation in *Drosophila.*

3.2 Results

3.2.1 Identification of Hsa21 *Drosophila* orthologues

An extra copy of Hsa21 genes in people with DS is the genetic cause of increased amyloid deposition with age in this population. To narrow down potential modifiers of Aβ toxicity and accumulation that are also known to be on Hsa21, using *Drosophila* orthologues of Hsa21 genes needed to be identified. In the reference list, I included all Hsa21 genes that have an extra functional copy in the Tc1 mouse model. I used the 'DRSC integrative ortholog prediction tool' (DIOPT), which combines 19 different orthologue prediction tools to determine the most likely orthologue for each gene (Hu *et al.*, 2011). This identified 159 *Drosophila* orthologues of which I selected those with high or moderate scores. The resulting list consisted of 88 *Drosophila* orthologues, corresponding to 77 Hsa21 genes. Next, I searched for single gene overexpression lines that were publicly available to order from *Drosophila* stock centres. This included transgenic UAS-ORF (FlyORF) and misexpression insertion P(EP) lines (Bloomington Drosophila Stock Center). EP lines are generated by random transposable P-element insertion. These p-elements contain UAS regulatory sequences and when they insert into the promoter of a gene of interest in the correct orientation, they can be used for mis-expression of downstream genes (Rørth, 1996). Maps in flybase.org were used to ensure the correct directionality of the insertions. For Hsa21 genes, with multiple *Drosophila* orthologues, I selected those with the highest score that had available overexpression lines. As a result, the final list of genes to be screened as modifiers of Aβ toxicity and accumulation included 35 *Drosophila* orthologues of the equivalent number of Hsa21 genes (Table 3.1). To achieve a homogeneous genetic background,

all lines were backcrossed at least six times into the w^{1118} background prior to screening.

Table 3.1 List of *Drosophila* genes and their human orthologues included in the genetic modifier screen.

DIOPT rank of moderate or high indicates the likelihood of correct orthologue prediction.

Human Gene name	*Drosophila* gene name	DIPOT rank
PKNOX1	*achi*	moderate
AGPAT3	*Agpat3*	high
PRMT2	*Art8*	moderate
ATP5J/ATP5PF	*ATPsynCF6*	high
CBS	*Cbs*	high
GRIK1	*clumsy*	moderate
ADARB1	*DIP1*	moderate
DSCAM	*Dscam4*	high
GABPA	*Ets97D*	high
HLCS	*Hcs*	high
LTN1	*Ltn1*	high
DYRK1A	*mnb*	high
MRPL39	*mRpL39*	high
ITGB2	*mys*	moderate
RRP1B	*Nnp-1*	high
POFUT2	*O-fut2*	high
PFKL	*Pfk*	moderate
PCNT	*Plp*	high
ETS2	*pnt*	moderate
TPTE	*Pten*	moderate
TMPRSS2	*Sb*	moderate
MX2/MX1	*shi*	moderate

TRAPPC10	*SIDL*	high
TIAM1	*sif*	high
SIK1	*Sik2*	moderate
SIM2	*sim*	high
SAMSN1	*SKIP*	high
SOD1	*Sod1*	high
USP16	*Usp16-45*	moderate
USP25	*Usp47*	moderate
WDR4	*wuho*	high
RBM11	*CG11454*	moderate
PWP2	*CG12325*	moderate
ABCG1	*CG17646*	moderate
SCAF4	*CG4266*	high
LRRC3	*CG42709*	high

Due to constraints regarding a lack of suitable orthologues or availability of overexpression lines and technical issues (e.g. fly lines not surviving to the backcrossing stage) many Hsa21 genes could not be included in my screen (Table S3.1). A number of these genes have been implicated in AD-DS such as *BACE2*, *SUMO3*, *DOPEY2* and *TTC3* and may therefore play a role in modifying amyloid pathology when overexpressed. Notably, the Tc1 mouse also carries an additional functional copy of 49 keratin-associated protein genes, which I excluded from my study due to a lack of evidence for their expression in the human brain.

3.2.2 Screening for modifiers of amyloid-β toxicity

Genetic modifications have been shown to have the potential to significantly impact the negative geotaxis response. I therefore used the negative geotaxis assay to determine whether co-overexpression of Aβ42 with an Hsa21 orthologue in adult

neurons could modify climbing speed with age compared with expression of Aβ42 alone. For this I included four different conditions per gene of interest: 1) flies that carry the *UAS-Aβx2*, *elavGS* constructs and a Hsa21 orthologue fed on food with added RU-486 to induce pan-neuronal over expression of Aβ and the Hsa21 orthologue, 2) flies carrying the *UAS-Aβx2*, *elavGS* only, fed on food with added RU-486 to induce expression, 3) flies of the same genotype as (1) but fed on food containing a vehicle control for RU-486 so that transcription of Aβ or the Hsa21 orthologue is not activated, 4) flies of the same genotype as (2) but food containing a vehicle control so that Aβ is not transcriptionally activated. The negative geotaxis experiment was performed at regular intervals throughout the flies' lifespan to assess the rate at which locomotor function declines with age. Average height climbed 15 seconds after being knocked to the bottom of a vial was plotted over time. Due to technical limitations regarding the number of vials that fit on one experimental device (drosoflipper), climbing experiments were divided into nine different batches. Each batch contained all four experimental conditions with 5x15 flies per condition.

Across all conditions tested, climbing speed decreased with age and, as has been previously shown, induction of Aβ42 expression in adult neurons resulted in a significant climbing defect compared to uninduced controls, suggesting that this peptide is sufficient to impair locomotor function with age in *Drosophila* (Figure 3.3). Out of 35 Hsa21 orthologue lines, 29 pan-neuronally co-overexpressing Aβ42 and *achi*; *Agpat3; Art; Cbs; clumsy; DIP1; Dscam4; Ets97D; Ltn1; mRpL39; mys; Nnp-1; O-fut2; Pfk; Plp; pnt; Pten; SIDL; sif; Sik2; sim; Sod1; Usp16-45; wuho; CG11454; CG12325; CG17464; CG4266* or *CG42709* showed no significant interaction between climbing speed with age and genotype in the induced (+RU) condition (Figure 3.3) This suggests that overexpression of these Hsa21 orthologues does not modify the flies' response to Aβ42 toxicity in the context of this measure of neuromotor function. Notably, *UAS-Aβx2*, *elavGS/UAS-Cbs, UAS-Aβx2*, *elavGS/UAS-mRpL39, UAS-Aβx2*, *elavGS/UAS-CG12325* flies showed a faster decline in climbing speed with age when expression was not induced (-RU), suggesting that the site of integration of the p-elements may worsen locomotor function for these genotypes.

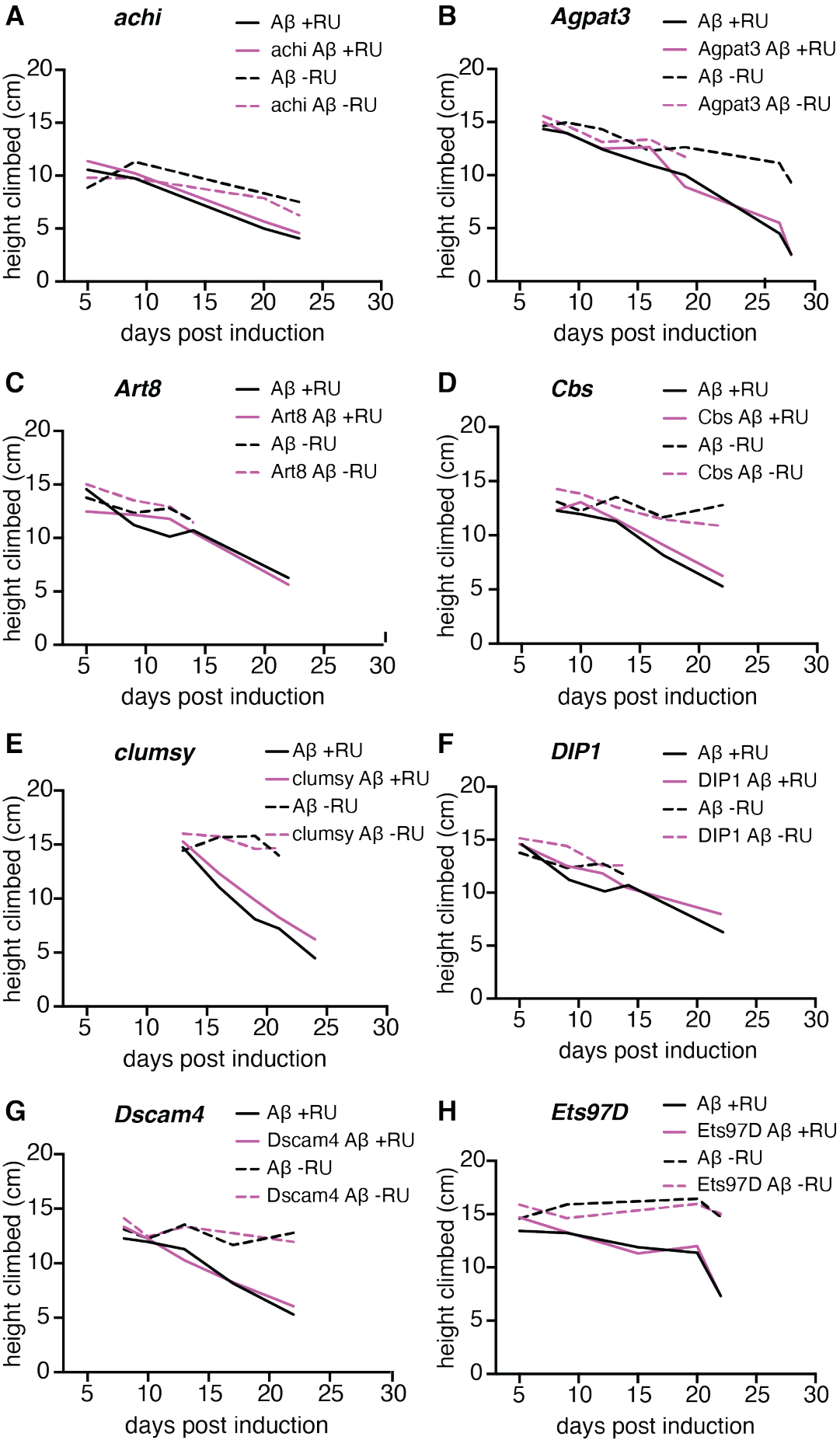
A
achi
Aβ +RU
achi Aβ +RU
Aβ -RU
achi Aβ -RU
B
Agpat3
Aβ +RU
Agpat3 Aβ +RU
Aβ -RU
Agpat3 Aβ -RU
C
Art8
Aβ +RU
Art8 Aβ +RU
Aβ -RU
Art8 Aβ -RU
D
Cbs
Aβ +RU
Cbs Aβ +RU
Aβ -RU
Cbs Aβ -RU
E
clumsy
Aβ +RU
clumsy Aβ +RU
Aβ -RU
clumsy Aβ -RU
F
DIP1
Aβ +RU
DIP1 Aβ +RU
Aβ -RU
DIP1 Aβ -RU
G
Dscam4
Aβ +RU
Dscam4 Aβ +RU
Aβ -RU
Dscam4 Aβ -RU
H
Ets97D
Aβ +RU
Ets97D Aβ +RU
Aβ -RU
Ets97D Aβ -RU
height climbed (cm)
0
5
10
15
20
5
10
15
20
25
30
days post induction

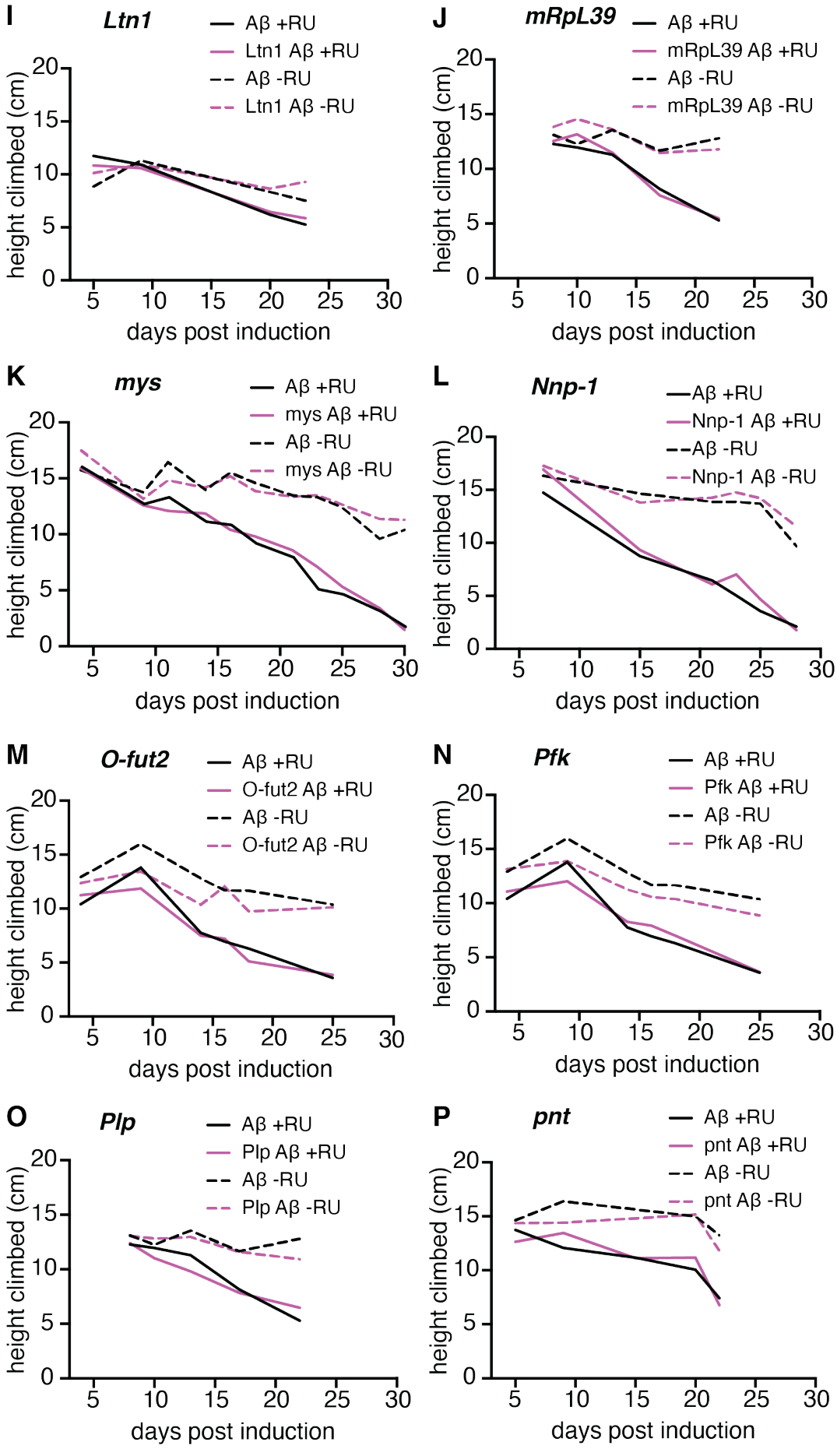
I
Ltn1
Aβ +RU
Ltn1 Aβ +RU
Aβ -RU
Ltn1 Aβ -RU
height climbed (cm)
days post induction
J
mRpL39
Aβ +RU
mRpL39 Aβ +RU
Aβ -RU
mRpL39 Aβ -RU
height climbed (cm)
days post induction
K
mys
Aβ +RU
mys Aβ +RU
Aβ -RU
mys Aβ -RU
height climbed (cm)
days post induction
L
Nnp-1
Aβ +RU
Nnp-1 Aβ +RU
Aβ -RU
Nnp-1 Aβ -RU
height climbed (cm)
days post induction
M
O-fut2
Aβ +RU
O-fut2 Aβ +RU
Aβ -RU
O-fut2 Aβ -RU
height climbed (cm)
days post induction
N
Pfk
Aβ +RU
Pfk Aβ +RU
Aβ -RU
Pfk Aβ -RU
height climbed (cm)
days post induction
O
Plp
Aβ +RU
Plp Aβ +RU
Aβ -RU
Plp Aβ -RU
height climbed (cm)
days post induction
P
pnt
Aβ +RU
pnt Aβ +RU
Aβ -RU
pnt Aβ -RU
height climbed (cm)
days post induction

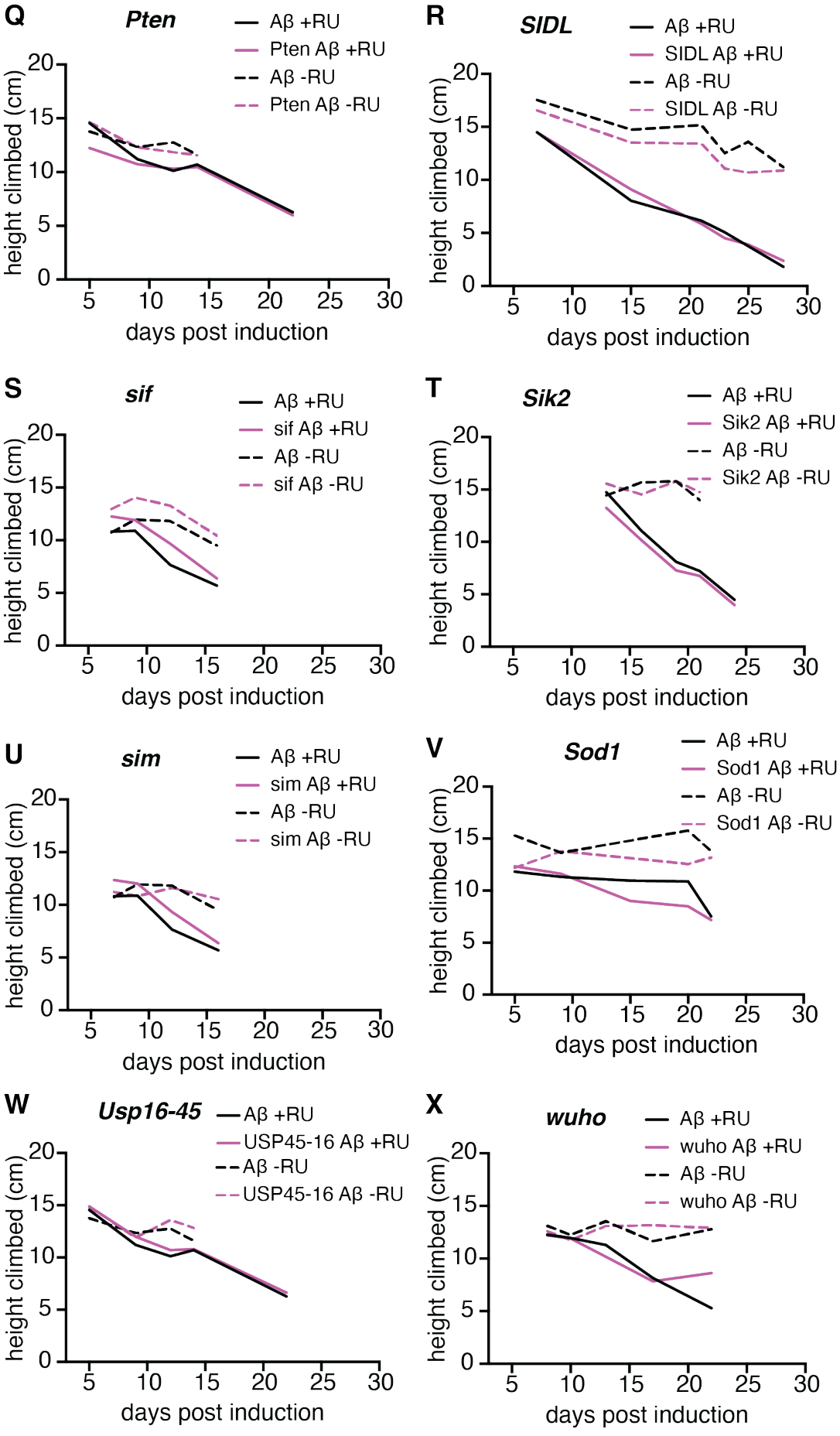
Q
Pten
Aβ +RU
Pten Aβ +RU
Aβ -RU
Pten Aβ -RU
height climbed (cm)
days post induction
R
SIDL
Aβ +RU
SIDL Aβ +RU
Aβ -RU
SIDL Aβ -RU
height climbed (cm)
days post induction
S
sif
Aβ +RU
sif Aβ +RU
Aβ -RU
sif Aβ -RU
height climbed (cm)
days post induction
T
Sik2
Aβ +RU
Sik2 Aβ +RU
Aβ -RU
Sik2 Aβ -RU
height climbed (cm)
days post induction
U
sim
Aβ +RU
sim Aβ +RU
Aβ -RU
sim Aβ -RU
height climbed (cm)
days post induction
V
Sod1
Aβ +RU
Sod1 Aβ +RU
Aβ -RU
Sod1 Aβ -RU
height climbed (cm)
days post induction
W
Usp16-45
Aβ +RU
USP45-16 Aβ +RU
Aβ -RU
USP45-16 Aβ -RU
height climbed (cm)
days post induction
X
wuho
Aβ +RU
wuho Aβ +RU
Aβ -RU
wuho Aβ -RU
height climbed (cm)
days post induction

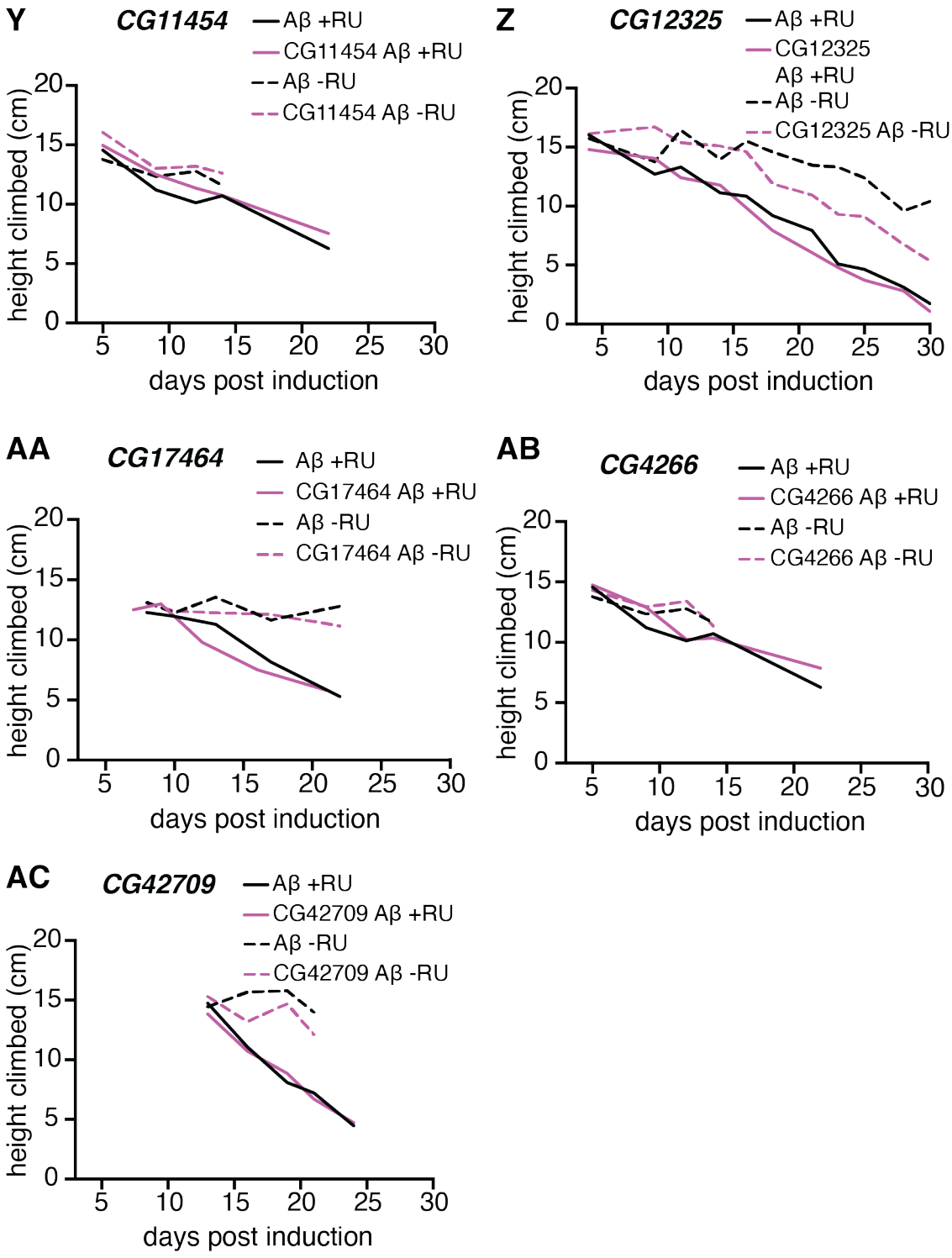

Figure 3.3 Negative geotaxis assays of flies overexpressing an Hsa21 orthologue together with Aβ42 for the non-significant interactions.

Average height climbed across the lifespan by flies pan-neuronally expressing Aβ42, with (pink lines) or without (black lines) overexpression of an Hsa21 orthologue in adult neurons (solid lines, +RU) and uninduced controls (dashed lines, -RU). n = 75 flies per

condition. All p-values refer to simple linear regression of the interaction between age and genotype unless stated otherwise (Table 3.2). Genotypes: (A-AC) *UAS-Aβx2*, *elavGS,* (A) *UAS-Aβx2, elavGS/UAS-achi* (B) *UAS-Aβx2, elavGS/UAS-Agpat3* (C) *UAS-Aβx2, elavGS/UAS*-Art8 (D) *UAS-Aβx2, elavGS/UAS-Cbs* (E) *UAS-Aβx2, elavGS/UAS-clumsy* (F) *UAS-Aβx2, elavGS/UAS-DIP1* (G) *UAS-Aβx2, elavGS/UAS-Dscam4* (H) *UAS-Aβx2, elavGS/ UAS-Ets97D* (I) *UAS-Aβx2, elavGS/UAS-Ltn1* (J) *UAS-Aβx2, elavGS/UAS-mRpL39* (K) *UAS-Aβx2, elavGS/UAS-mys* (L) *UAS-Aβx2, elavGS/UAS-Nnp-1* (M) *UAS-Aβx2, elavGS/UAS-O-fut2* (N) *UAS-Aβx2, elavGS/UAS-Pfk* (O) *UAS-Aβx2, elavGS/UAS-Plp* (P) *UAS-Aβx2, elavGS/UAS-pnt* (Q) *UAS-Aβx2, elavGS/UAS-Pten* (R) *UAS-Aβx2, elavGS/UAS-SIDL* (S) *UAS-Aβx2, elavGS/UAS-sif* (T) *UAS-Aβx2, elavGS/UAS-Sik2* (U) *UAS-Aβx2, elavGS/UAS-sim* (V) *UAS-Aβx2, elavGS/UAS-Sod1* (W) *UAS-Aβx2, elavGS/UAS-Usp16-45* (X) *UAS-Aβx2, elavGS/UAS-wuho* (Y) *UAS-Aβx2, elavGS/UAS-CG11454* (Z) *UAS-Aβx2, elavGS/UAS-CG12325* (AA) *UAS-Aβx2, elavGS/UAS-CG17464* (AB) *UAS-Aβx2, elavGS/UAS-CG4266* (AC) *UAS-Aβx2, elavGS/UAS-CG42709.* Full statistical results are presented in Table S3.2.

Table 3.2 Linear model of induced (+RU) Aβ expressing flies compared with co-overexpression of a Hsa21 orthologue.

Statistically significant results are highlighted in green, borderline significance (p<0.1) is highlighted in orange.

Gene		p-values		Gene		p-values	
		+RU	-RU			+RU	-RU
A	*achi*	0.847	0.200	P	*pnt*	0.619	0.819
B	*Agpat3*	0.833	0.500	Q	*Pten*	0.077	0.233
C	*Art8*	0.236	0.175	R	*SIDL*	0.843	283
D	*Cbs*	0.379	0.001	S	*sif*	0.587	0.144
E	*clumsy*	0.239	0.380	T	*Sik2*	0.234	0.938
F	*DIP1*	0.267	0.380	U	*sim*	0.466	0.444
G	*Dscam4*	0.985	0.324	V	*Sod1*	0.067	0.637
H	*Ets97D*	0.606	0.697	W	*Usp16-45*	0.896	0.435
I	*Ltn1*	0.068	n = too small	X	*wuho*	0.257	0.228
J	*mRpL39*	0.439	0.03	Y	*CG11454*	0.615	0.191
K	*mys*	0.181	0.307	Z	*CG12325*	0.191	5.79e-13
L	*Nnp-1*	0.064	0.101	AA	*CG7464*	0.922	0.251
M	*O-fut2*	0.964	0.783	AB	*CG4266*	0.596	0.654
N	*Pfk*	0.612	0.083	AC	*CG42709*	0.270	0.196
O	*Plp*	0.063	0.119				

Pan-neuronal co-overexpression of Aβ42 and *ATPsynCF6, Hcs, mnb, Sb, SKIP or Usp47* was found to modify height climbed with age (Figure 3.4). Of those, *Hcs, mnb, Sb, SKIP* and *Usp47* significantly rescued the climbing defect of Aβ42 expressing flies, suggesting that overexpression of these genes may improve how the flies respond to the toxic expression of Aβ42 (Figure 3.4B-F). Notably, when *mnb* was overexpressed, the rescue was due to a slower climbing speed at day 5 compared to Aβ expressing flies, reducing the slope of decline with age. The rate of decline did not significantly differ from day 9 onwards (p = 0.8517).

Conversely, overexpression of *ATPsynCF6* worsened the phenotype such that the rate of decline in climbing speed was more rapid compared to expression of Aβ42 alone (Figure 3.4A). Notably, for *UAS-Aβx2*, *elavGS/UAS-Hcs, UAS-Aβx2*, *elavGS/UAS-Sb and UAS-Aβx2*, *elavGS/UAS-Usp47* climbing speed also declined more slowly with age in the -RU condition. To assess whether the observed rescue in the +RU conditions may be due to factors other than overexpression of the target gene itself, I included 'RU' as a co-factor in the linear model. This is to determine whether induction of Aβ and Hsa21 orthologue expression has an effect on the locomotor phenotype (if so, the effect will be significant). For *Hcs,* the effect of overexpression remained significant (Table 3.3). However, for *Sb* and *Usp47,* the interaction between age and genotype was no longer significant suggesting that the observed rescue in the +RU condition may not be due to neuronal overexpression of the gene (Table 3.3).

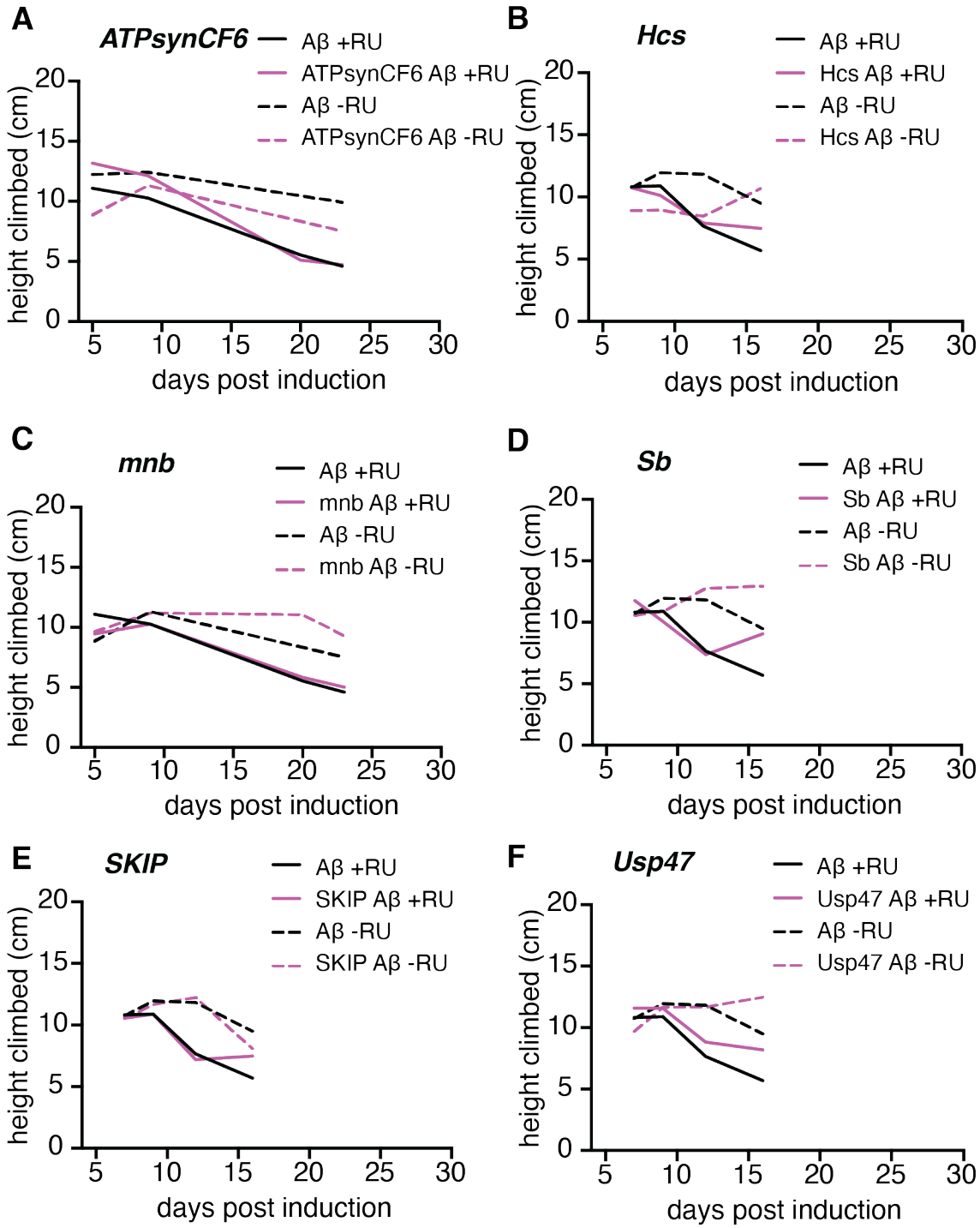

Figure 3.4 Negative geotaxis assays of flies overexpressing six Hsa21 orthologues together with Aβ42 that exhibited significant interactions.

Average height climbed across the lifespan by flies pan-neuronally expressing Aβ42, with (pink lines) or without (black lines) overexpression of a Hsa21 orthologue in adult neurons (solid lines, +RU) and uninduced controls (dashed lines, -RU). All p-values refer to simple linear regression of the interaction between age and genotype unless stated otherwise (Table 3.3). Genotypes: *(A-F) UAS-Aβx2*, *elavGS,* (A) *UAS-Aβx2*,

elavGS/UAS-ATPsynCF6, (B) *UAS-Aβx2*, *elavGS/UAS-Hcs,* (C) *UAS-Aβx2*, *elavGS/UAS-mnb,* (D) *UAS-Aβx2*, *elavGS/UAS-Sb,* (E) *UAS-Aβx2*, *elavGS/UAS-SKIP,* (F) *UAS-Aβx2*, *elavGS/UAS-Usp47*. Full statistical results are presented in Table S3.3.

Table 3.3 Linear model of induced (+RU) Aβ expressing flies compared with co-overexpression of a Hsa21 orthologue.

Statistically significant results are highlighted in green, borderline significance (p<0.1) is highlighted in orange.

Gene		**p-values**		
		+RU	**-RU**	**effect of RU**
A	*ATPsynCF6*	0.002	0.780	-
B	*Hcs*	0.015	0.011	0.001
C	*mnb*	0.043	0.863	
D	*Sb*	0.001	0.0003	0.990
E	*SKIP*	0.039	0.365	
F	*Usp47*	0.043	0.002	0.091

Due to the large number of lines that were screened in this study, negative geotaxis experiments had to be divided across multiple batches. To compare the homogeneity of control flies within the -RU and +RU conditions, I ran a linear model to test for batch effect. There was a significant difference in height climbed with age between batches both within the -RU and +RU conditions, highlighting the importance of having controls for each experimental batch (Figure 3.5).

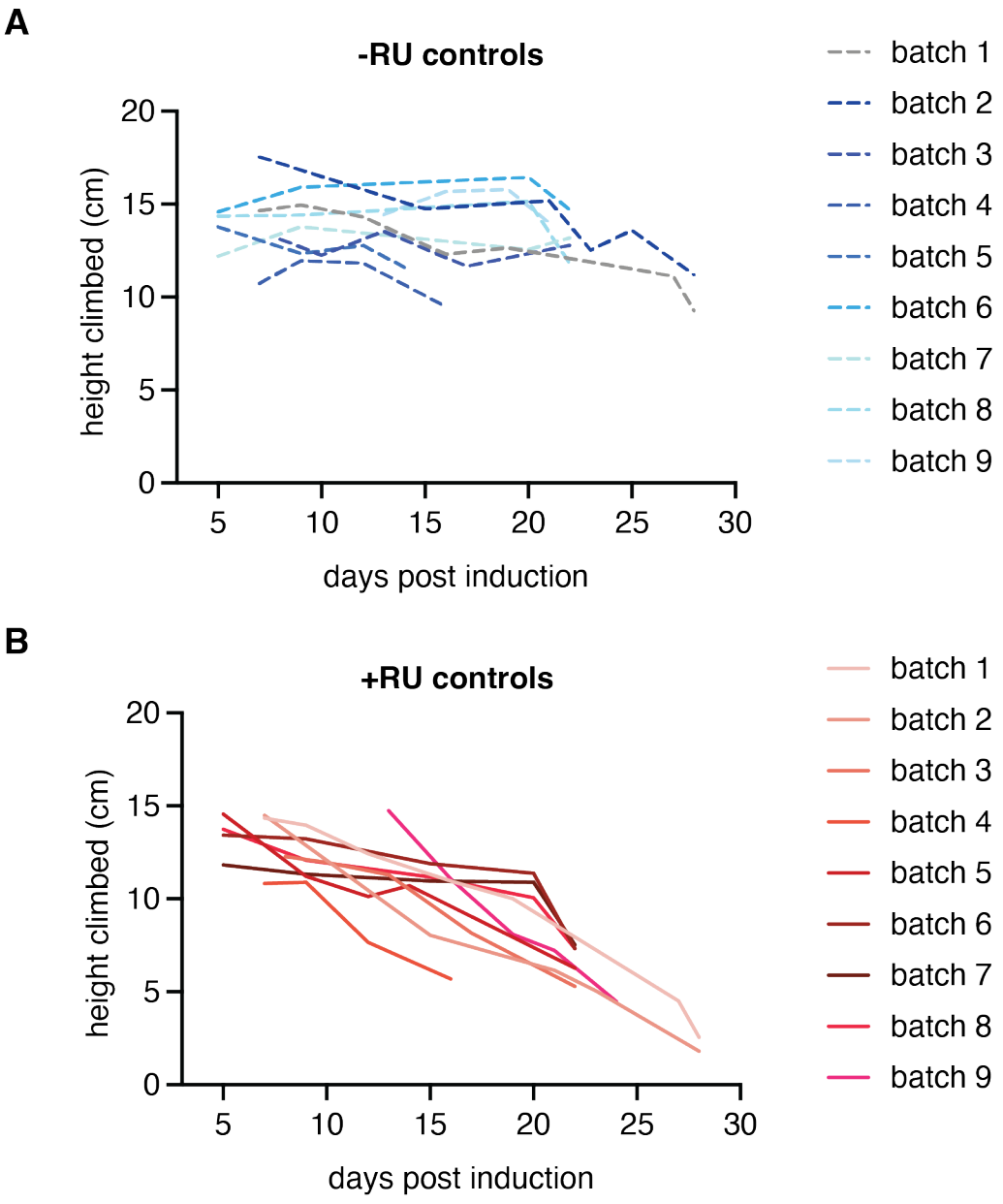

Figure 3.5 -RU and +RU controls from all nine experimental batches.

(A) Average height climbed with age of *UAS-Aβx2*, *elavGS* control flies fed on -RU food varies significantly across nine experimental batches (n = 75 flies per condition, simple linear regression, $p < 0.0001$). (B) Height climbed with age of *UAS-Aβx2*, *elavGS* control flies fed on +RU food varies significantly across nine experimental batches (n = 75 flies per condition, simple linear regression, $p = 0.0245$).

3.2.3 Work-up of Aβ42 ELISA in *Drosophila*

Flies expressing human Aβ in adult neurons accumulate Aβ42 in the brain (Yu *et al.*, 2020; Catterson *et al.*, 2023). To determine whether additional overexpression of Hsa21 orthologues can modify Aβ accumulation in addition to or independent of modifying Aβ toxicity, I measured the amount of Aβ42 in fly heads using an ELISA assay. For this, we worked up our own ELISA protocol rather than using a commercially available kit. Firstly, we conducted a pilot experiment based on an existing ELISA protocol, using antibody 6E10 that recognises human Aβ at positions 3-8 (EFRHDS), and which was first developed for the detection of cerebrovascular amyloid (Kim *et al.*, 1988). We tested *UAS-Aβx2*, *elavGS* flies that had expression of Aβ induced for 10 days and *UAS-Aβx2*, *elavGS* flies that were fed on media without expression inducing RU-486, used as a negative control. Induced *UAS-Aβx2*, *elavGS* flies showed a significant increase in Aβ42 accumulation compared to -RU controls of the same genotype (Figure 3.6).

ELISA assays can measure the amount of protein present in a sample through the use of primary antibodies that specifically bind the target of interest (Aβ42 in the case of this study), which is then bound by a detectable secondary antibody. The efficacy of the primary antibody can vary depending on the protein and the concentration at which it is present. Therefore, we trialled a range of dilutions between 1:10 and 1:1280 of primary 6E10 antibody. Dilutions of 1:40-1:160 gave similar values, suggesting that the antibody works effectively for our samples within this range. We decided the optimised working concentration would be 1:40 (Figure 3.6A).

Subsequently, I wanted to understand how Aβ42 accumulates in fly heads with age, to determine the most appropriate age for measuring potential modification of Aβ42 levels induced by overexpression of Hsa21 orthologues. I used *UAS-Aβx2*, *elavGS* flies that had been induced for 5, 10, 15 and 20 days. Aβ42 significantly increased between days 5 – 15 and plateaued between days 15-20 (Figure 3.6B). To screen for

Aβ42 accumulation, I therefore decided to induce expression for 10 days to allow for both increases and decreases in the protein to be detectable.

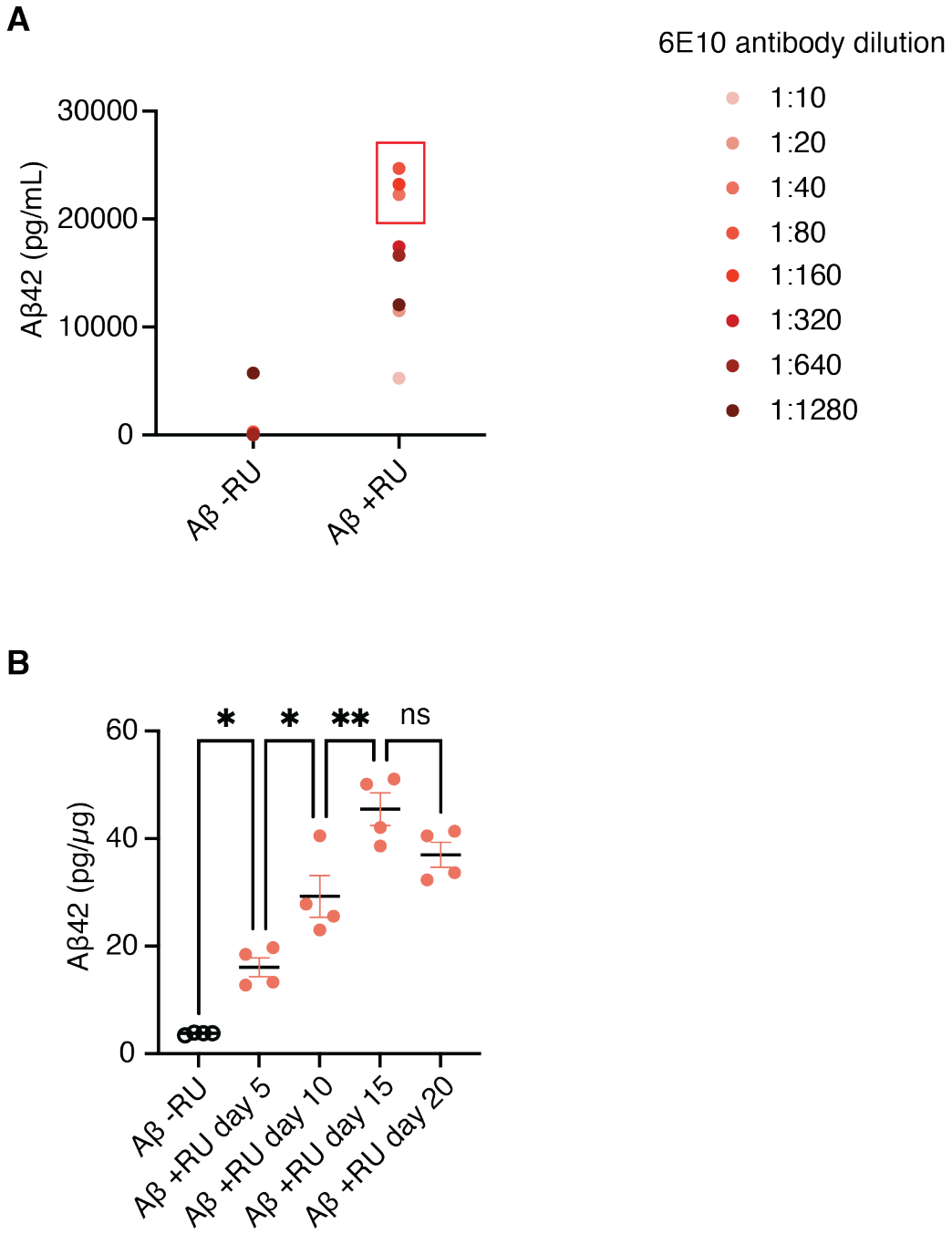

Figure 3.6 Work-up of Aβ42 ELISA.

(A) ELISA of *UAS-Aβx2*, *elavGS* flies kept on +RU media for 10 days and *UAS-Aβx2*, *elavGS* -RU controls. n = 2, with 10 fly heads per biological replicate. (B) ELISA of *UAS-Aβx2*, *elavGS* flies fed on +RU media for 5, 10, 15 or 20 days (red dots) and -RU controls (black circles) normalised to total protein by BCA assay. One-way ANOVA with Tukey's multiple comparisons test F (4, 15) = 41.92, p = 0.0001, day 5-10 p =

0.0177, day 10-15 $p = 0.0035$, day 15-20 $p = 0.1862$. Data are presented as mean ± SEM, n = 4 with 10 fly heads per biological replicate. *Work-up of the ELISA protocol was led by Dr Nathan Woodling.*

3.2.4 Screening for modifiers of amyloid-β accumulation

Subsequently, I used our optimised ELISA protocol to determine whether overexpression of an Hsa21 orthologue was sufficient to modify Aβ42 accumulation. Pan-neuronal co-overexpression of Aβ42 and *Dscam4, Cbs, sif, CG17646, wuho, Hcs, Sb, SKIP, Usp47, Art8, DIP1, Pten, Usp16-45, CG11454, CG4266, Agpat3, mys, CG12325, pnt, Ets97D, sim, achi, Ltn1, ATPsynCF6, mnb,* or *SIDL* did not result in a change to the amount of total Aβ42 present in fly heads compared with expression of Aβ42 alone (Figure 3.7). Notably, this includes genotypes that showed a change in climbing speed with age, suggesting that this observed neuromotor effect was independent of the amount of Aβ42 accumulating in the fly model. There was a trend towards increased Aβ42 when *mnb* or *SKIP* are overexpressed but this did not reach statistical significance (Table 3.4).

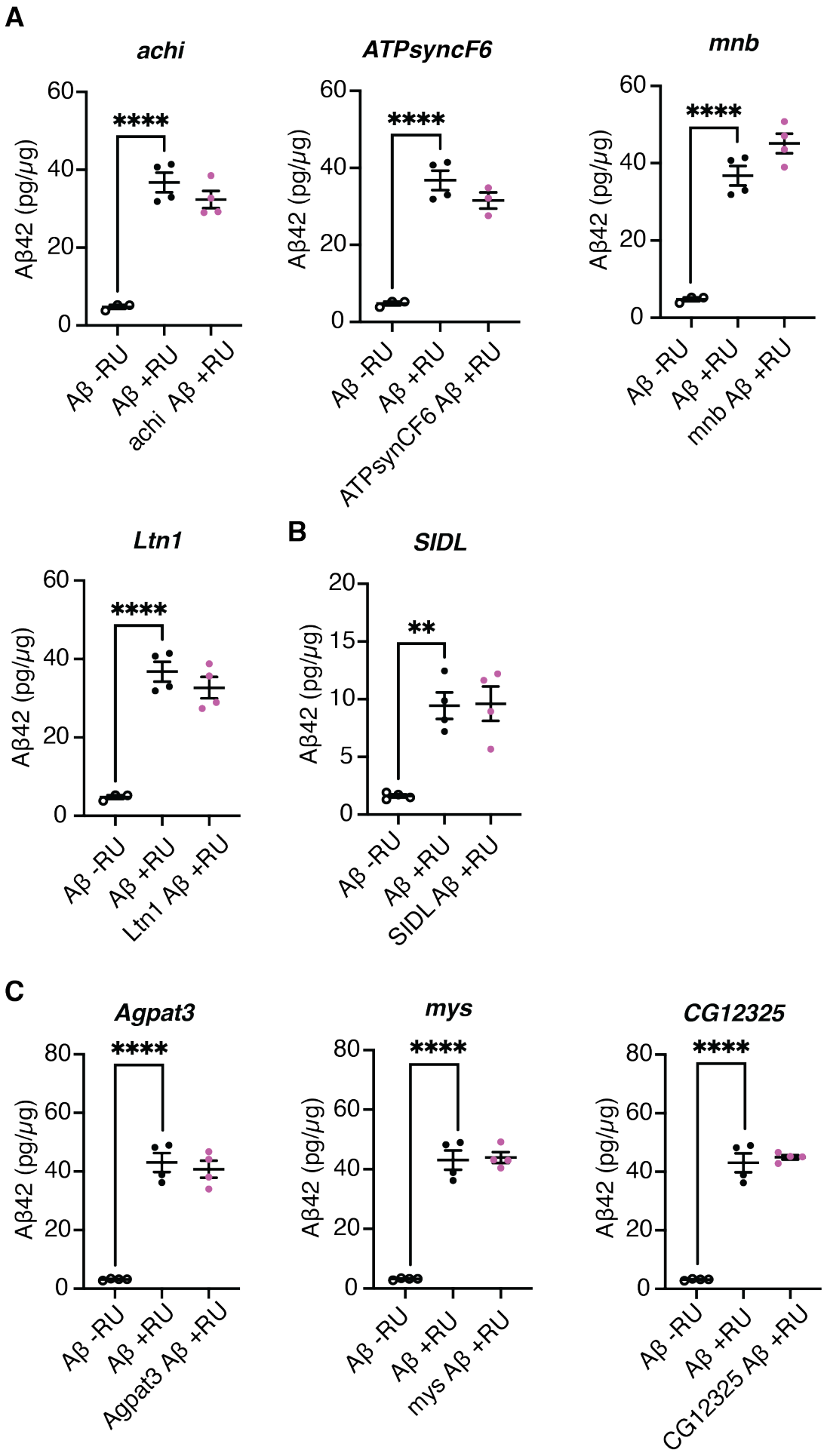
A
achi
ATPsyncF6
mnb
Aβ42 (pg/μg)
****
Aβ -RU
Aβ +RU
achi Aβ +RU
ATPsynCF6 Aβ +RU
mnb Aβ +RU
B
Ltn1
SIDL
**
Ltn1 Aβ +RU
SIDL Aβ +RU
C
Agpat3
mys
CG12325
Agpat3 Aβ +RU
mys Aβ +RU
CG12325 Aβ +RU

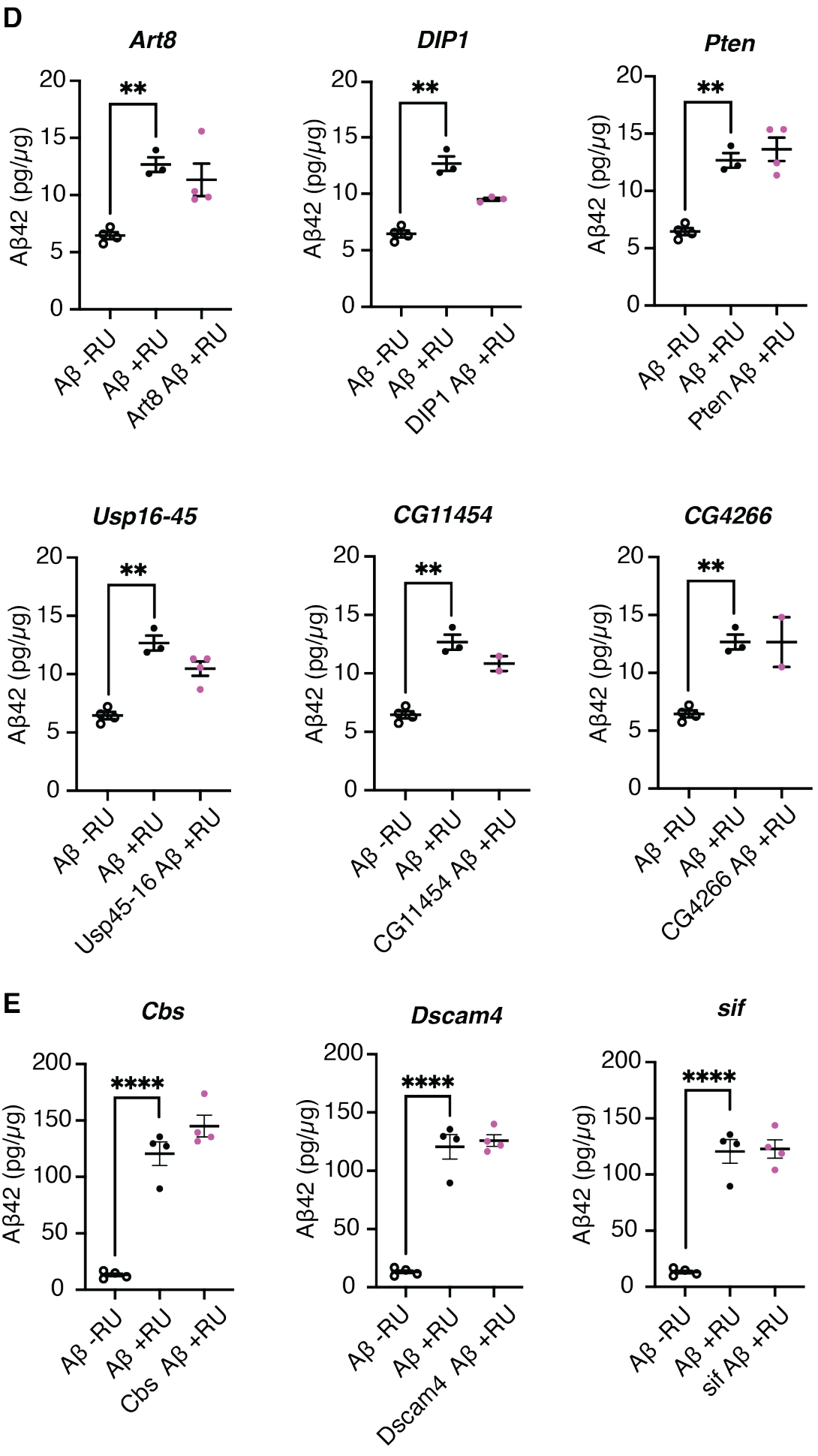
D
Art8
DIP1
Pten
Usp16-45
CG11454
CG4266
Aβ42 (pg/μg)
Aβ -RU
Aβ +RU
Art8 Aβ +RU
DIP1 Aβ +RU
Pten Aβ +RU
Usp45-16 Aβ +RU
CG11454 Aβ +RU
CG4266 Aβ +RU
**
E
Cbs
Dscam4
sif
****
Cbs Aβ +RU
Dscam4 Aβ +RU
sif Aβ +RU

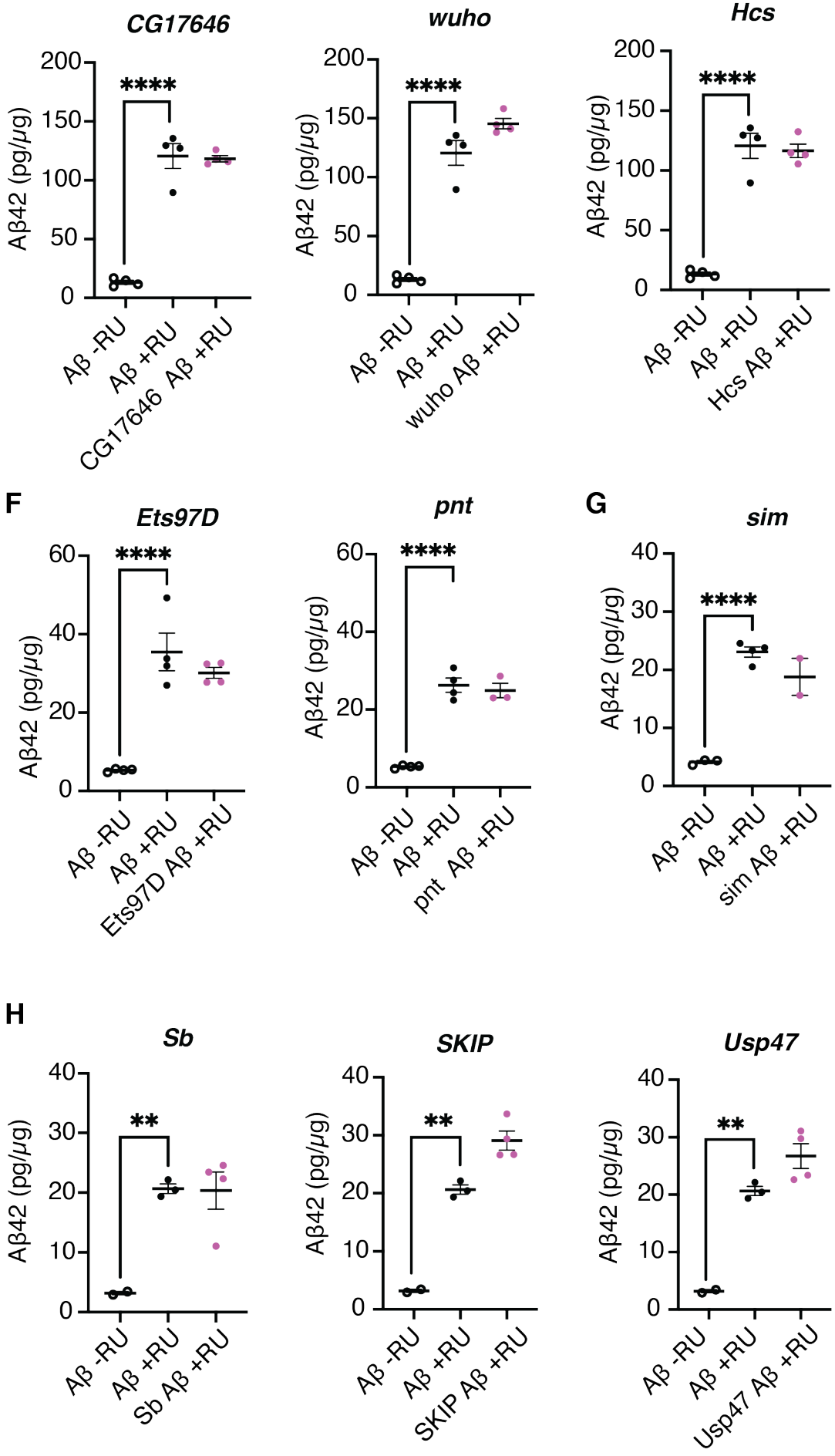
CG17646
wuho
Hcs
Aβ42 (pg/μg)
****
Aβ -RU
Aβ +RU
CG17646 Aβ +RU
wuho Aβ +RU
Hcs Aβ +RU
F
Ets97D
pnt
G
sim
Ets97D Aβ +RU
pnt Aβ +RU
sim Aβ +RU
H
Sb
SKIP
Usp47
**
Sb Aβ +RU
SKIP Aβ +RU
Usp47 Aβ +RU

Figure 3.7 ELISA of Hsa21 overexpression lines that did not modify Aβ42 accumulation.

(A-H) Amount of total Aβ42 normalised to total protein by BCA assay measured in fly heads. Expression of Aβ42 in adult neurons for 10 days significantly increased Aβ42 compared to -RU controls (black circles) (A-C, E-G $p < 0.0001$, D, H $p = 0.002$). There was no significant difference between *UAS-Aβx2*, *elavGS* +RU (black dots) and *UAS-Aβx2*, *elavGS/UAS-overexpression line* +RU (pink dots). Panel letters represent separate ELISA plates. Data are presented as mean ± SEM per gene. ** = $p < 0.01$, **** = $p < 0.0001$. n = 2-4, 10 fly heads per biological replicate per gene. Genotypes: (A-H) *UAS-Aβx2*, *elavGS,* (A) *UAS-Aβx2, elavGS/UAS-achi, UAS-Aβx2, elavGS/UAS-ATPsynCF6, UAS-Aβx2, elavGS/UAS-mnb, UAS-Aβx2, elavGS/ UAS-Ltn1,* (B) *UAS-Aβx2, elavGS/ UAS-SIDL.* (C) *UAS-Aβx2, elavGS/UAS-Agpat3, UAS-Aβx2, elavGS/UAS-mys, UAS-Aβx2, elavGS/UAS-CG12325.* (D) *UAS-Aβx2, elavGS/UAS-*Art8, *UAS-Aβx2, elavGS/UAS-DIP1, UAS-Aβx2, elavGS/UAS-Pten, UAS-Aβx2, elavGS/UAS-Usp16-45, UAS-Aβx2, elavGS/UAS-CG11454, UAS-Aβx2, elavGS/UAS-CG4266* (AC) *UAS-Aβx2* (E) *UAS-Aβx2, elavGS/UAS-Cbs, UAS-Aβx2, elavGS/UAS-Dscam4, UAS-Aβx2, elavGS/UAS-sif, UAS-Aβx2, elavGS/UAS-CG17464, UAS-Aβx2, elavGS/UAS-wuho, UAS-Aβx2, elavGS/UAS-Hcs* (F) *UAS-Aβx2, elavGS/UAS-Ets97D, UAS-Aβx2, elavGS/UAS-pnt,* (G) *UAS-Aβx2, elavGS/UAS-sim.* (H) *UAS-Aβx2, elavGS/UAS-Sb, UAS-Aβx2, elavGS/UAS-SKIP, UAS-Aβx2, elavGS/UAS-Usp47.*

Table 3.4 One-way ANOVA with Dunnett's multiple comparison.

p-values columns refer to Dunnett's multiple comparison of pan-neuronal co-overexpression of Aβ42 and Hsa21 orthologues compared with Aβ42 expression alone. Multiple comparisons included all conditions from the same plate where +RU controls are the same. Borderline significance ($p < 0.1$) is highlighted in orange.

	Gene	One-way ANOVA	p-value multiple comparisons		Gene	One-way ANOVA	p-value multiple comparisons
A	*achi*	F (5, 16) = 29.35, $p <$ 0.0001	0.541	E	*Cbs*	F (8, 27) = 39.97, $p <$ 0.0001	0.082
	ATPsynCF6		0.448		*Dscam4*		0.994
	mnb		0.073		*sif*		> 0.999
	Ltn1		0.608		*CG17464*		> 0.999
B	*SIDL*	F (4, 14) = 4.821 p = 0.012	> 0.999		*wuho*		0.074
C	*Agpat3*	F (5, 18) = 64.70, $p <$ 0.0001	0.928		*Hcs*		0.999
	mys		0.999	F	*Ets97D*	F (2, 9) = 31.05 $p <$ 0.0001	0.758
	CG12325		0.968		*pnt*	F (2, 8) = 69.24 $p <$ 0.0001	0.360
D	*Art8*	F (8, 21) = 5.049, p = 0.001	0.907	G	*sim*	F (2, 6) = 63.76 $p <$ 0.0001	0.122
	DIP1		0.238	H	*Sb*	F (4, 12) = 14.45 p = 0.002	>0.999
	Pten		0.981		*SKIP*		0.066
	Usp16-45		0.528		*Usp47*		0.226
	CG11454		0.837				
	CG4266		> 0.999				

Three of the screened Hsa21 orthologues were sufficient to modify total Aβ42 accumulation, independent of changes in Aβ toxicity. Pan-neuronal overexpression of *Plp* and *Nnp-1* significantly increased total Aβ42 in fly heads, whereas *Sod1* was sufficient to reduce levels of Aβ42 (Figure 3.8).

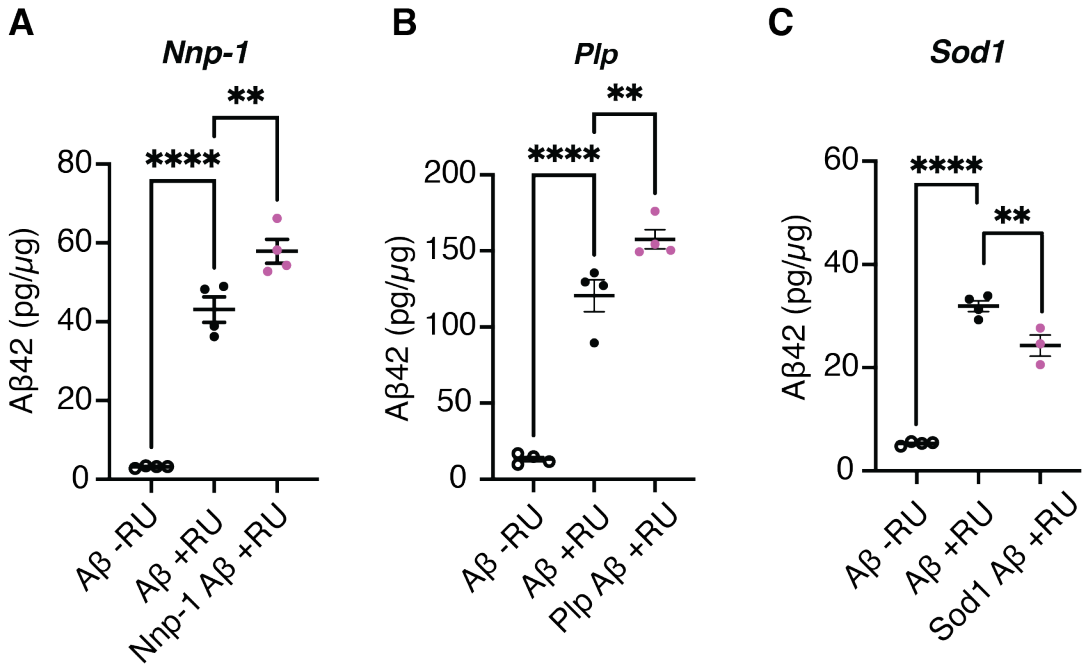

Figure 3.8 ELISA of Hsa21 overexpression lines that modified Aβ42 accumulation.

Total Aβ42 normalised to total protein by BCA assay measured in fly heads. Expression of Aβ42 in adult neurons for 10 days (black dots) significantly increased Aβ42 compared to -RU controls (black circles). (A, B) There was a significant increase in Aβ42 when *Nnp-1* or *Plp* were overexpressed in adult neurons (Table 3.5). (C) pan-neuronal overexpression of *Sod1* resulted in a significant decrease in Aβ42 (Table 3.5). n = 3-4, 10 fly heads per biological replicate. Data are presented as mean ± SEM. ** = $p < 0.01$, **** = $p < 0.0001$. Genotypes: (A, B, C) *UAS-Aβx2*, *elavGS* and (A) *UAS-Aβx2*, *elavGS/UAS-Nnp-1,* (B) *UAS-Aβx2*, *elavGS/UAS-Plp,* (C) *UAS-Aβx2*, *elavGS/UAS-Sod1.*

Table 3.5 One-way ANOVA with Dunnett's multiple comparison of pan-neuronal co-overexpression of Aβ42 and Hsa21 orthologues compared with Aβ42 expression alone.

p-values columns refer to Dunnett's multiple comparison of pan-neuronal co-overexpression of Aβ42 and Hsa21 orthologues compared with Aβ42 expression alone. Multiple comparisons included all conditions from the same plate. Significant multiple comparisons are highlighted in green.

	Gene	One-way ANOVA	p-value multiple comparisons
A	*Nnp-1*	F (5, 18) = 64.70, p <0.0001	p = 0.001
B	*Plp*	F (2, 9) = 111.2, p <0.0001	p = 0.004
C	*Sod1*	F (8, 27) = 39.97, p <0.0001	p = 0.004

3.2.5 Re-screen of identified targets

An initial screen identified six Hsa21 orthologues, *ATPsynCF6, Hcs, mnb*, *Sb, SKIP* and *Usp47,* as potential modifiers of Aβ toxicity in *Drosophila*. In order to validate those findings, I repeated the negative geotaxis assays for these identified hits (Figure 3.9). Interestingly, *mnb* was the only Hsa21 orthologue where the initial significant rescue of the Aβ induced climbing defect could be replicated. Notably, *UAS-Aβx2*, *elavGS/UAS-mnb* flies also showed a significant rescue in climbing speed in the uninduced condition (Figure 3.9B). When 'RU' was included as a co-factor in the linear model, the interaction of genotype and age remained significant, indicating that induction of Aβ and *mnb* expression significantly modified climbing speed with age. Thus, the observed rescue in the induced condition can be attributed to *mnb* overexpression.

Overexpression of *SKIP* also showed a trend towards significance of modified climbing speed with age in the replication study ($p \leq 0.1$, Figure 3.9D). However, modification of Aβ toxicity with age was not replicated for *ATPsynCF6, Hcs*, *Sb* and *Usp47* overexpression, demonstrating the importance of re-screening (Figure 3.9A,C). Repeats of *Usp47* and *ATPsynCF6* will be further discussed in Chapters 4 and 5, respectively. Due to a lack of expression of its Hsa21 orthologue in the human brain, I decided to exclude *Sb* from further characterisation (Krause *et al.*, 2022). These findings suggest that negative geotaxis assays in the fly are susceptible to environmental and genetic confounding factors which will be discussed in section 3.3.

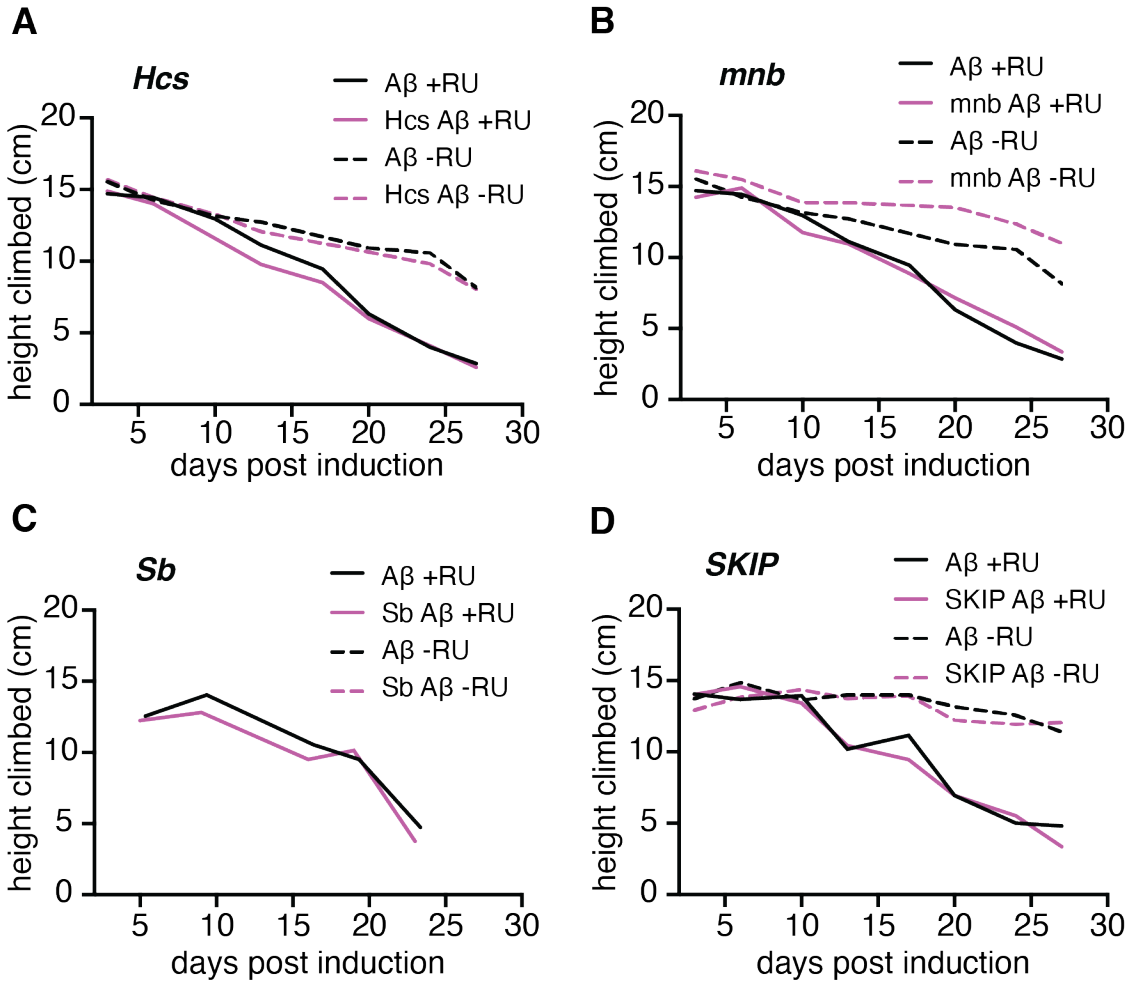

Figure 3.9 Re-screen of hits identified in the initial screen.

Average height climbed across the lifespan by flies pan-neuronally expressing Aβ42, with (pink lines) or without (black lines) overexpression of an Hsa21 orthologue in adult

neurons (solid lines, induced by RU-486) and uninduced controls (dashed lines). n = ~ 75 flies per condition. All p-values refer to simple linear regression of the interaction between age and genotype unless stated otherwise (Table 3.6). Genotypes: (A-D) *UAS-Aβx2*, *elavGS* (A) *UAS-Aβx2*, *elavGS/UAS-Hcs,* (B) *UAS-Aβx2*, *elavGS/UAS-mnb,* (C) *UAS-Aβx2*, *elavGS/UAS-Sb,* (D) *UAS-Aβx2*, *elavGS/UAS-SKIP*. Full statistical results are presented in Table S3.4.

Table 3.6 Linear models of induced (+RU) Aβ expressing flies compared with co-overexpression of an Hsa21 orthologue.

Statistically significant results are highlighted in green, borderline significance ($p < 0.1$) is highlighted in orange.

Gene		**p-values**		
		+RU	-RU	effect of RU
A	*Hcs*	0.667	0.948	-
B	*mnb*	0.043	0.0174	0.005
C	*Sb*	0.127	-	-
D	*SKIP*	0.097	0.257	-

3.2.6 Assessment of Hsa21 orthologue expression levels

To confirm that the observed impact on climbing speed can be attributed to overexpression of the Hsa21 orthologues, I measured their mRNA levels in heads of flies induced for 15 days by RT-qPCR. *ATPsynCF6, mnb, SKIP* and *Usp47* mRNA levels were significantly increased compared to uninduced *UAS-Aβx2*, *elavGS* controls. *Hcs* showed a trend towards elevated levels of its transcript. However, there was a large range of expression levels between biological replicates and the increase compared with controls was not statistically significant despite an observed rescue compared to flies overexpressing Aβ alone (Figure 3.10).

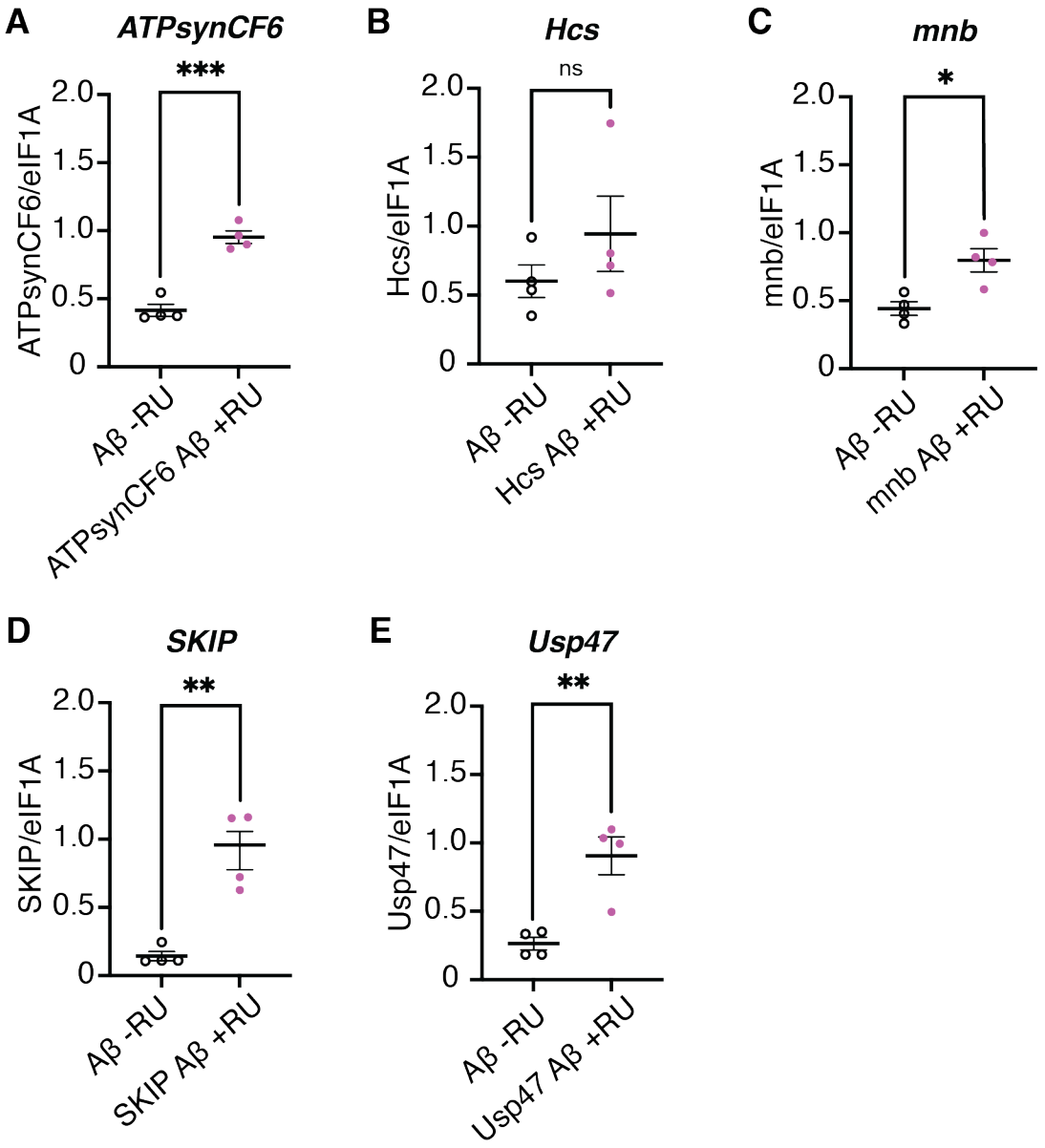

Figure 3.10 Expression levels of Hsa21 orthologues identified as phenotypic hits in the screen.

ATPsynCF6, Hcs, mnb, SKIP and *Usp47* (pink dots) mRNA levels compared to -RU controls (black circles) measured by RT-qPCR. mRNA levels are relative to eIF1A. Data are presented as mean ± SEM. * = $p < 0.05$, ** = $p < 0.01$, *** = $p < 0.001$. P-values refer to two-tailed unpaired t-test (Table 3.7). Genotypes: (A-E) *UAS-Aβx2, elavGS,* (A) *UAS-Aβx2, elavGS/UAS-ATPsynCF6,* (B) *UAS-Aβx2, elavGS/UAS-Hcs, UAS-Aβx2,* (C) *UAS-Aβx2, elavGS/UAS-mnb,* (D) *UAS-Aβx2, elavGS/UAS-SKIP,* (E) *UAS-Aβx2, elavGS/UAS-Usp47*.

Table 3.7 Unpaired t-test of induced (+RU) Aβ expressing flies with co-overexpression of a Hsa21 orthologue compared with uninduced *UAS-Aβx2*, *elavGS* flies.

Statistically significant results are highlighted in green.

	Gene	t statistic	p-value
A	*ATPsynCF6*	t(6) = 8.435	0.0002
B	*Hcs*	t(6) = 1.150	0.294
C	*mnb*	t(6) = 3.607	0.011
D	*SKIP*	t(6) = 5.343	0.002
E	*Usp47*	t(6) = 4.399	0.0046

3.2.7 Assessment of changes in the soluble and insoluble fractions of Aβ42

In AD, Aβ first accumulates in a soluble state before aggregating into fibrils and plaques. Transgenic expression of Aβ42 in *Drosophila* results in the accumulation of both soluble and insoluble Aβ42. A positive correlation between insoluble Aβ42 levels and worsening of the climbing deficit phenotype has been reported (Sofola *et al.*, 2010; Rogers *et al.*, 2012). I therefore wanted to determine whether there was a change in the soluble or insoluble fraction that could explain the modification in climbing speed observed in my screen. Initially, I ran a pilot experiment, adapting my total Aβ42 ELISA protocol to separate the soluble and insoluble fractions. For this, the Diethanolamine (DEA) soluble fraction was obtained as the supernatant following high-speed centrifugation (135,000 rcf). To generate the insoluble fraction, the remaining pellets were suspended in formic acid before being solubilised. For the pilot study, I used *UAS-Aβx2*, *elavGS* flies that had been fed on -RU or +RU containing food for 10 days. In both fractions, levels of Aβ42 were lower in the -RU compared to +RU conditions, although with n = 1 per condition, statistically significant differences could not be confirmed. The majority of Aβ42 was found to be present in the insoluble form (Figure

3.11A). Subsequently, I used this protocol for an independent set of samples from the total Aβ42 ELISA to test for changes in the distribution of Aβ42 between the soluble and insoluble fractions in my phenotypic screen hits.

In the soluble fraction, there was no significant difference between the induced and uninduced flies which may be due to overall low levels of this form of Aβ42 in fly heads or strong leakage of Aβ expression in the -RU condition. Flies overexpressing *mnb* and Aβ42 had significantly increased soluble Aβ levels compared with expression of Aβ42 alone. Overexpression of *ATPsynCF6, Hcs, Usp47* or *SKIP* did not result in modified accumulation of soluble Aβ42 (Figure 3.11B). In the insoluble fraction, Aβ42 levels were found to be significantly higher in +RU compared with -RU flies. No significant modification of insoluble Aβ42 levels was observed by over-expression of any of the Hsa21 orthologues studied here, compared with the control +RU condition (Figure 3.11C). However, overall levels of Aβ42 in the insoluble fraction were lower than expected based on the pilot experiment and published data (Catterson *et al.*, 2023). This may be due to the aggregated forms of Aβ42 not being fully solubilised during sample preparation, resulting in less Aβ42 being detected by the ELISA. In summary, these data indicate that levels of accumulation in the soluble fraction can occur independently of changes in total Aβ42.

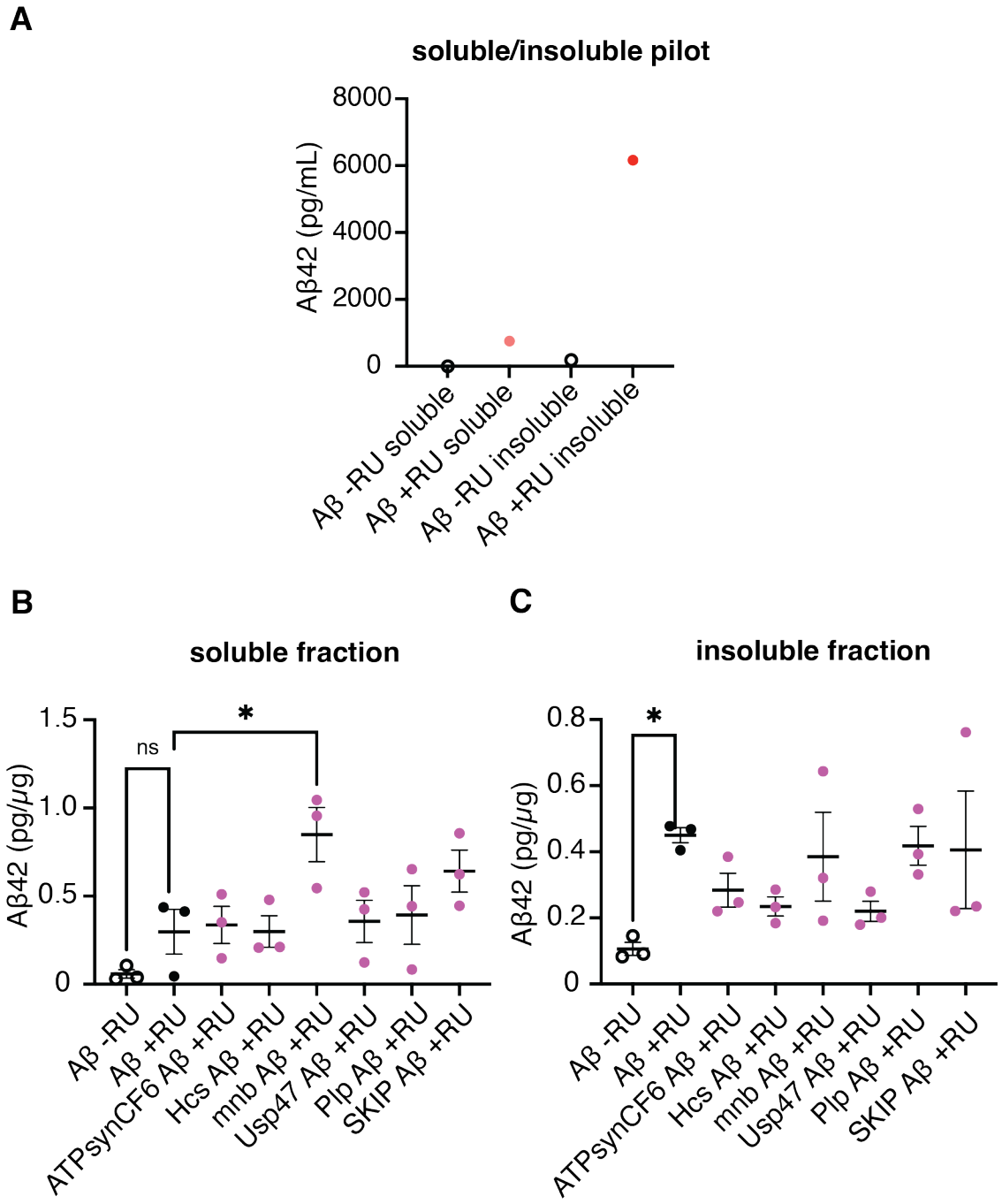

Figure 3.11 ELISA of the soluble and insoluble Aβ42 fraction for Hsa21 orthologue phenotypic hits identified in the screen.

Amount of soluble and insoluble Aβ42 measure by ELISA and normalised to total protein by BCA assay in fly heads induced for 10 days. (A) pilot experiment of *UAS-Aβx2*, *elavGS* flies induced (red dots) and uninduced (black circles) for 10 days. n = 1, 50 fly heads per biological replicate. (B) Soluble Aβ42 levels. One-way ANOVA with

Dunnett's multiple comparisons test, F (7, 16) = 3.987, $p = 0.010$, -RU (black circles) vs +RU controls (black dots) $p = 0.59$. n = 3, 30 fly heads per data point (Table 3.8). (C) Insoluble Aβ42 levels. One-way ANOVA with Dunnett's multiple comparisons test, F (7, 16) = 1.994, $p = 0.120$, -RU vs +RU controls $p = 0.012$ (Table 3.8). * = $p < 0.05$. Data are presented as mean ± SEM. Genotypes: *UAS-Aβx2*, *elavGS, UAS-Aβx2*, *elavGS/UAS-ATPsynCF6, UAS-Aβx2*, *elavGS/UAS-Hcs, UAS-Aβx2*, *elavGS/UAS-mnb, UAS-Aβx2 elavGS/UAS-SKIP, UAS-Aβx2*, *elavGS/UAS-Usp47*.

Table 3.8 One-way ANOVA with Dunnett's multiple comparisons test.
All p-values refer to one-way ANOVA with Dunnett's multiple comparisons test of +RU control vs overexpression line. Statistically significant results are highlighted in green, borderline significant ($p < 0.1$) results are highlighted in orange.

	soluble	**insoluble**
Gene	**p-value**	**p-value**
ATPsynCF6	> 0.999	0.188
Hcs	> 0.999	0.093
mnb	0.027	0.599
Usp47	> 0.999	0.075
SKIP	> 0.999	0.7190

3.3.8 Lifespans of Hsa21 orthologue hits

Negative geotaxis assays are a measure of locomotor and neuronal health and can be an indicator of how flies respond to the toxic expression of Aβ42 when an Hsa21 orthologue is overexpressed. To explore whether the identified orthologues could also modify Aβ induced decrease in survival, I next performed lifespan assays. For this, I compared lifespan curves of induced *UAS-Aβx2*, *elavGS* flies which had a median lifespan of 36.5 days with those overexpressing one of the identified Hsa21 orthologues, in addition to Aβ42. *UAS-Aβx2*, *elavGS/UAS-Hcs* flies had an extended overall lifespan suggesting that the initially observed climbing rescue (Figure 3.4B) is also reflected in increased longevity of the flies (Figure 3.11A). Pan-neuronal

overexpression of *mnb* or SKIP did not significantly impact lifespan of Aβ expressing flies in these experiments (Figure 3.12B,C). Pan-neuronal overexpression of *Usp47* or *ATPsynCF6* also did not result in a significant change in longevity in the presence of Aβ expression (these are presented in their dedicated Chapters 4 and 5, respectively).

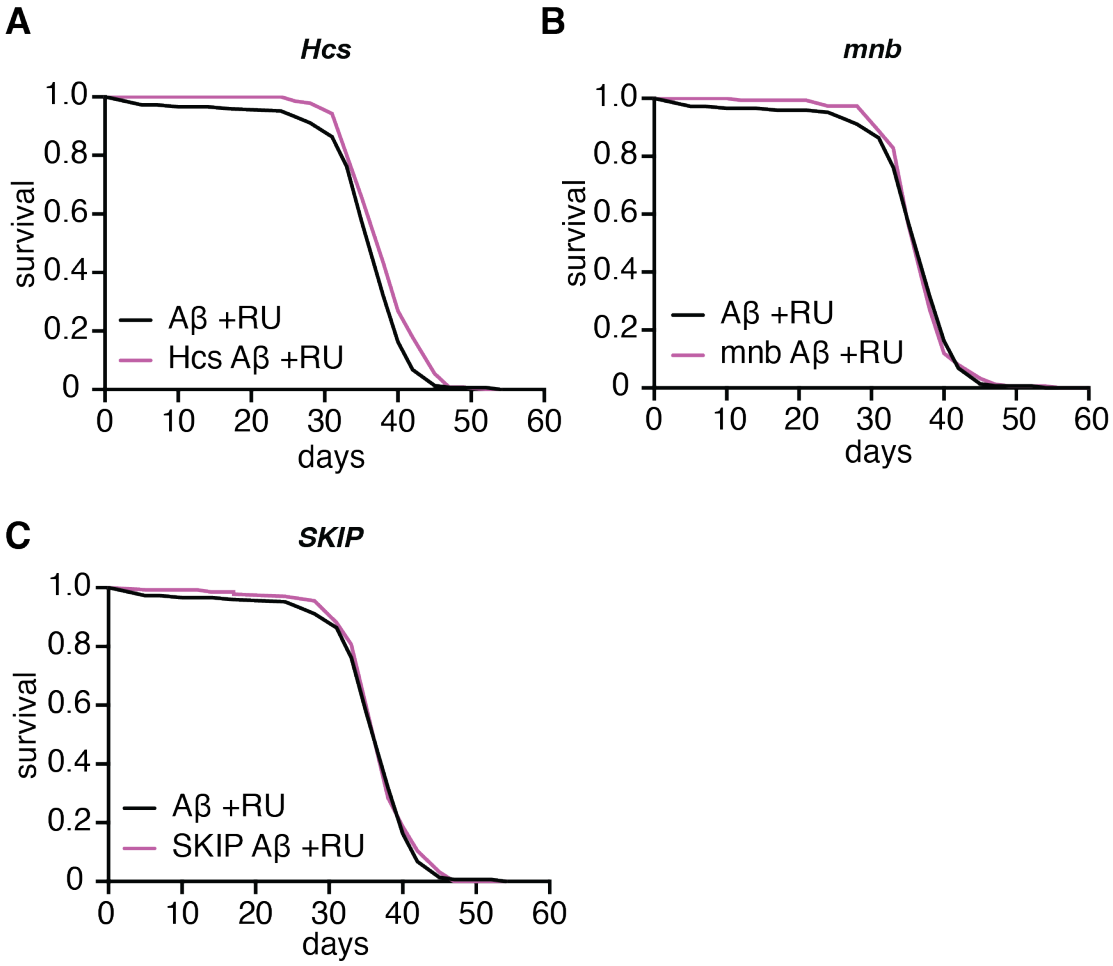

Figure 3.12 Lifespans of Hsa21 orthologue hits identified in the screen.

Lifespan curves of *UAS-Aβx2*, *elavGS* flies (black line) compared with those co-overexpressing an Hsa21 orthologue (pink line). n = ~150 flies per condition. All p-values refer to log-rank test. (A) Lifespan of induced *UAS-Aβx2*, *elavGS* flies was significantly extended by overexpression of *Hcs* (p = 0.0247). (B) Lifespan of flies overexpressing *mnb* did not differ significantly from controls (p = 0.519). (C) Lifespan of flies overexpressing *SKIP* flies did not differ significantly from controls (p = 0.740). Genotypes: (A-C) *UAS-Aβx2*, *elavGS* (A) *UAS-Aβx2*, *elavGS/UAS-Hcs,* (B) *UAS-*

Aβx2, *elavGS/UAS-mnb* (C) *UAS-Aβx2*, *elavGS/UAS-SKIP.* Full statistical results are presented in Table S3.5.

3.3 Discussion

3.3.1 Summary of findings

For this *Drosophila* screen, I identified 76 orthologues of Hsa21 genes, triplicated in the Tc1 mouse model of DS. Of those, 35 could be investigated to assess whether their pan-neuronal overexpression can modify Aβ toxicity and accumulation. During an initial screen using the negative geotaxis assay as a readout, five overexpression lines, *Hcs, mnb, Sb, SKIP* and *Usp47*, rescued the Aβ induced climbing defect whereas *ATPsynCF6* worsened the phenotype. With the exception of *mnb*, this occurred independently of changes in Aβ accumulation, suggesting that Hsa21 orthologues can modify the flies' response to Aβ without changing the amount of the peptide that accumulates in my model system.

Additionally, flies overexpressing the Hsa21 orthologues, *Nnp-1* and Plp had increased levels of total Aβ42 whereas overexpression of *Sod1* was sufficient to decrease Aβ42 in heads after 10 days of induction. Flies co-overexpressing Aβ42 and *mnb* showed a decrease in soluble Aβ42. This demonstrates that the level of Aβ present in fly heads does not necessarily predict climbing speed in this model. Of the identified hits, *mnb* was the only gene that consistently rescued the climbing defect. We decided to further investigate Hsa21 orthologues that resulted in a phenotypic modification when co-overexpressed with Aβ to determine whether toxicity extended beyond locomotor function.

Further investigation of the initially identified hits demonstrated that the observed changes in neuromotor function or amyloid accumulation were not reflected in changes in lifespan of Aβ expressing flies when *mnb, SKIP*, or *Usp47* were co-

overexpressed. However, in addition to rescuing the climbing defect, the lifespan of induced *UAS-Aβx2*, *elavGS* flies was significantly extended when *Hcs* was also expressed in adult neurons. Overall, my *Drosophila* screen identified candidate genes of Aβ42 toxicity and accumulation whose orthologues may impact amyloid pathology in AD-DS when overexpressed (Table 3.9).

Table 3.9 Summary of findings from the *Drosophila* screen of Hsa21 orthologues.

Changes in negative geotaxis, total, soluble and insoluble Aβ and lifespan of Aβ expressing flies co-overexpressing *ATPsynCF6, Hcs, mnb, Nnp-1, Plp, Sb, SKIP, Sod1 or Usp47* compared with those expressing Aβ alone. Green = rescue/decrease, red = exacerbation/increase, orange = borderline significant increase.

Gene Name	Negative geotaxis defect	Total Aβ42 accumulation	Soluble Aβ42 accumulation	Insoluble Aβ42 accumulation	Lifespan
ATPsynCF6	worsened	no change	no change	no change	no change
Hcs	rescued	no change	no change	no change	extended
mnb	rescued	no change	increase	no change	no change
Nnp-1	no change	increase	-	no change	-
Plp	no change	increase	no change	no change	-
Sb	rescued	no change	no change	no change	-
SKIP	rescued	no change	no change	no change	no change
Sod1	no change	decrease	-	no change	-
Usp47	rescued	no change	no change	no change	no change

3.3.2 Potential mechanisms of modified Aβ toxicity by overexpression of Hsa21 orthologues

DYRK1A is the most extensively studied gene whose orthologue *mnb* was identified as a consistent modifier of Aβ toxicity and accumulation in our study. This Hsa21 encoded gene is a member of the DYRK family of kinases and is ubiquitously expressed throughout life with particularly high expression levels in the central nervous system (CNS), including neuronal cells and, to a lesser extent, astrocytes and microglia (Martí *et al.*, 2003; Wegiel *et al.*, 2004; Atas-Ozcan *et al.*, 2021). Within the brain, DYRK1A phosphorylation of tyrosine, serine and threonine sites targets proteins involved in cytoskeletal formation, impacting neurogenesis and is sufficient to inhibit neuronal morphology and proliferation in vitro and in vivo when overexpressed (Yabut *et al.*, 2010; Martinez De Lagran *et al.*, 2012). It is known to be dosage sensitive in the DS brain and has also been found to be upregulated in AD (Ferrer *et al.*, 2005; Kimura *et al.*, 2007; Palmer *et al.*, 2021).

During AD pathogenesis, DYRK1A has been implicated in APP processing through hyperphosphorylation of threonine residues on APP and PSEN1 in vitro and mouse models (Ryoo *et al.*, 2008; Ryu *et al.*, 2010). In agreement with our study which saw an increase in soluble Aβ in *mnb* overexpressing flies (and a borderline significant increase in total Aβ42), these studies observed an increase in Aβ when *DYRK1A* was overexpressed. Notably, the mouse studies proposed an interaction of DYRK1A with the APP amyloidogenic processing pathway rather than a direct impact on Aβ. The *Drosophila* orthologue *mnb* is thought to be functionally conserved with *DYRK1A* as its overexpression has also been shown to impact the neurodegenerative phenotype in flies. Pan-neuronal overexpression of *mnb* (without co-overexpression of Aβ) resulted in worsened climbing ability and shortened lifespan (Lowe, Usowicz and Hodge, 2019). Additionally, pharmacological inhibition of mnb has been shown to partially rescue the locomotor deficit and lifespan of flies pan-neuronally expressing Aβ42 (Zhu, Parsons, Foley, *et al.*, 2022). My results stand in contrast to these findings, indicating a potential benefit of *mnb* overexpression. Importantly, the mechanism by

which overexpression of *mnb* rescued Aβ toxicity and accumulation in our work was independent of the rate of APP processing as our *Drosophila* model expresses Aβ directly. Therefore, *mnb* overexpression is more likely to impact Aβ by altering its toxicity and rate of clearance through increased kinase activity. Knockdown or inhibition of mnb in our model could provide further insight into how this protein may impact Aβ toxicity and accumulation.

We also observed a rescue of the climbing phenotype in flies co-overexpressing Aβ and *Hcs, Sb, SKIP* or *Usp47*. Notably, though I observed a rescue of both climbing speed with age and lifespan, *Hcs* was not significantly elevated as measured by qPCR. However, I measured mRNA levels of induced flies carrying constructs for both Aβ and *Hcs* overexpression and compared levels to uninduced flies carrying the Aβ construct as a negative control. It is therefore possible that the presence of Aβ lowered *Hcs* levels in these flies. To determine whether this is the case, mRNA levels should be reassessed using induced *elavGS/UAS-Hcs* flies with *elavGS* as a negative control. The mechanism by which *Hcs* or its human orthologue *HLCS* may interact with Aβ has not been previously investigated.

In *Drosophila*, *SKIP* codes for a potassium channel interacting protein with endogenous neuronal expression that has been implicated in olfactory function. Its human orthologue TMPRSS2 has not been studied in connection with AD-DS and is very lowly expressed in neurons, suggesting that my findings of an Aβ toxicity rescue may not translate to individuals with AD-DS (Y. Zhang *et al.*, 2016a). Similarly, *Sb* orthologue *SAMSN1* has very low levels of expression in human neurons (Y. Zhang *et al.*, 2016a). However, microglial expression of this Hsa21 gene is high and, moreover counter-intuitively there is some evidence of decreased protein abundance in DS foetal brains (Cheon *et al.*, 2003). Additionally, this gene has been identified as a LOAD GWAS gene that became significantly upregulated in microglia when exposed to Aβ, though an underlying mechanism for this has not been elucidated (Sierksma *et al.*, 2020). There is evidence that Hsa21 orthologues of two further modifiers of Aβ toxicity *Usp47* and *ATPsynCF6*, identified in our screen, may be linked to AD

pathology in individuals with DS. This will be discussed in more detail in Chapters 4 and 5. 1

3.3.3 Potential mechanisms of modified Aβ accumulation by Hsa21 orthologues

My screen identified four potential modifiers of Aβ accumulation: *mnb* (discussed above), *Nnp-1, Plp,* and *Sod1*. Of these, *Nnp-1* and *Plp* were sufficient to raise total Aβ levels when pan-neuronally overexpressed for 10 days. *Nnp-1* and its human orthologue RRP1 code for ribosomal RNA processing genes with low levels of expression in the CNS. There is no previous knowledge of their potential role in AD-DS. The Hsa21 orthologue of *Plp, PCNT*, has been found to be dosage sensitive in leucocytes isolated from DS individuals (Salemi *et al.*, 2013). Though it is known to be expressed in neurons, whether this gene is overexpressed in the DS brain and whether it interacts indirectly or directly with Aβ is not known.

My ELISA results show a decrease in total Aβ42 levels in response to *Sod1* overexpression. The function of *Sod1* and its human orthologue *SOD1* which codes for an enzyme that facilitates the conversion of superoxide radicals to molecular oxygen and hydrogen peroxide (H_2O_2) has been mostly studied in relation to amyotrophic lateral sclerosis (ALS), another neurodegenerative condition (Şahin *et al.*, 2017). Although activity level varies by cell type, an increase in SOD1 dosage has been observed in the brains from individuals with DS, leading to an overproduction of H_2O_2 (Gulesserian *et al.*, 2001). An increasing number of studies are also implicating SOD1 in AD and it has been identified as a shared risk factor gene for AD and AD-DS (Sharma *et al.*, 2020). One study examining its activity in cell culture found Aβ directly interacts with SOD1, impairing its enzymatic activity (Eun *et al.*, 2009). Therefore, despite a lack of alteration to the neuromotor phenotype, an interaction between Aβ and Sod1 may result in lowered Aβ levels in my *Drosophila* model system, though the mechanism by which this occurred is not clear. Although modification in climbing speed of the identified modifiers of Aβ accumulation (*Nnp-1, Plp* and *Sod1*) did not

reach statistical significance, all three had p-values < 0.07 for the age and genotype interaction term in the +RU conditions, suggesting a potential subtle effect of locomotor function.

Interestingly, my data indicate that an increase in Aβ42 level was not necessarily reflected in a worsening of the Aβ42 climbing defect and vice versa. Overexpression of *Plp* showed a trend towards slower climbing speed with age in line with increased accumulation of Aβ42. Surprisingly, the Aβ42 induced climbing defect showed a trend towards being rescued despite increased Aβ42 levels when *Nnp-1* was overexpressed. Similarly, a borderline non-significant worsening of climbing speed was observed in *Sod1* overexpressing flies with significantly lower levels of Aβ42. Overall, these results suggest that the potential modest changes in Aβ42 accumulation resultant from over-expression of Hsa21 orthologues in the fly model used here may not be sufficient to affect the negative geotaxis phenotype. Moreover, in my model system, I observed modified climbing speeds in the absence of any significant changes in total Aβ42 levels.

Hsa21 orthologues that when over-expressed rescue or worsen the climbing performance of flies in the negative geotaxis assay did not present modified total Aβ42 levels. I therefore wanted to determine whether the observed changes in neuromotor function could be attributed to altered levels of the soluble and insoluble fractions of Aβ. With the exception of *mnb* (which resulted in a significant increase), soluble Aβ42 levels were not altered by overexpression of these hits. Within the insoluble fraction, none of the tested hits led to a change in Aβ42, though there was a trend towards lower levels for *Hcs* and *Usp47*, consistent with their climbing rescue ($p < 0.1$). Overall levels of insoluble Aβ were lower than expected in relation to soluble levels based on my pilot experiment and published data (Catterson *et al.*, 2023). Notably, Catterson *et al.* investigated flies that were 1.5 weeks older than those in my study which would result in higher levels of Aβ. Repeating my experiment, ensuring the full solubilisation of aggregated Aβ during sample preparation, would give insight into whether insoluble Aβ may have been underestimated.

3.3.4 Genes of interest that could not be investigated in this study

Human chromosome 21 contains over 230 protein coding genes. Despite 35 genes that were included in this genetic modifier screen, there are also many whose effect on Aβ42 biology could not be investigated. Notably, these include genes that have previously been implicated in AD-DS. Firstly, overexpression of the β-secretase gene *BACE2* resultant from trisomy of human chromosome 21 has been proposed to act as a suppressive factor of Aβ pathology in individuals who have DS (Alić *et al.*, 2021). BACE2 has been proposed to act via two potential mechanisms; either as a θ-secretase (degrading the APP β-CTF and preventing the formation of Aβ), or as an Aβ-degrading protease. Notably, only its putative role as an Aβ-degrading protease can be investigated in my model system. The *Drosophila* orthologue *CG17134* was not included due to a lack of available overexpression lines. Notably, endogenous *BACE2* expression in human neurons is low, suggesting that any potential findings due to overexpression of the fly orthologue in neurons may not translate to its role in AD-DS (Y. Zhang *et al.*, 2016a).

Another notable gene that is missing from my study with no publicly available overexpression lines is SUMO family protein *smt3*. Its human orthologue *SUMO3* codes for a protein involved in post-translational modification (Hochstrasser, 2001). In vitro, overexpression of SUMO2/3 has been shown to reduce Aβ generation through polysumoylation of APP (Li *et al.*, 2003). In contrast, another study found that overexpression of *SUMO3* significantly increased full-length and C-terminal fragments of APP as well as Aβ production, proposing that this may be a result of increased γ-secretase concentration (Dorval *et al.*, 2007). By cloning *smt3*, an inducible overexpression line could be created to investigate whether overexpression of *smt3* can modify Aβ toxicity and accumulation in *Drosophila*.

3.3.5 Strengths and limitations of this *Drosophila* screen

Much of the AD-DS mechanistic research has been carried out using rodent models, with a particular focus on mice. However, this comes with many ethical challenges of using animals for research as well as a high cost and longer experimental timelines, making them unsuitable for large-scale genetic screens. In recent years, there have been major advances in the development of experimental techniques that provide a full replacement of animals, including cell culture and organoids for AD-DS research (Y. Wu *et al.*, 2022; Watson and Meharena, 2023). While these systems are biologically relevant to AD-DS because of their use of human rather than animal cells, they can only capture the effects on isolated cell types. The advantage of using *Drosophila* for this genetic modifier screen is that despite the genetic and physiological differences to humans, they provide an effective and quick way to assess the effects of overexpressing Hsa21 orthologues at an organismal level. Furthermore, I was able to track these effects throughout the lifetime of the same animals.

Rodent models of amyloid pathology carry human or mouse *APP/App* gene (many with FAD mutations) that is processed to form Aβ (Mucke *et al.*, 2000; Saito *et al.*, 2014). Therefore, changes to Aβ toxicity or accumulation as a result of Hsa21 overexpression could be due to the way APP is processed and may reflect an artefactual interaction of Hsa21 orthologues and the effect of FAD causal mutations. In contrast, the *Drosophila* model of AD used in our study allowed us to isolate the impact of raised Aβ levels specifically, in the absence of this potential confound. Additionally, the Aβx2 fly model was specifically developed to mimic APP duplication and the expression of wildtype Aβ in our model closely mimics the genetics of AD-DS (Casas-Tinto *et al.*, 2011).

Another important difference between DS, where Hsa21 genes are triplicated in all cells from development through to adulthood (with the exception of the rare mosaic form) and our modelling approach is the restriction of Hsa21 orthologue overexpression to adult neurons. This allows us to isolate the effects of overexpression during the life-stage when Aβ accumulates in the brain of individuals with DS, from the

developmental effects of overexpression of these genes. However, this also presents a limitation of our approach, as increased levels of Hsa21 genes during development may impact how DS individuals respond to Aβ toxicity in adulthood. Overall, we found that overexpression of only a small proportion of screened Hsa21 orthologues was sufficient to modify Aβ toxicity and accumulation in our initial screen despite evidence that an extra copy of their orthologues exacerbates Aβ aggregation and toxicity in a mouse model of AD-DS (Wiseman *et al.*, 2018). However, there are some important differences between the two approaches. In the mouse study, the observed effects of having an extra copy of most Hsa21 genes may have required the interaction of multiple genes which could not be modelled in our single gene screen approach. Additionally, the Tc1 mouse model used by Wiseman *et al.* is mosaic, meaning that not all cells carry the additional human chromosome which may confound results relating to the effect of gene triplication on AD-DS (O'Doherty *et al.*, 2005).

Several technical limitations should be considered when interpreting results. Firstly, statistical analysis of the negative geotaxis assay assumes each individual fly to be a separate biological replicate, resulting in a high n number (Sofola *et al.*, 2010; Rogers *et al.*, 2012). Therefore, very small differences in climbing speed with age can become statistically significant. This was particularly notable when *mnb* was found to significantly rescue the Aβ induced climbing defect in my initial screen. The linear model assessed differences in the rate of decline which was found to be lower compared with expression of Aβ alone. Notably, this lower rate of decline was driven by a slower climbing speed on day 5 only. However, induced *UAS-Aβx2*, *elavGS/UAS-mnb* flies maintained a significant rescue during the rescreen, suggesting that its overexpression slows neuromotor decline with age. As was observed with other genes identified as modifiers of Aβ toxicity, marginal effects may be difficult to replicate in a biological system where subtle environmental changes can influence phenotypic readouts (Hoffman *et al.*, 2021). An alternative way of assessing the negative geotaxis response is a more recently developed automated system that calculates the velocity of flies per vial (Spierer *et al.*, 2021). This allows for faster processing of the data and may also improve replicability.

Secondly, a potential reason for the low repeatability between experiments in this study may be attributable to the *Drosophila* food. Although the media recipe remained consistent throughout my work, there was an unavoidable change in the batch of yeast, a major component of the flies' diet. Within our laboratory, this is known to affect several experimental outcomes. In my case, during the negative geotaxis assays, flies initially started dying around day 30, which was reduced by about a week after a change in yeast batch. Climbing assays were terminated when >10% of flies had died. This was to avoid misinterpreting dead flies as not having climbed in the analysis and assessing climbing speed of flies biased to be longer lived. However, this resulted in a lack of consistency across all screened lines. To increase repeatability of hits, future screens should therefore ensure consistent components of fly media throughout all experiments.

Finally, differences in the genetic background may also have contributed to overexpression lines not showing robust rescue or worsening of the climbing phenoptype. All fly lines were backcrossed at the start of the initial screen and may have genetically drifted by the time they were being rescreened.

Three of the Hsa21 orthologues included in our screen that did not show a modification of the Aβ induced climbing defect have been implicated in affecting locomotor function in the literature. (1) the Hsa21 encoded gene *DSCAM* has four paralogues (*Dscam1, 2, 3* and *4*) in *Drosophila*. A study investigating ubiquitous overexpression of *Dscam1* found that it was sufficient to impair locomotor activity and modify synaptic function at the larval stage (Lowe, Hodge and Usowicz, 2018b). However, in our study, overexpression was restricted to adult neurons and any impairment in neuromotor function due to overexpression of *Dscam4* may have been masked by co-overexpression of Aβ. (2) *Pfk*, another gene included in our screen, has previously been shown to rescue locomotor deficits when overexpressed in motor neurons in a *Drosophila* model of ALS (Manzo *et al.*, 2019). However, in our screen, pan-neuronal overexpression did not rescue the Aβ induced locomotor deficit, suggesting that the published rescue may be specific to their investigated model of neurodegeneration. (3) We did not find a significant interaction between co-overexpression of Aβ and *Cbs*

with climbing speed across the lifespan. Shaposhnikov *et al*. showed that overexpression of *Cbs* was sufficient to rescue the locomotor phenotype with age (measured by an alternative readout of sponateous locomotor activity) when overexpressed ubiquitously but did not investigate its role in the presence of amyloid (Shaposhnikov *et al*., 2018).

3.3.6 Hsa21 genes to follow up in human post-mortem brain tissue

To determine whether the *Drosophila* orthologues of Hsa21 genes identified as modifiers of Aβ toxicity and accumulation in my initial screen may impact Aβ pathology in individuals with DS, I next selected two genes of interest to investigate in human post-mortem brain tissue. Based on previous knowledge of their potential and established connection to AD-DS, as well as known neuronal expression, I selected two genes. Firstly, the *Usp47* orthologue *USP25* and secondly the *ATPsynCF6* orthologue *ATP5J* to determine whether they are dosage sensitive in AD-DS compared with EOAD and healthy, age-matched controls.

Chapter 4: Validation and characterisation of Usp47/USP25

4.1 Introduction

Proteostasis requires a balance between translation and protein degradation and is disturbed in many neurodegenerative diseases, including AD, leading to aberrant protein aggregation and cognitive decline (Hipp, Park and Hartl, 2014; Thibaudeau, Anderson and Smith, 2018). The autophagy-lysosomal pathway (ALP) and the ubiquitin proteosome system (UPS) play crucial roles in maintaining this balance. The UPS accounts for over 80% of proteolysis, including of Aβ and tau (López Salon et al., 2000). This pathway comprises a cascade of events involving three ubiquitin-activating enzymes that post-translationally modify proteins by adding ubiquitin molecules which can lead to selective degradation by the proteasome (Li and Ye, 2008). During this process, ubiquitin is added to a lysine (K) residue on the target protein ranging from one molecule (monoubiquitination) to polyubiquitin chains of varying lengths and topologies. This creates a unique 'ubiquitin code' essential for a variety of cellular functions, including K48 linked polyubiquitination for proteasomal degradation (Chau *et al.*, 1989; Boughton, Krueger and Fushman, 2020). Ubiquitination is counteracted by removal of ubiquitin molecules through deubiquitinating enzymes (DUBs). This eliminates the proteasomal degradation signal and leads to the stabilisation of the substrate protein. The human genome encodes around 100 DUBs that are divided into two main classes of metalloproteases and cystine proteases based on their structure and function. Within the larger superfamily of cysteine proteases, ubiquitin specific proteases (USPs) make up one of six families. USPs hydrolyse isopeptide and peptide bonds, deubiquitinating their substrate proteins (Clague, Urbé and Komander, 2019).

One member of the USP family is ubiquitin specific peptidase 25 (*USP25*), encoded on the long arm of Hsa21 at 21q21.1**.** *USP25* has three splice variants, two of which (*USP25a* and *USP25b*) are expressed in several tissues, including the CNS, whereas *USP25m* is muscle specific (Valero *et al.*, 2001). USP25 has known specificity for both K48 and K63 linkages which are ubiquitination sites for proteasomal and lysosomal protein degradation (Korolchuk, Menzies and Rubinsztein, 2010; Zhang *et al.*, 2013; Ohtake *et al.*, 2018). Intracellularly, in addition to being present in the nucleus and cytosol, USP25 has been observed to localise to the endoplasmic reticulum (ER), a potential APP processing site (Hartmann *et al.*, 1997; Zhu *et al.*, 2021; Zheng *et al.*, 2022). Misfolded Aβ has been shown to cause ER stress which triggers the ER-associated protein degradation (ERAD) pathway that eliminates misfolded proteins via ubiquitination for proteasomal degradation (Hiller *et al.*, 1996; Jung *et al.*, 2015). USP25 was found to counteract ERAD leading to an increase in APP half-life in the presence of USP25 (Blount *et al.*, 2012). Thus, it was hypothesised that USP25 contributes to the stabilisation of APP, reducing its proteasomal degradation and thus resulting in its accumulation (Figure 4.1).

A potential role of USP25 in AD pathogenesis was supported by evidence from a familial AD mouse model (5xFAD) (Zheng *et al.*, 2021). In these animals, overexpression of human *USP25* was associated with exacerbated cognitive impairment and neuroinflammation through microglial activation. Conversely, these effects were rescued by ablation or inhibition of USP25, suggesting that it is both necessary and sufficient to regulate microglial homeostasis in AD. A direct link between USP25 and amyloid pathology in DS has recently been identified in the same mouse model (Zheng *et al.*, 2022). Overexpression of *USP25* was sufficient to increase APP and β-secretase BACE1 abundance leading to elevated amyloid plaque load, whereas genetic deletion of mouse *Usp25* in 5xFAD mice resulted in reduced amyloid burden. Mechanistically, USP25 was confirmed to deubiquitinate APP and BACE1 leading to their trafficking to the Golgi apparatus where β-secretase activity is favourable, increasing Aβ generation (Figure 4.1) (Zheng *et al.*, 2022). Notably, whether APP processing at the Golgi and its stabilisation through USP25 deubiquitination take place in neuronal cell types was not confirmed in this study.

Taken together, these results implicate increased levels of USP25 in playing a crucial role in exacerbating amyloid pathology in AD-DS through the reduction of APP and BACE1 degradation via the proteosome and lysosome.

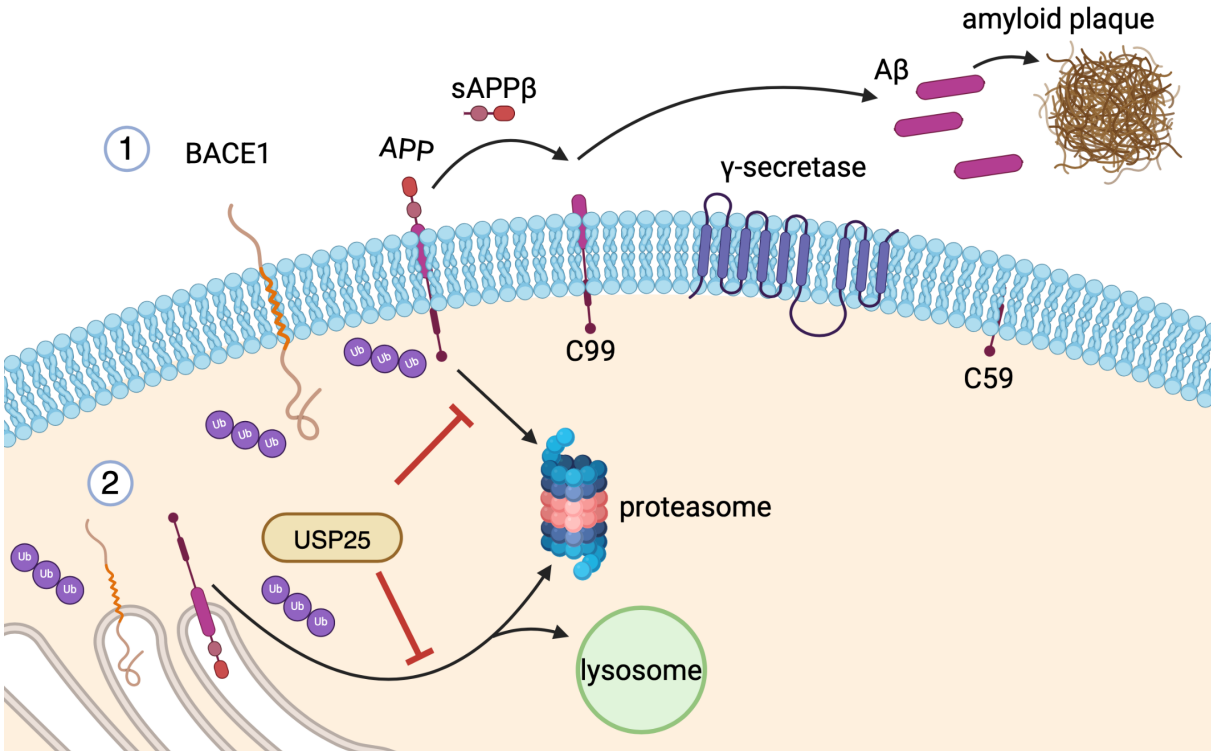

Figure 4.1 USP25 increases Aβ accumulation via deubiquitination of APP and BACE1.

(1) The amyloidogenic pathway comprises the sequential cleavage of APP by β-secretase (BACE1) and γ-secretase, generating Aβ that aggregates into amyloid plaques. (2) USP25 has been proposed to stabilise APP through deubquitination of both APP and BACE1, reducing their degradation by the proteasome/lysosome, thus increasing the amount of Aβ generated. Additionally, USP25 has been proposed to elevate Aβ accumulation through raising BACE1 concentration at the Golgi where its increased activity results in a higher turnover of APP cleavage. Based on (Liu *et al.*, 2021; Zheng *et al.*, 2022).

Importantly, the role of USP25 can vary between cell types and whether this mechanism is present in neurons has not been investigated. Additionally, although DUBs are highly conserved, their target proteins may vary between organisms, raising the possibility that USP25 also impacts amyloid pathology in other ways in the brain

of individuals who have AD-DS. Therefore, while these studies have demonstrated a role of USP25 in modulating APP processing, whether it also has an effect on downstream amyloid pathology through the direct interaction with Aβ is not known.

Deubiquitinases play an important role throughout *Drosophila* development and adulthood and have been implicated in photoreceptor differentiation, post-synaptic function, heat stress resistance and intestinal homeostasis (Bajpe *et al.*, 2008; Wang *et al.*, 2017; Cui *et al.*, 2020; Zhao *et al.*, 2024). Deubiquitination by Usp47 has been found to impact several signalling pathways. During development, Usp47 may act as an activator of the Wnt-β-catenin signalling pathway which is crucial for patterning of the embryo (Shi *et al.*, 2015; Kassel *et al.*, 2023). Furthermore, Usp47 impacts signalling through the RAS/MAPK pathway, a driver of cellular proliferation (Ashton-Beaucage *et al.*, 2016). The deubiquitinase was found to counteract E2/3 ligases that ubiquitinate MAPK for proteasomal degradation. Consequently, knockdown of *Usp47* reduced MAPK signalling in *Drosophila* larvae. In the adult, *Usp47* mutants with reduced expression of the gene exhibited a 'rough eye' phenotype, indicative of aberrant eye development (Bajpe *et al.*, 2008). At the molecular level, this was attributed to the stabilisation of the transcriptional repressor ttk involved in cell fate determination, driving cells towards a nonneuronal fate in the developing eye. However, Usp47 has not been previously studied in relation to locomotor activity, or in interaction with Aβ.

Our *Drosophila* model that directly expresses Aβ42 allowed us to isolate the effects of its fly orthologue *Usp47* on Aβ. The observed phenotypic rescue in neuromotor function of pan-neuronal *Usp47* overexpression in our initial fly screen suggested that it may positively impact Aβ toxicity. To determine whether USP25 may modify Aβ toxicity in AD-DS we wanted to understand whether it is overexpressed at the protein level in individuals with this condition. While USP25 abundance has been shown to be increased in the brains of foetuses with DS, dosage sensitivity in the adult brain of individuals with AD-DS has not been determined. Considering the potential implications of USP25 overexpression in AD-DS, understanding how its expression

and protein abundance is changed in DS compared to euploid individuals will provide insight into further mechanisms of increased AD vulnerability in DS.

Aims of this chapter were to determine:

1. whether the rescue of Aβ toxicity by *Usp47,* observed in the initial screen, can be replicated and whether fly longevity is altered by pan-neuronal overexpression of *Usp47* in adult *Drosophila* expressing Aβ42.
2. whether its human orthologue USP25 has increased abundance in the brains of individuals who had AD-DS compared with euploid control brain samples and may therefore impact amyloid pathology.

4.2 Results

4.2.1 Selection of Usp47, a target to follow up in human post-mortem brain tissue

When selecting a target to follow up in human post-mortem brain tissue, I took several factors into consideration. Firstly, I conducted a literature search on PubMed of the identified hits using the terms “human gene name” with either “Down Syndrome” or “Alzheimer’s disease”. Secondly, I searched through studies examining differential gene expression in samples of tissues from individuals who had DS to examine whether my genes of interest are known to be dosage sensitive in DS. Lastly, I used https://brainrnaseq.org and the RNA single cell feature of https://www.proteinatlas.org to confirm endogenous gene expression in neurons to ensure overexpression of the Hsa21 gene would be of biological relevance to APP processing in AD-DS, which is known to occur principally in neurons (Figure 4.2) (Y. Zhang *et al.*, 2016b; Karlsson *et al.*, 2021).

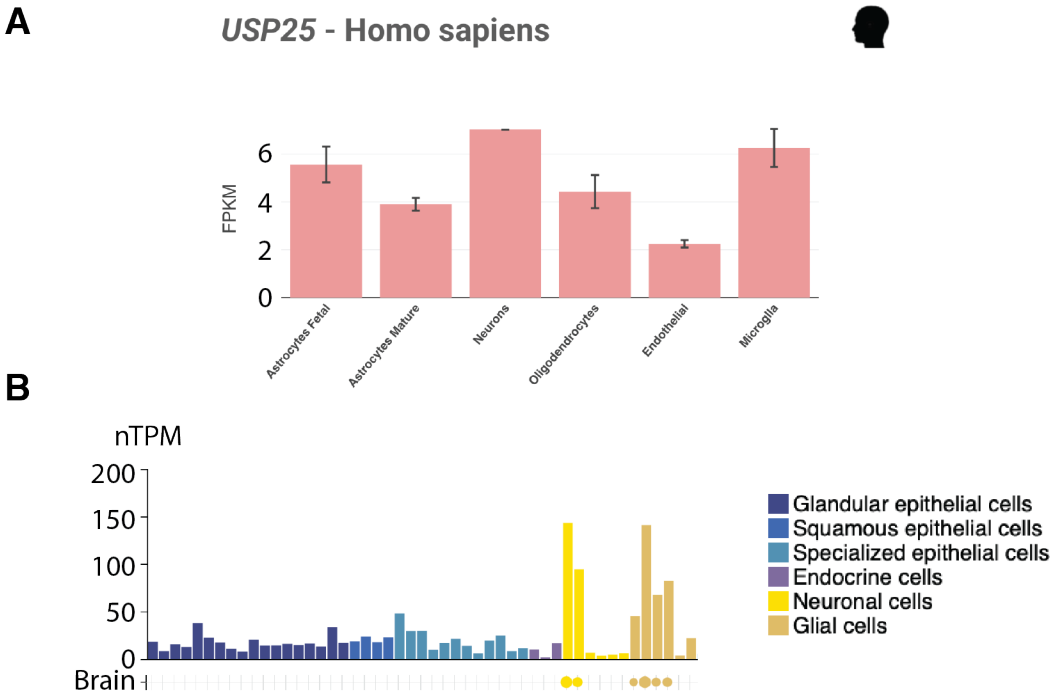

Figure 4.2 Expression patterns of *USP25* in human.

(A) *USP25* expression in CNS cell types as measured in fragments per kilobase million (FPKM), neuronal expression = 7.028 FPKM. Adapted from https://brainrnaseq.org (Y. Zhang *et al.*, 2016). (B) Single cell expression of *USP25* in the brain measured as normalised transcript per million (nTPM). Yellow bar/circle (left) = excitatory neurons, 143.0 nTPM, yellow bar/circle (right) = inhibitory neurons, 94.4 nTPM. Adapted from https://www.proteinatlas.org/ENSG00000155313-USP25/single+cell (Karlsson *et al.*, 2021).

To assess whether Usp47 orthologue USP25 may act in a conserved manner to modify Aβ toxicity in the human brain, I performed multiple sequence alignment of Usp47 (a and d) and USP25 (a and b) isoforms expressed in the brain using the UniPort Align tool (Figure 4.3) (Madeira *et al.*, 2024). Analysis comparing Usp47, spanning 1375 amino acids and USP25, spanning 1055 amino acids, showed a ~22% conservation in amino acid identity between human and *Drosophila melanogaster* orthologues of this deubiquitinase and 100% similarity within species isoforms (Table 4.1). Some of the conserved amino acid sequence fall within functional domains of the USP25 protein, including the N-terminal ubiquitin-interacting motifs (positions 97-116 and 123-140), responsible for the recognition and recruitment of ubiquitin molecules

(UniPort). This inter-species comparison demonstrates moderate sequence similarity, suggesting that proteins have a similar structure but differences are likely to be present that may affect their specificity.

```
CLUSTAL O(1.2.4) multiple sequence alignment


sp|Q9UHP3|UBP25_HUMAN      ------------------------------------------------------------ 0
sp|Q24574|UBPE_DROME       MTDKESEQCTVSVFDQTPGSEQKKINVVVRSHFTVKRVIDLIGTQFSYEKFELLLQPHDN 60


sp|Q9UHP3|UBP25_HUMAN      ------------------------------------------------------------ 0
sp|Q24574|UBPE_DROME       KDLVNLNALESQLMYEVAGFEPQLKNHLILLPSGSWDGDVTKRFELPIKRVVVKKVMKSD 120


sp|Q9UHP3|UBP25_HUMAN      ------------------------------------------------------------ 0
sp|Q24574|UBPE_DROME       GEKAKSPATGEKKKRVVGEKTKKKPASGSSSPSKAKTTSEDSLAKTSISSESSPEKTSKI 180


sp|Q9UHP3|UBP25_HUMAN      -------------------------MTVE---------QNVLQQSAA--QKHQQTFLNQL 24
sp|Q24574|UBPE_DROME       KTTAAKISKPGSEKAPRASPEECPELSTEINSKNTSSESPVAKKTAKVTSKPTLELLSPI 240
                                                  ::.*         . * :::*   .*    :*. :

sp|Q9UHP3|UBP25_HUMAN      REITGINDT------QILQQALKDSNGNLELAVAFLTAKNAKTPQQEE--TTYYQTALPG 76
sp|Q24574|UBPE_DROME       KPSSPIKELDCEPVDTLSKQQLSE---QLQ---LYPQGRNLISPVDDAPSDLFISDAEQL 294
                           :  : *::        : :* *.:   :*:    :  .:*  :* ::     : . *

sp|Q9UHP3|UBP25_HUMAN      NDRYISVGSQA----------------DTNVIDLTGDDKDDLQRAIALSLAESNRAFRET 120
sp|Q24574|UBPE_DROME       SDDDLALGASASPTMLGPGYDYGAPTGDSDVEGVTGVTDPSTIGTDDGTYPALSNFYRRK 354
                           .*  :::*:.*               *::* .:**  . .   :   :    .. :*..

sp|Q9UHP3|UBP25_HUMAN      GITDEEQAISRVLEASIAENKACLKRTPTEVWRDSRNPYDRKRQDKAPVGLKNVGNTCWF 180
sp|Q24574|UBPE_DROME       YGGDELRAWQRVNTTGA----DFVSSATTET---EAEARQASLGPRGYVGLVNQAMTCYL 407
                              ** :* .**  :.       :. : **.   . :  : .   :. *** * . **::

sp|Q9UHP3|UBP25_HUMAN      SAVIQSLFNLLEFRRLVLNYKPPSNAQDLPRNQKEHRNLPFMRELRYLFALLVGTKRKYV 240
sp|Q24574|UBPE_DROME       NSLLQALFMTPEFRNALYRWEFDND--------NEAKNIPYQLQK--LFLNLQTSPKAAV 457
                           .:::*:**   ***. : .::  .:        :* :*:*:  :   **  *  : :  *

sp|Q9UHP3|UBP25_HUMAN      DPSRAVEILKDAFK---SNDSQQQDVSEFTHKLLDWLEDAFQMKAEEETDEEKPKNPMVE 297
sp|Q24574|UBPE_DROME       ETTD----LTRSFGWDSTEAWQQHDIQELCRVMFDALEHKFKNTK--------QANLISN 505
                           : :     *. :*    ::  **:*:.*: : ::* **. *: .           * : :

sp|Q9UHP3|UBP25_HUMAN      LFYGRFLAV-GVLEG-KKFENTEMFGQYPLQVNGFKD------LHECL----EAAMIEGE 345
sp|Q24574|UBPE_DROME       LYEGKMNDYVKCLECNTEKTREDTFLDIPLPVRPFGSSSAYGSIEEALRAFVQPETLDGN 565
                           *: *::      **  .:  . : * : ** *. * .      :.*.*    :   ::*:
```

```
sp|Q9UHP3|UBP25_HUMAN      IESLHS--ENSGKSGQEHWFTELPPVLTFELSRFEFNQALGRPEKIHNKLEFPQVLYLDR 403
sp|Q24574|UBPE_DROME       NQYLCEKCKKKCDAHKGLHFKSFPYILTLHLKRFDFDYQTMHRIKLNDRVTFPQTLNLNT 625
                            : * .  ::. .: :   *..:* :**:.*.**:*:    :  *::::: ***.* *:

sp|Q9UHP3|UBP25_HUMAN      YMHRNREITRIKREEIKRLKDYLTVLQQRLERYLSYGSGPKRFPLVDVLQYALEFASSKP 463
sp|Q24574|UBPE_DROME       FINRSGNSGEQNSQL---------------------------------------------- 640
                           :::*. :  . : :

sp|Q9UHP3|UBP25_HUMAN      VCTSPVDDIDASSPPSGSIPSQTLPSTTEQQGALSSELPSTSPSSVAAISSRSVIHKPFT 523
sp|Q24574|UBPE_DROME       --NGTVDDCS--TADSGSAM---------EDDNLSSGVVTTAS----------------- 670
                             .. *** .  :  ***           ::. *** : :*:

sp|Q9UHP3|UBP25_HUMAN      QSRIPPDLPMHPAPRHITEEELSVLESCLHRWRTEIENDTRDLQESISRIHRTIELMYSD 583
sp|Q24574|UBPE_DROME       -------------------------S------SQHENDLNDEDEGIDMSSSTS--KSAK 696
                                                   *      :: *** .* :*.*.    *     :.

sp|Q9UHP3|UBP25_HUMAN      KSMIQVPYRLHAVLVHEGQANAGHYWAYIFDHRESRWMKYNDIAVTKSSWEELVRDSFGG 643
sp|Q24574|UBPE_DROME       QGSGPYLYELFAIMIHSGSASGGHYYAYIKDFDNNEWFCFNDQNVTSITQEDIQ-RSFGG 755
                           :.     *.*.*:::*.*.*..***:*** *. :..*: :**  **. : *::   ****

sp|Q9UHP3|UBP25_HUMAN      YRNASAYCLMYINDKAQFLIQ-EEFNKETGQPLVGIETLPPDLRDFVE-------EDNQR 695
sp|Q24574|UBPE_DROME       PNG-SYYSSAYTSSTNAYMLMYRQVDAKRNELVAKVADFPEHIKTLLPKLHSEEETRVSR 814
                            .. * *.  * ...  :::  .:.: : .: :. :  :* .:: ::          .*

sp|Q9UHP3|UBP25_HUMAN      FEKELEEWDAQLAQKALQEKLLASQKLRESETSVTTAQAAGDPEYLEQPSRSDFS--KHL 753
sp|Q24574|UBPE_DROME       LGRHITVTDLALPD----------------------LYKPRVYFYNPSLKKMKITRVY 850
                           : :.:   *  * :                            *: :** ..:.  :

sp|Q9UHP3|UBP25_HUMAN      KEET--IQII---------------TKASHEHEDKSPETVLQSAIKLEYARLVKLAQED 795
sp|Q24574|UBPE_DROME       VSQSFNINLVLMSAYEMLNVEQFAPLSRCRLVAYNSSMDTIIQSLESCTDPAL-----TE 905
                            .::  *:::               ::.     :.* :*::**  .     *      :

sp|Q9UHP3|UBP25_HUMAN      TPPETDYRLHHVVVYFIQNQAPKKIIEKTLLEQFGDRNLSFDERCHNIMKVAQAKLEMIK 855
sp|Q24574|UBPE_DROME       LRAAQNYSLDFLLEYRAEDQ---------------------------------EFEVYP 931
                                :* *..:: *  ::*                                  ::*:

sp|Q9UHP3|UBP25_HUMAN      PEEVNLEEYEEWHQDYRKFRETTMYLIIGLENFQRESYIDSLLFLICAYQNNKELLSKGL 915
sp|Q24574|UBPE_DROME       PNGI------TW----YVFK-------VDLSTMA----MDGP-FLV--YSAARE------ 961
                           *: :       *      *:       :.*..:     :*.  **:  *.  :*

sp|Q9UHP3|UBP25_HUMAN      YRGHDEELISHYRRECLLKLNEQAAE------------LFESGEDREVNNGLI---IMN- 959
sp|Q24574|UBPE_DROME       -----REASDVLRRSIALRLHISEQQFLLATVRATVPKAFVSYDPHPTPEALQHLQNMAN 1016
                                .*  .  **.  *:*: .  :             * * : : . :.*     *

sp|Q9UHP3|UBP25_HUMAN      -EF--IVPFLPLLLVDEMEEKDILAVEDM----------------------------RN 987
sp|Q24574|UBPE_DROME       TQFKSITYFYLNVPNTDAATLEMLGVPTVESVECASGGDVVDAAMMNGVAPGHMSSSNDY 1076
                            :*  *. *   :   :    ::*.*  :

sp|Q9UHP3|UBP25_HUMAN      RWCSYLGQEMEPHLQEKLTD-------------------------------------FL 1009
sp|Q24574|UBPE_DROME       DWRRYKRDLVEPMSQPSPSHGHESNSEDSSLSDGDRTLVETDNMAHRGGGDSQVSSTSHS 1136
                            *  *  : :**  * . :.                                      .

sp|Q9UHP3|UBP25_HUMAN      PKLL---------DCSMEI------------KSFHEPPKLPSYSTH------ELCERF-- 1040
sp|Q24574|UBPE_DROME       PQLSSPEDEAASHDAMMRVHAYCNGNGSYAAADVVDPLLLPTSTNHFFYATKVECVDVVG 1196
                           *:*          *. *.:             .. :*  **: :.*        *  .
```

Figure 4.3 Multiple sequence Alignment of human USP25 and *Drosophila* Usp47. Alignment of amino acid sequence of USP25a and Usp47. Generated using Clustal Omega Multiple Sequence Alignment (MSA) (Madeira *et al.*, 2024). * = positions with a single, fully conserved residue, : = positions with conservation between amino acid groups of similar properties. [1] outlines conservation in the UBI domain, [2] outlines conservation in the ubiquitin interacting

Table 4.1 Amino acid conservation between Usp47 and USP25.

Percentage Identity Matrix of MSA between Usp47 isoforms a and d and USP25 isoforms a and b, generated using UniPort. UniPort IDs: Usp47a (Q24574-1), Usp47d (Q24574-2), USP25a (Q9UHP3-2), USP25b (Q9UHP3-1).

	Usp47a	Usp47d	USP25a	USP25b
Usp47a	100%	100%	22.11%	22.17%
Usp47d	100%	100%	22.29%	22.35%
USP25a	22.11%	22.29%	100%	100%
USP25b	22.17%	22.35%	100%	100%

4.2.2 Effects of *Usp47* overexpression on *Drosophila* climbing and lifespan

In my initial genetic modifier screen of Hsa21 orthologues, pan-neuronal overexpression of *Usp47* was found to partially rescue the Aβ induced climbing defect, suggesting that it may act as a modifier of Aβ toxicity in *Drosophila*. To confirm our findings, we repeated the negative geotaxis assay. However, in this repeat, although climbing speed of *UAS-Aβx2*, *elavGS/UAS-Usp47* was overall greater compared to flies expressing Aβ alone, the rate of decline was not significantly altered (Figure 4.4).

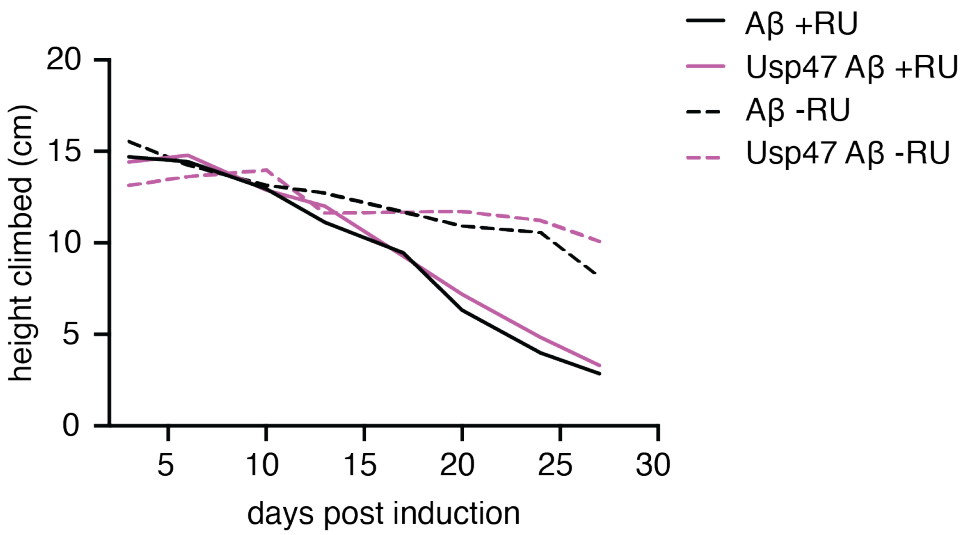

Figure 4.4 Re-screen of Usp47 negative geotaxis assay.

Average height climbed across the lifespan by flies pan-neuronally expressing Aβ42, with (pink lines) or without (black lines) overexpression of *Usp47* in adult neurons (solid lines, induced by RU-486) and uninduced controls (dashed lines). n = ~ 75 flies per condition. Simple linear regression of the effect of interaction between age and genotype: +RU $p = 0.259$, -RU $p = 0.001$. Genotype: *UAS-Aβx2*, *elavGS* and *UAS-Aβx2*, *elavGS/UAS-Usp47.* Full statistical results are presented in Table S4.1.

Next, I wanted to investigate whether the initially observed rescue of Aβ toxicity may also be reflected in a modification of longevity in our AD model. To test this, I compared the lifespan of Aβ expressing flies with those additionally overexpressing *Usp47* in adult neurons and their respective uninduced controls. As expected, induction of Aβ expression significantly reduced median lifespan from 57.5 to 36.5 days. Overexpression of *Usp47* did not significantly modify the overall lifespan of Aβ expressing flies, although median lifespan was shortened to 34 days while maximum lifespan was extended from 41 to 45 days (Figure 4.5A). Interestingly, for the same genotypes the p-element insertion upstream of *Usp47* was sufficient to significantly increase median lifespan in flies encoding two tandem copies of Aβ42 even when expression was not induced by RU-486 (Figure 4.5A). This may suggest that the insertional effect itself is beneficial to fly health. Alternatively, due to potential leakiness of the UAS/GeneSwitch overexpression system, Aβ and Usp47 may also be expressed at low levels in the -RU condition. Therefore, this trend may be observed if low level overexpression confers a beneficial effect whereas overexpression at higher levels is detrimental. To determine whether the observed trend towards a shortened median lifespan in the induced *Usp47* and Aβ co-overexpressing flies was specific to Aβ toxicity, I wanted to investigate whether overexpression of *Usp47* alone would alter *Drosophila* lifespan independently of Aβ. Pan-neuronal overexpression of *Usp47* in adulthood was sufficient to reduce median lifespan from 59 to 48.5 days suggesting that it is detrimental to overall fly health (Figure 4.5B). The control line with neuronal driver (elavGS) alone confirmed no significant effect of RU (Figure 4.5B). In summary, these data indicate that overexpression of *Usp47* is sufficient to shorten fly lifespan but does not significantly exacerbate reduced longevity induced by neuronal expression of Aβ42.

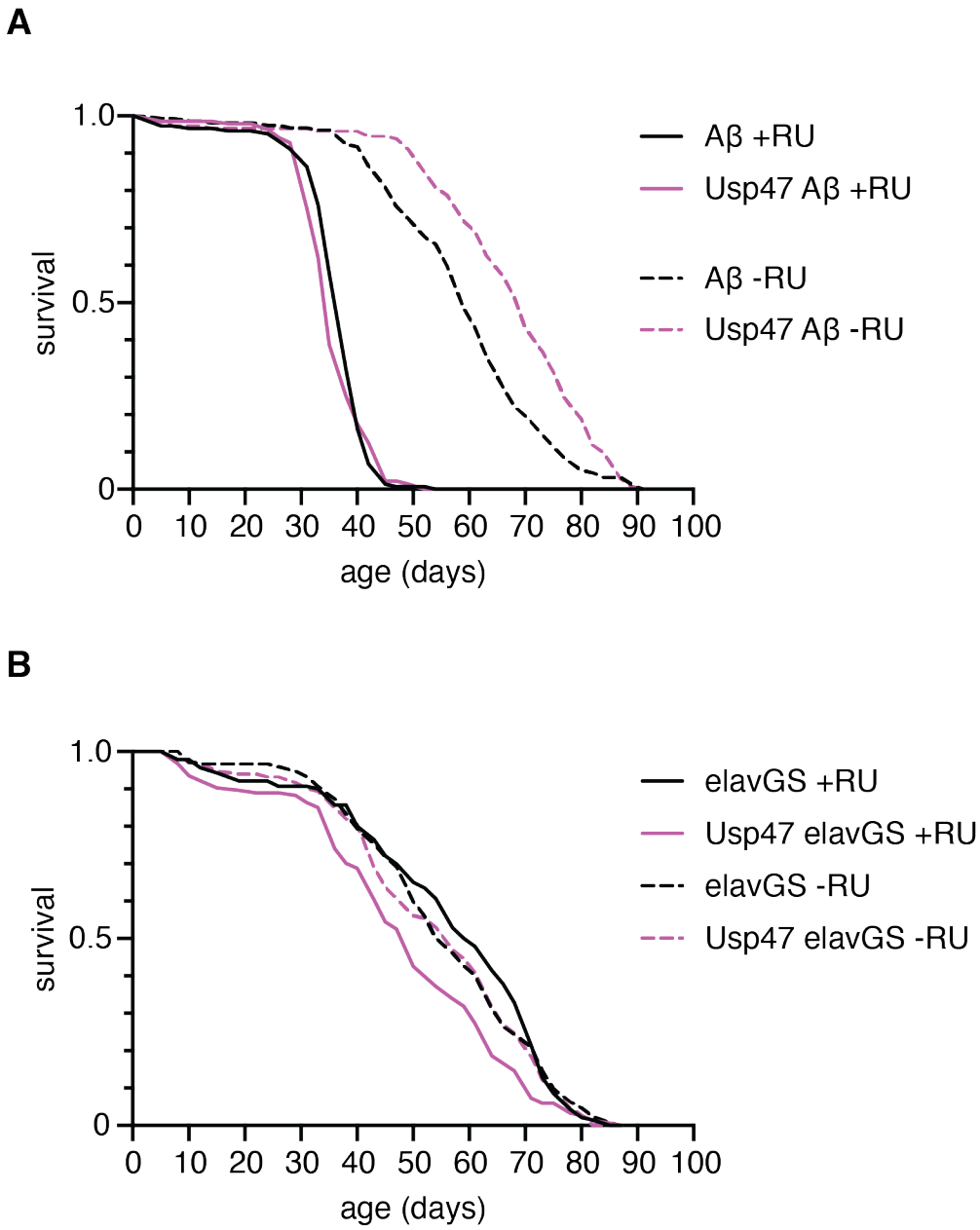

Figure 4.5 Lifespan of flies overexpressing *Usp47* in adult neurons.

(A) Lifespan curves of Aβ expressing flies (solid lines) with (pink lines) or without (black lines) pan-neuronal co-overexpression of *Usp47* induced by RU-486 and uninduced controls (dashed lines). Log-rank test of *Usp47* and Aβ co-overexpression versus Aβ expression alone, +RU p = 0.187, -RU p = 0.005. (B) Lifespan curves of flies expressing neuronal diver elavGS (solid lines) with (pink lines) or without (black lines) co-expression of Usp47 induced by RU-486 and uninduced controls (dashed lines). +RU p = 0.0004, -RU p = 0.532. n = ~150 flies per condition. Genotypes: (A) *UAS-Aβx2*, *elavGS, UAS-Aβx2*, *elavGS/UAS-Usp47* (B) *elavGS, elavGS/UAS-Usp47.* Full statistical results are presented in Table S4.2.

4.2.3 Selection of human post-mortem brain tissue cases for investigating targets of interest

To determine whether the human *Usp47* orthologue *USP25* may impact amyloid pathology in individuals with DS, I wanted to investigate whether triplication of this gene resulted in the upregulation of USP25 protein abundance in the brain of individuals with AD-DS. In this study, I compared cases of individuals with trisomy 21 and Alzheimer's disease pathology (AD-DS) with individuals who had EOAD (without known mutations in *APP*, *PSEN1* or *PSEN2*) and healthy euploid individuals (healthy ageing). Two cohorts of cases (set 1 and 2) were sourced from the South West Dementia Brain Bank (SWDBB), University of Bristol, UK and a third cohort was provided by the Newcastle Brain Tissue Resource (NBTR), Newcastle University, UK. Cohort 1 were samples of the temporal cortex (Brodmann Area 21), cohort 2 and 3 were samples of frontal cortex (Brodmann Area 10).

Within the SWDBB cohort 1, healthy ageing (HA) cases had a significantly higher mean age compared to the AD-DS cases but there was no significant difference between HA and EOAD or between EOAD and AD-DS. For cases obtained from NBTR, age did not significantly differ among case types. For SWDBB cohort 2, HA cases had a significantly higher mean age compared to the AD-DS and EOAD samples but there was no significant difference in age between AD-DS and EOAD cases (Figure 4.6A). Across all cohorts, there was no significant difference in post-mortem interval (PMI) among case types (Figure 4.6B). Combining all three cohorts, there was no overall significant difference in gender distribution across case types (HA 11 female and 10 male, EOAD 13 female and 8 male, AD-DS 15 female and 7 male (χ^2 1.139 df 2 p = 0.566). The distribution of *APOE* alleles was also evenly spread across case types (χ2 2.159 df 4 p = 0.707).

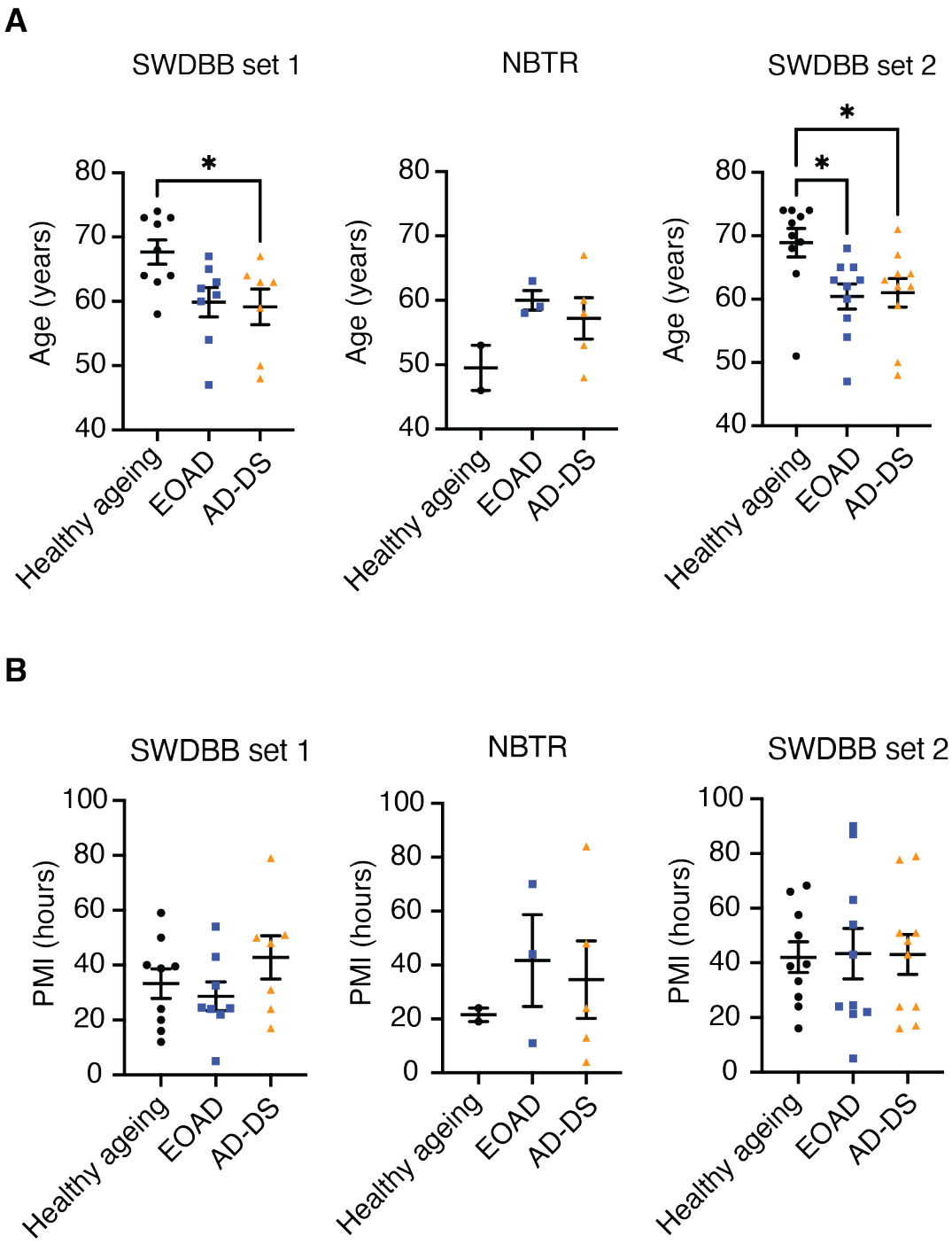

Figure 4.6 Case demographics of post-mortem brain samples.

Demographics of samples from three cohorts. SWDBB set 1: HA n = 9, EOAD n = 8, AD-DS n = 7; NBTR: HA n = 2, EOAD n = 3, AD-DS n = 5; SWDBB set 2: HA n = 10, EOAD n = 10, AD-DS n = 10. P-values refer to one-way ANOVA followed by pairwise comparison with Bonferroni multiple comparisons test. * = $p < 0.05$. (A) age distribution across case types. SWDBB1: F (2, 21) = 4.496, $p = 0.024$, HA vs EOAD $p = 0.064$, HA vs AD-DS $p = 0.0478$, EOAD vs AD-DS $p > 0.999$. NBTR: F (2, 7) = 1.958, p =

0.211, HA vs EOAD $p = 0.241$, HA vs AD-DS $p = 0.416$, EOAD vs AD-DS $p = 0.901$. SWDBB set 2: F (2, 27) = 4.848, $p = 0.016$, HA vs EOAD $p = 0.029$, HA vs AD-DS $p = 0.046$, EOAD vs AD-DS $p > 0.999$. (B) PMI across case types. There is no significant difference in PMI across case types. SWDBB set 1: F (2, 21) = 1.313, $p = 0.290$, HA vs EOAD $p > 0.999$, HA vs AD-DS $p = 0.840$, EOAD vs AD-DS $p = 0.376$. NBTR: F (2, 7) = 0.2912, $p = 0.756$, HA vs EOAD $p = 0.852$, HA vs AD-DS $p = 0.939$, EOAD vs AD-DS $p = 984$. SWDBB set 2: F (2, 27) = 0.008133, $p = 0.992$, HA vs EOAD $p > 0.999$, HA vs AD-DS $p > 0.999$, EOAD vs AD-DS $p > 0.999$.

4.2.4 Work-up of anti-USP25 antibodies for western blot

In individuals with DS, *USP25* has been found to be upregulated at the transcript level in several tissues and cell types, including neurons and microglia (Palmer *et al.*, 2021). To understand whether USP25 protein is also dosage sensitive in AD-DS, I examined three cohorts of human post-mortem brain tissue comparing AD-DS, EOAD and HA cases using western blots. To optimise experimental conditions, I trialled two anti-USP25 antibodies. Firstly, we probed membranes containing fibroblasts from trisomic and disomic individuals as well as mouse brain, with the polyclonal antibody ab246948 at dilutions of 1:1000, 1:2000 and 1:5000. β-actin was used as a loading control. Bands for USP25 at the expected 122kDa could be visualised on all three blots but were most clearly visible at a dilution of 1:1000 (Figure 4.7A). Continuing with this dilution, we wanted to determine the antibody's linear range where the signal is proportional to the amount of protein present using human post-mortem brain tissue obtained from HA cases. For this we loaded 4 different volumes of sample in two-fold increments ranging from 2.5-20μg (Figure 4.7B). This confirmed the relationship between the amount of protein loaded and relative USP25 signal detected was linear, suggesting that USP25 signal would be proportional to the amount of protein present when loading between 2.5-20μg of sample onto the gel (Figure 4.7C and D). Notably, although this anti-USP25 antibody allowed us to visualise USP25, blots also presented several non-

specific bands some of which were stronger than those corresponding to USP25, suggesting a lack of specificity.

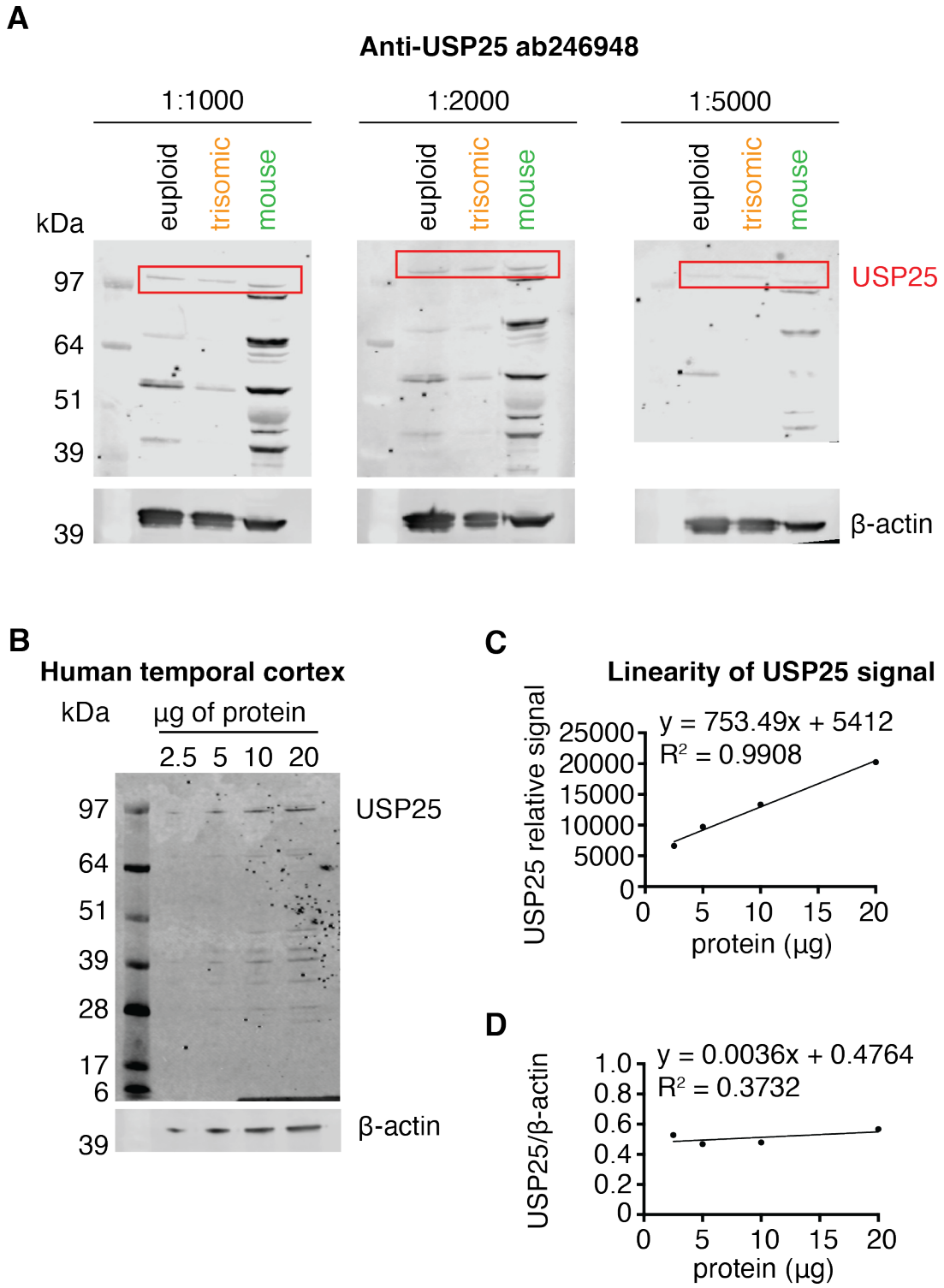

Figure 4.7 Workup and linearity of anti-USP25 antibody ab246948.

(A) Western blots testing anti-USP25 antibody ab246948 probed at concentrations of 1:1000, 1:2000 and 1:5000 to confirm specificity and determine optimal concentration

using euploid and trisomy 21 human fibroblast and mouse brain samples. USP25 was visualised at the expected 122kDa size. Bands were most clearly visible at a concentration of 1:1000. Anti-β-actin (A5441) was used as a control. (B) Western blot of human temporal cortex loaded at four different amounts 2.5μg, 5μg, 10μg and 20μg to test for signal linearity of anti-USP25 antibody ab246948. β-actin (A5441) was used as a loading control. (C) Linearity of USP25 signal vs amount of protein loaded, R^2 = 0.9908, p = 0.005, y = 753.49x + 5412. (D) Correlation between USP25 signal normalised to β-actin vs amount of protein loaded, R^2 = 0.3732, p = 0.389, y = 0.0036x + 0.4764, p = 0.389). *Sample preparation and loading was carried out by a member of the Wiseman lab.*

Secondly, we tested the monoclonal anti-USP25 antibody ab187156 (clone: EPR15019) at a dilution of 1:1000. As above, USP25 could be visualised at the expected 122kDa (Figure 4.8A). To determine the linearity of ab187156, we repeated the protocol of ab246948 which showed a linear relationship between USP25 signal and amount of protein loaded (Figure 4.8B). USP25 signal normalised to β-actin remained relatively steady with increasing protein concentrations (Figure 4.8C). Although some non-specific bands were also visible using this antibody, they were fewer/weaker compared with ab246948. This is consistent with monoclonal antibodies having lower cross-reactivity, resulting in fewer non-specific bands, compared to polyclonal antibodies. Therefore, we decided to proceed with this anti-USP25 ab187156 to investigate our AD-DS, EOAD and HA samples.

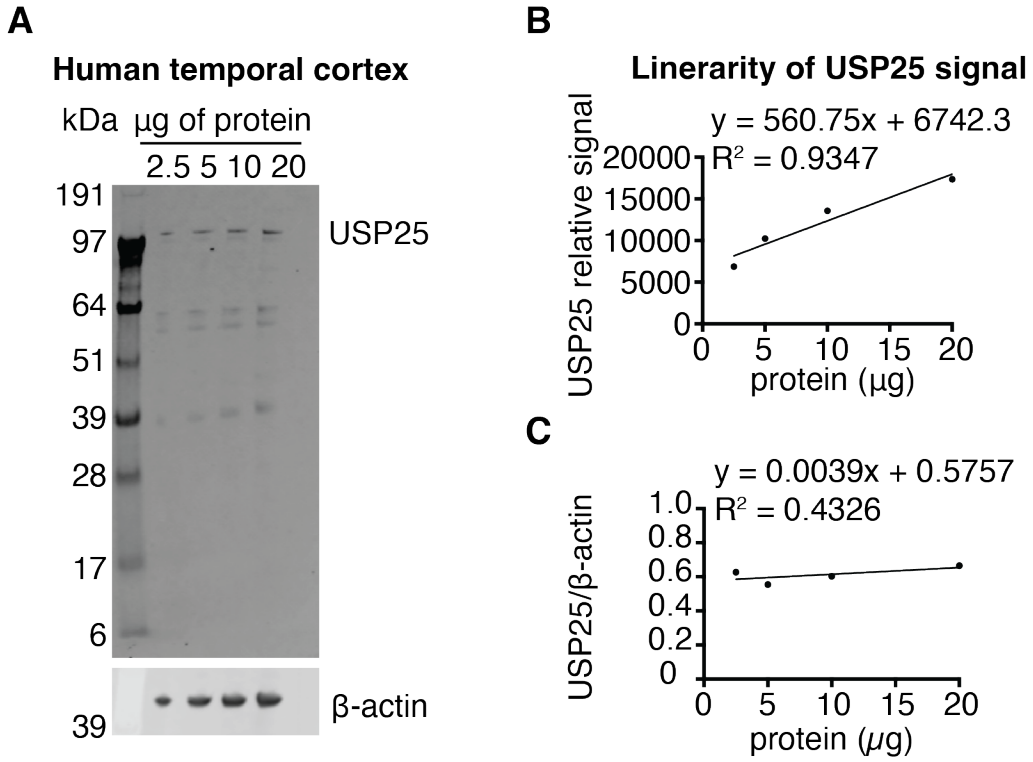

Figure 4.8 Workup and linearity of anti-USP25 antibody ab187156.

(A) Western blot of human temporal cortex loaded at four different amounts: 2.5µg, 5µg, 10µg and 20µg to test for signal linearity of anti-USP25 antibody ab187156 (EPR15019) diluted 1:1000. USP25 was visualised at the expected 122kDa size. Anti-β-actin (A5441) was used as a loading control. (B) Linearity of USP25 signal vs amount of protein loaded, $R^2 = 0.9347$, $p = 0.033$, y = 560.75x + 6742.3. (C) USP25 signal normalised to β-actin vs amount of protein loaded, $R^2 = 0.342$) y = 0.003926x + 0.5757. *Sample preparation and loading was carried out by a member of the Wiseman lab.*

4.2.5 Assessing dosage sensitivity of USP25 protein in human post-mortem brain tissue

Using the anti-USP25 antibody ab187156 at our optimised conditions, we proceeded to probe human post-mortem brain tissue from BA21 in the temporal cortex obtained from the SWDDB (cohort 1), consisting of 9 HA, 8 EOAD and 7 AD-DS cases. The

first technical repeat showed an overall low level of signal with considerable variation between samples (Figure 4.9A). To confirm our findings and account for lane bias, we repeated the experiment, randomising the order of our samples loaded onto the gel. The second replicate exhibited similarly low levels of USP25 signal with samples 16, 9, 15, and 10 exhibiting darker bands compared with the first repeat (Figure 4.9B). Subsequently, we selected these 4 samples that showed at least a 5-fold increase in USP25 signal on gel 2 compared with gel 1 to test in an additional technical repeat, loading samples in duplicate. This repeat showed bands comparable to replicate 2 for all samples tested, suggesting a possible technical issue in gel 1 that led to an underestimation of USP25 protein present in the samples (Figure 4.9C). To determine the amount of protein present in each sample, we averaged results from all technical repeats, normalising each USP25 signal datapoint to its β-actin loading control and to the gel average. Outlier test identified 1 HA and 1 AD-DS sample, which were removed from the analysis. There was no statistically significant difference in relative USP25 signal among HA, EOAD and AD-DS, though there was a trend towards lowered USP25 abundance in AD-DS temporal cortex (Figure 4.9D). Thus, based on this cohort of human post-mortem brain tissue, it could not be concluded whether USP25 is dosage sensitive at the protein level in the temporal cortex of people who had AD-DS compared with euploid control samples.

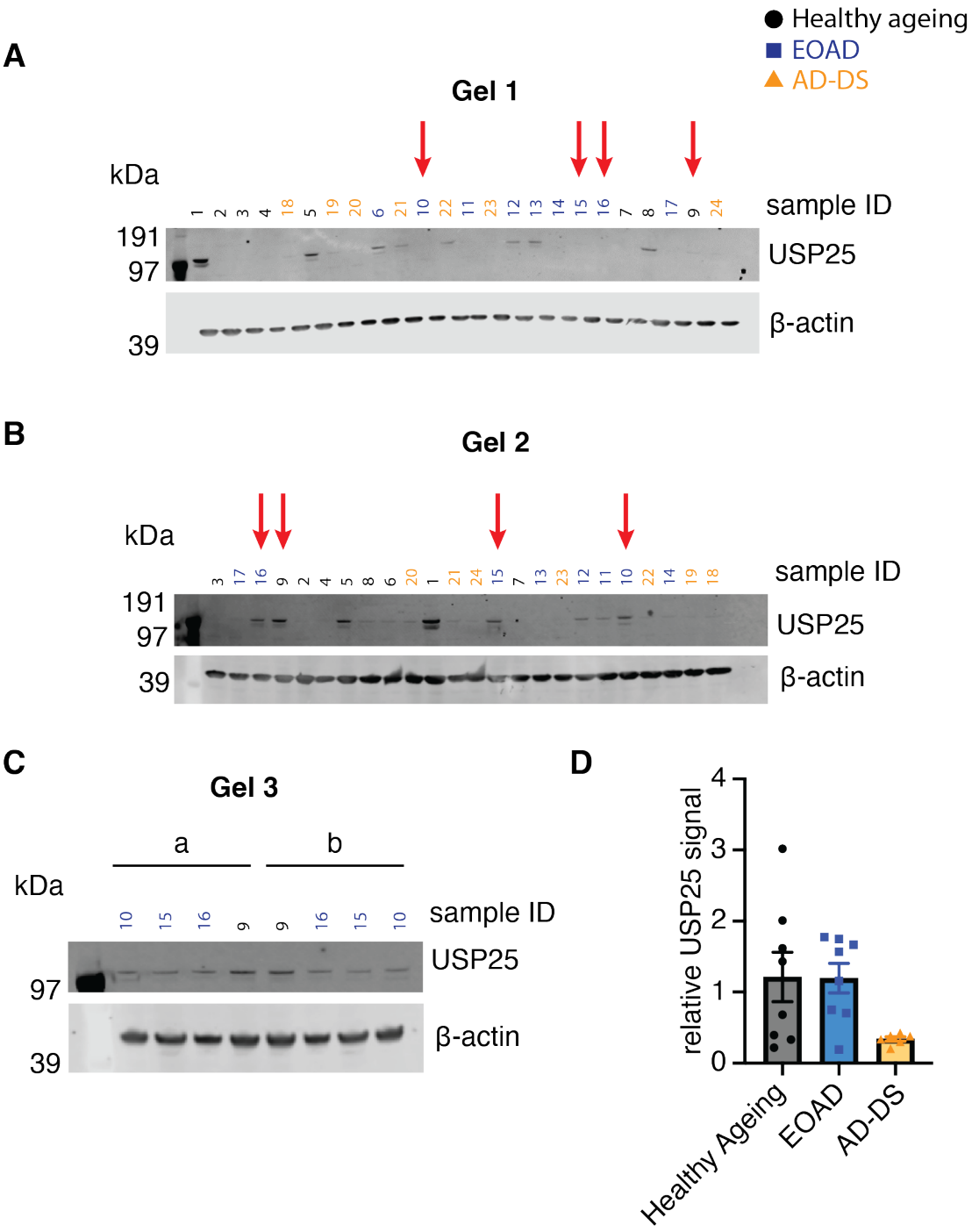

Figure 4.9 Relative USP25 protein levels in human post-mortem temporal cortex. Western blots of 24 human temporal cortex samples (BA21). Anti-USP25 antibody ab187156 (EPR15019) was used to probe for USP25 protein abundance in the HA, EOAD and AD-DS cases. Anti-β-actin (A5441) was used as a loading control. HA n = 9 (black), EOAD n = 8 (blue), AD-DS n = 7 (orange). Sample ID colours indicate case type: black = HA, blue = EOAD, yellow = AD-DS. (A, B) Western blot image showing

bands for USP25 at expected band size of 122 kDa and β-actin (expected size 42kDa) loaded in two different orders (generated using RAND() function in excel). Red arrows point to samples that showed substantial inter-gel variability in relative USP25 level between gels 1 and 2, defined as > 5-fold difference in USP25 signal between gels. (C) Technical repeat of samples marked by red arrows in (A) and (B). These outlier samples were loaded in two different orders (a and b) on gel 3. (D) Relative signal of USP25 normalised to β-actin and gel average. Signal was averaged across all three technical repeats. ROUT Identify Outliers (Q = 1%), 1 HA and 1 AD-DS sample removed. One-way ANOVA with Šídák's multiple comparisons test of cleaned data, $F(2, 19) = 3.328$, $p = 0.058$, HA vs EOAD $p > 0.999$, HA vs AD-DS $p = 0.094$, EOAD vs AD-DS $p = 0.103$ Data are presented as mean ± SEM. *Sample preparation and loading was carried out by a member of the Wiseman lab.*

To increase the number of biological replicates, we subsequently probed a second independent set of 10 human post-mortem brain tissue samples. These were obtained from the NBTR and consisted of 2 HA, 3 EOAD and 5 AD-DS prefrontal cortex (BA10) tissue. Firstly, we probed for USP25 using anti-USP25 antibody ab187156 (Figure 4.10A). There was no significant difference in relative USP25 signal among HA, EOAD and AD-DS cases, though there was a trend towards reduced levels in EOAD compared with HA (Figure 4.10B). These results were confirmed using anti-USP25 antibody ab246948 on the same cohort. Therefore, the addition of this cohort of samples was not sufficient to determine the dosage sensitivity of USP25 protein in AD-DS.

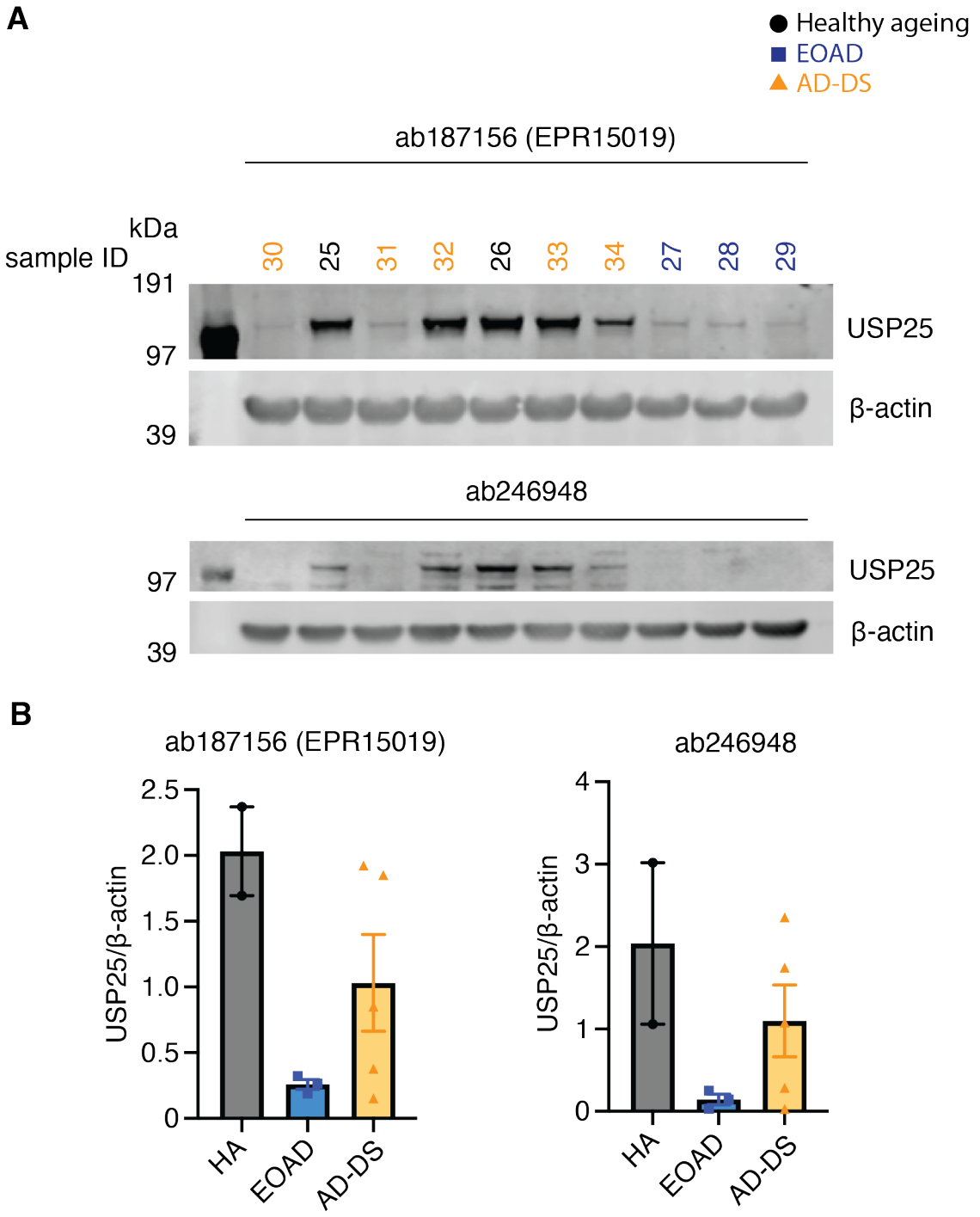

Figure 4.10 Relative USP25 protein levels in human post-mortem pre-frontal cortex

(A) Western blot of 10 human prefrontal cortex (BA10) samples probed with anti-USP25 ab187156 (EPR15019) and ab246948. HA = 2, EOAD = 3, AD-DS = 5. Anti-β-actin (A5441) was used as a loading control. Sample ID colours indicate case type: black = HA, blue = EOAD, yellow = AD-DS. (B) Quantification of USP25 protein level relative to β-actin and gel average. One-way ANOVA with Šídák's multiple

comparisons test, ab187156: F (2, 7) = 4.514, p = 0.055, HA vs EOAD p = 0.059, HA vs AD-DS p = 0.287, EOAD vs AD-DS p = 0.379. ab246948: F (2, 7) = 2.685, p = 0.136, HA vs EOAD p = 0.158, HA vs AD-DS p = 0.586, EOAD vs AD-DS p = 0.473. Data are presented as mean ± SEM. *Sample preparation and loading was carried out by a member of the Wiseman lab.*

Based on the results from the investigated cohorts, I wanted to calculate the sample size required to determine whether USP25 is dosage sensitive in AD-DS and whether its level is altered by disease. For this, I performed a power calculation using the case type specific means and standard deviations from our collected data. To detect whether there is a difference in USP25 levels between HA and AD-DS, the required sample size was calculated to be 14 samples per case type. Determining whether EOAD affects USP25 levels in human post-mortem brain tissue would require 12 HA and 12 EOAD samples, exceeding the number of examined samples thus far (Table 4.2).

Table 4.2 Power calculation for USP25 western blots.

T-test mean difference between two independent means, one-tail.

	HA (group 1) vs AD-DS (group 2)	**HA (group 1) vs EOAD (group 2)**
calculated effect size	0.9715028	1.049346
error	0.05	0.05
power	0.8	0.8
sample size group one	14	12
sample size group two	14	12
actual power	0.8044696	0.8009976

Informed by the power calculation, we wanted to increase our sample size further to determine whether the observed trend of lowered USP25 level in disease would reach statistical significance. We were able to source a third, larger cohort of human post-mortem prefrontal cortex samples from SWDBB (cohort 2). This cohort consisted of

10 HA, 10 EOAD and 10 AD-DS cases (Figure 4.11A). As with previous cohorts we probed membranes with anti-USP25 antibody ab187156 and β-actin as a loading control. Outlier analysis identified 1 sample from HA and EOAD and 2 samples from AD-DS cases which were removed from further statistical analysis. For this cohort, relative USP25 protein abundance was significantly lower in EOAD and AD-DS samples compared with healthy euploid controls. There was no significant difference in USP25 abundance between EOAD and AD-DS case types (Figure 4.11B).

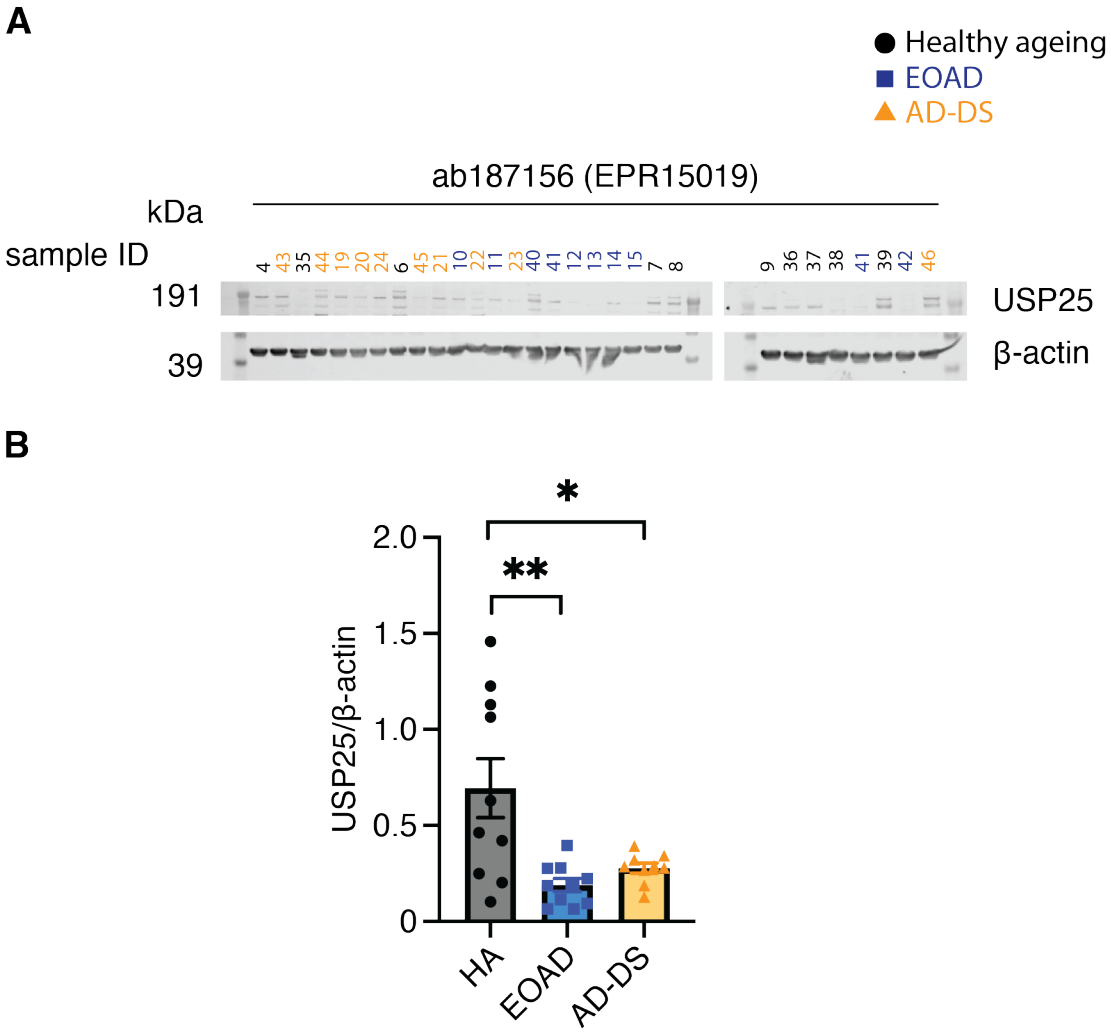

Figure 4.11 Relative USP25 protein levels in an independent set of human post-mortem prefrontal cortex samples.

(A) Western blot of 30 human prefrontal cortex (BA10) samples probed with anti-USP25 ab187156. Anti-β-actin (A5441) was used as a loading control. Sample ID colours indicate case type: black = HA, blue = EOAD, yellow = AD-DS. (B)

Quantification of USP25 protein abundance relative to β-actin signal and gel average. One-way ANOVA with Šídák's multiple comparisons test, F (2, 26) = 8.273, $p = 0.002$, HA vs EOAD $p = 0.002$, HA vs AD-DS $p = 0.015$, EOAD vs AD-DS $p = 0.891$. Data are presented as mean ± SEM. *Sample preparation and loading was carried out by a member of the Wiseman lab.*

4.2.6 Additional potential confounders affecting USP25 protein level

Western blots did not show a significant difference in relative USP25 signal between HA, EOAD and AD-DS samples for SWDBB1 and NBTR cohorts but relative USP25 abundance was found to be significantly decreased in EOAD and AD-DS cases in the SWDBB2 cohort compared with euploid controls. Furthermore, the amount of signal detected varied considerably between samples within cohorts and case types. I therefore wanted to investigate whether there were confounding factors that may influence the intensity of USP25 signal. As part of the experimental design, post-mortem brain tissue samples were selected to match for potential confounding factors, including age and PMI, as closely as possible among case types. However, due to a limited number of samples available, particularly of brain tissue from individuals who had AD-DS, age at death for this case type was significantly lower in both cohorts obtained from the SWDBB. Therefore, I examined whether USP25 signal correlated with age but this interaction was not found to be statistically significant (Figure 4.12A). Average PMI was not significantly different among case types for all cohorts but variance within conditions was large. However, I also found no significant correlation between PMI and relative USP25 signal detected by western blot, suggesting USP25 protein level was not confounded by age or PMI (Figure 4.12B). Additionally, we investigated the effect of age, PMI, sex, brain region, and brain bank and their interactions with a univariate general linear model. Braak stage was not included as a co-factor as this information was not available for all samples. An effect of brain region (BA), brain bank as well as the interaction of brain bank and region, was detected.

Additionally, consistent with significant effects of case type on USP25 signal abundance observed in only one of three cohorts, there was a significant interaction between brain bank and case type (status). Sex, age and PMI did not correlate with USP25 signal (Table 4.3).

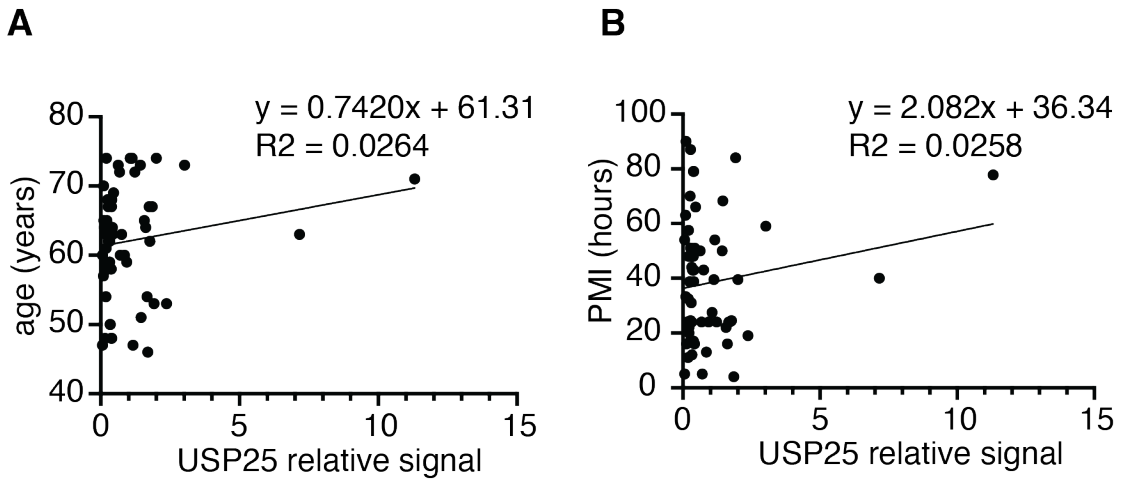

Figure 4.12 USP25 signal intensity is not correlated with PMI or age at death. (A) Linear correlation between age at death and relative USP25 signal (probed with ab187156) across all three cohorts is low by simple linear regression, $R^2 = 0.0264$, $p = 0.199$. Line of best fit y = 0.7420x + 61.31. (B) Linear correlation between post-mortem interval (PMI) and relative USP25 signal across all three cohorts is low by simple linear regression, $R^2 = 0.0258$, $p = 0.205$. Line of best fit y = 2.082x + 36.34.

Table 4.3 Univariate general linear model of potential confounding factors influencing USP25 signal intensity.

Tests of Between-Subjects Effects					
Dependent Variable: USP25 relative signal					
Source	Type III Sum of Squares	df	Mean Square	F	P-value
sex	1265.668	1	1265.668	0.229	0.635
region	642637.341	1	642637.341	116.071	<.001
bank	287271.081	1	287271.081	51.886	<.001
status	104.223	2	52.112	0.009	0.991
age	302.424	1	302.424	0.055	0.816
PMI	946.540	1	946.540	0.171	0.681
region * bank	.000	0	.	.	.
bank * status	662685.300	2	331342.650	59.846	<.001
region * status	1336935.538	2	668467.769	120.737	<.001

As AD pathology progresses, neuronal count decreases across multiple brain regions (Gómez-Isla *et al.*, 1997). In individuals with DS, neurodevelopmental differences cause an underlying neuronal deficit present from the early stages of development (Wegiel *et al.*, 2022). EOAD and AD-DS cases investigated in this study were classified as late-stage disease (Braak stage IV-VI) at which point substantial brain atrophy has taken place. To determine whether this expected reduction in neuronal number in AD-DS and EOAD compared with HA controls could be detected in our post-mortem brain tissue samples we probed membranes from all three cohorts with the neuron specific marker β3-tubulin (Figure 4.13A).

Within the SWDBB cohorts, relative β3-tubulin signal was not significantly different among case types, though there was a trend towards lower levels with disease (Figure 4.13B). For samples obtained from the NBTR, prefrontal cortex tissue from EOAD cases had significantly lower levels of β3-tubulin compared with HA controls, suggesting that neuronal count was lower in these samples. AD-DS cases also showed a trend towards lowered levels of this neuronal protein but this did not reach statistical significance (Figure 4.13B). To investigate whether USP25 protein abundance differs between case-types when accounting for neuronal abundance, I normalised USP25 signal to β3-tubulin. Across all cohorts there was no significant

difference in USP25 level relative to β3-tubulin suggesting that neuronal loss due to EOAD did not fully account for a lower amount of USP25 signal detected by western blot (Figure 4.13C).

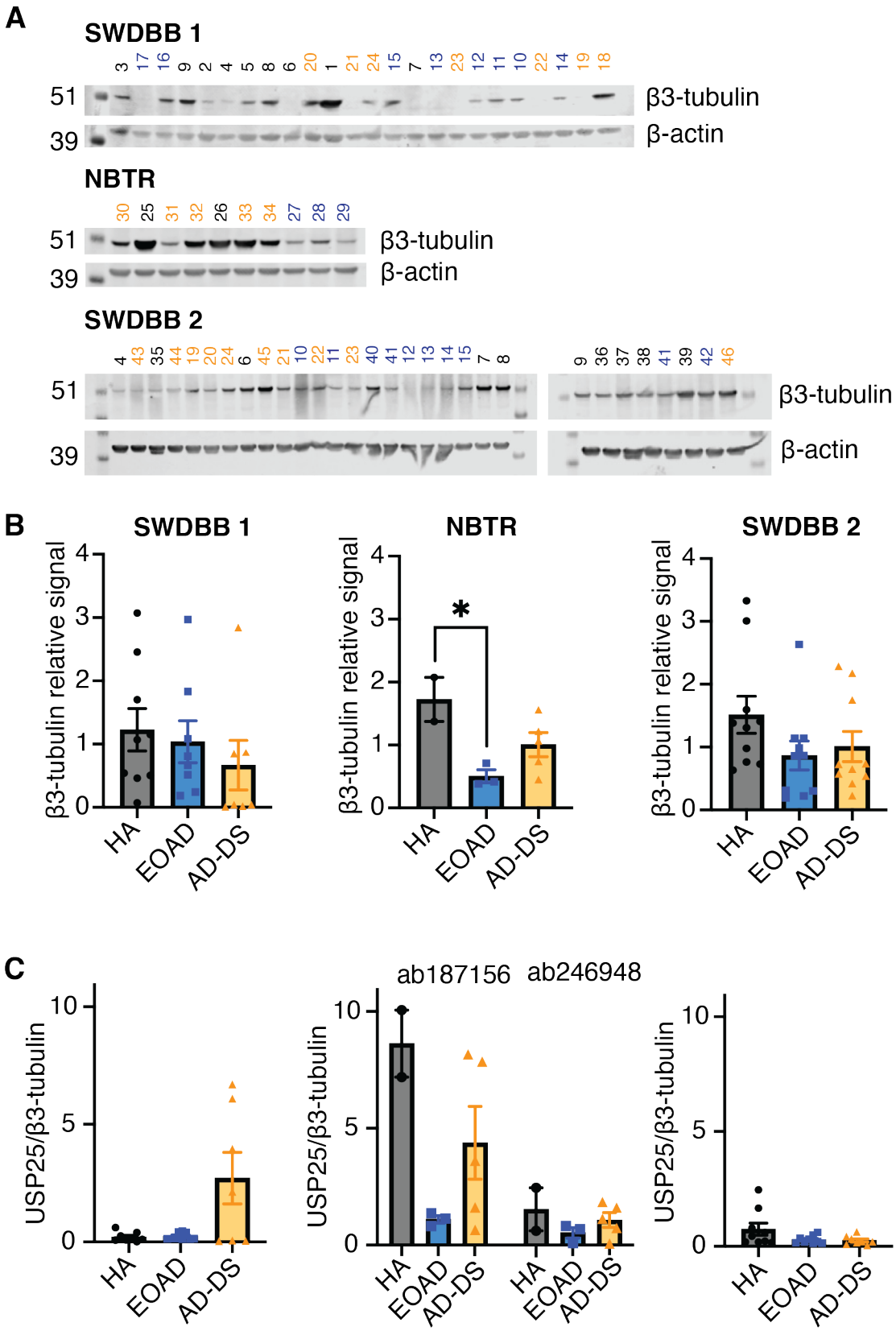

Figure 4.13 Neuronal abundance in AD-DS, EOAD and HA controls.

(A) Western blot of 64 human post-mortem temporal and prefrontal cortex samples from individuals with AD-DS, EOAD and HA controls (3 cohorts). Membranes were

probed with neuron-specific marker β3-tubulin, with β-actin as a loading control. (B) Relative β3-tubulin level normalised to β-actin and gel average measured in three cohorts. One-way ANOVA with Šídák's multiple comparisons test, SWDBB1: F (2, 21) = 0.6288, p = 0.543, HA vs EOAD p = 0.973, HA vs AD-DS p = 0.623, EOAD vs AD-DS p = 0.860. NBTR: F (2, 7) = 5.983, p = 0.031, HA vs EOAD p = 0.031, HA vs AD-DS p = 0.175, EOAD vs AD-DS p = 0.314. SWDBB2: F (2, 27) = 1.757, p = 0.192, HA vs EOAD p = 0.236, HA vs AD-DS p = 0.439, EOAD vs AD-DS p = 0.973. (C) USP25 signal normalised to β3-tubulin and gel average measured in SWDBB1, NBTR and SWDBB2 cohorts. One-way ANOVA with Šídák's multiple comparisons test, SWDBB1: F (2, 19) = 3.698, p = 0.044, HA vs EOAD p = 0.998, HA vs AD-DS p = 0.089, EOAD vs AD-DS p = 0.067, NBTR: two-way ANOVA with Tukey's multiple comparisons test, F (2, 14) = 3.140, p = 0.975 (interaction), F (1, 14) = 0.001438, p = 0.970 (case type), F (2, 14) = 6.582, p = 0.01 (antibody), ab187156 HA vs EOAD p = 0.059, HA vs AD-DS p = 0.287, EOAD vs AD-DS p = 0.379, ab246948 HA vs EOAD p = 0.462, HA vs AD-DS p = 0.867, EOAD vs AD-DS p = 0.730, SWDBB2: one-way ANOVA with Šídák's multiple comparisons test, F (2, 23) = 2.691, p = 0.089, HA vs EOAD p = 0.172, HA vs AD-DS p = 0.155, EOAD vs AD-DS p = 0.999. Data are presented as mean ± SEM. *Sample preparation and loading was carried out by a member of the Wiseman lab.*

To determine whether USP25 abundance was significantly different among case types, I combined data from all three cohorts. Overall, relative USP25 signal was significantly affected by case type and this effect was different between cohorts when normalised to β-actin or β3-tubulin (Figure 4.14A,B, Tables 4.4, 4.5). When USP25 was normalised to β-actin, pair-wise comparisons revealed a significantly reduced abundance in AD-DS cases when compared with EOAD and healthy ageing control cases in the SWDBB cohort 1 samples of temporal cortex. Similarly, in the NBTR cohort, the abundance of USP25 when normalised to β-actin was lower in both AD-DS and EOAD compared with healthy ageing controls. However, no effect of case type was detected in the SWDBB cohort 2 samples. Normalising USP25 to the neuronal marker β3-tubulin altered the between case-type differences in both samples of temporal cortex from the SWDBB cohort and samples of prefrontal cortex from the

NBTR (Figure 4.14B, Table 4.5). In contrast to an overall trend towards reduced USP25 abundance in AD-DS and EOAD when normalising to β-actin, normalising to β3-tubulin resulted in significantly higher levels of USP25 in AD-DS compared with EOAD and HA controls in SWDBB cohort 1 samples of temporal cortex. In the NBTR samples of prefrontal cortex, in addition to significantly reduced levels of USP25 being detected in EOAD compared with healthy ageing, USP25 normalised to β3-tubulin was also found to be decreased in AD-DS cases compared with healthy-ageing controls. However, as with the previous result in temporal cortex levels of USP25 normalised to β3-tubulin were elevated in AD-DS compared with EOAD. No significant differences between case types were observed when normalising USP25 to the neuronal marker β3-tubulin in the SWDBB samples of prefrontal cortex (cohort 2).

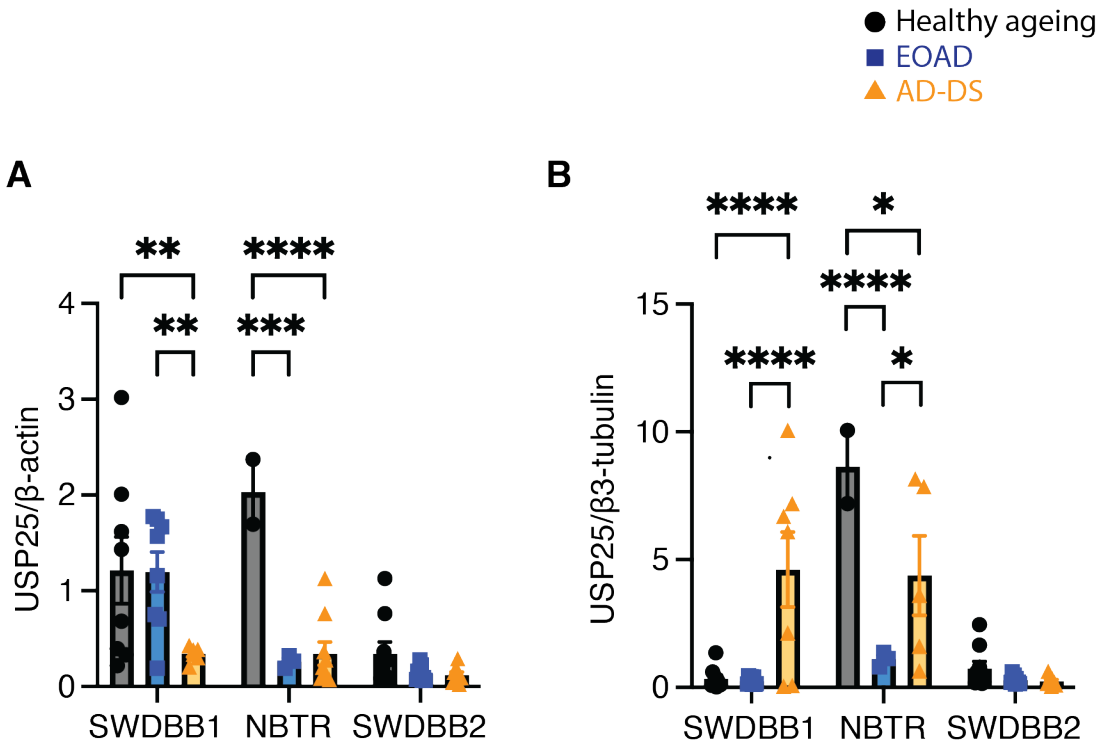

Figure 4.14 Summary of USP25 abundance in human post-mortem temporal and prefrontal cortex of AD-DS, EOAD and healthy ageing cases.

Quantification of USP25 protein levels normalised to β-actin and β3-tubulin across all three cohorts. HA n = 21, EOAD n = 21, AD-DS n = 22. (A) USP25 protein levels relative to β-actin. Two-way ANOVA with Tukey's multiple comparisons, F (4, 53) = 4.967, $p = 0.002$ (interaction), F (2, 53) = 15.90, $p < 0.0001$ (case type), F (2, 53) =

15.41, $p < 0.0001$ (brain bank) (Table 4.4). (B) USP25 relative to β3-tubulin, Two-way ANOVA with Tukey's multiple comparisons, F (4, 52) = 10.30, $p < 0.0001$ (interaction), F (2, 52) = 20.96, $p < 0.0001$ (case type), F (2, 52) = 12.36, $p < 0.0001$ (brain bank) (Table 4.5). * $p < 0.05$, ** $p < 0.01$. *** $p < 0.001$, **** $p < 0.0001$. Data are presented as mean ± SEM.

Table 4.4 Two-way ANOVA with Tukey's multiple comparisons test for USP25/β-actin across all three cohorts.

Significant differences are highlighted in green.

SWDBB1	**HA vs EOAD**	0.997
	HA vs AD-DS	0.003
	EAOD vs AD-DS	0.004
NBTR	**HA vs EOAD**	0.0004
	HA vs AD-DS	<0.0001
	EAOD vs AD-DS	0.962
SWDBB2	**HA vs EOAD**	0.613
	HA vs AD-DS	0.596
	EAOD vs AD-DS	0.998

Table 4.5 Two-way ANOVA with Tukey's multiple comparisons test for USP25/β3-tubulin across all three cohorts.

Significant differences are highlighted in green.

SWDBB1	**HA vs EOAD**	0.993
	HA vs AD-DS	<0.0001
	EAOD vs AD-DS	<0.0001
NBTR	**HA vs EOAD**	<0.0001
	HA vs AD-DS	0.012
	EAOD vs AD-DS	0.029

SWDBB2	**HA vs EOAD**	0.836
	HA vs AD-DS	0.805
	EAOD vs AD-DS	0.998

4.3 Discussion

4.3.1 Summary of findings

Usp47 was selected as one of the genes identified as a modifier of Aβ toxicity in the initial *Drosophila* screen to investigate further, due to its known role in APP stabilisation when overexpressed, leading to an increase in Aβ (Zheng *et al.*, 2022). Initial investigation indicated a beneficial effect of Usp47 co-overexpression on locomotor function of Aβ expressing flies which was independent of a change in total and soluble/insoluble levels of Aβ. I started by characterising *Usp47* further to assess its effect on fly lifespan. There was a trend towards shortened lifespan when *Usp47* was co-overexpressed with Aβ but this effect did not reach statistical significance. Interestingly, flies of the same genotype had a significant lifespan extension in the uninduced condition. Due to the insertion of a transposable element in the unregulated upstream region of the gene, *Usp47* may be overexpressed even in the -RU condition. To distinguish between potential interactions of Usp47 with Aβ and the effects of *Usp47* overexpression itself on fly longevity, I assessed lifespan of Usp47 flies lacking transgenic Aβ42. These results showed that pan-neuronal overexpression of *Usp47* is sufficient to significantly reduce *Drosophila* lifespan, suggesting that *Usp47* has a detrimental effect on longevity when overexpressed in adult neurons independent of modifying Aβ toxicity.

Due to their central role in maintaining proteostasis, DUBs are highly conserved with 44 encoded in the *Drosophila* genome (flybase.org). Although *Drosophila Usp47* is the most closely matched orthologue of *USP25* (best hit), sequence alignment is below 25% which may imply some functional differences (Rost, 1999). To establish whether

the human orthologue *USP25* may impact AD pathology in individuals with DS, we wanted to determine if this Hsa21 gene is dosage sensitive at the protein level in AD-DS. We quantified USP25 abundance by western blot in a total of 64 samples of temporal and prefrontal cortex post-mortem brain tissue obtained as three cohorts including AD-DS, EOAD and HA case types. Including all three cohorts, USP25 abundance was significantly affected by case type, with significantly lowered abundance in AD-DS compared with healthy euploid controls in the SWDBB1 cohort as well as in both EOAD and AD-DS samples in the NBTR cohort. USP25 signal was not found to correlate with age, PMI or sex but was significantly impacted by brain region and brain bank. There was an overall trend towards lower neuronal abundance in AD-DS and EOAD cases, consistent with the known loss of neurons that occurs in Alzheimer's disease (Gómez-Isla *et al.*, 1997). Normalising USP25 signal to the neuronal marker β3-tubulin did not change results for SWDBB2 but showed a significantly higher normalised USP25 abundance in AD-DS compared with EOAD and HA in the SWDBB cohort 1 of the temporal cortex and in AD-DS compared to EOAD in prefrontal cortex in the NBTR cohort. This indicated that neuronal loss may contribute to the reduced USP25 signal observed in EOAD and AD-DS in my initial analysis. Importantly, overall USP25 signal was low across all three cohorts with several samples showing bands that were not clearly distinguishable from the background signal. Therefore, findings should be interpreted with caution. However, a trend towards reduced USP25 abundance in AD-DS and EOAD was observed in all three cohorts but the relative contribution of a decrease in USP25 expression and in reduction in cell number could not be conclusively determined.

4.3.2 Expression profiles and function of USP25 in AD and DS

Individuals with DS carry an extra copy of genes encoded on Hsa21 including *USP25*. However, mRNA and protein abundance of Hsa21 genes in this population are not always present at 1.5-fold compared to euploid individuals (Lockstone *et al.*, 2007). At the transcript level, overexpression of *USP25* has been observed in a number of

tissues and cell types from individuals with DS as well as DS derived iPSCs (de Toma, Sierra and Dierssen, 2021; Palmer *et al.*, 2021). Upregulation of *USP25* was also observed in a lymphoblastoid cell line from a DS individual compared with a euploid control (Granese *et al.*, 2013). In a culture of cortical neurons differentiated from an individual with DS and disomic sibling, 212 genes across all chromosomes were significantly upregulated in trisomic samples including *USP25* with a fold-change of 1.26 (Gonzales *et al.*, 2018). An increased expression of *USP25* in the brain has been supported by single nucleus RNA (snRNA) sequencing of prefrontal cortex from people with DS and euploid controls. Although, not all brain cell types sequenced showed an upregulation of *USP25*, transcript abundance was significantly higher in excitatory neurons, microglia and pericytes in the DS cohort compared to non-DS samples (Palmer *et al.*, 2021). Notably, this study included samples from individuals with DS who were ≤ 32 years of age and lacked AD neuropathological hallmarks, although some AD pathology would be expected in this age group (Benejam *et al.*, 2020).

In our study, western blot analysis of temporal and prefrontal cortex found USP25 protein abundance was not significantly increased in human post-mortem brain tissue in individuals who had AD-DS compared to AD alone and healthy ageing controls indicating a disconnect between transcript and protein levels of this Hsa21 encoded gene. Importantly, elevated transcript of Hsa21 genes due to an extra copy, does not necessarily translate to increased protein abundance. This was highlighted in a recent multi-omics study revealing that, in the brain of individuals with DS, directionality of fold change at the mRNA and protein level only overlapped for 70% of genes (Rastogi *et al.*, 2024). This study compared post-mortem hippocampal and cortex tissue from individuals with DS (mean age of 36 years) and age-matched euploid controls and found no significant differential expression in USP25 at the gene and transcript level by bulk RNA sequencing. Interestingly, USP25 was not detected by proteomics in this work suggesting that overall level of this protein is low in post-mortem brain tissue, though the number of samples were limited to ~10 per condition making it harder to detect smaller differences. Therefore, even if overexpression of *USP25* transcript was found to be dosage sensitive into middle and old age in DS in the presence of amyloid

pathology, protein abundance could be unchanged or even decreased compared with age-matched healthy controls. USP25 protein abundance has been found to be increased in trisomic fetal brains and its overexpression during development has been linked to reduced neurogenesis in a mouse model of DS (Cai *et al.*, 2023). However, whether and how protein dosage sensitivity changes with age had not been previously investigated (Zheng *et al.*, 2021).

In our study we observed a trend towards reduced USP25 abundance in case types with AD pathology (AD-DS and EOAD). Mechanistically, during AD pathogenesis, a build-up of Aβ disturbs cellular calcium homeostasis inducing ER stress (Kuchibhotla *et al.*, 2008). USP25 has been shown to be reduced under conditions of ER stress providing a possible link between amyloid pathology and decreased USP25 protein in AD (Blount *et al.*, 2012). Comparison of USP25 protein level in LOAD and healthy age-matched controls found no difference in abundance between case types. Interestingly, this study discovered a positive correlation between USP25 protein level and APP/BACE1/Aβ42 abundance suggesting that higher levels of USP25 are associated with amyloid pathology.

Another important consideration is that abundance of USP25 protein does not provide information about its functional activity. In vitro, catalytic activity determined by oligomerisation states of USP25 has been shown to impact substrate stabilisation (Gersch *et al.*, 2019). Interestingly, overexpression of USP25 lead to inhibition of catalytic activity through tetramerisation of the protein. Therefore, measuring monoubiquitin levels could provide insight into whether USP25 function is altered in AD-DS. A recent study found significant inter-person variability in baseline USP activity proposing that this indicates that people with lowered activity are more vulnerable to increased protein accumulation in neurodegenerative diseases including AD (Hsieh *et al.*, 2024).

4.3.3 Technical limitations of analysing human post-mortem brain tissue

Power calculations based on our results from the SWDBB1 and NTBR cohorts suggested that we would require 14 AD-DS and HA control samples to test our hypothesis that USP25 protein is dosage sensitive in AD-DS. However, due to a high number of samples where USP25 signal was barely above background levels, increasing sample size would yield more reliable results. Unfortunately, access to post-mortem brain tissue from individuals who had DS is limited, particularly in the UK and within the time frame of this project we were only able to acquire 22 AD-DS and 21 HA cases. With the introduction of the Human Tissue Act (2004) (HTA), banking of new DS samples became very limited. This is because the HTA includes a pre-requisite of informed consent but the process for acquiring this has not been well adapted to individuals with ID, though some recent progress is being made to address this (Baumer *et al.*, 2022). Therefore, many of the samples available were banked several decades ago using now outdated protocols for tissue handling that varied between brain banks. This poses a potential confounding factor that may impact the degree of protein degradation that takes place post-mortem, in agreement with our findings that brain bank significantly impacted average USP25 abundance across case types. When analysing samples, it is therefore important to match AD-DS, EOAD and control samples from the same brain bank as was done in our study, to ensure that any detected differences between case types are of biological relevance.

Recently, increasing effort has been made to overcome this barrier with the establishment of the Down Syndrome Biobank Consortium that aims to collect and distribute brain tissue from individuals with DS at different ages and provide common protocols used by brain banks during tissue processing (Aldecoa *et al.*, 2024). Notably, in our study, brain bank was not identified as a factor influencing USP25 signal, suggesting that it did not significantly contribute to the observed variability in USP25 abundance in our samples.

Another limiting factor of working with post-mortem brain tissue is the rapid protein degradation that occurs between time of death and freezing of the tissue, underlining the importance of matching PMI between case types. This has been found to be particularly important for western blot analysis of frozen brain tissue where a significant reduction in protein integrity was observed when the PMI exceeded 22 hours, which was the case for several majority of our samples (Blair *et al.*, 2016). While multiple linear regression analysis suggested that variability in PMI between samples did not confound USP25 protein abundance, extended PMI periods may have contributed to an overall reduction in this protein, making detection technically challenging. Another confounding factor that can affect protein abundance is the temperature of the tissue before being frozen (Blair *et al.*, 2016). This factor is independent of PMI and was not controlled for in our study and may explain some of the variability in USP25 signal. To determine whether USP25 is dosage sensitive at the transcript level a member of the Wiseman lab also attempted to quantify mRNA levels by qPCR in the same samples. Unfortunately, subsequent RNA integrity number (RIN) analysis revealed that mRNA quality was too low to be reliably quantified in our samples. In future, it would be interesting to investigate USP25 mRNA in post-mortem brain tissue from individuals with AD-DS compared with EOAD and control cases to determine whether a trend toward reduced USP25 transcript in disease can also be observed.

4.3.4 Conclusion

Our study has indicated that the Hsa21 encoded USP25 protein product shows a trend towards decreased abundance in AD-DS and EOAD cortex cases despite evidence for its overexpression at the transcript level in trisomic neurons (Palmer *et al.*, 2021). This suggests that AD pathology may impact Hsa21 protein abundance and highlights that dosage sensitivity of Hsa21 proteins can vary across the lifespan in individuals with DS. In future experiments, increasing the number of samples as well as investigating post-mortem brain tissue from younger trisomic individuals, and whether

USP25 abundance correlates with APP/Aβ in AD-DS, could provide insight into how USP25 abundance changes with age and the onset of amyloid pathology.

Chapter 5: Validation and characterisation of ATPsynCF6/ATP5J

5.1 Introduction

DS and AD share several pathological hallmarks, including mitochondrial dysfunction. Mitochondria are essential multifunctional organelles that, aside from their role in calcium homeostasis, immune signalling and apoptosis, produce 90 % of cellular ATP (Lehninger, A., Nelson, D. and Cox, 1993; Rizzuto *et al.*, 2012; Jin *et al.*, 2017). Their double membrane structure surrounds the mitochondrial matrix and is separated by the intermembrane space (IMS). The site of energy release is located at the highly folded cristae of the inner mitochondrial membrane (IMM) and is comprised of several protein complexes that serve as electron carriers in the electron transport chain (ETC). Oxidative phosphorylation (OXPHOS) is the process by which ATP is produced in the ETC. Electrons are initially donated from NADH and $FADH_2$ to complex I and II, respectively. In a cascade of events, electrons are transferred along the ETC via enzymes and complex III and IV, where oxygen acts as the electron acceptor. This transfer results in the pumping of protons into the IMS, creating a proton gradient. Movement of protons back into the matrix through complex V allows for the conversion of ADP + Pi into ATP (Figure 5.1) (Zhao *et al.*, 2019). While the majority of mitochondrial genes are encoded in the nucleus, mitochondria contain their own self-replicating DNA (mtDNA), consisting of circular loops encoding 13 protein components of the OXPHOS system (Garcia *et al.*, 2017). Quality control of mtDNA replication is low compared to nuclear DNA and this is compensated for by dynamic fission/fusion events to maintain mitochondrial genetic homogeneity (Chan, 2012).

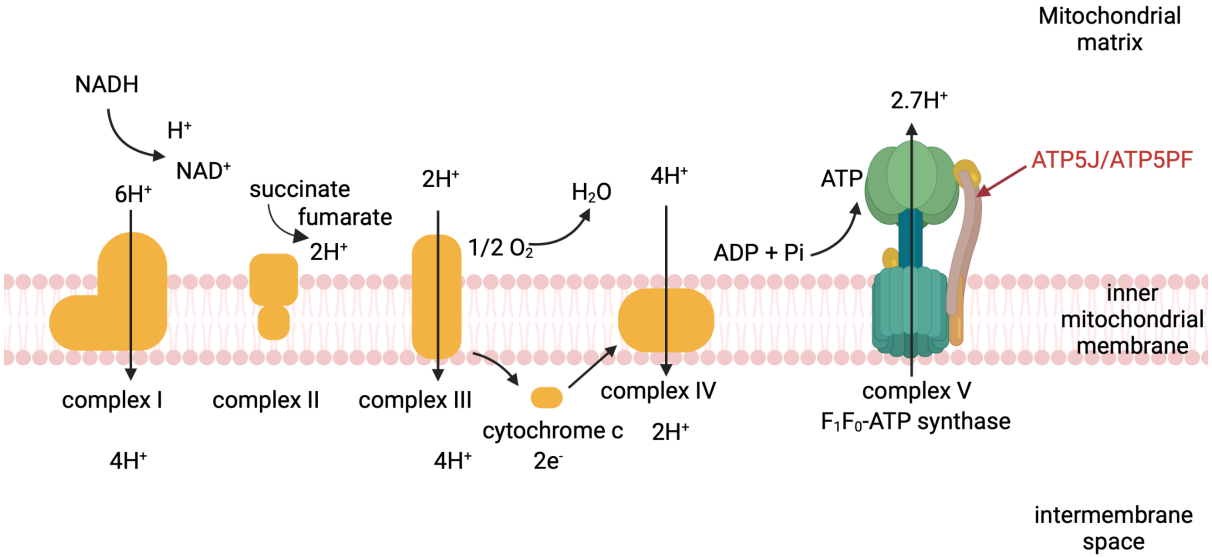

Figure 5.1 Oxidative phosphorylation occurs along the mitochondrial electron transport chain.

The ETC is embedded in the IMM and consists of protein complexes I-V and enzymes. Transfer of electrons along the complexes allows for the pumping of protons from the matrix into the IMS, creating a membrane potential. A reverse flux of protons through complex V is coupled to the conversion of ADP + Pi to ATP. Complex V is comprised of two multi-protein subunits (F0 and F1), including Hsa21 encoded ATP5J/ATP5PF as part of the F0 subunit. Created with biorender.com.

Unlike in the general population, where mitochondrial health declines with age, in individuals with trisomy 21, disturbed mitochondrial structure and function is present from development through to adulthood. This includes alterations of mitochondrial dynamics driven by increased fission and breakdown of the mitochondrial network as well as dysregulated OXPHOS resulting in lower energy efficiency (Piccoli *et al.*, 2013; Shah *et al.*, 2019; Zamponi and Helguera, 2019). Higher levels of oxidative stress and resulting DNA damage have been observed in individuals who have DS and this has been proposed as an early contributor to AD-DS neuropathology (Head *et al.*, 2001; Coskun and Busciglio, 2012). The causative mechanisms are not fully understood. In part, triplication of Hsa21 encoded genes, including *SOD1* and *APP,* may contribute to oxidative damage in tissues from people who have DS (Cenini *et al.*, 2011). Mitochondrial dysfunction has been hypothesised to present a compensatory

response to increased oxidative damage related to trisomy 21, leading to adaptive downregulation of mitochondrial function and thus reducing the impact of ROS production during OXPHOS (Helguera *et al.*, 2013). However, reduced energy release has detrimental effects on cellular function.

The brain is particularly vulnerable to these pathologies as neurogenesis and neuronal function are processes with high energy demands (Valenti *et al.*, 2010a). Animal studies have demonstrated the necessity of efficient OXPHOS function for neurogenesis and during development and adulthood (Khacho *et al.*, 2017). Thus, impairment in ATP production has been proposed as a contributor to reduced neurogenesis in the brain of fetuses with trisomy 21 (Bayona-Bafaluy *et al.*, 2021). Specifically, trisomy 21 cultured cells, including neurons, exhibit increased fragmentation of the mitochondrial network with shorter mitochondria and impaired mitochondrial transport (Helguera *et al.*, 2013; Izzo *et al.*, 2017). Furthermore, impairment of the ATP synthase has been observed in trisomy 21 skin fibroblasts, leading to an energy deficit in these cells (Valenti *et al.*, 2010a). Hsa21 encodes several nuclear encoded mitochondrial genes (NEMGs) that are either regulators of OXPHOS or are themselves part of the ETC. These include components of the ATP synthase *ATP5J* and *ATP5PO* as well as *NRIP1, SUMO3, PKNOX1*, *APP* and *RCAN1* that function as modulators of the mitochondrial biogenesis master regulator PGC-1α (Fernandez-Marcos and Auwerx, 2011). Overexpression of these genes has also been linked to increased generation of ROS in cells isolated from people with DS (Helguera *et al.*, 2013). Expression of Hsa21 NEMGs and their regulators has been found to be downregulated in trisomy 21 cells (Krapfenbauer *et al.*, 1999; Mao *et al.*, 2003; Piccoli *et al.*, 2013).

In the general population, cellular energy release declines as a result of decreasing mitochondrial health with age and this effect is exacerbated in neurodegenerative diseases, including AD, particularly affecting sporadic forms of AD (Swerdlow and Khan, 2004). Therefore, many of the above-described mitochondrial pathologies present throughout life in people who have DS are also observed in LOAD. Firstly, disturbed fusion/fission dynamics associated with upregulation of mitochondrial fission

genes have been observed in post-mortem cortical tissue from AD patients (Pickett *et al.*, 2018). Interestingly, this differential expression was positively correlated with Aβ load in these samples (Manczak, Calkins and Reddy, 2011). Secondly, decreased ATP production associated with increased ROS release has also been observed in cortical brain regions (Troutwine *et al.*, 2022). Furthermore, the function of several ETC protein complexes was found to be reduced in brain tissue from people who had AD compared to non-demented controls (Troutwine *et al.*, 2022). Another study discovered that ATP synthase stalk subunit OSCP protein was downregulated in the human post-mortem brain from people who had AD, where it co-localised with Aβ, leading to disruption of ATP synthase function (Beck *et al.*, 2016). Overexpression of OSCP in cultured neurons rescued this phenotype, highlighting that downregulation of ATP synthase proteins may be sufficient to induce mitochondrial dysfunction. Lastly, Aβ has been observed to localise to mitochondria in brain tissue from individuals who had AD, leading to ROS leakage, mitochondrial dysfunction and apoptosis (Lustbader *et al.*, 2004). Taken together, these studies suggest that Aβ pathology may trigger or exacerbate mitochondrial dysfunction in AD.

The crucial role of OXPHOS for energy metabolism through the synthesis of ATP is conserved between *Drosophila* and humans. In *Drosophila,* expression of OXPHOS genes, including *ATPsynCF6,* follows a coordinated pattern, peaking during late embryonic and pupal stages followed by another rise in expression during early adulthood (Curcio *et al.*, 2024). Mutations and loss of function of OXPHOS components has been associated with altered mitochondrial morphogenesis, impaired mtDNA maintenance, reduced neuromotor function and lifespan (Fukuoh *et al.*, 2014; Hegde, Vogel and Feany, 2014; Sawyer *et al.*, 2017; Kowada *et al.*, 2021). Furthermore, mutations in the ATPsynC gene, a component of the F1 domain within the ATP synthase complex, result in developmental delay and locomotor defects (including climbing) (Lovero *et al.*, 2018). *ATPsynCF6* codes for a protein that forms part of the peripheral stalk connecting the F0 and F1 domains of the ATP synthase complex. However, phenotypes associated with mutations or misexpression of this gene have not yet been elucidated.

Our initial fly screen identified ATP synthase peripheral stalk subunit 6 (*ATP5J*) orthologue, *ATPsynCF6,* as a negative modifier of Aβ toxicity in the context of neuromotor decline. *ATP5J* (also referred to as *ATP5PF*) codes for a protein subunit of the ATP synthase peripheral stalk and is required for the interaction between the F0 (membrane spanning complex) and the F1 (soluble catalytic core) complexes (Figure 5.1). Despite accumulating evidence for the role of ATP synthase function in mitochondrial dysregulation in DS and AD, the potential role of ATP5J has not been investigated in this context.

Aims of this chapter were to determine:

1. whether the worsening of Aβ induced locomotor dysfunction by pan-neuronal co-overexpression of *ATPsynCF6* in adult *Drosophila,* observed in the initial screen, extends to additional phenotypes.
2. whether its human orthologue ATP5J is dosage sensitive at the protein level in human post-mortem brain samples from individuals who had AD-DS and may therefore impact amyloid pathology.

5.2 Results

5.2.1 Selection of *ATPsynCF6* as a target to follow up in human post-mortem brain tissue

Mitochondrial dysfunction, and in particular disruption of the ETC presents a shared pathology of AD and DS (Ashleigh, Swerdlow and Beal, 2023; K. L. Tan *et al.*, 2023). Our initial fly screen identified *ATPsynCF6* as a modifier of Aβ toxicity when overexpressed in adult neurons independent of altering Aβ accumulation (Figures 3.3 and 3.6). Its human orthologue *ATP5J* is encoded on Hsa21 and is therefore present in 3 copies in individuals with DS. To determine whether ATP5J may act as a modifier

of amyloid toxicity in the brain, I confirmed its endogenous neuronal expression using https://www.proteinatlas.org (Figure 5.2).

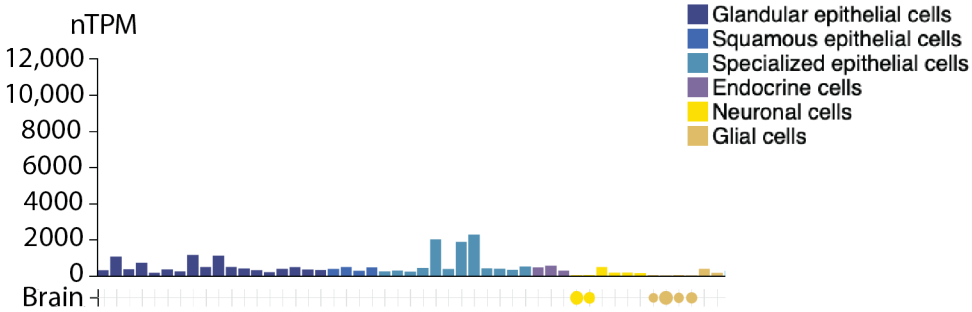

Figure 5.2 Expression patterns of *ATP5J* in human.

Single cell expression of *ATP5J* in the brain measured as normalised transcript per million (nTPM). Yellow circle (left) = excitatory neurons, 31.9 nTPM, yellow circle (right) = inhibitory neurons, 38.2 nTPM. Figure adapted from https://www.proteinatlas.org/ENSG00000154723-ATP5PF/single+cell (Karlsson *et al.*, 2021).

Additionally, to determine whether ATP5J and ATPsynCF6 likely show functional conservation, I performed multiple sequence alignment of *Drosophila* ATPsynCF6 and human ATP5J amino acid sequences (Figure 5.3). ATPsynCF6 encodes 3 isoforms of identical amino acid sequence spanning 106 amino acids, whereas ATP5J isoforms (1) and (2) code for 2 proteins comprising 108 and 116 amino acids, respectively. Across the full length of the protein, analysis showed a 40.78% conservation in amino acid identity between the two orthologues and 100% similarity between ATP5J isoforms (Table 5.1). This degree of similarity suggests functional conservation between ATPsynCF6 and ATP5J, making it a suitable orthologue.

```
CLUSTAL O(1.2.4) multiple sequence alignment


sp|P18859|ATP5J_HUMAN      MILQRLFRFSSVIRSAVSVHLRRNIGVTAVAFNKELDPIQKLFVDKIREYKSKRQTSGGP 60
sp|Q24407|ATP5J_DROME      MLSQSLLSGM----RVLRTEARRNFGIVAPALNKASDPIQQLFLDKVREYKQKSA-GGKL 55
                           *: * *:        .: .. ***:*:.* *:**  ****:**:**:****.*   .*

sp|P18859|ATP5J_HUMAN      VDASSEYQQELERELFKLKQMFG---NADMNTFPTFKFEDPKFEVIEKPQA  108
sp|Q24407|ATP5J_DROME      VDSNPDIERELKTELDRVAKQFGSDGKTDMLKFPEFQFPDVKVDPITQAPQ  106
                           **:. : ::**: ** :: : **   ::** .** *:* * *.: * :
```

Figure 5.3 Multiple sequence alignment of human ATP5J and *Drosophila* ATPsynCF6.

Alignment of amino acid sequence of ATPsynCF6 and ATP5J. Generated using Clustal Omega Multiple Sequence Alignment (MSA) (Madeira *et al.*, 2024). * = positions with a single, fully conserved residue, : = positions with conservation between amino acid groups of similar properties.

Table 5.1 Amino acid conservation between ATPsynCF6 and ATP5J.

Percentage Identity Matrix of multiple sequence alignment between ATPsynCF6 and ATP5J, generated using UniPort. UniPort IDs: ATPsynCF6 (Q24407), ATP5J (1) (P18859), ATP5J (2) (P18859-1).

	ATPsynCF6	**ATP5J (1)**	**ATP5J (2)**
ATPsynCF6	100%	40.78%	40.78%
ATP5J (1)	40.78%	100%	100%
ATP5J (2)	40.78%	100%	100%

5.2.2 Further investigation of the effects of *ATPsynCF6* overexpression on *Drosophila* climbing and lifespan

To further characterise co-overexpression of Aβ and *ATPsynCF6*, we first repeated the negative geotaxis assay to confirm worsening of the neuromotor phenotype due to *ATPsynCF6*. During this biological repeat assessment, overexpression of *ATPsynCF6* in Aβ expressing neurons resulted in slower climbing speed at each time point compared with Aβ +RU control flies. However, unlike during the initial screen, the rate of decline in climbing speed with age was not significantly altered by

overexpression of *ATPsynCF6* (Figure 5.4). This suggests that there was an overall difference in how this genotype responded during the negative geotaxis assay between the repeats.

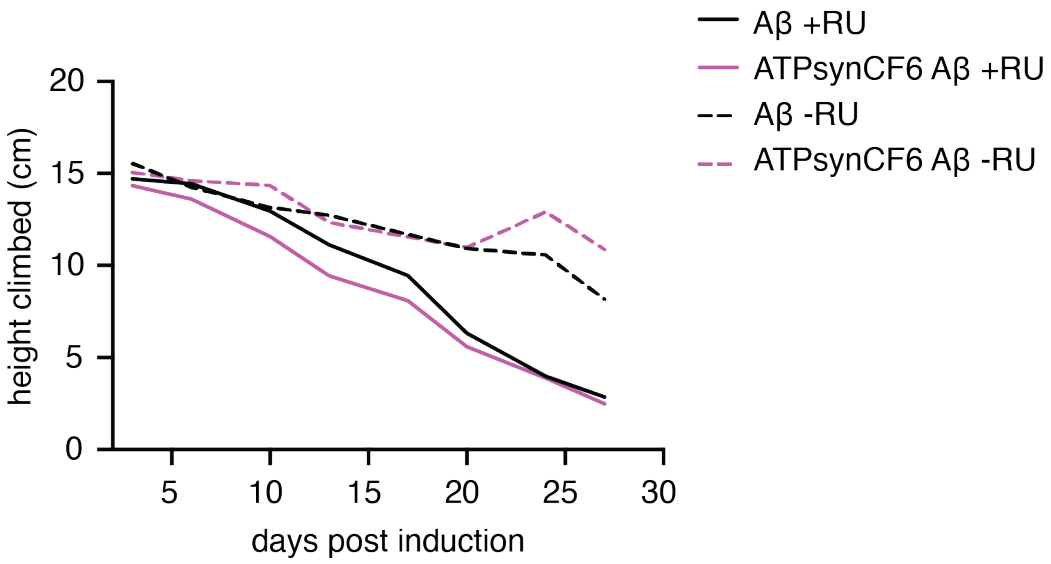

Figure 5.4 Re-screen of *ATPsynCF6* negative geotaxis assay

Average height climbed across the lifespan by flies pan-neuronally expressing Aβ42, with (pink lines) or without (black lines) overexpression of *ATPsynCF6* in adult neurons (solid lines, induced by RU-486) and uninduced controls (dashed lines). n = ~ 75 flies per condition. All p-values refer to simple linear regression. Genotype, +RU: $p = 0.002$, -RU $p = 0.225$. Age:genotype interaction: +RU $p = 0.403$, -RU $p = 0.002$. Genotypes: *UAS-Aβx2*, *elavGS* and *UAS-Aβx2*, *elavGS/UAS-ATPsynCF6.* Full statistical results are presented in Table S5.1.

Next, I wanted to investigate whether a modification of Aβ toxicity through overexpression of *ATPsynCF6* could impact fly longevity (Figure 5.5). In the induced (+RU) condition, pan-neuronal overexpression of *ATPsynCF6* reduced median and maximum lifespan from 36.5 to 34 days and 41 to 39 days, respectively. Although small, this shortening in lifespan was statistically significant and consistent with *ATPsynCF6* worsening the health of Aβ expressing flies observed in the initial fly screen. Notably, in the -RU condition, flies of the same genotype showed a large and significant extension in median lifespan from 59 to 66.6 days (Figure 5.5). Cox proportional hazards model found a significant interaction between genotype and RU,

indicating that *UAS-Aβx2*, *elavGS/UAS-ATPsynCF6* affects lifespan differently in the -RU and +RU conditions and thus, overexpression of *ATPsynCF6* modifies fly lifespan. The observed extension of the uninduced (-RU) condition indicates that the presence of the *UAS-ATPsynCF6* construct is advantageous to the *UAS-Aβx2*, *elavGS* genotype. However, whether this is due to leakage of *ATPsynCF6* expression in the absence of RU-486 would require quantification of *ATPsynCF6* expression of these flies by qPCR.

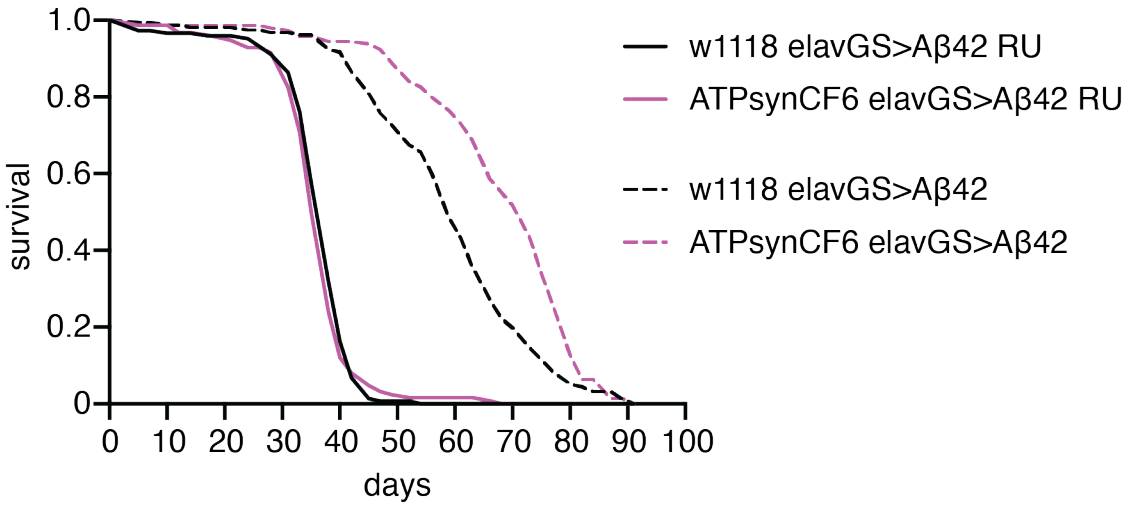

Figure 5.5 Lifespan of flies co-overexpressing Aβ and *ATPsynCF6* in adult neurons

Lifespan curves of Aβ expressing flies (solid lines) with (pink lines) or without (black lines) pan-neuronal co-overexpression of *ATPsynCF6* induced by RU-486 and uninduced controls (dashed lines). Log-rank test of *ATPsynCF6* and Aβ co-overexpression versus Aβ expression alone, +RU $p = 0.038$, -RU $p = 9.22E-08$. Cox proportional hazards: genotype $p = 2.65E-05$, RU $p < 2E-16$, genotype:RU interaction $p = 0.0003$. Genotypes: *UAS-Aβx2*, *elavGS* and *UAS-Aβx2*, *elavGS/UAS-ATPsynCF6.* Full statistical results are presented in Table S5.2.

5.2.3 Work-up of anti-ATP5J antibodies for western blot

To understand whether *ATP5J*, the human orthologue of *ATPsynCF6*, may impact Aβ toxicity in the brain of individuals who have AD-DS, we wanted to determine whether an additional copy of this Hsa21 encoded gene results in increased protein levels. For this we trialled anti-ATP5J antibodies at varying concentrations to optimise conditions for western blot, using fibroblast samples from trisomy 21 and euploid individuals. Firstly, we tested the polyclonal antibody ab224139 but were not able to visualise bands at the expected 13 kDa for either human fibroblast samples and an additional sample of mouse brain tissue at dilutions of 1:1000, 1:2000 or 1:5000 (Figure 5.6A). Secondly, we used a different polyclonal anti-ATP5J antibody (14114-1-AP) at the recommended dilution of 1:1000. This resulted in several non-specific bands but none at 13 kDa (Figure 5.6B). Lastly, we probed a membrane with euploid and trisomy 21 fibroblast samples with the polyclonal antibody PA5-29202 at dilutions of 1:1000 and 1:2000. In addition to several non-specific bands, we were able to visualise faint bands around 13 kDa (Figure 5.6C). To increase band intensity, we increased the primary antibody concentration to 1:500, which resulted in clearly visible bands at the expected molecular mass (Figure 5.6D). Therefore, PA5-29202 at a dilution of 1:500 was selected to be used to probe human post-mortem brain tissue for the abundance of ATP5J.

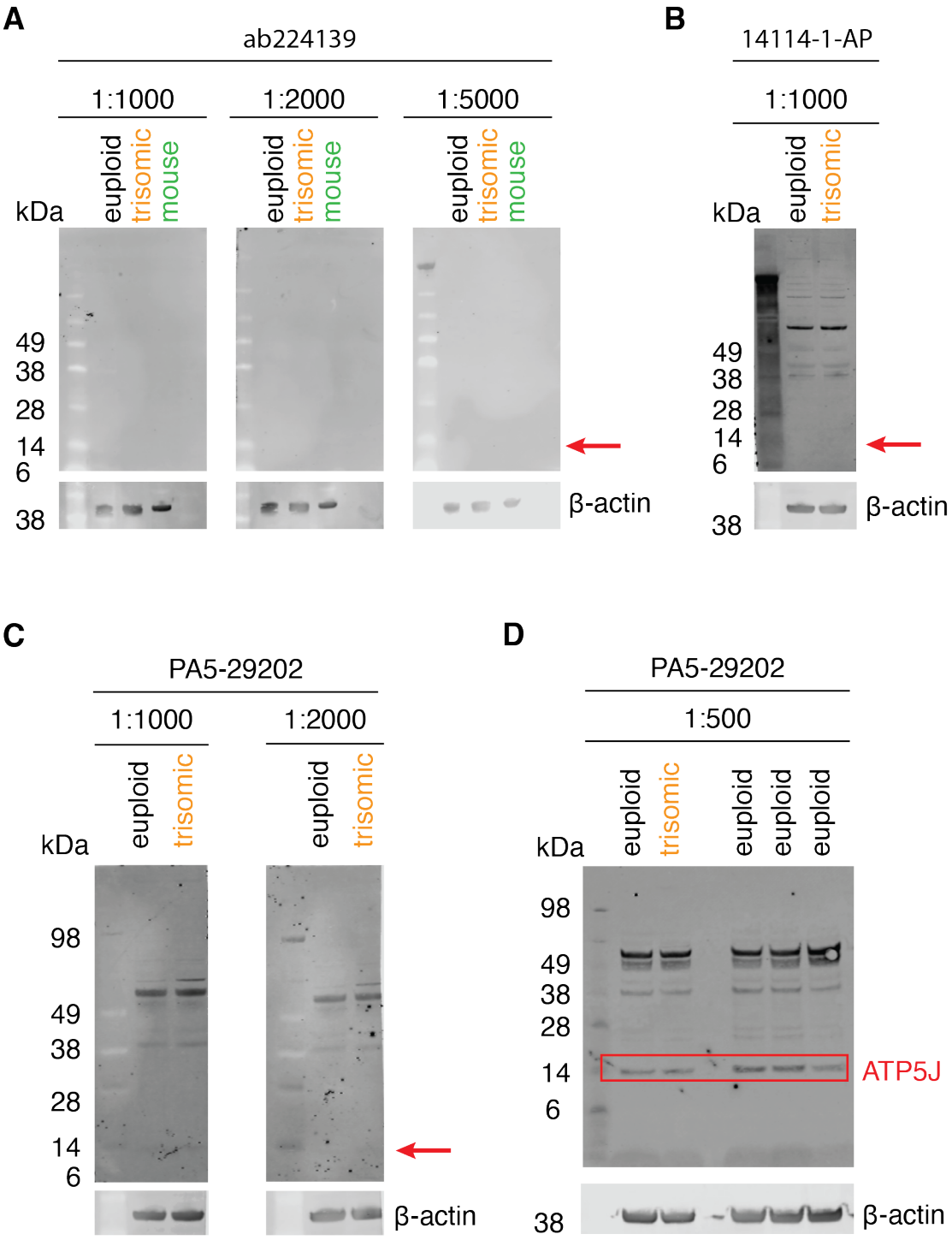

Figure 5.6 Work up of antibodies to visualise ATP5J protein in human brain samples by western blot.

Western blots testing anti-ATP5J antibodies at the indicated dilutions, using euploid and trisomy 21 human fibroblast and mouse brain samples. Anti-β-actin (A5441) was used as a loading control. Red arrows indicate the level at which a band for ATP5J would be expected. (A) Anti-ATP5J ab224139 probed at 1:1000, 1:2000 and 1:5000.

(B) Anti-ATP5J 14114-1-AP probed at 1:1000. (C) Anti-ATP5J PA5-29202 probed at 1:1000 and 1:2000. (D) Anti-ATP5J PA5-29202 probed at 1:500. The red box outlines bands at the expected molecular mass of ~13k Da.

5.2.4 Assessing dosage sensitivity of ATP5J protein in human post-mortem brain tissue

To investigate whether ATP5J abundance is altered in AD-DS or EOAD cortex compared to healthy euploid controls, we probed human post-mortem brain tissue samples from the same cohorts as detailed in chapter 4. The first examined cohort was temporal cortex (BA21), set 1 from SWDBB consisting of 9 HA, 8 EOAD and 7 AD-DS cases. ATP5J could not be quantified due to the absence of a clear band at the expected molecular mass (Figure 5.7). This lack of signal was not the result of a technical issue with the western blot itself, as β-actin bands were clearly visualised, suggesting that ATP5J abundance was too low to be detected in this cohort of samples.

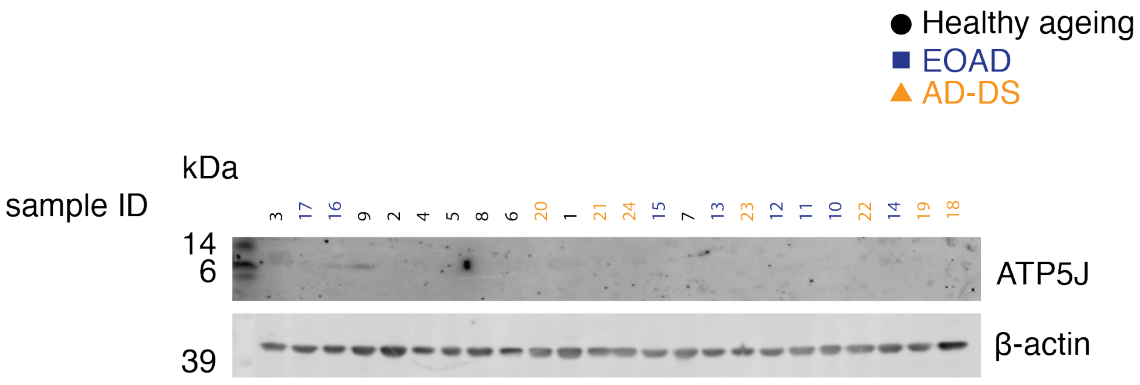

Figure 5.7 ATP5J protein abundance in human post-mortem BA21 temporal cortex.

Western blots of 24 human temporal cortex samples (BA21). Anti-ATP5J antibody PA5-29202 (1:500) was used to probe for ATP5J protein abundance in the HA, EOAD and AD-DS cases. Anti-β-actin (A5441) was used as a loading control. HA n = 9,

EOAD n = 8, AD-DS n = 7. Sample ID colours indicate case type: black = HA, blue = EOAD, yellow = AD-DS. *Sample preparation, loading and transfer was carried out by a member of the Wiseman lab.*

To determine whether a lack of bands for ATP5J in the SWDBB set 1 was specific to this cohort of samples or representative of ATP5J abundance being too low to visualise in human post-mortem brain tissue, we probed a second cohort obtained from the NBTR consisting of prefrontal cortex (BA10) with 2 HA, 3 EOAD and 5 AD-DS samples. For this cohort, quantifiable bands were visible at the expected molecular mass (Figure 5.8A). Analysis of the relative ATP5J signal found no significant difference between case types, suggesting that this protein is not dosage sensitive in AD-DS and remains unchanged in EOAD compared with healthy ageing (Figure 5.8B).

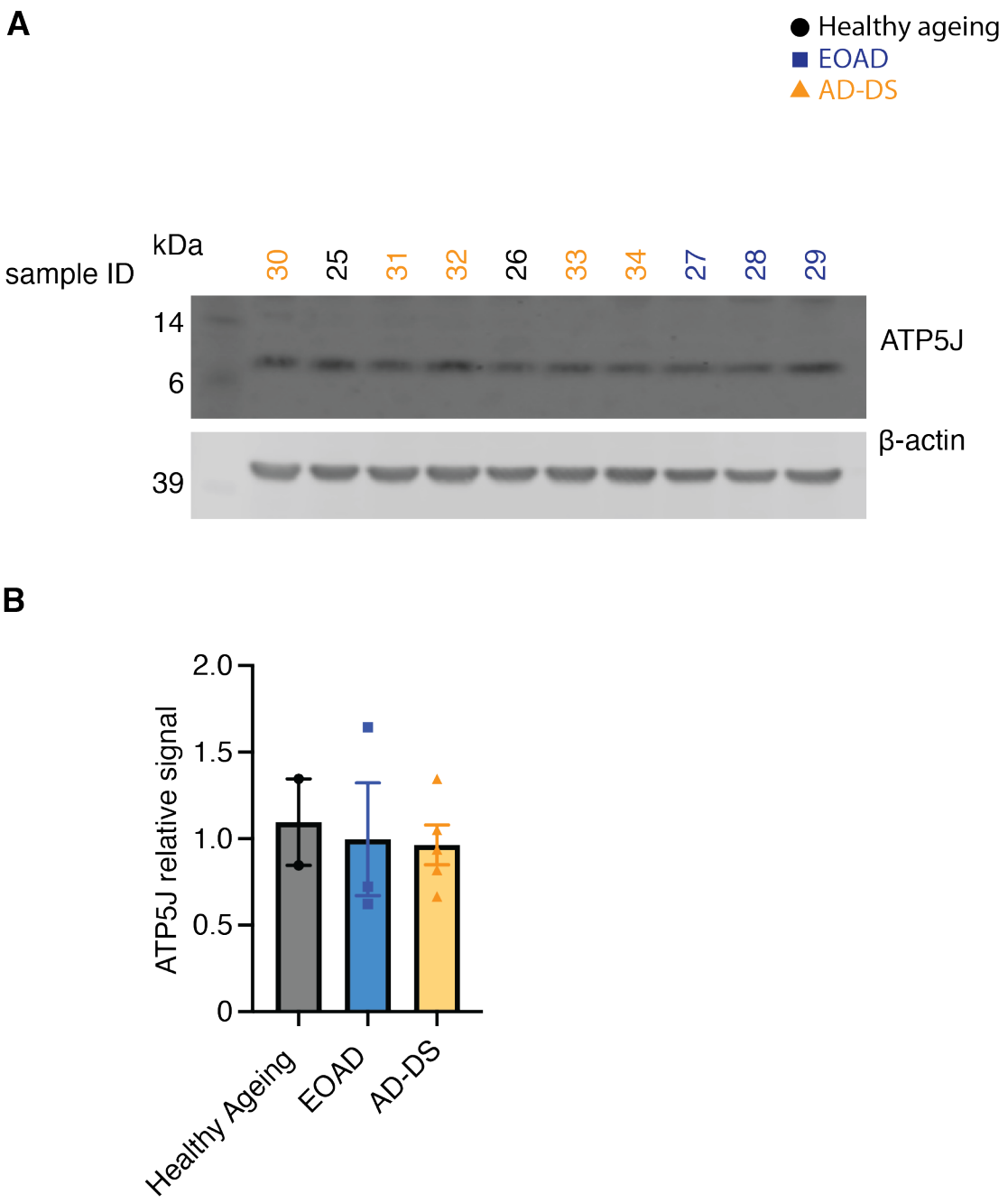

Figure 5.8 Relative ATP5J protein levels in human post-mortem pre-frontal cortex.

(A) Western blot of 10 human prefrontal cortex (BA10) samples probed with anti-ATP5J antibody PA5-29202 (1:500). HA = 2, EOAD = 3, AD-DS = 5. Anti-β-actin (A5441) was used as a loading control. Sample ID colours indicate case type: black = HA, blue = EOAD, yellow = AD-DS. (B) Quantification of ATP5J signal normalised to β-actin and gel average. One-way ANOVA with Tukey's multiple comparisons test, F

(2, 7) = 0.08590, $p = 0.919$, HA vs. EOAD $p = 0.957$, HA vs AD-DS $p = 0.911$, EOAD vs AD-DS $p = 0.992$. Data are presented as mean ± SEM. *Sample preparation, loading and transfer was carried out by a member of the Wiseman lab.*

To increase the sample size of our experiment we investigated a third cohort of human post-mortem brain tissue. This SWDBB2 cohort comprised 10 HA, 10 EOAD and 10 AD-DS cases of prefrontal cortex (BA10). Western blot probing for ATP5J showed bands of varying intensities at the expected 13 kDa molecular mass (Figure 5.9A). Quantification of relative ATP5J signal showed no dosage sensitivity of this protein in AD-DS. There was a trend towards decreased abundance of ATP5J in EOAD samples compared with HA controls but this did not reach statistical significance (Figure 5.9B).

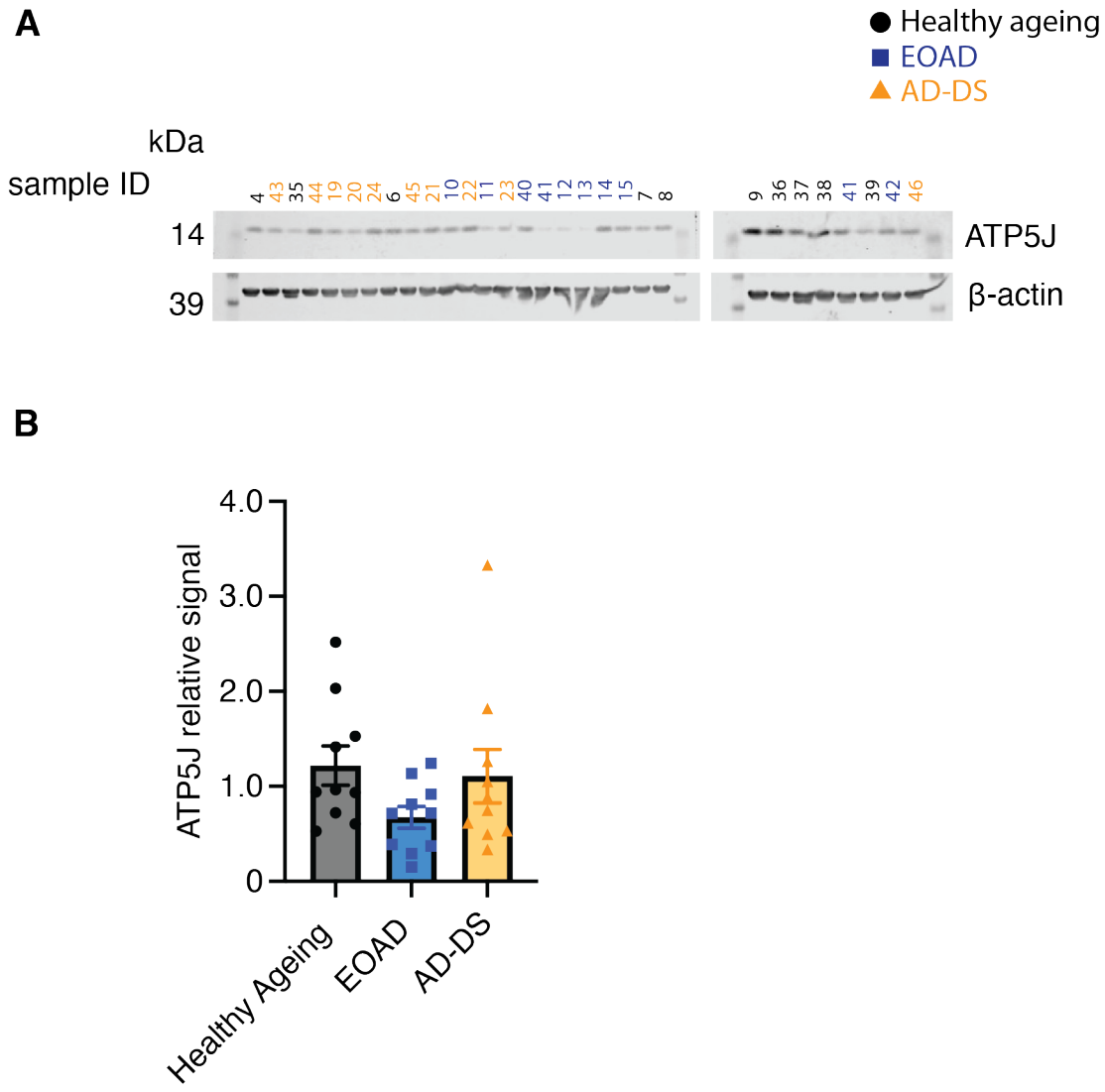

Figure 5.9 Relative ATP5J protein levels in an independent set of human post-mortem pre-frontal cortex samples.

(A) Western blot of 30 human prefrontal cortex (BA10) samples probed with anti-ATP5J antibody PA5-29202. Anti-β-actin (A5441) was used as a loading control. (B) Quantification of ATP5J signal normalised to β-actin and gel average. One-way ANOVA with Tukey's multiple comparisons test, F (2, 27) = 1.834, p = 0.179, HA vs EOAD p = 0.184, HA vs AD-DS p = 0.927, EOAD vs AD-DS p = 0.335. Data are presented as mean ± SEM. *Sample preparation, loading and transfer was carried out by a member of the Wiseman lab.*

Despite not having more human post-mortem brain tissue samples available to examine at the time of this project, I wanted to calculate the number of samples that would be required to reliably determine whether the observed trend towards reduced ATP5J abundance in EOAD samples in the SWDBB2 cohort was representative of reduced levels of this protein in AD. Therefore, I performed a power calculation using the means and SDs per case type from the NBTR and SWDBB2 cohorts. Owing to both a small effect size (0.076) and large variability in ATP5J signal detected, the minimum sample size required to achieve a power of 0.8 was calculated to be 2138 samples of HA and AD-DS cases, far exceeding the number of banked brain samples from individuals who had AD-DS in the UK. Comparison of HA versus EOAD means and SDs showed a moderate effect size of 0.685 determining the required minimum sample size to be 28 per case type (Table 5.2). However, this is still greater than the 21 samples each of HA and EOAD cases that were available to me for this work.

Table 5.2 Power calculation for ATP5J western blots.

T-test mean difference between two independent means, one-tail.

	HA (group 1) vs AD-DS (group 2)	HA (group 1) vs EOAD (group 2)
calculated effect size	0.07606279	0.6850878
error	0.05	0.05
power	0.8	0.8
sample size group one	2138	28
sample size group two	2138	28
actual power	0.80000133	0.8122393

5.2.5 Potential confounding factors influencing ATP5J abundance in human post-mortem brain tissue.

Given the variability in signal intensity between samples, I wanted to determine whether other confounding factors may influence the amount of protein present. Firstly, I investigated whether there was a linear relationship between ATP5J signal and age-at-death, a potential confounding factor that was significantly higher in the SWDBB2 control cohort (Figure 4.2). Age at death was not found to be significantly correlated with the amount of signal detected across all samples (Figure 5.10A). Secondly, I examined the correlation between PMI and ATP5J relative signal. Simple linear regression analysis determined the slope of the fitted line to be significantly non-zero, implying a positive relationship between the two variables (Figure 5.10B). Notably, although an outlier test did not identify outliers in this dataset, the correlation was driven by a single high reading of ATP5J signal. Removal of this value from the model rendered the linear relationship non-significant (Figure 5.10C).

Lastly, I performed a univariate general linear model analysis to assess the combined effect of quantitative and categorical variables including age at death, PMI, sex, brain

bank and their interactions. PMI remained the only significant co-factor positively correlated with ATP5J abundance in our samples when the highest signal value was included (Table 5.3). Together, these findings suggest that the range in ATP5J signal detected by western blot was mainly due to inter-person variability in ATP5J abundance.

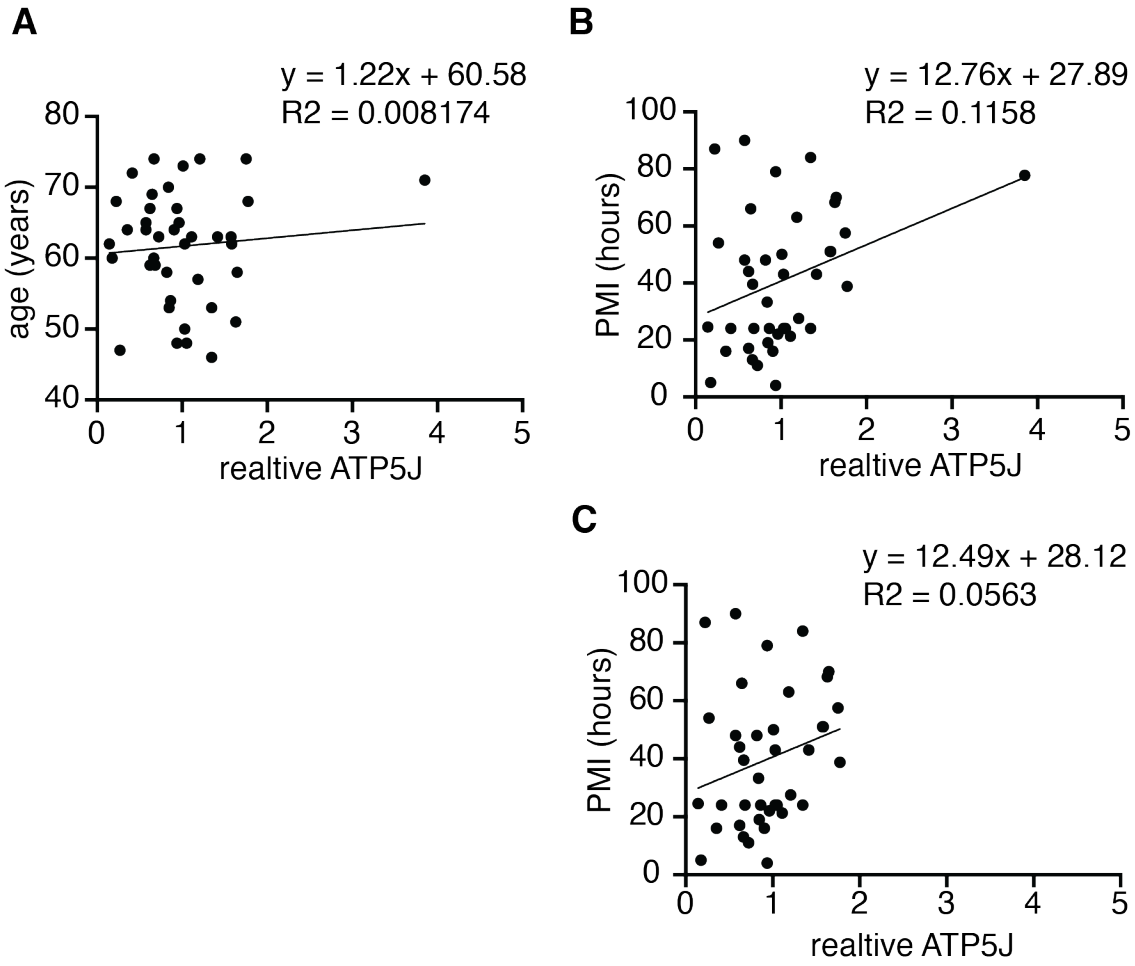

Figure 5.10 Correlation between relative ATP5J signal and age or PMI.

(A) Linear correlation between age-at-death and relative ATP5J signal across NBTR and SWDBB2 cohorts by simple linear regression, slope is not significantly non-linear, $R^2 = 0.008$, $p = 0.579$. Line of best fit y = 1.22x + 60.58. (B) Linear correlation between PMI and relative ATP5J signal across NBTR and SWDBB2 cohorts is low by simple linear regression, $R^2 = 0.1158$, $p = 0.032$. Line of best fit y = 12.76x + 27.89. No significant outliers were identified in this dataset by robust regression outlier test (ROUT) removal (Q = 1%). (C) Linear correlation between PMI and relative ATP5J

signal across NBTR and SWDBB2 cohorts with the highest PMI value removed. R^2 = 0.0563, p = 0.146. Line of best fit y = 12.49x + 28.12.

Table 5.3 Univariate general linear model of potential confounding factors influencing ATP5J signal intensity.

Tests of Between-Subjects Effects					
Dependent Variable: ATP5J relative signal					
Source	Type III Sum of Squares	df	Mean Square	F	P-value
age	0.037	1	0.037	0.096	0.759
PMI	1.906	1	1.906	4.976	0.034
Brain bank	0.076	1	0.076	0.197	0.66
sex	0.02	1	0.02	0.052	0.822
case type	0.952	2	0.476	1.243	0.305
brain bank * sex	0.608	1	0.608	1.588	0.218
brain bank * case type	0.579	2	0.289	0.755	0.48
sex * case type	0.674	2	0.337	0.88	0.426
Brain bank * sex * case type	0.002	1	0.002	0.004	0.948

To summarise our results of ATP5J abundance measured in prefrontal cortex samples, I assessed whether relative signal intensity varied significantly between case type and whether this effect differed between cohorts. The interaction between cohort and case type was not statistically significant, suggesting that the average signal per case type was not significantly affected by cohort. Additionally, neither cohort nor case type alone was found to have a significant effect on ATP5J abundance in our samples (Figure 5.11A). Due to the use of end-stage disease post-mortem brain tissue in our study, neuronal loss would be expected in EOAD and AD-DS samples compared with healthy euploid controls. We previously found a trend towards reduced neuronal abundance as measured by β3-tubulin in EOAD and AD-DS cases from the SWDBB2

cohort and a significant reduction in EOAD cases from the NBTR cohort (Figure 4.13). To determine whether ATP5J signal was correlated with neuronal abundance, I normalised ATP5J relative signal to relative β3-tubulin signal quantified in the same samples. Within both cohorts, ATP5J abundance did not differ significantly among case types relative to neuronal abundance. However, the interaction term between cohort and case type was borderline significant indicating a trend towards differing average ATP5J signal per case type between cohorts, underlining the importance of matching brain bank for AD-DS, EOAD and control samples (Figure 5.11B).

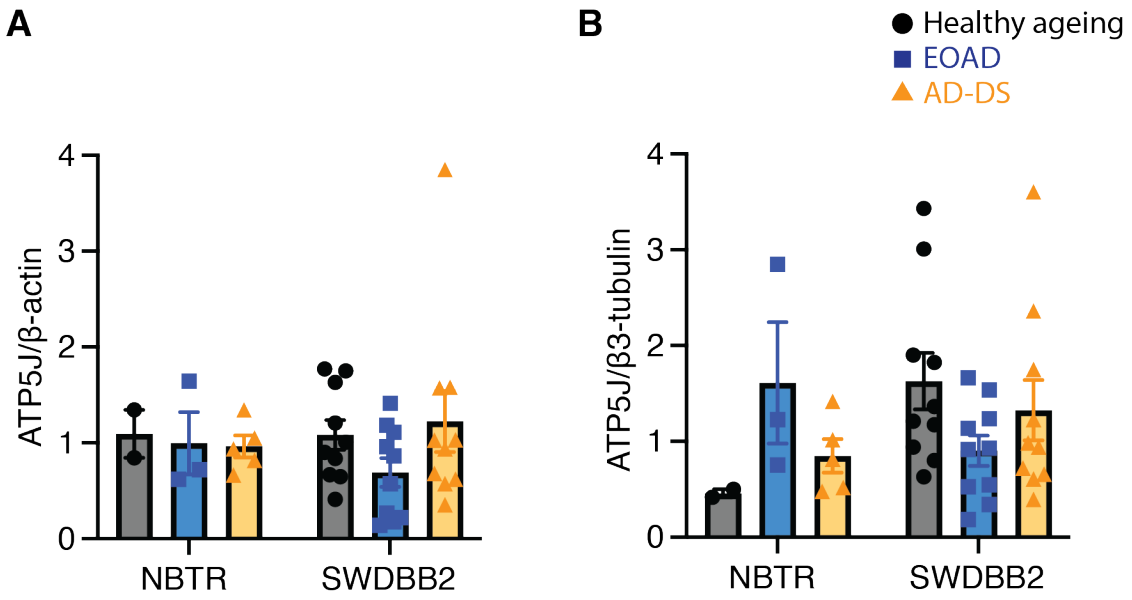

Figure 5.11 Summary of ATP5J abundance in human post-mortem brain tissue. Quantification of ATP5J signal among HA (black), EOAD (blue) and AD-DS (yellow) case types. (A) ATP5J signal normalised to β-actin and gel average divided by cohort. ATP5J abundance did not differ significantly between case types and was not significantly affected by cohort. Two-way ANOVA with Tukey's multiple comparisons test, F (2, 34) = 0.5176, p = 0.601 (interaction), F (2, 34) = 0.4601, p = 0.635 (case type), F (1, 34) = 0.0056, p = 0.941 (cohort). Multiple comparisons are presented in Table 5.4. (B) ATP5J signal normalised to β3-tubulin and gel average divided by cohort. ATP5J abundance relative to neuronal abundance did not differ significantly between case types and was not significantly affected by cohort, the interaction of the two cofactors was borderline significant. Two-way ANOVA with Tukey's multiple comparisons test, F (2, 34) = 2.847, p = 0.072 (interaction), F (2, 34) = 0.1708, p =

0.844 (case type), F (1, 34) = 1.020, p = 0.320 (cohort). Multiple comparisons are presented in Table 5.5. Data are presented as mean ± SEM.

Table 5.4 Two-way ANOVA with Tukey's multiple comparisons test for ATP5J/β-actin across all three cohorts.

NBTR	HA vs EOAD	0.998
	HA vs AD-DS	0.993
	EAOD vs AD-DS	>0.999
SWDBB2	HA vs EOAD	0.461
	HA vs AD-DS	0.951
	EAOD vs AD-DS	0.212

Table 5.5 Two-way ANOVA with Tukey's multiple comparisons test for ATP5J/β3-tubulin across all three cohorts.

NBTR	HA vs EOAD	0.274
	HA vs AD-DS	0.832
	EAOD vs AD-DS	0.409
SWDBB2	HA vs EOAD	0.124
	HA vs AD-DS	0.679
	EAOD vs AD-DS	0.478

5.3 Discussion

5.3.1 Summary of findings

In this chapter, I was interested in following up findings from my initial fly screen where *ATPsynCF6* was found to exacerbate Aβ toxicity when pan-neuronally overexpressed. Aβ toxicity has been associated with mitochondrial dysfunction in *Drosophila* models of AD, suggesting a mechanistic interaction in neurons (Wang and Davis, 2021). Individuals with DS and AD both present with mitochondrial dysfunction suggesting that an additional copy of NEMGs in DS may contribute to this phenotype. Thus, in addition to characterising *ATPsynCF6* overexpression in *Drosophila*, I also examined whether its orthologue ATP5J is dosage sensitive at the protein level in AD-DS brains.

Firstly, a biological repeat of the climbing assay showed that pan-neuronal overexpression of *ATPsynCF6* reduced climbing speed in Aβ expressing flies. However, the rate of decline with age was not significantly different. Exacerbation of the rate of decline in the initial screen, though significant, was small, suggesting that minor changes such as a different yeast batch used in the fly media may be sufficient to render the effect of *ATPsynCF6* overexpression non-significant. Secondly, using the same genotype comparisons, I observed whether *ATPsynCF6* overexpression would impact longevity. Consistent with a detrimental effect of *ATPsynCF6* in Aβ expressing flies, I observed a significant shortening of median lifespan in these flies. Conversely, in the -RU condition, lifespan was extended which may point to a pleiotropic effect of *ATPsynCF6* where very low levels of overexpression are beneficial to fly health, whereas higher level overexpression becomes detrimental. Measuring mRNA levels of uninduced *UAS-Aβx2*, *elavGS/UAS-ATPsynCF6* would reveal whether the Hsa21 orthologue is expressed at low levels in the -RU condition. RU-486 induces target gene expression in a dose-dependent manner (Osterwalder *et al.*, 2001). Therefore, repeating the experiment with lower doses of RU (and consequently

induction of lower levels of *ATPsynCF6*) would provide further insight into this hypothesis.

To determine whether a 1.5-fold increase in *ATP5J* gene dosage in DS may influence Aβ toxicity, I quantified its protein levels by western blot in cortex tissue from individuals with AD-DS, EOAD and HA controls. ATP5J could not be visualised in temporal cortex which may have been related to greater deterioration of overall protein in this cohort due to the greater age of the samples than in the frontal cortex cohorts, making the detection of low-level proteins technically challenging. Across the two prefrontal cortex cohorts (NBTR and SWDBB2), there was no significant difference in ATP5J abundance among case types, though there was a trend towards reduced levels in the SWDBB2 EOAD cases. This trend remained for the SWDBB2 frontal cortex cohort when ATP5J was normalised to neuronal marker β3-tubulin. In the NBTR prefrontal cortex cohort, this normalisation resulted in non-statistically significant higher relative ATP5J levels in EOAD cases compared with HA, though this only consisted of an n = 3. Notably, from the total number of samples investigated, we cannot be certain that ATP5J is not changed in AD-DS, as our study was underpowered.

To understand whether ATP5J variability could be explained by other factors, I conducted a univariate general linear model analysis, including age-at-death, PMI, brain bank and sex. PMI was found to be the only factor to significantly correlate with ATP5J signal. Surprisingly, these two factors were found to be positively correlated suggesting that an increase in ATP5J abundance is accompanied by an increase in PMI. This is contrary to what would be expected, as proteins begin to degrade post-mortem, leading to lower overall levels with increased PMI (Blair *et al.*, 2016). Importantly, this correlation was driven by a single high PMI value and exclusion of this data point from the analysis rendered the correlation insignificant, suggesting that for the majority of samples, variability in ATP5J signal cannot be explained by PMI. Overall, based on our data, we found ATP5J to be non-dosage sensitive at the protein level in the prefrontal cortex of individuals with AD-DS and unchanged in EOAD compared with matched healthy euploid controls.

5.3.2 Variability of mitochondrial gene expression and function in DS, AD and the general population

Our results showed substantial variability in ATP5J abundance between human post-mortem prefrontal cortex samples that did not significantly correlate with case type, age at death, PMI, sex or brain bank. This suggests that the primary source of ATP5J protein abundance may stem from differences between cell and tissue types as well as between individuals, irrespective of trisomy and disease status. Sub-areas of the cerebral cortex are mapped into BAs numbered 1-52, based on their cytoarchitecture (Brodmann, 1909). A recent cerebral proteome analysis revealed region-specific protein signatures, with 134 proteins exhibiting differential expression between at least 29 different BAs (Guo *et al.*, 2022). Overall, proteome signatures varied significantly between BA10 and BA21 regions based on functional differences between the temporal and frontal lobes. Additionally, proteomic signatures for a cluster of areas, including BA10, exhibited enrichment related to AD. Contrary to my findings, ATP5J had lower abundance in the BA10 (frontal cortex) compared to BA21 (temporal cortex), although importantly, post-mortem brain tissue for this study was isolated from a single case and therefore does not account for inter-individual variability. Another study focusing on the proteomic comparison of the frontal and temporal cortex did not find a significant difference in ATP5J protein abundance between these two areas, suggesting that a lack of ATP5J signal in our SWDBB1 temporal cortex cohort was due to technical limitations, such as poor tissue preservation, rather than to a physiologically lower level of the ATP5J protein in this brain region (Xu *et al.*, 2021). Notably, the samples of temporal cortex (SWDBB1) were sourced in 2014 and had previously been used by the Wiseman lab for another project, whereas the samples of frontal cortex (NBTR/SWDBB2) were sourced in 2022 for this and a related project (Wu *et al.*, 2023). This is likely to have contributed to lower detection in the SWDBB1 cohort as proteins are degraded during freeze-thaw cycles of the tissue.

Interestingly, evidence suggests that transcriptional brain-region variability outweighs differences between individuals (Hawrylycz *et al.*, 2012). However, inter-person variability in protein abundance is also likely to have contributed to the range of ATP5J

abundance observed in our samples (Kushner *et al.*, 2018). *Drosophila* experiments using large sample sizes can reduce the impact of this inter-individual variability in protein abundance observed in both human and *Drosophila*. Furthermore, experimental flies are crossed into a homogeneous genetic background and are exposed to the same level of the selective expression inducing RU-486 drug, resulting in comparable levels of overexpression of our gene of interest. While this provides the advantage to investigate how a pre-determined level of gene expression impacts phenotypic readouts, it does not take into account that, in humans, this response may vary between individuals based on their genetic background when the Hsa21 gene is overexpressed. Additionally, a growing number of AD risk alleles have been identified in recent years, raising the possibility that *ATP5J* alleles may influence increased vulnerability of AD in individuals in DS (Wang *et al.*, 2023). However, to date, no such alleles have been identified for *ATP5J*. Abundance of genes coding for OXPHOS components varies from person to person, with mtDNA showing the highest degree of variability. Expression levels of mtDNA encoded genes in the general population have been shown to vary by up to 100-fold between individuals independent of mtDNA copy number (Wang *et al.*, 2014). NEMGs have been found to be downregulated in hippocampal samples from individuals who had LOAD and fetal brains with trisomy 21, including a reduction in *ATP5J* expression but *ATP5J* transcript changes have not been detected in the brain of individuals with AD-DS (Mao *et al.*, 2005; Mastroeni *et al.*, 2017; Palmer *et al.*, 2021). Due to low RNA integrity, we were not able to quantify *ATP5J* mRNA abundance in our samples. Based on our western blot results, ATP5J protein abundance in AD-DS is not significantly changed compared to EOAD and non-AD euploid controls, suggesting that downregulation of OXPHOS activity in DS and AD is more likely to be driven by alterations in other mitochondrial genes.

Additionally, although mitochondrial function is known to decline with age in the general population and from a young age in DS, baseline activity levels have been suggested to be heritable (Swerdlow, Burns and Khan, 2014). This has led to the mitochondrial cascade hypothesis of AD that proposes that baseline mitochondrial activity increases the risk for certain individuals to develop sporadic AD by driving amyloid pathology (Swerdlow and Khan, 2004). Whether this mechanism also applies

to genetic forms of AD is not well understood. However, it raises the possibility that, as individuals with DS exhibit mitochondrial dysfunction from early life, this population will be particularly vulnerable to develop oxidative stress driven Aβ pathology (Ganguly and Kadam, 2022). In future, it would be interesting to assess how mitochondrial activity differs between AD-DS, EOAD and control cases. However, this is technically challenging as membrane potential (a readout of ATP synthase activity) is affected post-mortem, with evidence suggesting that a PMI of <10 hours would be required for isolation of mitochondria to perform these measurements, which is exceeded in the majority of samples we were able to obtain for our study (Barksdale *et al.*, 2010). Alternatively, measuring mitochondrial complex abundance may provide clues about dysregulation of OXPHOS in the brains of individuals with AD-DS.

5.3.3 Conclusion

In this chapter, we found no significant dosage sensitivity of ATP5J at the protein level in AD-DS post-mortem brain tissue and no significant change in its abundance in EOAD compared with age-matched healthy ageing controls, suggesting that triplication of this gene is not a driver of mitochondrial dysfunction in individuals with AD-DS. Investigating dysregulation of other mitochondrial genes in samples from individuals who had AD-DS could provide further mechanistic insight into this process.

Chapter 6: snRNA-sequencing analysis to identify other targets of interest and neuronal AD-DS gene expression signatures

6.1 Introduction

In the majority of cases, DS is caused by an extra complete copy of chromosome 21 being present in every cell, resulting in three copies of more than 230 protein coding genes as well as a currently unknown number of non-coding genes (e.g. miRNAs) and pseudogenes. While overexpression of several Hsa21 genes has been described in the literature, for many genes, the effect of triplication on the abundance of gene products has not been determined (Sleegers *et al.*, 2006). Investigating differential gene expression in tissues from people who had DS will further our understanding of how trisomy 21 gives rise to a range of pathologies present to varying degrees in individuals with DS.

It is known that trisomy 21 predisposes individuals with DS to several conditions including AD, with pathology developing decades earlier than in the general population (Lott and Head, 2019). While triplication of Hsa21 is known to be a genetic cause of early-onset AD, the underlying mechanisms of how the response to AD pathology is changed in people who have DS compared with euploid individuals is still being investigated. Importantly, having three copies of Hsa21 genes does not necessarily equate to a 1.5-fold increase in their transcript and protein levels in every cell and tissue type. Therefore, determining differences in the transcriptome and proteome in AD-DS compared with euploid individuals with AD will provide insight into how trisomy 21 affects AD in people who have DS, and can inform the processes that underlie differences in disease development and progression. Understanding these differences is crucial for developing AD-modifying therapies that can be used to treat AD-DS. Furthermore, key aspects of pathology and clinical progression of AD are similar in

DS and the general population indicating that the potential treatment benefits may extend to other forms of AD, albeit with several key differences including the earlier age of onset, higher levels of CAA and the presence of unique dense amyloid plaque structures.

An increasing number of omics studies have assessed transcriptomic and proteomic profiles in a range of tissues and cell types from individuals with DS and AD. Many studies have focused on transcript level changes employing methods including microarrays, qPCR and RNA sequencing (Olmos-Serrano *et al.*, 2016; Shi *et al.*, 2016; Palmer *et al.*, 2021; Rastogi *et al.*, 2024). While bulk RNA sequencing can reveal average tissue specific changes in gene expression between different conditions, the development of single cell/single nuclei RNA sequencing techniques (scRNA-seq/snRNA-seq) provides resolution at the single cell level. Notably, isolation of single neurons is particularly challenging due to their fragility and interconnectedness within the tissue, making the faster, nuclei isolation protocols favourable for frozen post-mortem brain tissue (Li and Wang, 2021; Cuevas-Diaz Duran *et al.*, 2022).

In AD, several transcriptomic studies of the post-mortem brain have revealed brain region, disease stage and sex specific gene expression profiles (Grubman *et al.*, 2019; Mathys *et al.*, 2019; Guennewig *et al.*, 2021; Sziraki *et al.*, 2023). A large scale scRNA-seq study examining 6 anatomical brain regions from individuals with and without AD recently identified neuronal subtypes that exhibit increased vulnerability to AD and share differentially expressed marker genes (Mathys *et al.*, 2024). However, the transcriptome of neuronal cell types was found to be particularly variable across brain regions compared with other cell types. Interestingly, this study also found cell type specific DEG signatures associated with neuritic plaques and NFTs demonstrating an interaction between gene expression and AD pathology.

Transcriptomic techniques are also being harnessed to gain insight into gene expression changes in DS tissues across the lifespan, demonstrating that dysregulation is not confined to Hsa21 genes but is present across all chromosomes (Lockstone *et al.*, 2007; Y. Chen *et al.*, 2023). This gene expression dysregulation is

present from the early foetal stages where trisomy 21 has been associated with upregulation of genes involved in neuronal differentiation, synaptic transmission, immune response and white matter defects (Olmos-Serrano *et al.*, 2016). Within the same study, analysis of DEGs across different ages and brain regions revealed spatiotemporal differences in gene dosage sensitivity in the DS brain, with region and age accounting for a larger amount of variability compared to genotype. A meta-analysis of DS transcriptomic differential expression datasets identified clusters of DEGs that were consistently dysregulated across studies enriched for GO categories associated with inflammation, a hallmark pathology of DS (Flores-Aguilar *et al.*, 2020; Huggard *et al.*, 2020; de Toma, Sierra and Dierssen, 2021). Bulk transcriptomic studies average expression levels across multiple cell types within the same tissue but cannot determine whether observed differential gene expression is due to changes in the levels of gene products present in each cell or an altered ratio of cell types within the tissue. This is particularly important for the study of trisomy 21 in which developmental differences are known to alter the abundance of specific brain cell-types (Russo, Sousa and Bhattacharyya, 2024). snRNA-seq data support the contribution of both factors, revealing changes in the excitatory and inhibitory neuron ratios as well as cell type specific profiles of DEGs in the DS brain (Palmer *et al.*, 2021). However, whether this change in neuronal cell type ratio is altered with the development and progression of AD-DS is not yet understood.

Importantly, while these studies provide insight into transcriptional changes in AD and DS, endogenous compensatory mechanisms mediate a poor correlation between transcriptome and proteome, including in cortical brain regions (Carlyle *et al.*, 2017). In the adult DS brain, discrepancies between differentially expressed genes, transcripts and proteins have been observed, with changes being region-specific even when accounting for differences in cell type composition between trisomic and disomic samples (Rastogi *et al.*, 2024). Enrichment of pathways associated with dysregulated genes and proteins exhibit only a small overlap, indicating that those identified in transcriptomic studies do not capture the full extent of functional changes resulting from trisomy 21. Notably, these findings are from young DS individuals lacking evidence of amyloid pathology. Therefore, the relative contribution of trisomy 21 and

AD to differential gene and protein abundance have not been determined. To address this research gap, the Wiseman lab conducted an snRNA-seq study comparing cell type specific DEGs in the prefrontal cortex of individuals with AD-DS, EOAD and healthy euploid controls (Farrell *et al.,* in preparation). For my study, I was interested in neuronal differential gene expression signatures and how their associated enriched pathways may differ between age-matched AD-DS and EOAD brains.

Aims of this chapter were to:

1. determine whether Hsa21 orthologues of genes identified as modifiers of Aβ toxicity in the initial *Drosophila* screen are dosage sensitive at the transcript level in different neuronal cell types in AD-DS compared with EOAD and healthy ageing (HA) controls.
2. investigate enriched pathways associated with upregulated and downregulated genes in excitatory and inhibitory neurons and whether they are shared or unique between AD-DS and EOAD.
3. identify Hsa21 genes of interest whose orthologues were not included in the *Drosophila* screen to investigate as potential modifiers of Aβ toxicity/accumulation based on their dosage sensitivity in AD-DS neurons.

6.2 Results

6.2.1 Case demographics

SnRNA-seq preparation and data processing was carried out by Dr Yazead Buhidma (Lashely lab, IoN, UCL) and Dr Clíona Farrell (Wiseman lab, UK DRI at UCL) at UCL Genomics. Samples were obtained from the NBTR consisting of prefrontal cortex (BA10) post-mortem-brain tissue isolated from 4 HA, 4 EOAD and 8 AD-DS cases. All HA cases lacked AD pathology (Braak stage 0), all EOAD cases were Braak stage VI. Four AD-DS cases were Braak stage VI, whereas 4 cases did not have Braak staging

but neuropathological examination revealed severe amyloid plaque load and NFT. Causal mutations for EOAD cases were not known as they had not been sequenced for *APP*, *PSEN1* or *PSEN2* mutations. Case types were matched for age (one-way ANOVA, $F(2, 13) = 2.640$, $p = 0.109$), PMI (one-way ANOVA, $F(2, 13) = 0.698$, $p = 0.515$) and *APOE* genotype where known and possible. Sex was distributed equally among AD-DS cases, with the HA cohort skewed towards male cases (3 male, 1 female) and the EOAD cohort skewed towards female cases (1 male, 3 female).

6.2.2 Differential gene expression in neuronal populations

snRNA-seq data can identify signatures of gene dysregulation at the single cell level in AD-DS compared with EOAD and control brains. In my *Drosophila* screen I restricted overexpression of Aβ and Hsa21 orthologues to adult neurons to assess the effect on amyloid toxicity and accumulation. Therefore, in this snRNA sequencing dataset, I was interested in neuronal signatures of differential gene expression in AD-DS compared with EOAD and non-trisomic healthy controls. Sequencing recovered 89,649 nuclei with an average cell count of 5,603 per case (ranging from 1494-7888 cell counts, Table S6.1). A total of 38 distinct clusters were identified, including 8 excitatory and 4 inhibitory neuronal sub populations, comprising all the main neuronal subtypes based on their expression patterns. In neuronal cell types, out of 31,743 detected genes, 343 and 106 genes were found to be significantly upregulated (false discovery rate (FDR) < 0.05) in excitatory and inhibitory neurons, respectively in AD-DS compared to HA prefrontal cortex. Of those that were upregulated, 63 genes in excitatory neurons and 38 genes in inhibitory neurons were Hsa21 encoded (Table 6.1). Across all neuronal subclusters, AD-DS versus control cases exhibited the highest number of upregulated genes, with some clusters showing an equal or greater number of downregulated genes. As expected, the number of upregulated Hsa21 genes as a proportion of all upregulated genes was also greatest for this case type comparison, independent of the number of dysregulated genes per cell type (Figure 6.1A). Only 2 Hsa21 triplicated genes (*APP* in excitatory neuron cluster 1 and

RIPPLY3 in excitatory neuron cluster 6) were significantly downregulated in AD-DS neurons. Interestingly, all neuronal subtypes also exhibited upregulated expression of several Hsa21 genes in AD-DS compared to EOAD samples, suggesting that dysregulation of these genes is caused or exacerbated by trisomy 21 rather than AD alone (Figure 6.1B). This is supported by only a small number of genes being upregulated in EOAD compared with controls, with Hsa21 genes making up a low proportion of these DEGs (Figure 6.1C).

Table 6.1 Hsa21 genes upregulated in excitatory and inhibitory neuronal cell types in brain samples from individuals who had AD-DS compared with HA controls.

Excitatory neurons				**Inhibitory neurons**	
NCAM2	*BRWD1*	*UBEG2G*	*SLC19A1*	*APP*	*KCNJ6*
APP	*DOPB1*	*PKNOX1*	*VPS26C*	*TTC3*	*TMEM50B*
DSCAM	*DYRK1A*	*NRIP1*		*TIAM1*	*AGPAT3*
BACE2	*CRYZL1*	*SCAF4*		*NCAM2*	*MORC3*
TTC3	*PDXK*	*BTG3*		*SON*	*BACE2*
PTTG1IP	*PRMT2*	*IFNAR2*		*ITSN1*	*PKNOX1*
GRIK1	*HUNK*	*SOD1*		*PRMT2*	*DIP2A*
LSS	*MORC3*	*CBR1*		*DSCAM*	*PDE9A*
KCNJ6	*C2CD2*	*CXADR*		*MX1*	*IFNAR1*
TIAM1	*SYNJ1*	*ADAMST1*		*PDXK*	*ATP5PO*
EVA1C	*COL18A1*	*TMEM50B*		*GRIK1*	*C2CD2*
TRAPPC10	*USP25*	*RUNX1*		*BRWD1*	*AT5PF*
SON	*ADARB1*	*USP16*		*HLCS*	*USP25*
ETS2	*HLCS*	*SLC37A1*		*CXADR*	*PAXBP1*
PCP4	*ABCG1*	*RCAN1*		*SYNJ1*	*DONSON*
TRPM2	*PCNT*	*PCBP3*		*PCNT*	*BACH1*
ZBTB21	*MX1*	*PFKL*		*SOD1*	*IFNAR2*
PAXBP1	*C21orf91*	*MRPS6*		*GET1*	*USP16*
DIP2A	*PDE9A*	*TSPEAR*		*DYRK1A*	
ITSN1	*BACH1*	*SUMO3*		*TRAPPC10*	

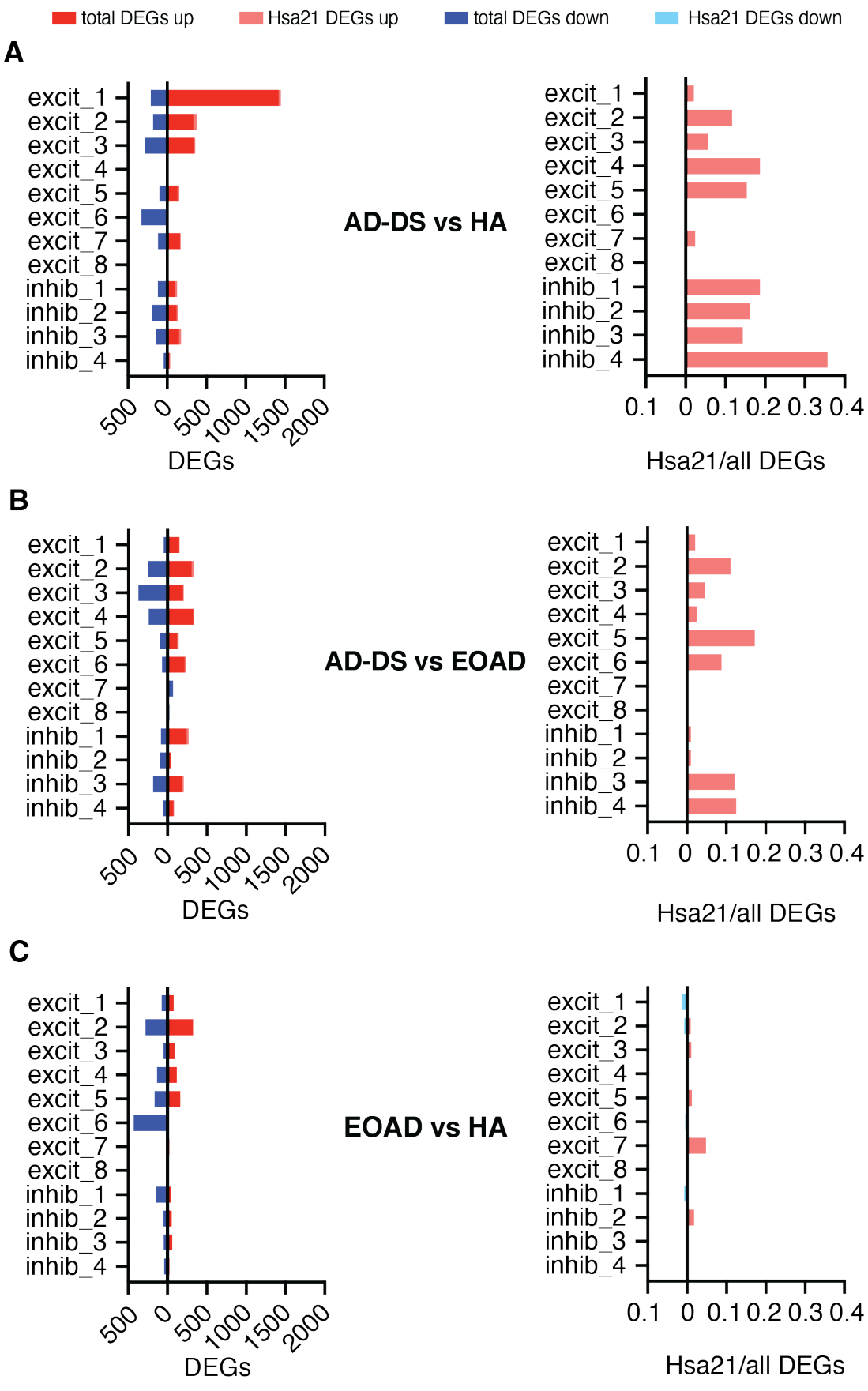
total DEGs up
Hsa21 DEGs up
total DEGs down
Hsa21 DEGs down
A
excit_1
excit_2
excit_3
excit_4
excit_5
excit_6
excit_7
excit_8
inhib_1
inhib_2
inhib_3
inhib_4
500 0 500 1000 1500 2000
DEGs
AD-DS vs HA
0.1 0 0.1 0.2 0.3 0.4
Hsa21/all DEGs
B
AD-DS vs EOAD
C
EOAD vs HA

Figure 6.1 Differentially expressed genes in excitatory and inhibitory neuron clusters.

Significant DEGs (FDR <0.05, percentage detection (pct) > 0 in the analysed cell types) in excitatory neuron clusters 1-8 and inhibitory neuron clusters 1-4. Case type comparisons: (A) AD-DS vs HA, (B) AD-DS vs EOAD, (C) EOAD vs HA. Each case type comparison shows the total number of DEGs per cluster that were significantly up (red) or downregulated (blue) and the proportion of Hsa21/total DEGs per cluster that were significantly up or downregulated.

6.2.3 Differential expression of genes of interest from the *Drosophila* screen

Subsequently, I was interested in whether genes I identified as hits for Aβ toxicity modifiers in my initial *Drosophila* screen were upregulated at the transcript level in AD-DS prefrontal cortex neurons. Of those that I did not investigate further in human post-mortem brain tissue, *DYRK1A* was significantly overexpressed in AD-DS compared with HA in four excitatory and three inhibitory neuron sub clusters, consistent with previously observed dosage sensitivity of this gene in the DS brain (Palmer *et al.*, 2021). Notably, there was no significant difference in its mRNA level in AD-DS compared with EOAD as well as in EOAD compared with HA (Figure 6.2B). Therefore, upregulation of *DYRK1A* cannot be attributed to AD pathology in these cases.

HLCS, whose fly orthologue *Hcs* was found to rescue Aβ toxicity, was also upregulated in several neuronal cell types in AD-DS compared with both HA and EOAD cases (Figure 6.2C). *SAMSN1*, the Hsa21 orthologue of *Drosophila Sb* that rescued the Aβ induced climbing defect in my fly screen exhibited no significant change in expression in AD-DS samples which may also reflect its low endogenous expression in neuronal cell types (Figure 6.2D). Similarly, *TMPRSS2*, the human orthologue of *SKIP*, which exhibited a beneficial effect on *Drosophila* locomotor function in the initial screen, was not dysregulated in neurons from individuals with AD-DS compared with EOAD and

HA cases. Detection of this gene was absent or very low in neuronal cell types in the Farrell *et al.* dataset, consistent with published neuronal expression patterns of this gene (X. Zhang *et al.*, 2016; Karlsson *et al.*, 2021).

Based on our western blot results, USP25 showed a trend towards reduced abundance with AD in temporal and prefrontal cortex samples. Notably, the 10 samples obtained from the NBTR and examined by western blot belonged to the same cases and brain region as for the snRNA-seq dataset. In contrast to protein abundance in AD-DS, at the transcript level, *USP25* was significantly increased in 2 excitatory and 2 inhibitory neuron clusters in comparison to euploid HA control and in 2 excitatory and 1 inhibitory neuron clusters when compared with EOAD cases. Additionally, a significant downregulation was present in excitatory neuron cluster 2 when comparing EOAD versus HA samples. These results support reduced USP25 levels in EOAD compared with AD-DS and HA case types, in agreement with our observed trend towards protein level reduction in EOAD brains (Figure 6.2E). Our quantification of ATP5J protein abundance in prefrontal cortex showed no significant change in AD-DS or EOAD compared with controls. Consistent with these findings, *ATP5J* transcript was not significantly altered in the majority of neuronal cell types, with the exception of a small upregulation of 0.1 logFC in one inhibitory neuron subcluster in AD-DS compared with controls (Figure 6.2A).

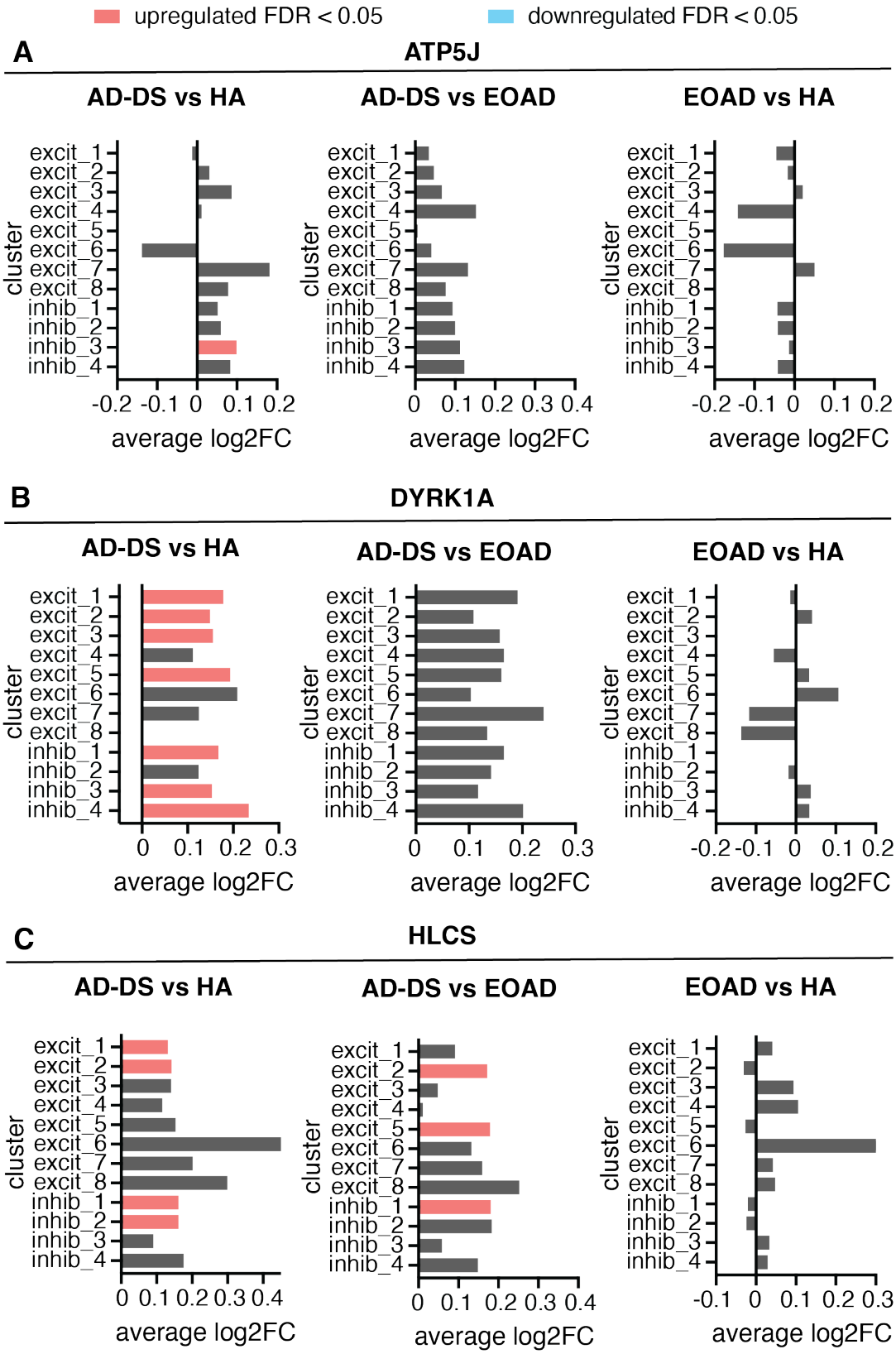
upregulated FDR < 0.05
downregulated FDR < 0.05
A
ATP5J
AD-DS vs HA
AD-DS vs EOAD
EOAD vs HA
cluster
excit_1
excit_2
excit_3
excit_4
excit_5
excit_6
excit_7
excit_8
inhib_1
inhib_2
inhib_3
inhib_4
-0.2 -0.1 0 0.1 0.2
0 0.1 0.2 0.3 0.4
average log2FC
B
DYRK1A
AD-DS vs HA
AD-DS vs EOAD
EOAD vs HA
0 0.1 0.2 0.3
C
HLCS
AD-DS vs HA
AD-DS vs EOAD
EOAD vs HA
-0.1 0 0.1 0.2 0.3

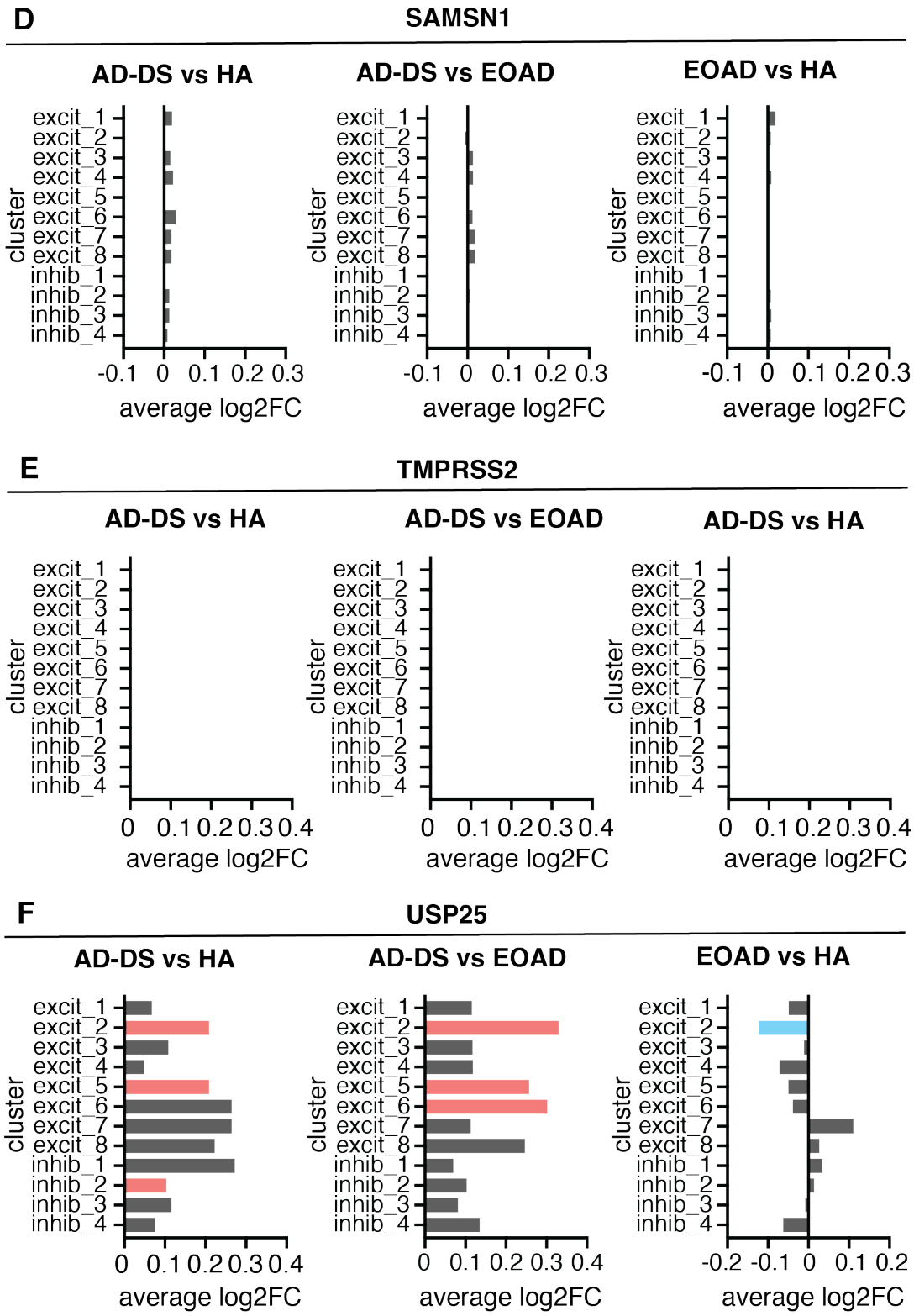

Figure 6.2 Neuronal expression profiles of genes of interest

(A-F) Average log_2 fold change (log2FC) of Hsa21 genes of interest in excitatory and inhibitory neuron clusters comparing AD-DS vs HA, AD-DS vs EOAD and EOAD vs HA case types. Significant upregulation (red) and significant downregulation (blue) by FDR < 0.05 and pct > 0 in the analysed cell types. Grey bars = log_2FC with FDR >

0.05). Genes of interest based on orthologues (*ATP5J/ATPsynCF6, DYRK1A/mnb, HLCS/Hcs, SAMSN1/Sb, TMPRSS2/SKIP, USP25/Usp47*), identified as modifiers of Aβ toxicity in the initial fly screen.

6.2.4 Dysregulated pathways in AD-DS and EOAD

Based on the observed dysregulation of gene expression in AD-DS prefrontal cortex neurons, I wanted to investigate whether up and downregulation of these genes was associated with distinct enriched biological processes in AD-DS and EOAD. I combined subclusters into inhibitory and excitatory neuronal cell types, separating up and downregulated genes per case type comparison. I performed gene ontology analysis, with all detected genes from the examined clusters set as the background genome. GO categories of biological processes were ranked from smallest to largest by FDR. Among all case type comparisons, both excitatory and inhibitory neuronal cell types exhibited dysregulated expression of genes involved in processes relating to neurodevelopment and synaptic function, suggesting that these are not unique to AD-DS (Figure 6.3). Processes relating to axons and cell projections were identified to be among the top 10 most significantly enriched pathways in inhibitory and excitatory neurons when comparing AD-DS samples with HA and EOAD, respectively. Dysregulated genes associated with these pathways included *HECW1, CNTN1, STMN4*, *MAP1B* and Hsa21 encoded *TIAM1* (Figure 6.3B,D). These GO categories were present in both up and downregulated DEGs for the AD-DS versus EOAD comparison within excitatory neuron clusters, suggesting dysregulation of gene expression results in disturbed axonal and dendritic development and function. Notably, genes involved in cell projection, including *CNTN1* and *NCDN,* were also upregulated in EOAD neurons compared with controls, indicating that AD pathology may contribute to the observed dysregulation of these processes in AD-DS. Interestingly, when comparing upregulated genes in EOAD versus HA samples for inhibitory neurons, 8 out of the top 10 most significantly enriched processes were GO terms relating to OXPHOS and the ETC (Figure 6.3F).

GO Biological Processes: Excitatory Neurons

A

AD-DS vs HA

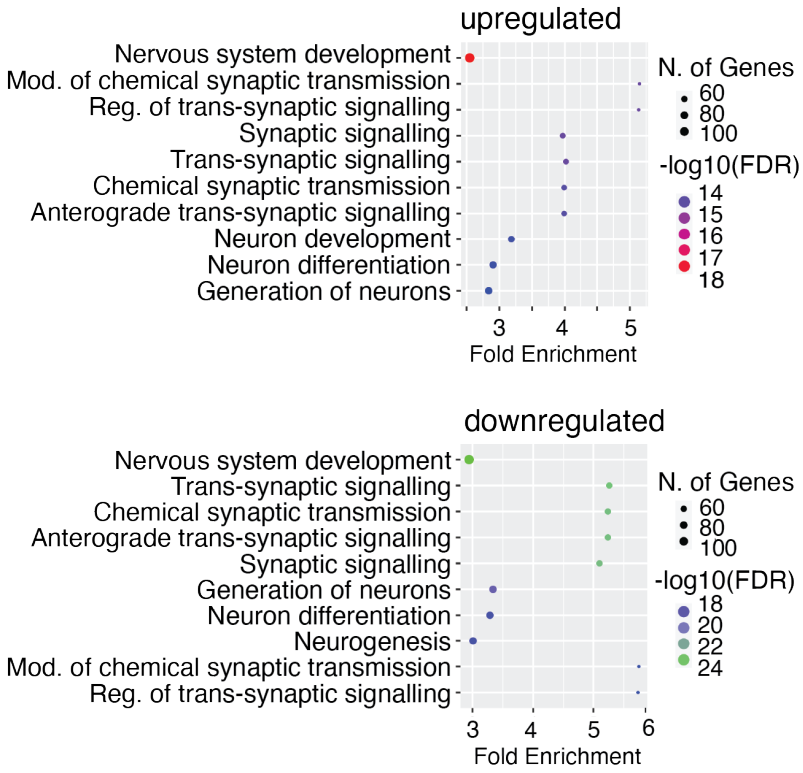

B

AD-DS vs EOAD

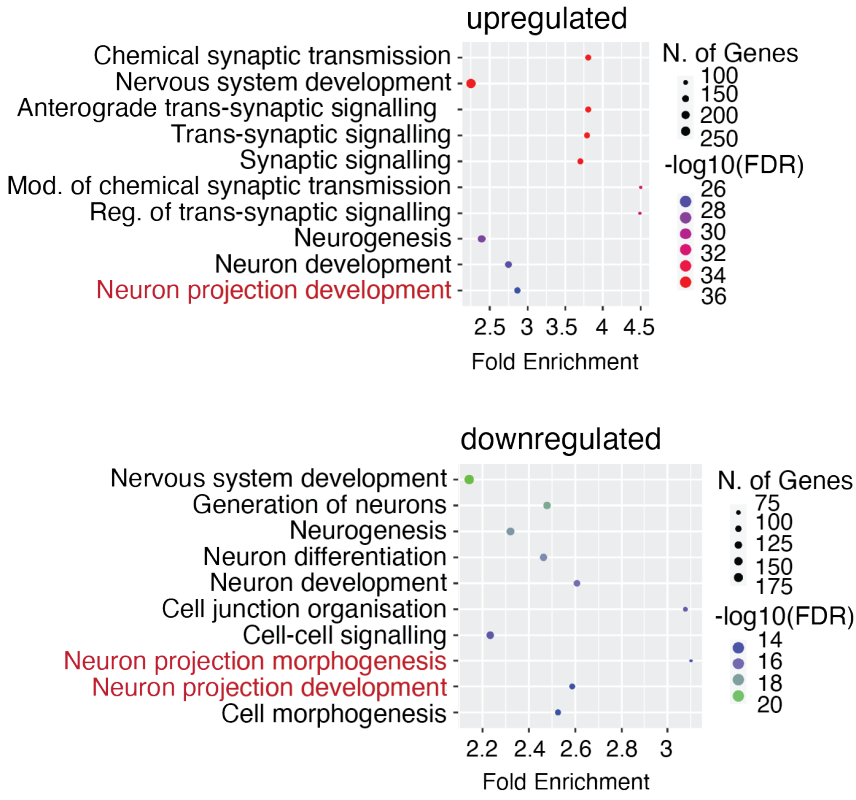

C

EOAD vs HA

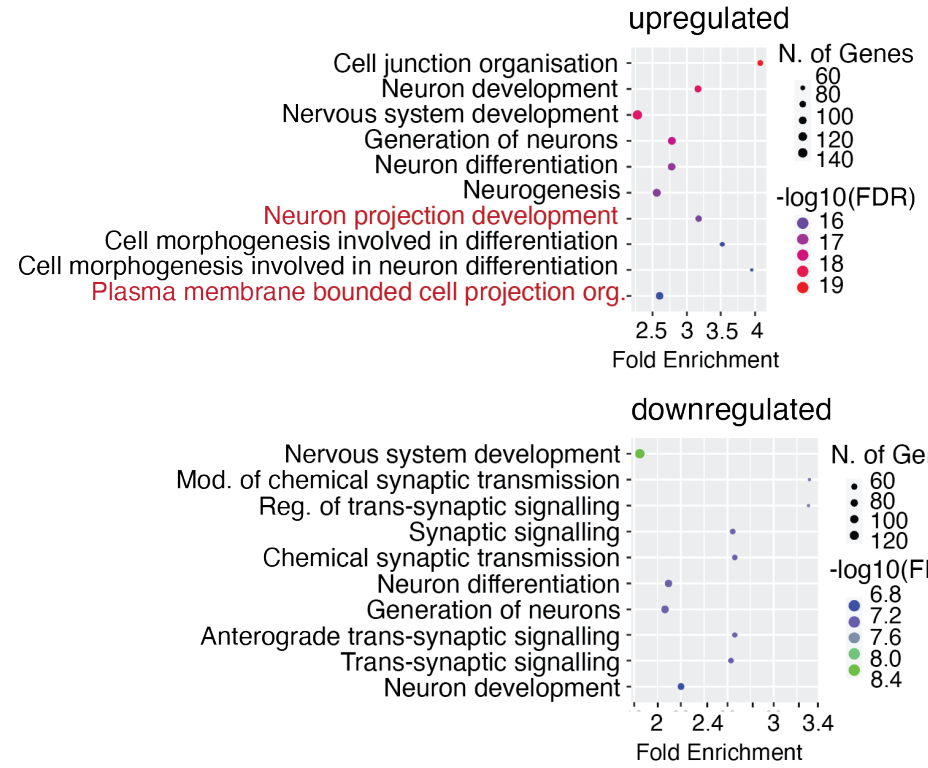

GO Biological Processes: Inhibitory Neurons

D

AD-DS vs HA

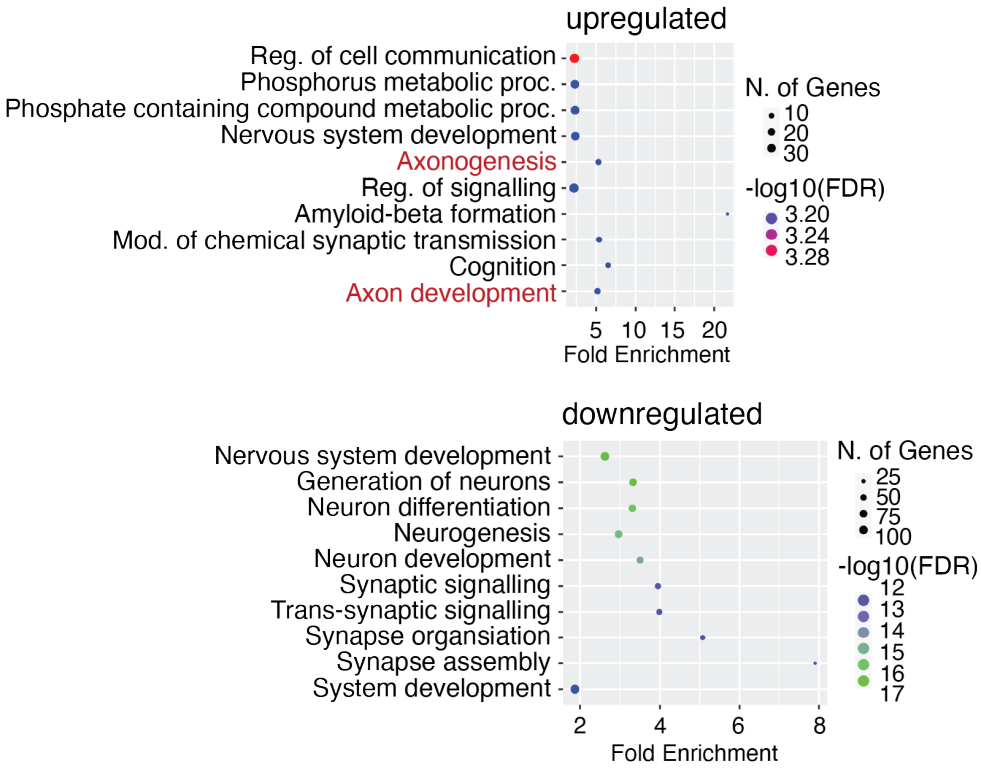

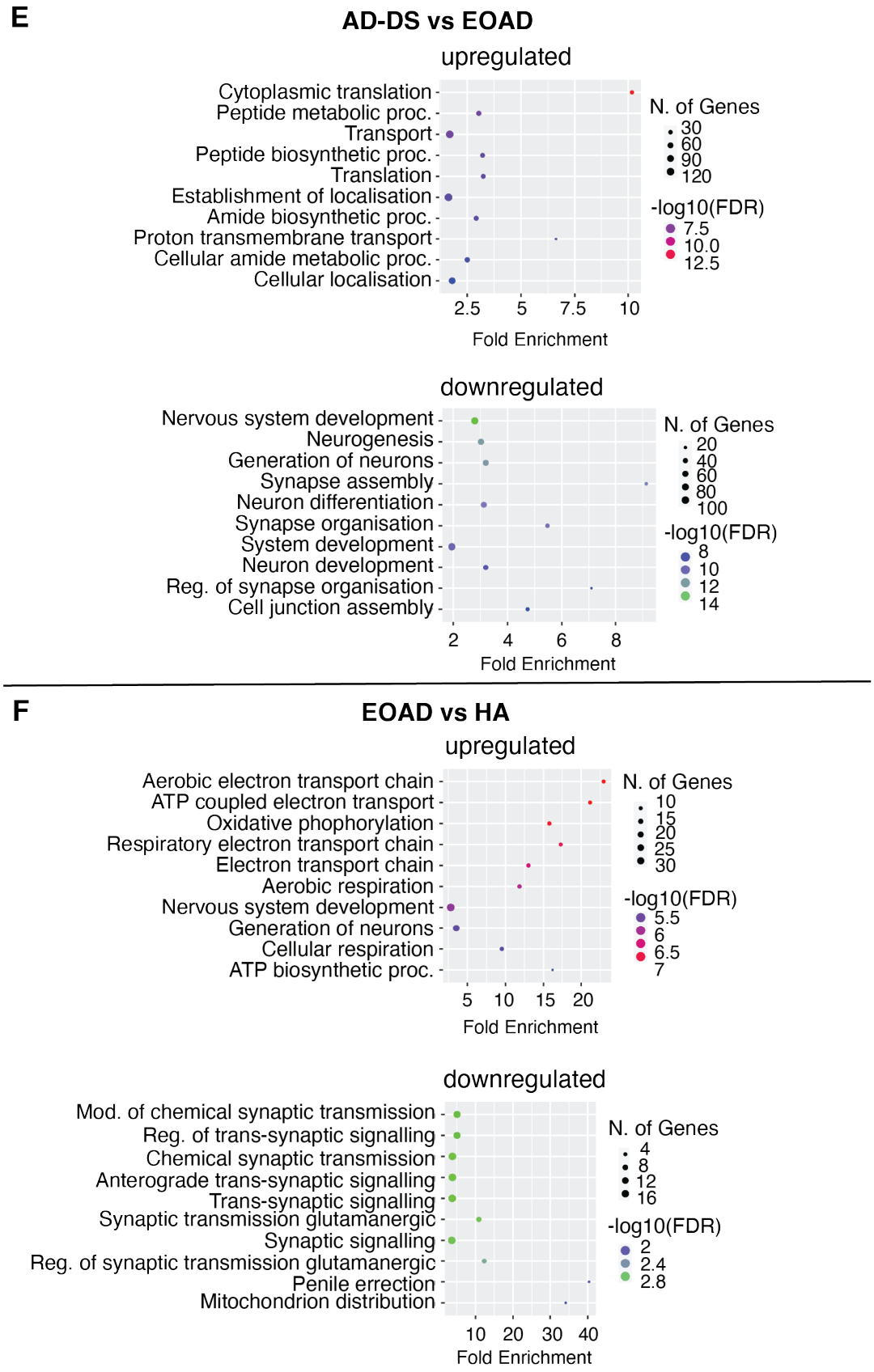

Figure 6.3 GO categories enriched in neuronal cell types in AD-DS and EOAD post-mortem prefrontal cortex.

Gene ontology biological processes. Gene lists included all significant DEGs per case type comparison and were distinct for upregulated and downregulated genes. Top 10 most significantly enriched GO categories are presented in the dotplot graphs ranked by FDR value (smallest at the top). GO categories relating to axons and cell projections are highlighted in red. Categories are arranged by fold enrichment along the x-axis. Circle sizes indicate the number of DEGs, circle colour indicates negative log10 transformed enrichment FDR value from smallest (up = red, down = green) to largest (blue). Plots of GO categories enriched in upregulated and downregulated DEGs in (A) AD-DS vs HA, (B) AD-DS vs EOAD and (C) EOAD vs HA excitatory neurons. Plots of GO categories enriched in upregulated and downregulated DEGs in (D) AD-DS vs HA, (E) AD-DS vs EOAD and (F) EOAD vs HA inhibitory neurons.

To determine the contribution of trisomy and AD to DEGs associated enriched pathways in neurons from individuals who had AD-DS, I compared significantly enriched GO terms (FDR < 0.05) in 4 categories: upregulated in AD-DS vs HA, upregulated in EOAD vs HA, downregulated in AD-DS vs HA and downregulated in EOAD vs HA. This comparison was carried out separately for combined excitatory and inhibitory neuron subclusters. Pathways upregulated in AD-DS vs HA (AD-DS up) only (not AD-DS down, EOAD up or EOAD down) were considered to be unique to AD-DS overexpressed genes. This comparison comprised 515 GO categories in excitatory neurons (circled in red, Figure 6.4A). The largest set of enriched pathways were related to regulation of metabolic processes, with several categories associated with apoptosis and neuronal myelination. Most significantly enriched pathways unique to downregulated genes in AD-DS only, related to synaptic transmission and action potential with several categories associated with dendritic extension (circled in blue, Figure 6.4A). Inhibitory neuronal cell types were comprised of half the number of clusters compared with excitatory neurons, exhibiting a lower number of DEGs and consequently fewer pathways associated with those genes. Comparison of GO categories showed 214 pathways unique to AD-DS upregulated DEGs and 163 enriched biological processes associated with downregulated genes (circled in red and blue, Figure 6.4B). Top upregulated processes in inhibitory neuronal cell types unique to AD-DS featured phosphorous and amyloid metabolism, whereas enrichment

of downregulated genes did not fall into a particular set of pathways but included postsynaptic organisation and neuron projection guidance.

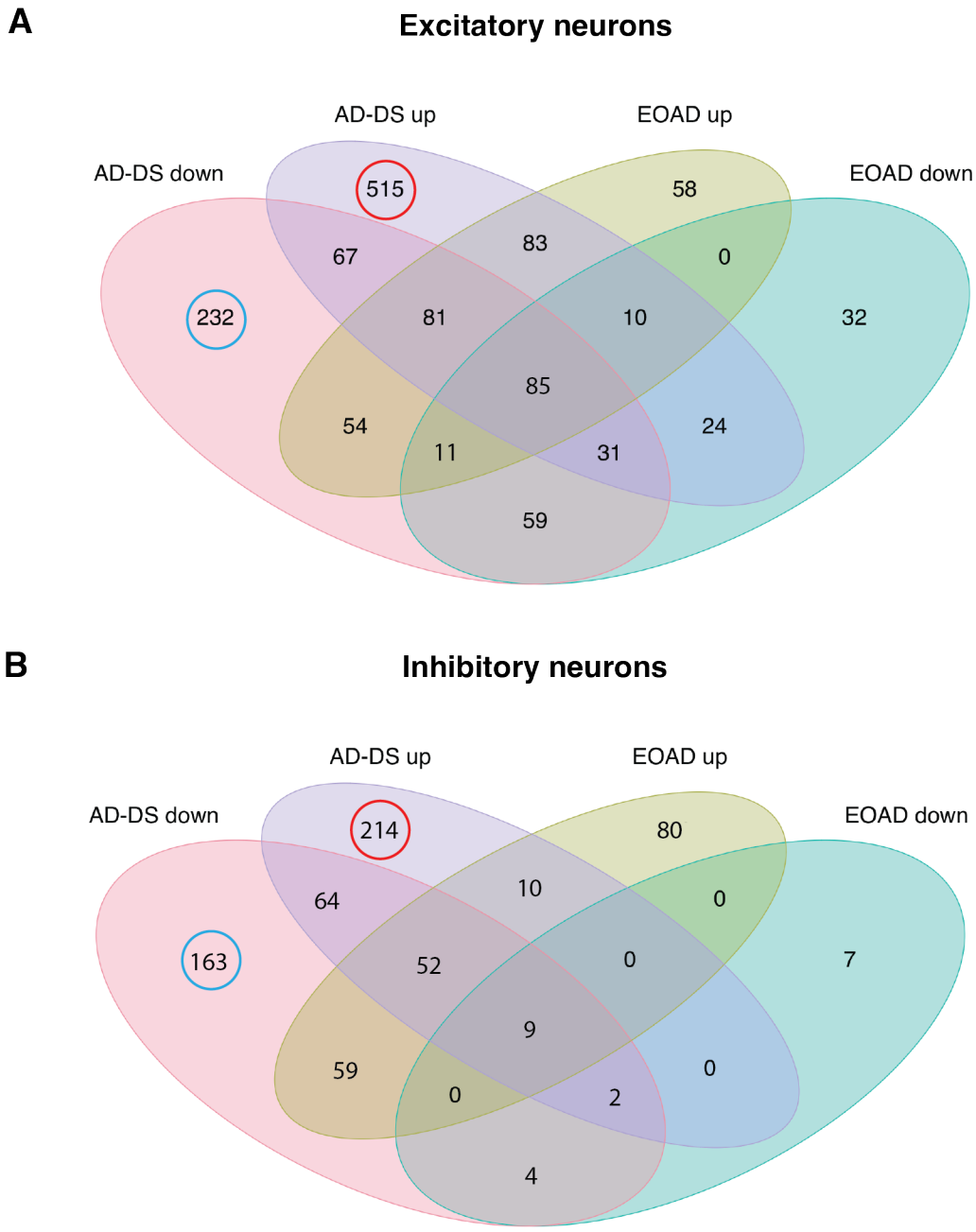

Figure 6.4 Shared and unique pathways enriched in AD-DS and EOAD compared with HA controls.

Venn Diagram of the number of GO categories of biological processes associated with upregulated and downregulated genes in AD-DS versus HA and EOAD vs HA samples for (A) excitatory and (B) inhibitory neuronal cell types. Categories associated with AD-DS upregulated (purple), downregulated (pink), EOAD upregulated (green) and

downregulated (turquoise) genes. Red circles outline the number of pathways uniquely enriched based on upregulated genes and blue circles outline the number of pathways uniquely enriched based on downregulated genes in AD-DS compared with control samples.

To validate our DEGs and associated GO category enrichment analysis, I compared the Farrell *et al.* data to a previously published dataset generated by snRNA sequencing of prefrontal cortex samples from individuals who had DS compared with age-matched euploid individuals (Palmer *et al.*, 2021). Both datasets sequenced post-mortem brain tissue samples from adjacent BAs of prefrontal cortex of individuals with trisomy 21. However, Palmer *et al.* included DS samples from younger individuals and noted an absence of AD pathology in their cases.

Separating upregulated and downregulated genes in excitatory and inhibitory neuronal populations, I repeated the GO analysis using this independent dataset. To match parameters of the DEG list available from the Palmer *et al.* study, I filtered my gene lists to only include those that had been detected in at least 10% of cells for the examined clusters. Overall, Palmer *et al.* profiled a smaller number of DEGs in excitatory and inhibitory neurons from trisomy 21 cases. The number of overlapping significant DEGs between the two datasets was greater for excitatory neurons compared with inhibitory neuron clusters (Figure 6.5). However, of the DEGs detected in the Palmer *et al.* study 37% and 32% were also found to be upregulated and downregulated in the Farrell *et al.* dataset respectively (Figure 6.5A). In the inhibitory neuron clusters, the Farrell *et al*. dataset identified 49% and 67% of up-and downregulated DEGs also found in the previously published dataset (Figure 6.5A). Biological processes associated with the identified DEGs also showed a significant overlap with ~50-65% for excitatory neurons and 32-100% for inhibitory neurons (Figure 6.5B). In addition to exact matches, many of the GO categories were also associated with closely related processes. This suggests DEGs and associated biological processes in prefrontal cortex neurons of individuals with DS share similarities in the presence and absence of AD pathology in DS.

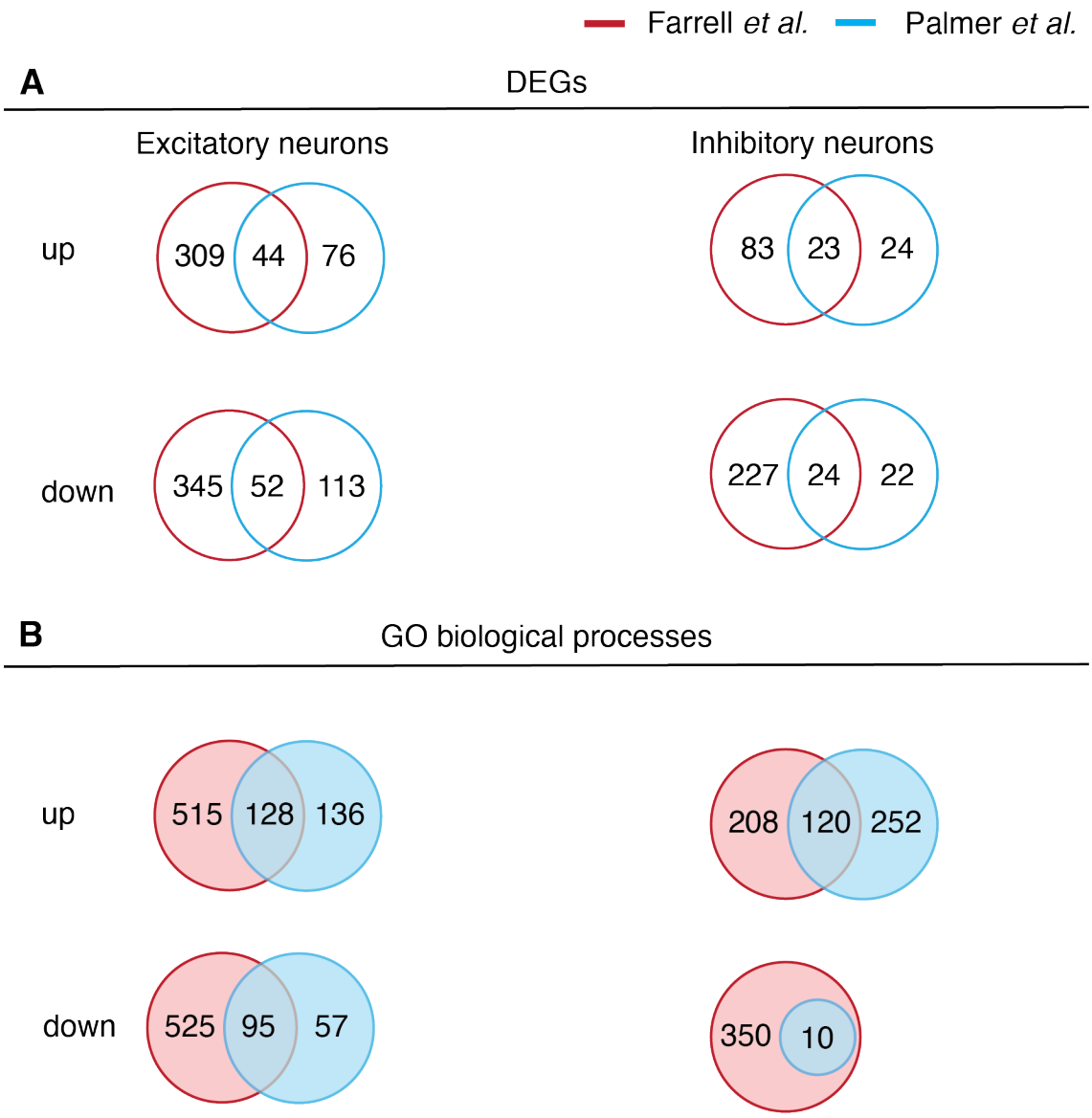

Figure 6.5 DEGs and associated biological processes in neurons comparing the Farrell *et al.* and Palmer *et al.* snRNA-seq datasets.

DEGs and associated gene ontology biological processes. Gene lists were derived from the (Farrell *et al.*, in preparation) and (Palmer *et al.*, 2021) snRNA-seq datasets and included all significant DEGs (FDR < 0.05, pct > 0.1) per case type comparison and were distinct for upregulated and downregulated genes. (A) Venn diagrams for the number of DEGs between DS or AD-DS and HA case types in excitatory and inhibitory neurons showing differences and overlaps between the Farrell *et al.* (red) and Palmer *et al.* (blue) datasets. (B) Venn diagrams for the number of significantly enriched (FDR < 0.05) GO biological process associated with DEGs from (A) showing

differences and overlaps between the Farrell *et al.* (red) and Palmer et al. (blue) datasets**.**

6.2.5 *TTC3* as a candidate modifier of Aβ pathology in AD-DS

During my *Drosophila* screen, I was unable to include several Hsa21 orthologues to investigate the effect of their neuronal overexpression on Aβ toxicity and accumulation, either because of a lack of suitable fly orthologues or because suitable overexpression lines were not publicly available. I was therefore interested in unscreened Hsa21 genes that were overexpressed in excitatory or inhibitory neurons in this snRNA-seq dataset and whether mRNA overexpression would be reflected in increased protein abundance. Unscreened Hsa21 genes that exhibited the highest logFC in excitatory neuron clusters were the transmembrane protein encoding gene neural cell adhesion molecule 2 (*NCAM2*)*, APP* and E3 ubquitin protein ligase tetratricopeptide repeat domain 3 (*TTC3*)*.* I was interested in the expression profile of *TTC3* as it has been identified as a risk variant of LOAD (Kohli *et al.*, 2016)*.* Overexpression was observed in 9 out of 12 AD-DS neuronal cell clusters compared with HA controls. Increased mRNA levels were likely due to an extra copy of this gene caused by trisomy 21, as levels in AD-DS were also elevated compared with EOAD samples and no significant increase was detected in EOAD versus control neurons (Figure 6.6). Notably, *TTC3* was also highly upregulated in DS neurons in the (Palmer *et al.*, 2021) dataset. Based on the observed dosage sensitivity in the brain of individuals who had DS at the transcript level, I wanted to measure its protein abundance in our previously tested set of human post-mortem prefrontal cortex samples by western blot. Unfortunately, despite several rounds of optimisation, due to technical challenges relating to antibody specificity and transfer of large proteins (~230 kDa), I was unable to visualise TTC3 within the timeframe of this project (Figure S6.1).

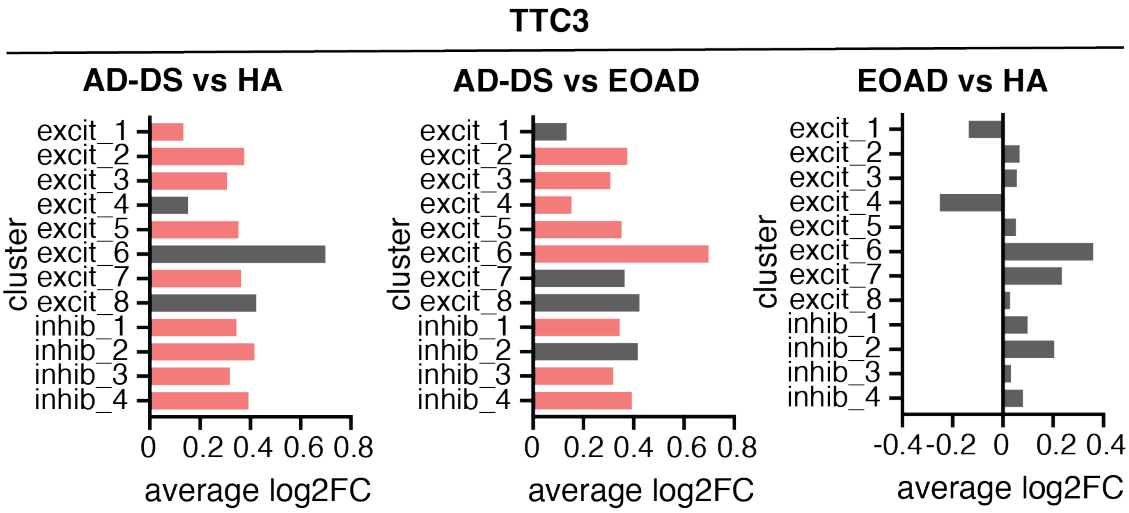

Figure 6.6 Neuronal expression profiles of *TTC3* in prefrontal cortex neurons. Average log_2 fold change of *TTC3* in excitatory and inhibitory neuron clusters comparing AD-DS vs HA, AD-DS vs EOAD and EOAD vs HA case types. Significant upregulation (red) by FDR < 0.05 and pct > 0 in the analysed cell types. Grey bars = log_2FC with FDR > 0.05.

6.3 Discussion

6.3.1 Summary of findings

In this chapter, I investigated differential gene expression in neuronal cell types generated by snRNA-seq comparing post-mortem prefrontal cortex brain tissue from individuals who had AD-DS or EOAD and healthy ageing control cases (Farrell *et al.*, in preparation). The number of upregulated genes was greatest in AD-DS samples compared with HA controls. Next, I examined dosage sensitivity of genes whose orthologues were identified as modifiers of Aβ toxicity in my *Drosophila* screen when overexpressed. This confirmed dosage sensitivity of previously investigated genes, *DYRK1A* and *USP25*, as well as identifying upregulation of *ATP5J* and *HLCS* in

several neuron clusters which has not been previously detected in prefrontal cortex from individuals with DS (Palmer *et al.*, 2021). However, overexpression was not present in all cell types sequenced, indicating cell type specific dosage effects. Overexpression of *USP25* at the transcript level stands in contrast to our findings of a trend towards lowered level of USP25 protein abundance in AD-DS in the same set of prefrontal cortex samples. This discrepancy between mRNA and protein abundance highlights the importance of integrating multi-omics data when investigating dosage sensitivity in DS, as changes in protein abundance are often required to elicit a functional response. However, significant downregulation of *USP25* was observed in a subcluster of excitatory neurons supporting the hypothesis that a trend towards reduced protein abundance in EOAD vs control prefrontal cortex tissue not only resulted from AD related neuronal loss but may also be attributed to reduced expression of this gene. In agreement with our western blot findings, *ATP5J* transcript was not significantly altered in AD-DS compared with EOAD or HA, indicating that this gene may be subject to dosage compensation in the DS brain. Gene ontology identified enriched biological processes associated with upregulated and downregulated genes, some of which are shared between AD-DS and EOAD, while others were uniquely enriched in AD-DS, indicating that these alterations are driven by trisomy 21 rather than AD pathology.

In the Farrell *et al.* snRNA-seq dataset, biological processes related to synaptic signalling were enriched in AD-DS compared with HA controls in excitatory and inhibitory neuronal cell types in agreement with a previous single cell study (Palmer *et al.*, 2021). In contrast, dysregulation of genes associated with functions relating to nervous system development featured among the top 10 most significantly enriched processes in excitatory but not inhibitory neurons from individuals with trisomy 21 compared with euploid controls in both studies. Dysregulation of genes associated with neuronal development in trisomy 21 excitatory neurons may indicate that these neuronal cell types are more sensitive to the impact of triplication of Hsa21 genes consistent with altered development of excitatory neurons observed in a trisomic iPSC derived cortical spheroid model (Li *et al.*, 2022). This is supported by evidence for an increase in the inhibitory to excitatory neuron ratio at different ages in DS (Palmer *et*

al., 2021). An important caveat in comparing snRNA-seq studies is that pipelines for determining cell types can vary between studies, confounding direct comparison of cell type specific DEGs (Andrews and Hemberg, 2018). For instance, Palmer *et al.*, identified a greater number of neuronal clusters compared with the Farrell at al dataset (Palmer *et al.*, 2021). This may be further complicated when sequencing trisomy 21 samples, where changes and cell type proportions that have been observed in the brain should be considered when interpreting changes in transcript abundance (Palmer *et al.*, 2021).

A limitation of my *Drosophila* screen was the lack of suitable orthologues and overexpression lines for several Hsa21 encoded genes whose effect on Aβ toxicity and accumulation could not be investigated. Therefore, to complement the screen, I used the Farrell *et al*. snRNA-seq dataset to identify genes overexpressed in AD-DS that could be potential modifiers of amyloid pathology in this population. *TTC3*, which codes for an E3 ubiquitin-protein ligase was identified as one of the most highly elevated Hsa21 genes in neuronal cell types from individuals who had AD-DS, in agreement with findings by (Palmer *et al.*, 2021). Through selective ubiquitination of proteins, TTC3 contributes to the maintenance of proteostasis, a process that is disrupted in both AD and DS (Hipp, Park and Hartl, 2014; Aivazidis *et al.*, 2017). A potential role of *TTC3* in AD pathogenesis was indicated by the discovery of a missense mutation as a rare genetic risk factor in LOAD (Kohli *et al.*, 2016). Introduction of this mutation into iPSCs that were differentiated into neuronal progenitor cells (NPCs) and forebrain neurons resulted in altered gene expression patterns, including upregulation of proteins in the PI3K-Akt pathway that is known to be dysregulated in AD (Rickle *et al.*, 2004; Cukier *et al.*, 2023). Morphological comparison of mutated versus normal neuronal cells showed that the *TTC3* missense mutation leads to alterations in neurite extension due to changes in cytoskeletal actin dynamics (Cukier *et al.*, 2023).

While neuronal overexpression of *TTC3* at the transcript level was also observed by (Palmer *et al.*, 2021) differential protein abundance has not been assessed in the brain from individuals with AD-DS. In my study, we attempted to quantify TTC3 protein

abundance in AD-DS, EOAD and HA post-mortem brain tissue samples but were not able to visualise the protein by western blot. Further optimisation, such as trialling alternative anti-TTC3 antibodies and further increasing transfer time, may permit quantification of TTC3 protein in human post-mortem brain tissue to assess whether increased expression translates to dosage sensitivity at the protein level and may therefore have functional consequences relating to amyloid pathology in AD-DS.

6.3.2 Dysregulation of biological processes in AD-DS and EOAD

Gene ontology of significantly dysregulated genes identified by snRNA-seq revealed several shared enriched biological processes, including categories related to neuronal development and synaptic function. These processes are known to be dysregulated in both AD and DS (Chen, Fu and Ip, 2019; Moreno-Jiménez *et al.*, 2019; Utagawa *et al.*, 2022). Synaptic plasticity has been proposed as a major contributor to cognitive impairment in individuals with DS. Reduced synaptic density and breakdown of synaptic function through decreased levels of synaptic proteins involved in trans-synaptic signalling has been observed in post-mortem frontal cortex tissue in AD-DS and AD but not younger trisomy 21 samples, suggesting that synapse breakdown in DS may be a response to AD pathology (Downes *et al.*, 2008; X. Q. Chen *et al.*, 2023). Consistent with these findings, snRNA-seq analysed in this study revealed significant downregulation of synaptic genes *SNAP25* and *SYT1* in AD-DS and EOAD excitatory neurons, extending this downregulation observed in LOAD to EOAD cases.

Another set of pathways consistently found among the most significantly enriched in neurons from individuals who had AD-DS were related to neuron projection/dendrites and axon development. Regulation of these processes is critical for establishing proper polarisation of neuronal cells (the formation of a single axon and multiple dendrites) (Schelski and Bradke, 2017). Dendrite morphology and plasticity is crucial for neuronal function and abnormalities have been associated with cognitive impairment in mice (Vanleeuwen and Penzes, 2012). Dysregulation of neuronal polarisation in DS is not well understood but several recent omics studies identified

differential expression of genes associated with axon and dendrite deficits in brains from individuals with trisomy 21 (Palmer *et al.*, 2021; Seol, Kwon and Kang, 2023; Rastogi *et al.*, 2024). Importantly, this signature was found to be conserved at the protein level, indicating that dysregulation of these genes results in functional consequences. Recent mechanistic evidence from DS mouse and human neuronal cell cultures suggests that polarisation deficits are due to multiple axon formation in DS compared with control neurons (Rastogi *et al.*, 2024). In AD, neuronal polarity is compromised although this has been mostly linked to dendritic spine loss (Mijalkov *et al.*, 2021). Notably, we found DEGs associated with neuron projection development were also present in excitatory neurons from AD-DS versus HA and EOAD as well as EOAD versus HA cases. Taken together, this indicates that trisomy 21 and AD may both contribute to neuronal polarisation deficits in AD-DS.

While several enriched biological processes were common to AD-DS and EOAD case types, EOAD samples uniquely exhibited a strong signature of OXPHOS related processes associated with upregulated genes in inhibitory neurons. This enrichment resulted from overexpression of several mitochondrial encoded genes, contrasting literature that suggests an overall reduction in mtDNA abundance in the post-mortem AD brain, although these studies included late-onset forms of AD (Bennett and Keeney, 2020; Harerimana *et al.*, 2023). However, in agreement with the Farrell *et al.* dataset, a recent scRNA-seq analysis identified an increase in OXPHOS related genes in prefrontal cortex neurons of LOAD samples, though this overexpression was confined to excitatory rather than inhibitory neurons in vulnerable cell populations (Mathys *et al.*, 2024).

6.3.3 Technical limitations

The snRNA-seq dataset generated by Farrell *et al.* compared gene expression in the prefrontal cortex (BA10) in post-mortem brain tissue from individuals with AD-DS, EOAD and HA controls. When interpreting findings, study limitations relating to sample

selection, sequencing and analysis should be considered. Sample size was confined to 8 AD-DS, 4 EOAD and 4 HA cases, including 2 AD-DS and 2 EOAD cases with low nuclei recovery. A small sample size may be underpowered to detect case type differences, particularly for lowly expressed genes and those with high inter-individual variation, mirroring limitations encountered in our western blot experiments. Additionally, 4 out of 8 excitatory neuron clusters had a cell count of 0-10 for multiple samples across all case types with EOAD cases being disproportionately affected. Combining excitatory neuron subclusters mitigated low cell count to a certain extent, however, DEGs and their associated enriched GO categories should still be interpreted with caution as expression levels may be underestimated, particularly in EOAD cases. Moreover, RNA quality (measured as RNA integrity number (RIN)) degrades post-mortem, making lowly expressed transcripts more likely to be missed in post-mortem tissue, although RIN values have been found to be independent of PMI (White *et al.*, 2018). Furthermore, trisomic and disomic samples with AD pathology represented end-stage disease (Braak stage V-VI) where substantial neuronal loss in the prefrontal cortex would be expected which may be selective for specific neuronal subtypes (Leng *et al.*, 2021).

DEGs that were up or downregulated in AD-DS but not EOAD can provide insight into the relative contributions of DS and AD to the observed gene expression dysregulation in AD-DS. However, disease aetiology may vary between AD-DS and AD in euploid cases. In AD-DS elevated Aβ levels are primarily driven by triplication of the Hsa21 encoded *APP* gene whereas familial mutations in *APP, PSEN1/2* were not confirmed in EOAD cases included in this study. An additional comparison with younger DS samples lacking AD pathology would capture trisomy 21 only driven changes in gene expression but availability of such samples is limited. Importantly, observed dysregulation in gene expression in the presence of AD pathology does not establish a direction of causality i.e. whether changes are disease causing or disease induced. Furthermore, this snRNA-seq study does not account for different alleles and splice variants which may influence the biological function of gene products. In future, increasing sample size, matching comparison groups for sex and sequencing

additional brain regions will allow findings to be confirmed and could reveal a greater extent of dysregulation in AD-DS that may have been missed in the current study.

6.3.4 Conclusion

Assessment of DEGs and their associated biological processes has revealed dosage sensitivity of candidate amyloid toxicity modifiers in AD-DS at the transcript level, including *ATP5J* and *USP25,* that were not significantly dysregulated at the protein level, indicating that dosage sensitivity of Hsa21 genes can differ between transcript and protein. While RNA sequencing provides a high-throughput assessment of gene expression patterns (including regulatory non-coding genes), complementing this approach the assessment of protein abundance provides additional information about potential functional consequences of the observed transcriptional changes. Moreover, the snRNA-seq study examined in this chapter provides a useful dataset in support of recently discovered changes in the brain from individuals with DS, such as dysregulation of neuronal polarisation and can be used to identify neuronal dosage sensitive genes in AD-DS that can be further investigated as candidate modifiers of AD progression in this population.

Chapter 7: Discussion

7.1 Summary of key results

Trisomy 21 is the greatest genetic risk factor for AD. Triplication of *APP* is known to be necessary and sufficient to cause AD-DS (Sleegers *et al.*, 2006; Doran *et al.*, 2017). However, in recent years, preclinical studies have indicated that other Hsa21 encoded genes, when present in three copies, can modify amyloid neuropathology and cognitive impairment (Wiseman *et al.*, 2018; Tosh *et al.*, 2021; Mumford *et al.*, 2022). Therefore, I wanted to investigate whether overexpression of single Hsa21 genes, other than *APP*, is sufficient to modify Aβ toxicity and accumulation. Subsequently, I investigated whether the abundance of Hsa21 orthologues of identified gene candidates is raised in human post-mortem brain tissue as a result of Hsa21 triplication in DS. Increased abundance at the transcript and protein level may have functional consequences, including modification of amyloid pathology in AD-DS.

A genetic modifier screen using *Drosophila* co-overexpressing Aβ42 and an Hsa21 orthologue in adult neurons identified *Hcs, mnb, Sb, SKIP* and *Usp47* as potential suppressors and *ATPsynCF6* as a potential enhancer of amyloid toxicity using a locomotor assay as a behavioural readout. Additionally, measurements of total Aβ42 protein abundance in fly heads identified *Nnp-1, Plp* and *Sod1* as potential modifiers of amyloid accumulation. Interestingly, there was no positive correlation between the total, soluble or insoluble Aβ42 levels and toxicity of the peptide, a phenomenon consistent with amyloid by itself being a poor predictor of clinical symptoms in patients with AD (Bejanin *et al.*, 2017). However, observed phenotypes were subtle, making reproducibility challenging. In DS, the observed impact of trisomy 21 on multiple body systems, including the CNS, may require the interaction of multiple genes, with the effects of single dosage sensitive genes being more subtle. Additionally, trisomy 21 fetuses are at a significantly increased risk of miscarriage, indicating that natural

selection results in individuals with DS who carry genetic variants compatible with life post-birth (Savva *et al.*, 2006).

To select genes for further investigation in human post-mortem brain tissue, I conducted a literature search for previous knowledge of their role in AD-DS and other forms of AD and whether their dosage sensitivity in the adult DS brain had been determined. The first gene of interest identified as a suppressor of amyloid toxicity in the initial *Drosophila* screen was the deubiquitinase *Usp47.* Rescue of Aβ42 induced toxicity as a result of *Usp47* overexpression was restricted to neuromotor function as I observed no significant effect on lifespan. Direct modification of Aβ toxicity represents a potential additional role of the human orthologue *USP25* which has been associated with raised amyloid plaque load through increasing levels of APP and BACE1 (Zheng *et al.*, 2022). *USP25* transcript abundance is increased in the brains of adults with DS, consistent with snRNA-seq data from the Wiseman lab showing dosage sensitivity in several neuronal cell types (Palmer *et al.*, 2021, Farrell *et al.*, in preparation). In contrast, my data suggest that USP25 protein abundance may be reduced in end-stage post-mortem brain tissue from individuals with AD-DS compared with EOAD and healthy age-matched controls, likely as a result of neuronal loss associated with AD pathology. Notably, conclusive interpretation was confounded by low signal detection. Confirming our findings would therefore require an increase in sample size. In summary, my analysis indicates that trisomy of Hsa21 raises *USP25* transcript at the single cell level in neurons. However, whether this results in elevated protein levels within trisomy 21 cells cannot be concluded from our study, as a loss of neurons in the examined late-stage disease brain tissue resulted in a reduction in the total amount of USP25 in samples from individuals who had AD-DS or EOAD compared with healthy ageing control cases.

The mitochondrial ETC component *ATPsynCF6* was identified as another gene of interest enhancing amyloid toxicity in the initial *Drosophila* screen, as mitochondrial dysfunction is a feature of both DS and AD (Valenti *et al.*, 2010b; Izzo *et al.*, 2017; Troutwine *et al.*, 2022). Downregulation of ETC components and regulators has been observed in DS and LOAD (Helguera *et al.*, 2013; Troutwine *et al.*, 2022). Aβ localises

to mitochondria where it interacts with mitochondrial proteins, contributing to the organelle's dysfunction (Lustbader *et al.*, 2004; Rhein *et al.*, 2009). A recent in vitro study found a correlation between increased intracellular Aβ accumulation and mitochondrial membrane depolarisation (Wilkins *et al.*, 2022). Furthermore, downregulation of ETC components (which has been observed in DS and AD) correlated with Aβ pathology in post-mortem prefrontal cortex tissue from non-demented individuals, indicating a possible mechanistic link between ETC proteins and amyloid pathology (Wilkins *et al.*, 2022). However, this study did not identify a specific involvement of *ATPsynCF6* orthologue *ATP5J*. Transcriptionally, *ATP5J* was not previously identified as a dosage sensitive gene in the DS adult brain. Analysis of the Farrell *et al.*, snRNA-seq data indicated marginal overexpression in one inhibitory neuron subtype in AD-DS compared with euploid controls. However, at the protein level, ATP5J abundance was not affected by case type in human post-mortem brain tissue, indicating that it is unlikely to impact amyloid pathology in AD-DS.

In my aim to identify Hsa21 candidate modifiers of amyloid toxicity and accumulation in AD-DS, I screened 35 *Drosophila* orthologues. The number of screened genes was limited by the existence of suitable orthologues and the availability of overexpression lines. Thus, the effects of almost 200 Hsa21 protein-coding genes were excluded from my study. To determine which of these genes may play a role in the modification of AD risk in DS, I searched the Farrell *et al.* snRNA-seq dataset of human post-mortem brain tissue for Hsa21 genes dysregulated in neurons from individuals who had AD-DS compared with EOAD and healthy ageing controls and determined their associated pathways. E3-ubiquitin ligase *TTC3* was significantly upregulated in trisomy 21 neuronal cell populations compared with both EOAD and healthy ageing control samples. Due to technical limitations, we were not able to determine its dosage sensitivity at the protein level. Given that a variant of this gene has been identified as an AD genetic risk factor which may act through disrupting neurite extension processes, *TTC3* poses an interesting target to explore as a candidate for modification of AD neuropathology in individuals with DS (Kohli *et al.*, 2016; Cukier *et al.*, 2023). Analysis of enriched pathways associated with DEGs in AD-DS compared with euploid controls showed dysregulation of synaptic signalling and neuronal development

across both excitatory and inhibitory neurons consistent with synaptic dysfunction in AD and DS (Chen, Fu and Ip, 2019; Moreno-Jiménez *et al.*, 2019; Utagawa *et al.*, 2022). Additionally, I found support for the dysregulation of pathways associated with neuron projection and axon development unique to AD-DS neurons which were recently identified in a multi-omics study of brain tissue from individuals with DS (Rastogi *et al.*, 2024). This illustrates the power of snRNA-seq datasets as hypothesis-generating tools that can complement pre-clinical studies in the identification of candidate genes in AD-DS research.

7.2 Dosage sensitivity in Down Syndrome

In our screen, we used *Drosophila* that were genetically modified to overexpress single Hsa21 orthologues in adult neurons. Observed changes in amyloid toxicity in these flies compared with controls could therefore be attributed to the direct or indirect effects of the increased transcript and protein dosage of that gene. To assess the potential clinical relevance of these findings for patients with AD-DS, whether candidate genes are also overexpressed in the brains of these individuals has to be investigated. A 1.5-fold increase in Hsa21 gene dose resulting in raised transcript and protein levels of the same magnitude is the most parsimonious explanation for the DS associated phenotypes. Indeed, overexpression of many Hsa21 genes has been found across multiple tissues, in both people with trisomy 21 and animal models of DS (Lockstone *et al.*, 2007; Palmer *et al.*, 2021; Farrell, Mumford and Wiseman, 2022; Rastogi *et al.*, 2024). However, several genes do not appear to be raised by 1.5-fold with levels comparable to or even lower than euploid controls, suggesting the presence of mechanisms that compensate for the increased dosage. Consistent with this hypothesis, analysis of the Farrell *et al.* snRNA-seq dataset revealed that RNA levels of several Hsa21 genes did not show a 1.5-fold increase across all brain cell types sequenced. Dosage compensation is an established process that occurs in many organisms such as *Drosophila,* where genes on the single X chromosome in males are upregulated 2-fold (Conrad and Akhtar, 2012). However, whether compensatory mechanisms apply to triplication of autosomal Hsa21 genes is not well

understood. Interestingly, subunits of protein complexes such as ATP5J may be more likely to be dosage compensated, as changes in their levels can impact the stoichiometry of subunits and, thus, the assembly of the protein complex. This is consistent with our observed lack of altered protein abundance of ATP5J in post-mortem brain tissue from individuals who had AD-DS (Veitia, 2003; Veitia and Birchler, 2015).

To determine whether genes are dosage sensitive, transcript levels are measured in trisomic and euploid controls (e.g. EOAD, healthy ageing) to identify differentially expressed genes. However, expression level is noisy, varying within the same individual depending on age and time of day and are tissue and cell type specific (Prandini *et al.*, 2007; Zhang *et al.*, 2014). Additionally, transcriptional profiles exhibit significant inter-person variability which can, in part, be attributed to single nucleotide polymorphisms. Many gene variants have been identified as increasing the risk of LOAD development in the general population, such as a missense mutation in the Hsa21 encoded *TTC3* gene (Kohli *et al.*, 2016; Kunkle *et al.*, 2019; Kretzschmar *et al.*, 2021). Furthermore, certain loci, termed expression quantitative trait loci (eQTLs), correlate with variability in mRNA levels, with certain variants being associated with lowered gene expression in the general population (Aguet *et al.*, 2017). This has led to the hypothesis that Hsa21 genes with a lower-than-expected transcript level in trisomy 21 cells may be associated with such eQTLs, contributing to their expression profile of less than 1.5-fold compared with euploid controls, although this has not yet been tested on large sample sizes (Hunter *et al.*, 2023).

Expression levels are further influenced by epigenetic mechanisms, transcriptional control and post-translational modifications, leading to gene expression diversity even between genetically identical organisms (Raser and O'Shea, 2005; Wright, Smith and Jiggins, 2022). This includes alternative splicing (AS) events that can result in diverse mRNA variants (and protein isoforms) not captured by differential gene expression analysis. AS is prevalent in the brain, affecting over 90% of human protein coding genes (Wang *et al.*, 2008; X. Zhang *et al.*, 2016; Song *et al.*, 2017). In the brain of individuals with DS, comparison of mRNA variant level differences with euploid

controls indicates that regulation of splicing by trisomy 21 may contribute to gene expression dysregulation (Rastogi *et al.*, 2024). Protein isoform diversity has also been reported in post-mortem brain tissue from patients with AD. Isoform quantification confirmed the expression of multiple *APP* isoforms as well as revealing previously unannotated isoforms of AD risk gene *TREM2* and Hsa21 encoded gene *WDR4,* further demonstrating the importance of considering splice variants when comparing differential gene expression between case types (Guerreiro *et al.*, 2013; Aguzzoli Heberle *et al.*, 2024). Importantly, assessing dosage sensitivity at the transcript level does not provide full functional information. Therefore, transcriptomic studies should be complemented by the assessment of protein abundance as protein level dosage compensation is a known mechanism in human cells (e.g. aneuploid cancer cells) (Schukken and Sheltzer, 2022). This discrepancy was highlighted in our measurements of protein level in human post-mortem brain tissue where USP25 showed a trend towards lowered abundance in AD-DS samples compared with control samples despite having been identified as dosage sensitive in snRNA-seq studies of brain tissue samples from individuals who had DS and AD-DS (Palmer *et al.*, 2021, Farrell *et al.*, in preparation).

In addition to biological variability in gene expression at the population level, analysis protocols of sequencing data may further complicate the assessment of dosage sensitivity in DS. A recent in vitro study found that modifying an RNA-seq analysis pipeline to account for trisomy, resulted in almost all Hsa21 genes exhibiting a ~1.5-fold increase in transcript, indicating that Hsa21 genes largely conform to the 150% increase in mRNA levels (Hunter *et al.*, 2023). However, the study only included a small sample size and thus, the contribution of dosage compensation for some Hsa21 genes cannot be excluded. Notably, the proportional increase in transcript dose has also been found in another in vitro study of human aneuploidies (Hwang *et al.*, 2021). Regardless of the source of gene expression variability, large enough sample sizes are of great importance to increase the likelihood of detecting true differences between AD-DS and control samples to understand whether candidate genes are overexpressed in cell types of interest. Therefore, a lack of detected overexpression of Hsa21 genes in the analysed Farrell *et al.* snRNA-seq dataset does not necessarily

imply a lack of dosage sensitivity, and detection may be improved by increased sample size and higher sequencing depth of samples.

7.3 Limitations of modelling AD-DS in this study

AD is sometimes considered to have a canonical progression of neuropathology. However, this is not universally true, and in recent years, there has been accumulating evidence for the heterogeneity amongst sporadic cases of the disease (Ferreira, Nordberg and Westman, 2020; Jutten *et al.*, 2021). This has led to the proposal of defined AD subtypes based on the order in which brain areas are affected by atrophy and the associated clinical presentation of symptoms. Interestingly, these differences cannot be detected by discrepancies in CSF biomarkers (Baumeister *et al.*, 2024). Genetic forms of AD display further differences and are characterised by an overproduction of Aβ due to mutations in or duplications of *APP* and genes implicated in its amyloidogenic processing (Tcw and Goate, 2017). Modelling AD-DS provides further challenges as the contribution of trisomy 21 to AD risk is multigenic (Wiseman *et al.*, 2018). Because of the complexity of this disease, selecting the most appropriate preclinical model requires careful consideration of the research question. In order to dissect the function of Hsa21 genes, non-mammalian models, including *Caenorhabditis elegans* (nematode worm) and *Danio rerio* (zebrafish), have previously been used to screen for phenotypes altered by loss-of-function or overexpression of Hsa21 orthologues (Edie *et al.*, 2018; Nordquist, Smith and Pierce, 2018).

In my thesis, we selected *Drosophila melanogaster* to determine which Hsa21 genes other than *APP* modify amyloid toxicity and accumulation when overexpressed. The advantage of this model system is that a large number of genes could be screened within a relatively short time frame, dissecting the functional consequences of single genes. Furthermore, overexpression of Aβ in our fly model mimics the increase in Aβ production in individuals with AD-DS while isolating the effects Aβ itself from the effect

of APP processing. However, this approach does not take into account genetic interactions that may be required to elicit an amyloid-modifying response, a phenomenon that has been observed in rodent models of AD-DS. For instance, an additional copy of the Hsa21 orthologue *Cstb* has been found to be insufficient to modify amyloid accumulation despite previous evidence that triplication of an Hsa21 syntenic region of genes including *Cstb* exacerbates amyloid pathology in a mouse model of AD-DS (Tosh *et al.*, 2021; Wu *et al.*, 2021). Genetic interactions between Hsa21 orthologues have been shown to have both additive and compensatory effects on early embryonic development in zebrafish, demonstrating that a lack of modification by a single gene does not preclude the possibility that its overexpression contributes to a particular DS phenotype by interacting with other genes (Edie *et al.*, 2018).

Furthermore, the spatiotemporal restriction of gene expression to adult neuronal cell types may influence the translatability of our findings. In >95% of DS cases, triplication of Hsa21 is present in every cell. Interestingly, although individuals mosaic for trisomy 21 may not exhibit signs of ID, they still appear to be at increased risk of developing EOAD compared with the general population, suggesting that triplication of Hsa21 in a subset of cells is sufficient to mediate AD risk (Ringman *et al.*, 2008; Potter, Granic and Caneus, 2016). However, expression patterns vary across cell types, and whether pan-neuronal overexpression of Hsa21 genes would be sufficient to modify the development of amyloid pathology in AD-DS has not been investigated. Therefore, overexpression of Hsa21 orthologues in tissues and cell types not considered in this thesis, may result in a different response to amyloid toxicity and accumulation. Additionally, induction of Hsa21 orthologue overexpression in adulthood excludes the potential developmental effect of trisomy 21 on Aβ toxicity and accumulation during adulthood in our *Drosophila* model. In DS fetuses, AD-associated pathological changes have been observed as early as 28 week's gestation, with intraneuronal Aβ beginning to accumulate in the first decade of life, indicating that the impact of Hsa21 gene dosage begins prior to adulthood (Cataldo *et al.*, 2000; Fortea *et al.*, 2021).

More broadly, despite cross-species conservation of many genes and pathways, *Drosophila* do not recapitulate the complexity of the human brain, comprising

substantially fewer neurons as well as exhibiting differences in defined brain regions, including those implicated in AD-DS (Court *et al.*, 2023). In addition to a lack of Hsa21 orthologous protein coding genes, the influence of non-coding genes on amyloid pathology was not investigated in our screen. Hsa21 is rich in lncRNAs that are differentially expressed in DS and may influence AD risk (Salemi *et al.*, 2021). Further important aspects of AD-DS known to influence amyloid pathology were not modelled in our genetic screen. Immune dysregulation, including lower numbers and functional impairment of immune cells, is present from childhood in individuals with DS, resulting in increased risk of infection and autoimmune conditions (Huggard *et al.*, 2020). Blood samples also show raised pro-inflammatory markers such as TNF-α, IL-1β and IFN–γ as well as increased interferon signalling which has been attributed to overexpression of the four Hsa21 encoded interferon receptor subunits *IFNAR1*, *IFNAR2*, *IFNGR2* and *IL10RB* (Zhang *et al.*, 2017; Araya *et al.*, 2019). Furthermore, these immune changes are accompanied by altered morphology and hyperactivation of microglia (Flores-Aguilar *et al.*, 2020; Pinto *et al.*, 2020). These immune phenotypes are also found in the presence of AD in individuals with trisomy 21, presenting a pathological difference to sporadic forms of AD (Wilcock *et al.*, 2015; Startin *et al.*, 2019). These peripheral and cellular immune effects could not be modelled in our screen, as *Drosophila* lack an adaptive immune system (Yu *et al.*, 2022).

Additionally, I investigated my research questions using female *Drosophila* only. Toxicity of pan-neuronal overexpression of Aβ has been observed in both sexes (Catterson *et al.*, 2023). However, sex differences in the *Drosophila* ageing process have been observed, raising the possibility of sex specific effects on Aβ toxicity and accumulation as a result of Hsa21 orthologue overexpression (Magwere, Chapman and Partridge, 2004; Regan *et al.*, 2016). In the general population, AD disproportionately affects women. Although sex differences are less prominent in AD-DS, differences in disease duration and age-specific prevalence have been observed, indicating that neuropathology may be impacted by sex (Lai *et al.*, 2020; Iulita *et al.*, 2023; Silverman *et al.*, 2023).

AD is characterised by both amyloid and tau hallmark pathologies. In this study, we sought to investigate the effects of hsa21 overexpression on amyloid accumulation and toxicity. However, similarly to amyloid pathology, the emergence of NFTs consisting of hyperphosphorylated tau protein also occurs decades earlier in individuals with DS compared with sporadic cases of AD (Fortea *et al.*, 2021). Furthermore, differences in the propagation of tau protein in AD-DS brains compared with other familial and sporadic AD cases indicate that trisomy may have a direct or downstream effect on the development of tau pathology (Condello *et al.*, 2022). *Drosophila* used in this study have been genetically engineered to model amyloid but not tau pathology. Screening for the effects of Hsa21 orthologue overexpression on phenotypes of flies co-expressing human tau may provide insight into the potential modification of tau pathology by trisomy 21.

In summary, when using model organisms to investigate human diseases, it is important to be aware of the animal and approach specific strengths and limitations in order to interpret the potential clinical relevance of findings. *Drosophila* offer a promising opportunity to perform high-throughput screens with the aim of identifying disease-modifying candidate genes. However, due to differences in their genetics and physiology, confirming findings in mammalian model systems, as well as human cell models, is critical to determine their clinical relevance for individuals with AD-DS.

7.4 Conclusion and future directions

In this study, I modelled the effect of increased single Hsa21 gene expression on amyloid toxicity and accumulation. Initial screening results indicated that pan-neuronal overexpression of a subset of Hsa21 orthologues was sufficient to modify the Aβ42 induced toxicity or accumulation. However, despite a previously observed exacerbation of amyloid pathology in a mouse model of AD-DS resulting from triplication of Hsa21 genes, including orthologues of those screened in this study, modifications were subtle and did not show robust effects during repeat experiments

(Wiseman *et al.*, 2018). This indicates that overexpression of many Hsa21 orthologues on their own may not be sufficient to modify Aβ toxicity, suggesting that genetic interactions are important for the observed exacerbation of AD pathology in mouse models of AD-DS. Furthermore, three copies of Hsa21 genes/orthologues are present throughout development in AD-DS rodent models, raising the possibility that their developmental effect outweighs their impact during adulthood. In future experiments, co-overexpressing Aβ and Hsa21 orthologues in *Drosophila* larvae could provide insight into the developmental contribution of single Hsa21 genes to amyloid pathology in AD-DS. In addition to genetic and physiological differences between mouse and fly models, there are several possibilities to explain these discrepancies. Firstly, the worsened amyloid pathology in the AD-DS mouse model may have been mediated by a gene or subset of genes that were not included in our *Drosophila* screen. Secondly, a combination of two or more screened Hsa21 orthologues may be necessary to substantially modify amyloid pathology with single genes only having marginal effects. Importantly, candidate modifiers of AD pathology are only of clinical relevance if they are dosage sensitive in AD-DS. My work determined USP25 and ATP5J as unlikely modifiers of amyloid toxicity and accumulation in individuals with AD-DS due to a lack of increased protein abundance in the brain compared with euploid healthy ageing control cases. Furthermore, I found discrepancies between RNA and protein abundance of Hsa21 genes in AD-DS post-mortem brain tissue, further highlighting the complexity of investigating the underlying genetics of AD risk in this population.

This raises the question of how best to approach the dissection of the genotype-phenotype relationship in AD-DS. Following on from findings that overexpression of genes other than *APP* is sufficient to modify amyloid pathology, segmental duplication mouse models have been used to further narrow down the genes mediating these effects, as well as regions of genes that may confer a protective effect against raised *APP* gene dosage (Tosh *et al.*, 2021; Mumford *et al.*, 2022). However, the type of AD model (expressing human *APP* or endogenous humanised mouse *App*) in these studies impacted how additional copies of Hsa21 orthologues modify Aβ accumulation. In the study by Tosh *et al.*, expression of human *APP* results in increased mortality rates and non-AD related phenotypes that may have masked the

protective effect of certain Hsa21 genes against amyloid pathology when present in three copies on AD (Sasaguri *et al.*, 2017; Tosh *et al.*, 2021). Therefore, complementary approaches will be required to dissect the impacts of an extra copy of Hsa21 genes in AD-DS development and progression. This could include multi-omics studies of AD-DS post-mortem brain tissue to identify differentially expressed genes and proteins and their associated pathways, providing insight into potentially synergistic genetic interactions. The mechanistic impact of this subset of genes could then be investigated in pre-clinical models both as single gene and grouped effects.

To reduce the use of mammalian animal models in line with 3Rs principles, we have confirmed that *Drosophila* present a suitable system for identifying Hsa21 mediated rescue and exacerbation of amyloid toxicity and accumulation provided genes of interest have suitable orthologues in the fly. For instance, *TTC3* is consistently upregulated in DS neurons, including in the dataset analysed in this thesis (Palmer *et al.*, 2021, Farrell *et al.*, in preparation). An orthologue of this gene was not included in our fly screen as there were no overexpression lines of *CG4235* publicly available. Notably, updated orthologue predictions now include *PpD3* as a likely orthologue of *TTC3* (DIOPT version 9). In future, co-overexpressing *PpD3* and Aβ42 could determine whether the *TTC3* orthologue is sufficient to modify amyloid induced toxicity in *Drosophila*. Furthermore, overexpressing not only single genes but also small groups of Hsa21 orthologues may expand findings by including the effects of selected genetic interactions. Such an approach in *Drosophila* has previously demonstrated that the interaction of three Hsa21 orthologues was required for impaired vesicle recycling and locomotor function with overexpression of each single gene not being sufficient to modify these phenotypes (Chang and Min, 2009).

In conclusion, investigating the underlying genetics of AD-DS is complex and requires a combined approach of complementary pre-clinical model systems as well as multi-omics studies of human brain tissue from individuals with AD-DS to identify potential targets for the treatment and prevention of AD development and progression. Furthering our understanding in this field is crucial for providing AD treatment options

for individuals with DS which also has the potential to alleviate the burden of other forms of AD.

References

Abramov, E. *et al.* (2009) ‘Amyloid-beta as a positive endogenous regulator of release probability at hippocampal synapses’, *Nature neuroscience*. Nat Neurosci, 12(12), pp. 1567–1576. doi: 10.1038/NN.2433.

Van Acker, Z. P., Bretou, M. and Annaert, W. (2019) ‘Endo-lysosomal dysregulations and late-onset Alzheimer’s disease: impact of genetic risk factors’, *Molecular Neurodegeneration 2019 14:1*. BioMed Central, 14(1), pp. 1–20. doi: 10.1186/S13024-019-0323-7.

Adams, M. D. *et al.* (2000) ‘The Genome Sequence of Drosophila melanogaster’, *Science*. American Association for the Advancement of Science, 287(5461), pp. 2185–2195. doi: 10.1126/SCIENCE.287.5461.2185.

Aguet, F. *et al.* (2017) ‘Genetic effects on gene expression across human tissues’, *Nature 2017 550:7675*. Nature Publishing Group, 550(7675), pp. 204–213. doi: 10.1038/nature24277.

Aguzzoli Heberle, B. *et al.* (2024) ‘Mapping medically relevant RNA isoform diversity in the aged human frontal cortex with deep long-read RNA-seq’, *Nature Biotechnology 2024*. Nature Publishing Group, pp. 1–12. doi: 10.1038/s41587-024-02245-9.

Aivazidis, S. *et al.* (2017) ‘The burden of trisomy 21 disrupts the proteostasis network in Down syndrome’, *PLoS ONE*. Public Library of Science, 12(4), p. e0176307. doi: 10.1371/JOURNAL.PONE.0176307.

Aldecoa, I. *et al.* (2024) ‘Down Syndrome Biobank Consortium: A perspective’, *Alzheimer’s & Dementia*. John Wiley & Sons, Ltd, 20(3), pp. 2262–2272. doi: 10.1002/ALZ.13692.

Alhajraf, F. *et al.* (2019) ‘Plasma amyloid and tau as dementia biomarkers in Down syndrome: Systematic review and meta-analyses’, *Developmental Neurobiology*. Wiley, 79(7), pp. 684–698. doi: 10.1002/dneu.22715.

Alić, I. *et al.* (2020) ‘Patient-specific Alzheimer-like pathology in trisomy 21 cerebral organoids reveals BACE2 as a gene dose-sensitive AD suppressor in human brain’, *Molecular Psychiatry 2020 26:10*. Nature Publishing Group, 26(10), pp. 5766–5788. doi: 10.1038/s41380-020-0806-5.

Alić, I. *et al.* (2021) ‘Patient-specific Alzheimer-like pathology in trisomy 21 cerebral organoids reveals BACE2 as a gene dose-sensitive AD suppressor in human brain’, *Molecular psychiatry*. Mol Psychiatry, 26(10), pp. 5766–5788. doi: 10.1038/S41380-020-0806-5.

Altmann, A. *et al.* (2024) ‘Towards cascading genetic risk in Alzheimer’s disease’, *Brain*. Oxford Academic, 147(8), pp. 2680–2690. doi: 10.1093/BRAIN/AWAE176.

Altuna, M., Giménez, S. and Fortea, J. (2021) ‘Epilepsy in Down Syndrome: A Highly Prevalent Comorbidity’, *Journal of Clinical Medicine 2021, Vol. 10, Page 2776*. Multidisciplinary Digital Publishing Institute, 10(13), p. 2776. doi: 10.3390/JCM10132776.

Alzheimer, A. (1907) ‘Uber eigenartige Erkrankung der Hirnrinde’, *Allg. Z. Psychiatr.*, 64, pp. 146–148. Available at: https://cir.nii.ac.jp/crid/1571135649977545216 (Accessed: 9 December 2024).

Andrews, T. S. and Hemberg, M. (2018) ‘Identifying cell populations with scRNASeq’, *Molecular Aspects of Medicine*. Pergamon, 59, pp. 114–122. doi: 10.1016/J.MAM.2017.07.002.

Antonarakis, S. E. *et al.* (1993) ‘Mitotic errors in somatic cells cause trisomy 21 in about 4.5% of cases and are not associated with advanced maternal age’, *Nature genetics*. Nat Genet, 3(2), pp. 146–150. doi: 10.1038/NG0293-146.

Antonarakis, S. E. *et al.* (2020) ‘Down syndrome’, *Nature Reviews Disease Primers 2020 6:1*. Nature Publishing Group, 6(1), pp. 1–20. doi: 10.1038/s41572-019-0143-7.

Araya, P. *et al.* (2019) ‘Trisomy 21 dysregulates T cell lineages toward an autoimmunity-prone state associated with interferon hyperactivity’, *Proceedings of the National Academy of Sciences of the United States of America*. National Academy of Sciences, 116(48), pp. 24231–24241. doi: 10.1073/PNAS.1908129116/SUPPL_FILE/PNAS.1908129116.SD06.XLSX.

Ashleigh, T., Swerdlow, R. H. and Beal, M. F. (2023) ‘The role of mitochondrial dysfunction in Alzheimer’s disease pathogenesis’, *Alzheimer’s & dementia : the journal of the Alzheimer’s Association*. Alzheimers Dement, 19(1), pp. 333–342. doi: 10.1002/ALZ.12683.

Ashton-Beaucage, D. *et al.* (2016) ‘The Deubiquitinase USP47 Stabilizes MAPK by Counteracting the Function of the N-end Rule ligase POE/UBR4 in Drosophila’, *PLOS Biology*. Public Library of Science, 14(8), p. e1002539. doi: 10.1371/JOURNAL.PBIO.1002539.

Atas-Ozcan, H. *et al.* (2021) ‘Dyrk1a from Gene Function in Development and Physiology to Dosage Correction across Life Span in Down Syndrome’, *Genes 2021, Vol. 12, Page 1833*. Multidisciplinary Digital Publishing Institute, 12(11), p. 1833. doi: 10.3390/GENES12111833.

Avgerinos, K. I. *et al.* (2024) ‘Critical assessment of anti-amyloid-β monoclonal antibodies effects in Alzheimer’s disease: a systematic review and meta-analysis highlighting target engagement and clinical meaningfulness’, *Scientific Reports 2024 14:1*. Nature Publishing Group, 14(1), pp. 1–12. doi: 10.1038/s41598-024-75204-8.

Baburamani, A. A. *et al.* (2020) ‘Assessment of radial glia in the frontal lobe of fetuses with Down syndrome’, *Acta neuropathologica communications*. Acta Neuropathol Commun, 8(1). doi: 10.1186/S40478-020-01015-3.

Bagaria, J., Bagyinszky, E. and An, S. S. A. (2022) ‘Genetics, Functions, and Clinical Impact of Presenilin-1 (PSEN1) Gene’, *International Journal of Molecular Sciences*. MDPI, 23(18), p. 10970. doi: 10.3390/IJMS231810970/S1.

Bajpe, P. K. *et al.* (2008) ‘Deubiquitylating enzyme UBP64 controls cell fate through stabilization of the transcriptional repressor tramtrack’, *Molecular and cellular biology*. Mol Cell Biol, 28(5), pp. 1606–1615. doi: 10.1128/MCB.01567-07.

Baksh, R. A. *et al.* (2023) ‘Multiple morbidity across the lifespan in people with Down syndrome or intellectual disabilities: a population-based cohort study using electronic health records’, *The Lancet. Public health*. Lancet Public Health, 8(6), pp. e453–e462. doi: 10.1016/S2468-2667(23)00057-9.

Balamurugan, K. *et al.* (2017) ‘Effect of Alzheimer Familial Chromosomal Mutations on the Amyloid Fibril Interaction with Different PET Tracers: Insight from Molecular Modeling Studies’, *ACS chemical neuroscience*. ACS Chem Neurosci, 8(12), pp. 2655–2666. doi: 10.1021/ACSCHEMNEURO.7B00215.

Barksdale, K. A. *et al.* (2010) ‘Mitochondrial viability in mouse and human postmortem brain’, *The FASEB Journal*. Wiley, 24(9), p. 3590. doi: 10.1096/FJ.09-152108.

Bateman, R. J. *et al.* (2006) ‘Human amyloid-beta synthesis and clearance rates as measured in cerebrospinal fluid in vivo’, *Nature medicine*. Nat Med, 12(7), pp. 856–861. doi: 10.1038/NM1438.

Baumeister, H. *et al.* (2024) ‘A generalizable data-driven model of atrophy heterogeneity and progression in memory clinic settings’, *Brain*. Oxford Academic, 147(7), pp. 2400–2413. doi: 10.1093/BRAIN/AWAE118.

Baumer, N. T. *et al.* (2022) ‘Conducting clinical trials in persons with Down syndrome: summary from the NIH INCLUDE Down syndrome clinical trials readiness working group’, *Journal of Neurodevelopmental Disorders*. BioMed Central Ltd, 14(1), p. 22. doi: 10.1186/S11689-022-09435-Z.

Bayona-Bafaluy, M. P. *et al.* (2021) ‘Down syndrome is an oxidative phosphorylation disorder’, *Redox Biology*. Elsevier, 41, p. 101871. doi: 10.1016/J.REDOX.2021.101871.

Beck, S. J. *et al.* (2016) ‘Deregulation of mitochondrial F1FO-ATP synthase via OSCP in Alzheimer’s disease’, *Nature Communications 2016 7:1*. Nature Publishing Group, 7(1), pp. 1–16. doi: 10.1038/ncomms11483.

Bejanin, A. *et al.* (2017) ‘Tau pathology and neurodegeneration contribute to cognitive impairment in Alzheimer’s disease’, *Brain : a journal of neurology*. Brain, 140(12), pp. 3286–3300. doi: 10.1093/BRAIN/AWX243.

Belfiori-Carrasco, L. F. *et al.* (2017) ‘A novel genetic screen identifies modifiers of age-dependent amyloid β toxicity in the Drosophila brain’, *Frontiers in Aging Neuroscience*. Frontiers Research Foundation, 9(MAR), p. 222073. doi: 10.3389/FNAGI.2017.00061/BIBTEX.

Bellenguez, C. *et al.* (2022) ‘New insights into the genetic etiology of Alzheimer’s disease and related dementias’, *Nature Genetics 2022 54:4*. Nature Publishing Group, 54(4), pp. 412–436. doi: 10.1038/s41588-022-01024-z.

Benejam, B. *et al.* (2020) ‘Diagnosis of prodromal and Alzheimer’s disease dementia in adults with Down syndrome using neuropsychological tests’, *Alzheimer’s & Dementia : Diagnosis, Assessment & Disease Monitoring*. John Wiley and Sons Inc, 12(1), p. e12047. doi: 10.1002/DAD2.12047.

Bennett, J. P. and Keeney, P. M. (2020) ‘Alzheimer’s and Parkinson’s brain tissues have reduced expression of genes for mtDNA OXPHOS Proteins, mitobiogenesis regulator PGC-1α protein and mtRNA stabilizing protein LRPPRC (LRP130)’, *Mitochondrion*. Mitochondrion, 53, pp. 154–157. doi: 10.1016/J.MITO.2020.05.012.

Blair, J. A. *et al.* (2016) ‘Individual Case Analysis of Postmortem Interval Time on Brain Tissue Preservation’, *PLOS ONE*. Public Library of Science, 11(3), p. e0151615. doi: 10.1371/JOURNAL.PONE.0151615.

Blount, J. R. *et al.* (2012) ‘Ubiquitin-Specific Protease 25 Functions in Endoplasmic Reticulum-Associated Degradation’, *PLOS ONE*. Public Library of Science, 7(5), p. e36542. doi: 10.1371/JOURNAL.PONE.0036542.

Boerwinkle, A. H. *et al.* (2023) ‘Comparison of amyloid burden in individuals with Down syndrome versus autosomal dominant Alzheimer’s disease: a cross-sectional study’, *The Lancet Neurology*. Elsevier, 22(1), pp. 55–65. doi: 10.1016/S1474-4422(22)00408-2.

Borelli, V. *et al.* (2015) ‘Plasma N-Glycome Signature of Down Syndrome’, *Journal of Proteome Research*. American Chemical Society, 14(10), pp. 4232–4245. doi: 10.1021/ACS.JPROTEOME.5B00356/SUPPL_FILE/PR5B00356_SI_002.PDF.

Boughton, A. J., Krueger, S. and Fushman, D. (2020) ‘Branching via K11 and K48 Bestows Ubiquitin Chains with a Unique Interdomain Interface and Enhanced Affinity for Proteasomal Subunit Rpn1’, *Structure*. Cell Press, 28(1), pp. 29-43.e6. doi: 10.1016/J.STR.2019.10.008/ATTACHMENT/F6DF5E35-6CBB-48CE-AB98-7E3ED1EF178D/MMC2.PDF.

Braak, H. and Braak, E. (1991) ‘Neuropathological stageing of Alzheimer-related changes’, *Acta Neuropathologica*. Springer-Verlag, 82(4), pp. 239–259. doi: 10.1007/BF00308809/METRICS.

Brand, A. and Perrimon, N. (1993) ‘Targeted gene expression as a means of altering cell fates and generating dominant phenotypes’, *Development (Cambridge, England)*, 118(2), pp. 401–415.

Brion, J. P. *et al.* (1985) ‘Mise en évidence immunologique de la protéine tau au niveau des lésions de dégénérescence neurofibrillaire de la maladie d’Alzheimer’, *Archives de biologie*, 95, pp. 229–235. Available at: http://hdl.handle.net/2013/ (Accessed: 9 December 2024).

Brodmann, K. (1909) ‘Vergleichende Lokalisationslehre der Grosshirnrinde in ihren Prinzipien dargestellt auf Grund des Zellenbaues’.

Burns, M. *et al.* (2003) ‘Presenilin Redistribution Associated with Aberrant Cholesterol Transport Enhances β-Amyloid Production In Vivo’, *Journal of Neuroscience*. Society for Neuroscience, 23(13), pp. 5645–5649. doi: 10.1523/JNEUROSCI.23-13-05645.2003.

Busciglio, J. *et al.* (2002) ‘Altered metabolism of the amyloid β precursor protein is associated with mitochondrial dysfunction in Down’s syndrome’, *Neuron*. Cell Press, 33(5), pp. 677–688. doi: 10.1016/S0896-6273(02)00604-9.

Cacace, R., Sleegers, K. and Van Broeckhoven, C. (2016) ‘Molecular genetics of early-onset Alzheimer’s disease revisited’, *Alzheimer’s & Dementia*. John Wiley & Sons, Ltd, 12(6), pp. 733–748. doi: 10.1016/J.JALZ.2016.01.012.

Cai, F. *et al.* (2023) ‘USP25 contributes to defective neurogenesis and cognitive impairments’, *FASEB journal : official publication of the Federation of American Societies for Experimental Biology*. FASEB J, 37(6). doi: 10.1096/FJ.202300057R.

Campbell, N. B. *et al.* (2023) ‘Extracellular Vesicle Treatment Alleviates Neurodevelopmental and Neurodegenerative Pathology in Cortical Spheroid Model of Down Syndrome’, *International journal of molecular sciences*. Int J Mol Sci, 24(4). doi: 10.3390/IJMS24043477.

Cao, W. *et al.* (2008) ‘Identification of novel genes that modify phenotypes induced by Alzheimer’s beta-amyloid overexpression in Drosophila’, *Genetics*. Genetics, 178(3), pp. 1457–1471. doi: 10.1534/GENETICS.107.078394.

Carlyle, B. C. *et al.* (2017) ‘A multiregional proteomic survey of the postnatal human brain’, *Nature Neuroscience 2017 20:12*. Nature Publishing Group, 20(12), pp. 1787–1795. doi: 10.1038/s41593-017-0011-2.

Carmona-Iragui, M. *et al.* (2021) ‘Diagnostic and prognostic performance and longitudinal changes in plasma neurofilament light chain concentrations in adults with Down syndrome: a cohort study’, *The Lancet Neurology*. Lancet Publishing Group, 20(8), pp. 605–614. doi: 10.1016/S1474-4422(21)00129-0.

Carmona-Iragui, M. *et al.* (2024) ‘Clinical and research application of fluid biomarkers in autosomal dominant Alzheimer’s disease and Down syndrome’, *EBioMedicine*. EBioMedicine, 108. doi: 10.1016/J.EBIOM.2024.105327.

Casas-Tinto, S. *et al.* (2011) ‘The ER stress factor XBP1s prevents amyloid-β neurotoxicity’, *Human Molecular Genetics*. Oxford Academic, 20(11), pp. 2144–2160. doi: 10.1093/HMG/DDR100.

Cataldo, A. M. *et al.* (2000) 'Endocytic Pathway Abnormalities Precede Amyloid β Deposition in Sporadic Alzheimer's Disease and Down Syndrome: Differential Effects of APOE Genotype and Presenilin Mutations', *The American Journal of Pathology*. Elsevier, 157(1), pp. 277–286. doi: 10.1016/S0002-9440(10)64538-5.

Catterson, J. H. *et al.* (2023) 'Protein retention in the endoplasmic reticulum rescues Aβ toxicity in Drosophila', *Neurobiology of Aging*. Elsevier, 132, pp. 154–174. doi: 10.1016/J.NEUROBIOLAGING.2023.09.008.

Cenini, G. *et al.* (2011) 'Association between frontal cortex oxidative damage and beta-amyloid as a function of age in Down syndrome', *Biochimica et Biophysica Acta*, 1822(2), p. 130. doi: 10.1016/J.BBADIS.2011.10.001.

Chan, D. C. (2012) 'Fusion and fission: Interlinked processes critical for mitochondrial health', *Annual Review of Genetics*. Annual Reviews Inc., 46(Volume 46, 2012), pp. 265–287. doi: 10.1146/ANNUREV-GENET-110410-132529/CITE/REFWORKS.

Chang, K. T. and Min, K. T. (2009) 'Upregulation of three Drosophila homologs of human chromosome 21 genes alters synaptic function: Implications for Down syndrome', *Proceedings of the National Academy of Sciences of the United States of America*. National Academy of Sciences, 106(40), pp. 17117–17122. doi: 10.1073/PNAS.0904397106/SUPPL_FILE/SM2.AVI.

Chau, V. *et al.* (1989) 'A multiubiquitin chain is confined to specific lysine in a targeted short-lived protein', *Science (New York, N.Y.)*. Science, 243(4898), pp. 1576–1583. doi: 10.1126/SCIENCE.2538923.

Chen, G. F. *et al.* (2017) 'Amyloid beta: structure, biology and structure-based therapeutic development', *Acta Pharmacologica Sinica 2017 38:9*. Nature Publishing Group, 38(9), pp. 1205–1235. doi: 10.1038/aps.2017.28.

Chen, J. H. *et al.* (2015) ‘Protection of TGF-β1 against neuroinflammation and neurodegeneration in Aβ1-42-induced Alzheimer’s disease model rats’, *PloS one*. PLoS One, 10(2). doi: 10.1371/JOURNAL.PONE.0116549.

Chen, J. Y. *et al.* (2013) ‘Dosage of Dyrk1a Shifts Cells within a p21-Cyclin D1 Signaling Map to Control the Decision to Enter the Cell Cycle’, *Molecular Cell*. Cell Press, 52(1), pp. 87–100. doi: 10.1016/J.MOLCEL.2013.09.009.

Chen, L. *et al.* (2022) ‘Global, Regional, and National Burden and Trends of Down Syndrome From 1990 to 2019’, *Frontiers in genetics*. Front Genet, 13. doi: 10.3389/FGENE.2022.908482.

Chen, X. Q. *et al.* (2023) ‘Reduced synaptic proteins and SNARE complexes in Down syndrome with Alzheimer’s disease and the Dp16 mouse Down syndrome model: Impact of APP gene dose’, *Alzheimer’s & Dementia*. John Wiley & Sons, Ltd, 19(5), pp. 2095–2116. doi: 10.1002/ALZ.12835.

Chen, Y. *et al.* (2023) ‘Single-cell landscape analysis reveals systematic senescence in mammalian Down syndrome’, *Clinical and Translational Medicine*. Wiley, 13(7), p. e1310. doi: 10.1002/CTM2.1310.

Chen, Y., Fu, A. K. Y. and Ip, N. Y. (2019) ‘Synaptic dysfunction in Alzheimer’s disease: Mechanisms and therapeutic strategies’, *Pharmacology & Therapeutics*. Pergamon, 195, pp. 186–198. doi: 10.1016/J.PHARMTHERA.2018.11.006.

Chêne, G. *et al.* (2015) ‘Gender and incidence of dementia in the Framingham Heart Study from mid-adult life’, *Alzheimer’s & dementia : the journal of the Alzheimer’s Association*. Alzheimers Dement, 11(3), pp. 310–320. doi: 10.1016/J.JALZ.2013.10.005.

Cheon, M. S. *et al.* (2003) ‘Protein levels of genes encoded on chromosome 21 in fetal Down syndrome brain: challenging the gene dosage effect hypothesis (Part II)’, *Amino acids*. Amino Acids, 24(1–2), pp. 119–125. doi: 10.1007/S00726-002-0337-1.

Cheon, M. S. *et al.* (2008) ‘Protein expression of BACE1, BACE2 and APP in Down syndrome brains’, *Amino acids*. Amino Acids, 35(2), pp. 339–343. doi: 10.1007/S00726-007-0618-9.

Chien, S. *et al.* (2002) ‘Homophila: human disease gene cognates in Drosophila’, *Nucleic Acids Research*. Oxford Academic, 30(1), pp. 149–151. doi: 10.1093/NAR/30.1.149.

Choi, S. H. *et al.* (2014) ‘A three-dimensional human neural cell culture model of Alzheimer’s disease’, *Nature*. Nature, 515(7526), pp. 274–278. doi: 10.1038/NATURE13800.

Clague, M. J., Urbé, S. and Komander, D. (2019) ‘Breaking the chains: deubiquitylating enzyme specificity begets function’, *Nature reviews. Molecular cell biology*. Nat Rev Mol Cell Biol, 20(6), pp. 338–352. doi: 10.1038/S41580-019-0099-1.

Cockerill, I. *et al.* (2018) ‘Blood-Brain Barrier Integrity and Clearance of Amyloid-β from the BBB’, *Advances in experimental medicine and biology*. Adv Exp Med Biol, 1097, pp. 261–278. doi: 10.1007/978-3-319-96445-4_14.

Cohen, A. D. *et al.* (2018) ‘Early striatal amyloid deposition distinguishes Down syndrome and autosomal dominant Alzheimer’s disease from late-onset amyloid deposition’, *Alzheimer’s & dementia : the journal of the Alzheimer’s Association*. Alzheimers Dement, 14(6), pp. 743–750. doi: 10.1016/J.JALZ.2018.01.002.

Cole, J. H. *et al.* (2017) ‘Brain-predicted age in Down syndrome is associated with beta amyloid deposition and cognitive decline’, *Neurobiology of Aging*. Elsevier, 56, pp. 41–49. doi: 10.1016/J.NEUROBIOLAGING.2017.04.006.

Condello, C. *et al.* (2022) ‘Aβ and tau prions feature in the neuropathogenesis of down syndrome’, *Proceedings of the National Academy of Sciences of the United States of America*. National Academy of Sciences, 119(46), p. e2212954119. doi: 10.1073/PNAS.2212954119/SUPPL_FILE/PNAS.2212954119.SAPP.PDF.

Conrad, T. and Akhtar, A. (2012) ‘Dosage compensation in Drosophila melanogaster: epigenetic fine-tuning of chromosome-wide transcription’, *Nature Reviews Genetics 2012 13:2*. Nature Publishing Group, 13(2), pp. 123–134. doi: 10.1038/nrg3124.

Coskun, P. E. and Busciglio, J. (2012) ‘Oxidative stress and mitochondrial dysfunction in Down’s syndrome: Relevance to aging and dementia’, *Current Gerontology and Geriatrics Research*, 2012. doi: 10.1155/2012/383170.

Court, R. *et al.* (2023) ‘Virtual Fly Brain—An interactive atlas of the Drosophila nervous system’, *Frontiers in Physiology*. Frontiers Media S.A., 14, p. 1076533. doi: 10.3389/FPHYS.2023.1076533/BIBTEX.

Crowther, D. C. *et al.* (2005) ‘Intraneuronal Aβ, non-amyloid aggregates and neurodegeneration in a Drosophila model of Alzheimer’s disease’, *Neuroscience*. Elsevier Ltd, 132(1), pp. 123–135. doi: 10.1016/j.neuroscience.2004.12.025.

Cuevas-Diaz Duran, R. *et al.* (2022) ‘Single-cell and single-nuclei RNA sequencing as powerful tools to decipher cellular heterogeneity and dysregulation in neurodegenerative diseases’, *Frontiers in Cell and Developmental Biology*. Frontiers Media S.A., 10, p. 884748. doi: 10.3389/FCELL.2022.884748/BIBTEX.

Cui, L. *et al.* (2020) ‘Deubiquitinase USP7 regulates Drosophila aging through ubiquitination and autophagy’, *Aging (Albany NY)*. Impact Journals LLC, 12(22), p. 23082. doi: 10.18632/AGING.104067.

Cukier, H. N. *et al.* (2023) ‘An Alzheimer’s disease risk variant in TTC3 modifies the actin cytoskeleton organization and the PI3K-Akt signaling pathway in iPSC-derived forebrain neurons’, *Neurobiology of aging*. Neurobiol Aging, 131, pp. 182–195. doi: 10.1016/J.NEUROBIOLAGING.2023.07.007.

Cummings, J. (2023) ‘Anti-Amyloid Monoclonal Antibodies are Transformative Treatments that Redefine Alzheimer’s Disease Therapeutics’, *Drugs*. Drugs, 83(7), pp. 569–576. doi: 10.1007/S40265-023-01858-9.

Curcio, R. *et al.* (2024) ‘Two functionally different mitochondrial phosphate carriers support Drosophila melanogaster OXPHOS throughout distinct developmental stages’, *Biochimica et Biophysica Acta (BBA) - Molecular Cell Research*. Elsevier, 1871(1), p. 119615. doi: 10.1016/J.BBAMCR.2023.119615.

Dar, N. J. and Glazner, G. W. (2020) ‘Deciphering the neuroprotective and neurogenic potential of soluble amyloid precursor protein alpha (sAPPα)’, *Cellular and molecular life sciences : CMLS*. Cell Mol Life Sci, 77(12), pp. 2315–2330. doi: 10.1007/S00018-019-03404-X.

Dashinimaev, E. B. *et al.* (2017) ‘Neurons Derived from Induced Pluripotent Stem Cells of Patients with Down Syndrome Reproduce Early Stages of Alzheimer’s Disease Type Pathology in vitro’, *Journal of Alzheimer’s disease : JAD*. J Alzheimers Dis, 56(2), pp. 835–847. doi: 10.3233/JAD-160945.

DeVos, S. L. *et al.* (2018) ‘Tau reduction in the presence of amyloid-β prevents tau pathology and neuronal death in vivo’, *Brain*. Oxford Academic, 141(7), pp. 2194–2212. doi: 10.1093/BRAIN/AWY117.

Doran, E. *et al.* (2017) 'Down Syndrome, Partial Trisomy 21, and Absence of Alzheimer's Disease: The role of APP', *Journal of Alzheimer's disease : JAD*. NIH Public Access, 56(2), p. 459. doi: 10.3233/JAD-160836.

Dorval, V. *et al.* (2007) 'Modulation of Aβ generation by small ubiquitin-like modifiers does not require conjugation to target proteins', *Biochemical Journal*. Portland Press, 404(2), pp. 309–316. doi: 10.1042/BJ20061451.

Dowjat, W. K. *et al.* (2007) 'Trisomy-driven overexpression of DYRK1A kinase in the brain of subjects with Down syndrome', *Neuroscience letters*. Neurosci Lett, 413(1), pp. 77–81. doi: 10.1016/J.NEULET.2006.11.026.

Down, J. L. H. (1866) 'Observations on an ethnic classification of idiots', *Heredity*, 21(4), pp. 695–697. doi: 10.1038/hdy.1966.69.

Downes, E. C. *et al.* (2008) 'Loss of synaptophysin and synaptosomal-associated protein 25-kDa (SNAP-25) in elderly Down syndrome individuals', *Neuropathology and applied neurobiology*. Neuropathol Appl Neurobiol, 34(1), pp. 12–22. doi: 10.1111/J.1365-2990.2007.00899.X.

Edie, S. *et al.* (2018) 'Survey of Human Chromosome 21 Gene Expression Effects on Early Development in Danio rerio', *G3 (Bethesda, Md.)*. G3 (Bethesda), 8(7), pp. 2215–2223. doi: 10.1534/G3.118.200144.

Espuny-Camacho, I. *et al.* (2017) 'Hallmarks of Alzheimer's Disease in Stem-Cell-Derived Human Neurons Transplanted into Mouse Brain', *Neuron*. Cell Press, 93(5), pp. 1066-1081.e8. doi: 10.1016/J.NEURON.2017.02.001/ATTACHMENT/F33F10BE-3CB9-4ED9-AC17-97092088D9B5/MMC4.PDF.

Eun, J. Y. *et al.* (2009) ‘Intracellular amyloid beta interacts with SOD1 and impairs the enzymatic activity of SOD1: implications for the pathogenesis of amyotrophic lateral sclerosis’, *Experimental & Molecular Medicine*. Korean Society for Biochemistry and Molecular Biology, 41(9), p. 611. doi: 10.3858/EMM.2009.41.9.067.

Farrell et al., (2025). 'Apolipoprotein E abundance is elevated in the brains of individuals with Down syndrome-Alzheimer’s disease', bioRxiv. doi:10.1101/2025.02.24.639862.

Farrell, C., Mumford, P. and Wiseman, F. K. (2022) ‘Rodent Modeling of Alzheimer’s Disease in Down Syndrome: In vivo and ex vivo Approaches’, *Frontiers in neuroscience*. Front Neurosci, 16. doi: 10.3389/FNINS.2022.909669.

De Felice, F. G. *et al.* (2008) ‘Alzheimer’s disease-type neuronal tau hyperphosphorylation induced by A beta oligomers’, *Neurobiology of aging*. Neurobiol Aging, 29(9), pp. 1334–1347. doi: 10.1016/J.NEUROBIOLAGING.2007.02.029.

Fernandez-Marcos, P. J. and Auwerx, J. (2011) ‘Regulation of PGC-1α, a nodal regulator of mitochondrial biogenesis’, *The American journal of clinical nutrition*. Am J Clin Nutr, 93(4). doi: 10.3945/AJCN.110.001917.

Fernandez, A. *et al.* (2024) ‘Cryo-EM structures of amyloid-β and tau filaments in Down syndrome’, *Nature structural & molecular biology*. Nat Struct Mol Biol, 31(6), pp. 903–909. doi: 10.1038/S41594-024-01252-3.

Ferreira, D., Nordberg, A. and Westman, E. (2020) ‘Biological subtypes of Alzheimer disease: A systematic review and meta-analysis’, *Neurology*. Neurology, 94(10), pp. 436–448. doi: 10.1212/WNL.0000000000009058.

Ferrer, I. *et al.* (2005) ‘Constitutive Dyrk1A is abnormally expressed in Alzheimer disease, Down syndrome, Pick disease, and related transgenic models’, *Neurobiology of disease*. Neurobiol Dis, 20(2), pp. 392–400. doi: 10.1016/J.NBD.2005.03.020.

Fertan, E. *et al.* (2024) ‘Cerebral organoids with chromosome 21 trisomy secrete Alzheimer’s disease-related soluble aggregates detectable by single-molecule-fluorescence and super-resolution microscopy’, *Molecular psychiatry*. Mol Psychiatry, 29(2), pp. 369–386. doi: 10.1038/S41380-023-02333-3.

Fisher, E. M. C. *et al.* (2017) ‘The integration site of theAPP transgene in the J20 mouse model of Alzheimer’s disease’, *Wellcome Open Research*. The Wellcome Trust, 2. doi: 10.12688/WELLCOMEOPENRES.12237.2.

Flores-Aguilar, L. *et al.* (2020) ‘Evolution of neuroinflammation across the lifespan of individuals with Down syndrome’, *Brain : a journal of neurology*. Brain, 143(12), pp. 3653–3671. doi: 10.1093/BRAIN/AWAA326.

Fortea, J. *et al.* (2020) ‘Clinical and biomarker changes of Alzheimer’s disease in adults with Down syndrome: a cross-sectional study’, *The Lancet*. Lancet Publishing Group, 395(10242), pp. 1988–1997. doi: 10.1016/S0140-6736(20)30689-9.

Fortea, J. *et al.* (2021) ‘Alzheimer’s disease associated with Down syndrome: a genetic form of dementia’, *The Lancet Neurology*. Elsevier, 20(11), pp. 930–942. doi: 10.1016/S1474-4422(21)00245-3.

Fortea, J. *et al.* (2024) ‘APOE4 homozygosity represents a distinct genetic form of Alzheimer’s disease’, *Nature Medicine 2024 30:5*. Nature Publishing Group, 30(5), pp. 1284–1291. doi: 10.1038/s41591-024-02931-w.

Franceschi, C. *et al.* (2019) ‘Accelerated bio-cognitive aging in Down syndrome: State of the art and possible deceleration strategies’, *Aging Cell*. Blackwell Publishing Ltd, 18(3), p. e12903. doi: 10.1111/ACEL.12903.

Fukami-Gartner, A. *et al.* (2023) ‘Comprehensive volumetric phenotyping of the neonatal brain in Down syndrome’, *Cerebral cortex (New York, N.Y. : 1991)*. Cereb Cortex, 33(14), pp. 8921–8941. doi: 10.1093/CERCOR/BHAD171.

Fukuoh, A. *et al.* (2014) ‘ Screen for mitochondrial DNA copy number maintenance genes reveals essential role for ATP synthase ’, *Molecular Systems Biology*. Springer Science and Business Media LLC, 10(6), p. 734. doi: 10.15252/MSB.20145117/SUPPL_FILE/MSB145117.REVIEWER_COMMENTS.PDF.

Ganguly, B. B. and Kadam, N. N. (2022) ‘Triplication of HSA21 on alterations in structure and function of mitochondria’, *Mitochondrion*. Elsevier, 65, pp. 88–101. doi: 10.1016/J.MITO.2022.05.007.

García-Cerro, S. *et al.* (2017) ‘Normalizing the gene dosage of Dyrk1A in a mouse model of Down syndrome rescues several Alzheimer’s disease phenotypes’, *Neurobiology of Disease*. Academic Press Inc., 106, pp. 76–88. doi: 10.1016/j.nbd.2017.06.010.

Garcia, I. *et al.* (2017) ‘The little big genome: the organization of mitochondrial DNA’, *Frontiers in bioscience (Landmark edition)*. Frontiers in Bioscience, 22(4), p. 710. doi: 10.2741/4511.

Gargano, J. W. *et al.* (2005) ‘Rapid iterative negative geotaxis (RING): A new method for assessing age-related locomotor decline in Drosophila’, *Experimental Gerontology*. doi: 10.1016/j.exger.2005.02.005.

Gauthier, S. *et al.* (2021) *World Alzheimer Report 2021: Journey through the diagnosis of dementia*.

Gersch, M. *et al.* (2019) 'Distinct USP25 and USP28 Oligomerization States Regulate Deubiquitinating Activity', *Molecular Cell*. Cell Press, 74(3), p. 436. doi: 10.1016/J.MOLCEL.2019.02.030.

Gerton, J. L. (2024) 'A working model for the formation of Robertsonian chromosomes', *Journal of cell science*. J Cell Sci, 137(7). doi: 10.1242/JCS.261912.

Gholipour, T. *et al.* (2017) 'The clinical and neurobehavioral course of Down syndrome and dementia with or without new-onset epilepsy', *Epilepsy & behavior : E&B*. Epilepsy Behav, 68, pp. 11–16. doi: 10.1016/J.YEBEH.2016.12.014.

Ghosh, U. *et al.* (2024) 'Cryo-EM structures reveal tau filaments from Down syndrome adopt Alzheimer's disease fold', *Acta neuropathologica communications*. Acta Neuropathol Commun, 12(1). doi: 10.1186/S40478-024-01806-Y.

Giffin-Rao, Y. *et al.* (2022) 'Altered patterning of trisomy 21 interneuron progenitors', *Stem Cell Reports*. Cell Press, 17(6), pp. 1366–1379. doi: 10.1016/J.STEMCR.2022.05.001/ATTACHMENT/21536F50-4A4C-4246-A99C-6C99E3DF729D/MMC8.PDF.

Glenner, G. G. and Wong, C. W. (1984a) 'Alzheimer's disease: initial report of the purification and characterization of a novel cerebrovascular amyloid protein', *Biochemical and biophysical research communications*. Biochem Biophys Res Commun, 120(3), pp. 885–890. doi: 10.1016/S0006-291X(84)80190-4.

Glenner, G. G. and Wong, C. W. (1984b) 'Alzheimer's disease and Down's syndrome: Sharing of a unique cerebrovascular amyloid fibril protein', *Biochemical and Biophysical Research Communications*, 122(3), pp. 1131–1135. doi: 10.1016/0006-291X(84)91209-9.

Gómez-Isla, T. *et al.* (1997) 'Neuronal loss correlates with but exceeds neurofibrillary tangles in Alzheimer's disease', *Annals of neurology*. Ann Neurol, 41(1), pp. 17–24. doi: 10.1002/ANA.410410106.

Gonzales, P. K. *et al.* (2018) 'Transcriptome analysis of genetically matched human induced pluripotent stem cells disomic or trisomic for chromosome 21', *PloS one*. PLoS One, 13(3). doi: 10.1371/JOURNAL.PONE.0194581.

de Graaf, G., Buckley, F. and Skotko, B. G. (2020) 'Estimation of the number of people with Down syndrome in Europe', *European Journal of Human Genetics 2020 29:3*. Nature Publishing Group, 29(3), pp. 402–410. doi: 10.1038/s41431-020-00748-y.

De Graaf, G., Buckley, F. and Skotko, B. G. (2017) 'Estimation of the number of people with Down syndrome in the United States', *Genetics in Medicine*. Nature Publishing Group, 19(4), pp. 439–447. doi: 10.1038/gim.2016.127.

Granese, B. *et al.* (2013) 'Validation of microarray data in human lymphoblasts shows a role of the ubiquitin-proteasome system and NF-kB in the pathogenesis of Down syndrome', *BMC Medical Genomics*. BioMed Central, 6(1), p. 24. doi: 10.1186/1755-8794-6-24.

Greeve, I. *et al.* (2004) 'Age-Dependent Neurodegeneration and Alzheimer-Amyloid Plaque Formation in Transgenic Drosophila', *The Journal of Neuroscience*. Society for Neuroscience, 24(16), p. 3899. doi: 10.1523/JNEUROSCI.0283-04.2004.

Gribble, S. M. *et al.* (2013) 'Massively Parallel Sequencing Reveals the Complex Structure of an Irradiated Human Chromosome on a Mouse Background in the Tc1 Model of Down Syndrome', *PLOS ONE*. Public Library of Science, 8(4), p. e60482. doi: 10.1371/JOURNAL.PONE.0060482.

Grigorova, M. *et al.* (2022) 'Amyloid- β and tau deposition influences cognitive and functional decline in Down syndrome', *Neurobiology of Aging*. Elsevier, 119, pp. 36–45. doi: 10.1016/J.NEUROBIOLAGING.2022.07.003.

Grubman, A. *et al.* (2019) 'A single-cell atlas of entorhinal cortex from individuals with Alzheimer's disease reveals cell-type-specific gene expression regulation', *Nature neuroscience*. Nat Neurosci, 22(12), pp. 2087–2097. doi: 10.1038/S41593-019-0539-4.

Guennewig, B. *et al.* (2021) 'Defining early changes in Alzheimer's disease from RNA sequencing of brain regions differentially affected by pathology', *Scientific Reports 2021 11:1*. Nature Publishing Group, 11(1), pp. 1–15. doi: 10.1038/s41598-021-83872-z.

Guerreiro, R. *et al.* (2013) 'TREM2 variants in Alzheimer's disease', *The New England journal of medicine*. N Engl J Med, 368(2), pp. 117–127. doi: 10.1056/NEJMOA1211851.

Guidi, S. *et al.* (2008) 'Neurogenesis impairment and increased cell death reduce total neuron number in the hippocampal region of fetuses with Down syndrome', *Brain pathology (Zurich, Switzerland)*. Brain Pathol, 18(2), pp. 180–197. doi: 10.1111/J.1750-3639.2007.00113.X.

Guidi, S. *et al.* (2011) 'Widespread proliferation impairment and hypocellularity in the cerebellum of fetuses with down syndrome', *Brain pathology (Zurich, Switzerland)*. Brain Pathol, 21(4), pp. 361–373. doi: 10.1111/J.1750-3639.2010.00459.X.

Gulesserian, T. *et al.* (2001) 'Superoxide dismutase SOD1, encoded on chromosome 21, but not SOD2 is overexpressed in brains of patients with Down syndrome', *Journal of investigative medicine : the official publication of the American Federation for Clinical Research*. J Investig Med, 49(1), pp. 41–46. doi: 10.2310/6650.2001.34089.

Guo, Z. *et al.* (2022) 'A Global Multiregional Proteomic Map of the Human Cerebral Cortex', *Genomics, Proteomics & Bioinformatics*. Elsevier, 20(4), pp. 614–632. doi: 10.1016/J.GPB.2021.08.008.

Gupta, K., Czerminski, J. T. and Lawrence, J. B. (2024) 'Trisomy silencing by XIST: translational prospects and challenges', *Human genetics*. Hum Genet, 143(7), pp. 843–855. doi: 10.1007/S00439-024-02651-8.

Haddadi, M. *et al.* (2016) 'Transgenic Drosophila model to study apolipoprotein E4-induced neurodegeneration', *Behavioural brain research*. Behav Brain Res, 301, pp. 10–18. doi: 10.1016/J.BBR.2015.12.022.

Hampel, H. *et al.* (2021) 'The β-Secretase BACE1 in Alzheimer's Disease', *Biological psychiatry*. Biol Psychiatry, 89(8), pp. 745–756. doi: 10.1016/J.BIOPSYCH.2020.02.001.

Hanseeuw, B. J. *et al.* (2019) 'Association of Amyloid and Tau With Cognition in Preclinical Alzheimer Disease: A Longitudinal Study', *JAMA Neurology*. American Medical Association, 76(8), pp. 915–924. doi: 10.1001/JAMANEUROL.2019.1424.

Hardy, J. A. and Higgins, G. A. (1992) 'Alzheimer's disease: The amyloid cascade hypothesis', *Science*. American Association for the Advancement of Science , 256(5054), pp. 184–185. doi: 10.1126/SCIENCE.1566067/ASSET/74A758CB-215F-4A8E-9AAA-05F4D89DA62A/ASSETS/SCIENCE.1566067.FP.PNG.

Harerimana, N. V. *et al.* (2023) 'The role of mitochondrial genome abundance in Alzheimer's disease', *Alzheimer's & Dementia*. John Wiley & Sons, Ltd, 19(5), pp. 2069–2083. doi: 10.1002/ALZ.12812.

Hartley, S. L. *et al.* (2024) ‘AT(N) biomarker profiles and Alzheimer’s disease symptomology in Down syndrome’, *Alzheimer’s & dementia : the journal of the Alzheimer’s Association*. Alzheimers Dement, 20(1), pp. 366–375. doi: 10.1002/ALZ.13446.

Hartmann, T. *et al.* (1997) ‘Distinct sites of intracellular production for Alzheimer’s disease A beta40/42 amyloid peptides’, *Nature medicine*. Nat Med, 3(9), pp. 1016–1020. doi: 10.1038/NM0997-1016.

Hasselmann, J. *et al.* (2019) ‘Development of a Chimeric Model to Study and Manipulate Human Microglia In Vivo’, *Neuron*. Neuron, 103(6), pp. 1016-1033.e10. doi: 10.1016/J.NEURON.2019.07.002.

Hassold, T. and Hunt, P. (2001) ‘To err (meiotically) is human: the genesis of human aneuploidy’, *Nature Reviews Genetics 2001 2:4*. Nature Publishing Group, 2(4), pp. 280–291. doi: 10.1038/35066065.

Hawrylycz, M. J. *et al.* (2012) ‘An anatomically comprehensive atlas of the adult human brain transcriptome’, *Nature 2012 489:7416*. Nature Publishing Group, 489(7416), pp. 391–399. doi: 10.1038/nature11405.

Head, E. *et al.* (2001) ‘Oxidation of Aβ and Plaque Biogenesis in Alzheimer’s Disease and Down Syndrome’, *Neurobiology of Disease*. Academic Press, 8(5), pp. 792–806. doi: 10.1006/NBDI.2001.0431.

Hegde, V. R., Vogel, R. and Feany, M. B. (2014) ‘Glia are critical for the neuropathology of complex I deficiency in Drosophila’, *Human molecular genetics*. Hum Mol Genet, 23(17), pp. 4686–4692. doi: 10.1093/HMG/DDU188.

Helguera, P. *et al.* (2013) 'Adaptive Downregulation of Mitochondrial Function in Down Syndrome', *Cell metabolism*, 17(1), p. 132. doi: 10.1016/J.CMET.2012.12.005.

Herault, Y. *et al.* (2017) 'Rodent models in Down syndrome research: Impact and future opportunities', *DMM Disease Models and Mechanisms*. Company of Biologists Ltd, pp. 1165–1186. doi: 10.1242/dmm.029728.

Hibaoui, Y. *et al.* (2014) 'Modelling and rescuing neurodevelopmental defect of Down syndrome using induced pluripotent stem cells from monozygotic twins discordant for trisomy 21', *EMBO molecular medicine*. EMBO Mol Med, 6(2), pp. 259–277. doi: 10.1002/EMMM.201302848.

Hiller, M. M. *et al.* (1996) 'ER Degradation of a Misfolded Luminal Protein by the Cytosolic Ubiquitin-Proteasome Pathway', *Science*. American Association for the Advancement of Science, 273(5282), pp. 1725–1728. doi: 10.1126/SCIENCE.273.5282.1725.

Hipp, M. S., Park, S. H. and Hartl, U. U. (2014) 'Proteostasis impairment in protein-misfolding and -aggregation diseases', *Trends in cell biology*. Trends Cell Biol, 24(9), pp. 506–514. doi: 10.1016/J.TCB.2014.05.003.

Hithersay, R. *et al.* (2019) 'Association of Dementia With Mortality Among Adults With Down Syndrome Older Than 35 Years.', *JAMA neurology*, 76(2), pp. 152–160. doi: 10.1001/jamaneurol.2018.3616.

Hochstrasser, M. (2001) 'SP-RING for SUMO: new functions bloom for a ubiquitin-like protein', *Cell*. Cell, 107(1), pp. 5–8. doi: 10.1016/S0092-8674(01)00519-0.

Hoffman, J. M. *et al.* (2021) 'Sex, mating and repeatability of Drosophila melanogaster longevity', *Royal Society open science*. R Soc Open Sci, 8(8). doi: 10.1098/RSOS.210273.

Hsieh, Y. C. *et al.* (2024) ‘Person-specific differences in ubiquitin-proteasome mediated proteostasis in human neurons’, *Alzheimer’s & Dementia*. John Wiley & Sons, Ltd, 20(4), pp. 2952–2967. doi: 10.1002/ALZ.13680.

Hu, Y. *et al.* (2011) ‘An integrative approach to ortholog prediction for disease-focused and other functional studies’, *BMC bioinformatics*. BMC Bioinformatics, 12(357). doi: 10.1186/1471-2105-12-357.

Huang, Y. *et al.* (2019) ‘Insulin signaling in Drosophila melanogaster mediates Aβ toxicity’, *Communications Biology 2019 2:1*. Nature Publishing Group, 2(1), pp. 1–14. doi: 10.1038/s42003-018-0253-x.

Huggard, D. *et al.* (2020) ‘Increased systemic inflammation in children with Down syndrome’, *Cytokine*. Cytokine, 127. doi: 10.1016/J.CYTO.2019.154938.

Hunter, S. *et al.* (2023) ‘Transcription dosage compensation does not occur in Down syndrome’, *BMC Biology*. BioMed Central Ltd, 21(1), pp. 1–15. doi: 10.1186/S12915-023-01700-4/FIGURES/3.

Hwang, S. *et al.* (2021) ‘Consequences of aneuploidy in human fibroblasts with trisomy 21’, *Proceedings of the National Academy of Sciences of the United States of America*. National Academy of Sciences, 118(6), p. e2014723118. doi: 10.1073/PNAS.2014723118/SUPPL_FILE/PNAS.2014723118.SD05.XLSX.

Ichimata, S. *et al.* (2022) ‘Patterns of Mixed Pathologies in Down Syndrome’, *Journal of Alzheimer’s Disease*. IOS Press BV, 87(2), pp. 595–607. doi: 10.3233/JAD-215675/ASSET/IMAGES/10.3233_JAD-215675-FIG3.JPG.

Ichimata, S. *et al.* (2023) ‘Distinct Molecular Signatures of Amyloid-Beta and Tau in Alzheimer’s Disease Associated with Down Syndrome’, *International journal of molecular sciences*. Int J Mol Sci, 24(14). doi: 10.3390/IJMS241411596.

Iijima-Ando, K. *et al.* (2008) 'Overexpression of neprilysin reduces alzheimer amyloid-beta42 (Abeta42)-induced neuron loss and intraneuronal Abeta42 deposits but causes a reduction in cAMP-responsive element-binding protein-mediated transcription, age-dependent axon pathology, and prem', *The Journal of biological chemistry*. J Biol Chem, 283(27), pp. 19066–19076. doi: 10.1074/JBC.M710509200.

Iulita, M. F. *et al.* (2023) 'Association of biological sex with clinical outcomes and biomarkers of Alzheimer's disease in adults with Down syndrome', *Brain communications*. Brain Commun, 5(2). doi: 10.1093/BRAINCOMMS/FCAD074.

Iwata, N. *et al.* (2001) 'Metabolic regulation of brain Abeta by neprilysin', *Science (New York, N.Y.)*. Science, 292(5521), pp. 1550–1552. doi: 10.1126/SCIENCE.1059946.

Izzo, A. *et al.* (2017) 'Metformin restores the mitochondrial network and reverses mitochondrial dysfunction in Down syndrome cells', *Human Molecular Genetics*. Oxford Academic, 26(6), pp. 1056–1069. doi: 10.1093/HMG/DDX016.

Jack, C. R. *et al.* (2019) 'The bivariate distribution of amyloid-β and tau: relationship with established neurocognitive clinical syndromes', *Brain : a journal of neurology*. Brain, 142(10), pp. 3230–3242. doi: 10.1093/BRAIN/AWZ268.

Jack, C. R. *et al.* (2024) 'Revised criteria for diagnosis and staging of Alzheimer's disease: Alzheimer's Association Workgroup', *Alzheimer's & dementia : the journal of the Alzheimer's Association*. Alzheimers Dement, 20(8), pp. 5143–5169. doi: 10.1002/ALZ.13859.

Jacobs, H. I. L. *et al.* (2018) 'Structural tract alterations predict downstream tau accumulation in amyloid-positive older individuals', *Nature Neuroscience 2018 21:3*. Nature Publishing Group, 21(3), pp. 424–431. doi: 10.1038/s41593-018-0070-z.

Jansen, W. J. *et al.* (2015) ‘Prevalence of Cerebral Amyloid Pathology in Persons Without Dementia: A Meta-analysis’, *JAMA*. American Medical Association, 313(19), pp. 1924–1938. doi: 10.1001/JAMA.2015.4668.

Jervis, G. A. (1948) ‘Early senile dementia in mongoloid idiocy’, *The American journal of psychiatry*. Am J Psychiatry, 105(2), pp. 102–106. doi: 10.1176/AJP.105.2.102.

Jin, H. S. *et al.* (2017) ‘Mitochondrial Control of Innate Immunity and Inflammation’, *Immune network*. Immune Netw, 17(2), pp. 77–88. doi: 10.4110/IN.2017.17.2.77.

Jin, M. *et al.* (2022) ‘Type-I-interferon signaling drives microglial dysfunction and senescence in human iPSC models of Down syndrome and Alzheimer’s disease’, *Cell stem cell*. Cell Stem Cell, 29(7), pp. 1135-1153.e8. doi: 10.1016/J.STEM.2022.06.007.

Johnson, N. R. *et al.* (2023) ‘Alzheimer’s disease phenotypes in human induced pluripotent stem cell-based models of Down syndrome’, *Alzheimer’s & Dementia*. John Wiley & Sons, Ltd, 19(S13), p. e080065. doi: 10.1002/ALZ.080065.

Jung, E. S. *et al.* (2015) ‘Acute ER stress regulates amyloid precursor protein processing through ubiquitin-dependent degradation’, *Scientific Reports 2015 5:1*. Nature Publishing Group, 5(1), pp. 1–9. doi: 10.1038/srep08805.

Jutten, R. J. *et al.* (2021) ‘Finding Treatment Effects in Alzheimer Trials in the Face of Disease Progression Heterogeneity’, *Neurology*. Neurology, 96(22), pp. E2673–E2684. doi: 10.1212/WNL.0000000000012022.

Karanth, S. *et al.* (2020) ‘Prevalence and Clinical Phenotype of Quadruple Misfolded Proteins in Older Adults’, *JAMA neurology*. JAMA Neurol, 77(10), pp. 1299–1307. doi: 10.1001/JAMANEUROL.2020.1741.

Karlsson, M. *et al.* (2021) ‘A single-cell type transcriptomics map of human tissues’, *Science advances*. Sci Adv, 7(31). doi: 10.1126/SCIADV.ABH2169.

Kasri, A. *et al.* (2024) ‘Amyloid-β peptide signature associated with cerebral amyloid angiopathy in familial Alzheimer’s disease with APPdup and Down syndrome’, *Acta neuropathologica*. Acta Neuropathol, 148(1), p. 8. doi: 10.1007/S00401-024-02756-4.

Kassel, S. *et al.* (2023) ‘USP47 deubiquitylates Groucho/TLE to promote Wnt-β-catenin signaling’, *Science Signaling*. American Association for the Advancement of Science, 16(771). doi: 10.1126/SCISIGNAL.ABN8372/SUPPL_FILE/SCISIGNAL.ABN8372_MDAR_REPRODUCIBILITY_CHECKLIST.PDF.

Kazuki, Y. *et al.* (2020) ‘A non-mosaic transchromosomic mouse model of down syndrome carrying the long arm of human chromosome 21’, *eLife*. eLife Sciences Publications Ltd, 9, pp. 1–29. doi: 10.7554/eLife.56223.

Kessissoglou, I. A. *et al.* (2020) ‘The Drosophila amyloid precursor protein homologue mediates neuronal survival and neuroglial interactions’, *PLOS Biology*. Public Library of Science, 18(12), p. e3000703. doi: 10.1371/JOURNAL.PBIO.3000703.

Khacho, M. *et al.* (2017) ‘Mitochondrial dysfunction underlies cognitive defects as a result of neural stem cell depletion and impaired neurogenesis’, *Human Molecular Genetics*. Oxford University Press, 26(17), pp. 3327–3341. doi: 10.1093/HMG/DDX217.

Kim, K. S. *et al.* (1988) ‘Production and characterization of monoclonal antibodies reactive to synthetic cerebrovascular amyloid peptide’, *Neurosci. Res. Commun.*, 2, pp. 121–130.

Kimura, R. *et al.* (2007) 'The DYRK1A gene, encoded in chromosome 21 Down syndrome critical region, bridges between beta-amyloid production and tau phosphorylation in Alzheimer disease', *Human molecular genetics*. Hum Mol Genet, 16(1), pp. 15–23. doi: 10.1093/HMG/DDL437.

Kohli, M. A. *et al.* (2016) 'Segregation of a rare TTC3 variant in an extended family with late-onset Alzheimer disease', *Neurology. Genetics*. Neurol Genet, 2(1). doi: 10.1212/NXG.0000000000000041.

Korolchuk, V. I., Menzies, F. M. and Rubinsztein, D. C. (2010) 'Mechanisms of cross-talk between the ubiquitin-proteasome and autophagy-lysosome systems', *FEBS letters*. FEBS Lett, 584(7), pp. 1393–1398. doi: 10.1016/J.FEBSLET.2009.12.047.

Kowada, R. *et al.* (2021) 'The function of Scox in glial cells is essential for locomotive ability in Drosophila', *Scientific reports*. Sci Rep, 11(1). doi: 10.1038/S41598-021-00663-2.

Krapfenbauer, K. *et al.* (1999) 'Differential display reveals deteriorated mRNA levels of NADH3 (complex I) in cerebellum of patients with Down syndrome', *Journal of neural transmission. Supplementum*. J Neural Transm Suppl, 57(57), pp. 211–220. doi: 10.1007/978-3-7091-6380-1_13.

Krause, S. A. *et al.* (2022) 'FlyAtlas 2 in 2022: enhancements to the Drosophila melanogaster expression atlas', *Nucleic acids research*. Nucleic Acids Res, 50(D1), pp. D1010–D1015. doi: 10.1093/NAR/GKAB971.

Kretzschmar, G. C. *et al.* (2021) 'GWAS-Top Polymorphisms Associated With Late-Onset Alzheimer Disease in Brazil: Pointing Out Possible New Culprits Among Non-Coding RNAs', *Frontiers in Molecular Biosciences*. Frontiers Media S.A., 8, p. 563. doi: 10.3389/FMOLB.2021.632314/BIBTEX.

Krinsky-McHale, S. J. *et al.* (2022) 'A modified Cued Recall Test for detecting prodromal AD in adults with Down syndrome', *Alzheimer's & Dementia: Diagnosis, Assessment & Disease Monitoring*. John Wiley & Sons, Ltd, 14(1), p. e12361. doi: 10.1002/DAD2.12361.

Krishtal, J. *et al.* (2017) 'In situ fibrillizing amyloid-beta 1-42 induces neurite degeneration and apoptosis of differentiated SH-SY5Y cells', *PloS one*. PLoS One, 12(10). doi: 10.1371/JOURNAL.PONE.0186636.

Kuchibhotla, K. V. *et al.* (2008) 'Abeta plaques lead to aberrant regulation of calcium homeostasis in vivo resulting in structural and functional disruption of neuronal networks', *Neuron*. Neuron, 59(2), pp. 214–225. doi: 10.1016/J.NEURON.2008.06.008.

Kunkle, B. W. *et al.* (2019) 'Genetic meta-analysis of diagnosed Alzheimer's disease identifies new risk loci and implicates Aβ, tau, immunity and lipid processing', *Nature Genetics 2019 51:3*. Nature Publishing Group, 51(3), pp. 414–430. doi: 10.1038/s41588-019-0358-2.

Kurabayashi, N. and Sanada, K. (2013) 'Increased dosage of DYRK1A and DSCR1 delays neuronal differentiation in neocortical progenitor cells', *Genes & Development*. Cold Spring Harbor Laboratory Press, 27(24), pp. 2708–2721. doi: 10.1101/GAD.226381.113.

Kushner, I. K. *et al.* (2018) 'Individual Variability of Protein Expression in Human Tissues', *Journal of Proteome Research*. American Chemical Society, 17(11), pp. 3914–3922. doi: 10.1021/ACS.JPROTEOME.8B00580/SUPPL_FILE/PR8B00580_SI_002.XLSX.

Lai, F. *et al.* (2020) 'Sex differences in risk of Alzheimer's disease in adults with Down syndrome', *Alzheimer's & dementia (Amsterdam, Netherlands)*. Alzheimers Dement (Amst), 12(1). doi: 10.1002/DAD2.12084.

Lana-Elola, E. *et al.* (2016) ‘Genetic dissection of Down syndrome-associated congenital heart defects using a new mouse mapping panel’, *eLife*, 5. doi: 10.7554/eLife.11614.

Lancaster, M. A. and Knoblich, J. A. (2014) ‘Generation of cerebral organoids from human pluripotent stem cells’, *Nature Protocols 2014 9:10*. Nature Publishing Group, 9(10), pp. 2329–2340. doi: 10.1038/nprot.2014.158.

Landes, S. D., Finan, J. M. and Turk, M. A. (2023) ‘Reporting Down syndrome on the death certificate for Alzheimer disease/unspecified dementia deaths’, *PloS one*. PLoS One, 18(2). doi: 10.1371/JOURNAL.PONE.0281763.

Lanoiselée, H. M. *et al.* (2017) ‘APP, PSEN1, and PSEN2 mutations in early-onset Alzheimer disease: A genetic screening study of familial and sporadic cases’, *PLOS Medicine*. Public Library of Science, 14(3), p. e1002270. doi: 10.1371/JOURNAL.PMED.1002270.

LaRocca, T. J. *et al.* (2021) ‘Amyloid beta acts synergistically as a pro-inflammatory cytokine’, *Neurobiology of Disease*. Academic Press, 159, p. 105493. doi: 10.1016/J.NBD.2021.105493.

Laufer, B. I. *et al.* (2019) ‘Whole genome bisulfite sequencing of Down syndrome brain reveals regional DNA hypermethylation and novel disorder insights’, *Epigenetics*. Epigenetics, 14(7), pp. 672–684. doi: 10.1080/15592294.2019.1609867.

Lee, K. J. *et al.* (2010) ‘Beta amyloid-independent role of amyloid precursor protein in generation and maintenance of dendritic spines’, *Neuroscience*. Neuroscience, 169(1), pp. 344–356. doi: 10.1016/J.NEUROSCIENCE.2010.04.078.

Lehninger, A., Nelson, D. and Cox, M. (1993) *Principles of Biochemistry*. Worth Publishers, New York. Available at: https://www.scirp.org/reference/referencespapers?referenceid=3522999 (Accessed: 31 October 2024).

LeJeune, J., Gautier, M. and Turpin, R. (1959) 'Study of somatic chromosomes from 9 mongoloid children [French]', *C.R. Hebd. Seances. Acad. Sci.*, 248, pp. 1721–1722.

Leng, F. and Edison, P. (2020) 'Neuroinflammation and microglial activation in Alzheimer disease: where do we go from here?', *Nature Reviews Neurology 2020 17:3*. Nature Publishing Group, 17(3), pp. 157–172. doi: 10.1038/s41582-020-00435-y.

Leng, K. *et al.* (2021) 'Molecular characterization of selectively vulnerable neurons in Alzheimer's disease', *Nature Neuroscience 2021 24:2*. Nature Publishing Group, 24(2), pp. 276–287. doi: 10.1038/s41593-020-00764-7.

Lenz, S. *et al.* (2013) 'Drosophila as a screening tool to study human neurodegenerative diseases', *Journal of neurochemistry*. J Neurochem, 127(4), pp. 453–460. doi: 10.1111/JNC.12446.

LeVine, H. *et al.* (2017) 'Down syndrome: Age-dependence of PiB binding in postmortem frontal cortex across the lifespan', *Neurobiology of aging*. Elsevier Inc., 54, p. 163. doi: 10.1016/J.NEUROBIOLAGING.2017.03.005.

Li, L. B. *et al.* (2012) 'Trisomy correction in Down syndrome induced pluripotent stem cells', *Cell stem cell*. Cell Stem Cell, 11(5), pp. 615–619. doi: 10.1016/J.STEM.2012.08.004.

Li, W. and Ye, Y. (2008) 'Polyubiquitin chains: functions, structures, and mechanisms', *Cellular and molecular life sciences : CMLS*. Cell Mol Life Sci, 65(15), pp. 2397–2406. doi: 10.1007/S00018-008-8090-6.

Li, X. and Wang, C. Y. (2021) 'From bulk, single-cell to spatial RNA sequencing', *International Journal of Oral Science 2021 13:1*. Nature Publishing Group, 13(1), pp. 1–6. doi: 10.1038/s41368-021-00146-0.

Li, Y. *et al.* (2003) 'Positive and negative regulation of APP amyloidogenesis by sumoylation', *Proceedings of the National Academy of Sciences of the United States of America*. National Academy of Sciences, 100(1), pp. 259–264. doi: 10.1073/PNAS.0235361100/ASSET/830337ED-AF99-49BA-A324-4E02FB8CFBA5/ASSETS/GRAPHIC/PQ0235361004.JPEG.

Li, Y. Y. *et al.* (2012) 'MiRNA-155 upregulation and complement factor H deficits in Down's syndrome', *NeuroReport*, 23(3), pp. 168–173. doi: 10.1097/WNR.0B013E32834F4EB4.

Li, Z. *et al.* (2022) 'Asynchronous excitatory neuron development in an isogenic cortical spheroid model of Down syndrome', *Frontiers in Neuroscience*. Frontiers Media S.A., 16, p. 932384. doi: 10.3389/FNINS.2022.932384/BIBTEX.

Liou, J. *et al.* (2025) 'A neuropathology case report of a woman with Down syndrome who remained cognitively stable: Implications for resilience to neuropathology', *Alzheimer's & dementia : the journal of the Alzheimer's Association*. Alzheimers Dement. doi: 10.1002/ALZ.14479.

Liu, B. *et al.* (2021) 'Deubiquitinating enzymes (DUBs): decipher underlying basis of neurodegenerative diseases', *Molecular Psychiatry 2021 27:1*. Nature Publishing Group, 27(1), pp. 259–268. doi: 10.1038/s41380-021-01233-8.

Liu, L. *et al.* (2024) 'Lecanemab and Vascular-Amyloid Deposition in Brains of People With Down Syndrome', *JAMA neurology*. JAMA Neurol, 81(10). doi: 10.1001/JAMANEUROL.2024.2579.

Lockstone, H. E. *et al.* (2007) 'Gene expression profiling in the adult Down syndrome brain', *Genomics*. Academic Press, 90(6), pp. 647–660. doi: 10.1016/J.YGENO.2007.08.005.

López Salon, M, Morelli, L, Castaño, EM, Soto, EF Pasquini, J. (2000) 'Defective ubiquitination of cerebral proteins in Alzheimer's disease', *J. Neurosci. Res.*, (62), pp. 302–310. doi: https://doi.org/10.1002/1097-4547(20001015)62:2<302::AID-JNR15>3.0.CO;2-L.

Lott, I. T. and Head, E. (2019) 'Dementia in Down syndrome: unique insights for Alzheimer disease research', *Nature Reviews Neurology*. Nature Publishing Group, pp. 135–147. doi: 10.1038/s41582-018-0132-6.

Lovero, D. *et al.* (2018) 'Characterization of Drosophila ATPsynC mutants as a new model of mitochondrial ATP synthase disorders', *PLOS ONE*. Public Library of Science, 13(8), p. e0201811. doi: 10.1371/JOURNAL.PONE.0201811.

Lowe, S. A., Hodge, J. J. L. and Usowicz, M. M. (2018a) 'A third copy of the Down syndrome cell adhesion molecule (Dscam) causes synaptic and locomotor dysfunction in Drosophila', *Neurobiology of disease*. Neurobiol Dis, 110, pp. 93–101. doi: 10.1016/J.NBD.2017.11.013.

Lowe, S. A., Hodge, J. J. L. and Usowicz, M. M. (2018b) 'A third copy of the Down syndrome cell adhesion molecule (Dscam) causes synaptic and locomotor dysfunction in Drosophila', *Neurobiology of Disease*. Academic Press Inc., 110, pp. 93–101. doi: 10.1016/j.nbd.2017.11.013.

Lowe, S. A., Usowicz, M. M. and Hodge, J. J. L. (2019) 'Neuronal overexpression of Alzheimer's disease and down's syndrome associated DYRK1A/minibrain gene alters motor decline, neurodegeneration and synaptic plasticity in Drosophila', *Neurobiology of Disease*. Academic Press Inc., 125, pp. 107–114. doi: 10.1016/j.nbd.2019.01.017.

Lu, J. *et al.* (2011) 'S100B and APP Promote a Gliocentric Shift and Impaired Neurogenesis in Down Syndrome Neural Progenitors', *PLOS ONE*. Public Library of Science, 6(7), p. e22126. doi: 10.1371/JOURNAL.PONE.0022126.

Lu, J. *et al.* (2012) 'OLIG2 over-expression impairs proliferation of human Down syndrome neural progenitors', *Human Molecular Genetics*. Oxford Academic, 21(10), pp. 2330–2340. doi: 10.1093/HMG/DDS052.

Luo, L., Tully, T. and White, K. (1992) 'Human amyloid precursor protein ameliorates behavioral deficit of flies deleted for Appl gene', *Neuron*. Neuron, 9(4), pp. 595–605. doi: 10.1016/0896-6273(92)90024-8.

Lustbader, J. W. *et al.* (2004) 'ABAD Directly Links Aβ to Mitochondrial Toxicity in Alzheimer's Disease', *Science*. American Association for the Advancement of Science, 304(5669), pp. 448–452. doi: 10.1126/SCIENCE.1091230/SUPPL_FILE/LUSTBADER.SOM.PDF.

Lv, X. *et al.* (2013) 'Exploring the differences between mouse mAβ(1-42) and human hAβ(1-42) for Alzheimer's disease related properties and neuronal cytotoxicity', *Chemical communications (Cambridge, England)*. Chem Commun (Camb), 49(52), pp. 5865–5867. doi: 10.1039/C3CC40779A.

Madabattula, S. T. *et al.* (2015) 'Quantitative Analysis of Climbing Defects in a Drosophila Model of Neurodegenerative Disorders', *Journal of Visualized Experiments : JoVE*. MyJoVE Corporation, 2015(100), p. 52741. doi: 10.3791/52741.

Madeira, F. *et al.* (2024) ‘The EMBL-EBI Job Dispatcher sequence analysis tools framework in 2024.’, *Nucleic Acids Research*. Oxford University Press, 52(W1), pp. W521–W525. doi: 10.1093/NAR/GKAE241.

Magwere, T., Chapman, T. and Partridge, L. (2004) ‘Sex Differences in the Effect of Dietary Restriction on Life Span and Mortality Rates in Female and Male Drosophila Melanogaster’, *The Journals of Gerontology: Series A*. Oxford Academic, 59(1), pp. B3–B9. doi: 10.1093/GERONA/59.1.B3.

Maia, L. F. *et al.* (2013) ‘Changes in amyloid-β and tau in the cerebrospinal fluid of transgenic mice overexpressing amyloid precursor protein’, *Science Translational Medicine*. American Association for the Advancement of Science, 5(194). doi: 10.1126/SCITRANSLMED.3006446/SUPPL_FILE/5-194RE2_SM.PDF.

Manczak, M., Calkins, M. J. and Reddy, P. H. (2011) ‘Impaired mitochondrial dynamics and abnormal interaction of amyloid beta with mitochondrial protein Drp1 in neurons from patients with Alzheimer’s disease: implications for neuronal damage’, *Human Molecular Genetics*. Oxford Academic, 20(13), pp. 2495–2509. doi: 10.1093/HMG/DDR139.

Mann, D. M. A. *et al.* (2018) ‘Patterns and severity of vascular amyloid in Alzheimer’s disease associated with duplications and missense mutations in APP gene, Down syndrome and sporadic Alzheimer’s disease’, *Acta neuropathologica*. Acta Neuropathol, 136(4), pp. 569–587. doi: 10.1007/S00401-018-1866-3.

Manzo, E. *et al.* (2019) ‘Glycolysis upregulation is neuroprotective as a compensatory mechanism in ALS’, *eLife*. Elife, 8. doi: 10.7554/ELIFE.45114.

Mao, R. *et al.* (2003) ‘Global up-regulation of chromosome 21 gene expression in the developing Down syndrome brain’, *Genomics*. Genomics, 81(5), pp. 457–467. doi: 10.1016/S0888-7543(03)00035-1.

Mao, R. *et al.* (2005) 'Primary and secondary transcriptional effects in the developing human Down syndrome brain and heart', *Genome Biology*. BioMed Central, 6(13), pp. 1–20. doi: 10.1186/GB-2005-6-13-R107/TABLES/10.

Martí, E. *et al.* (2003) 'Dyrk1A expression pattern supports specific roles of this kinase in the adult central nervous system', *Brain Research*. Elsevier, 964(2), pp. 250–263. doi: 10.1016/S0006-8993(02)04069-6.

Martín-Peña, A., Rincón-Limas, D. E. and Fernandez-Fúnez, P. (2018) 'Engineered Hsp70 chaperones prevent Aβ42-induced memory impairments in a Drosophila model of Alzheimer's disease', *Scientific Reports 2018 8:1*. Nature Publishing Group, 8(1), pp. 1–14. doi: 10.1038/s41598-018-28341-w.

Martinez De Lagran, M. *et al.* (2012) 'Dyrk1A influences neuronal morphogenesis through regulation of cytoskeletal dynamics in mammalian cortical neurons', *Cerebral cortex (New York, N.Y. : 1991)*. Cereb Cortex, 22(12), pp. 2867–2877. doi: 10.1093/CERCOR/BHR362.

Mastroeni, D. *et al.* (2017) 'Nuclear but not mitochondrial-encoded oxidative phosphorylation genes are altered in aging, mild cognitive impairment, and Alzheimer's disease', *Alzheimer's & Dementia*. John Wiley & Sons, Ltd, 13(5), pp. 510–519. doi: 10.1016/J.JALZ.2016.09.003.

Mathys, H. *et al.* (2019) 'Single-cell transcriptomic analysis of Alzheimer's disease', *Nature 2019 570:7761*. Nature Publishing Group, 570(7761), pp. 332–337. doi: 10.1038/s41586-019-1195-2.

Mathys, H. *et al.* (2024) 'Single-cell multiregion dissection of Alzheimer's disease', *Nature 2024 632:8026*. Nature Publishing Group, 632(8026), pp. 858–868. doi: 10.1038/s41586-024-07606-7.

Matsumoto, K. *et al.* (2006) ‘Overexpression of amyloid precursor protein induces susceptibility to oxidative stress in human neuroblastoma SH-SY5Y cells’, *Journal of Neural Transmission*. Springer, 113(2), pp. 125–135. doi: 10.1007/S00702-005-0318-0/METRICS.

Mawuenyega, K. G. *et al.* (2010) ‘Decreased clearance of CNS beta-amyloid in Alzheimer’s disease’, *Science (New York, N.Y.)*. Science, 330(6012), p. 1774. doi: 10.1126/SCIENCE.1197623.

McCarron, M. *et al.* (2017) ‘A prospective 20-year longitudinal follow-up of dementia in persons with Down syndrome’, *Journal of Intellectual Disability Research*. John Wiley & Sons, Ltd, 61(9), pp. 843–852. doi: 10.1111/JIR.12390.

Meijer, L., Chrétien, E. and Ravel, D. (2024) ‘Leucettinib-21, a DYRK1A Kinase Inhibitor as Clinical Drug Candidate for Alzheimer’s Disease and Down Syndrome’, *Journal of Alzheimer’s disease : JAD*. J Alzheimers Dis, 101(s1), pp. S95–S113. doi: 10.3233/JAD-240078.

Mertens, J. *et al.* (2018) ‘Aging in a Dish: iPSC-Derived and Directly Induced Neurons for Studying Brain Aging and Age-Related Neurodegenerative Diseases’, *Annual review of genetics*. Annu Rev Genet, 52, pp. 271–293. doi: 10.1146/ANNUREV-GENET-120417-031534.

Meuwese-Jongejeugd, A. *et al.* (2006) ‘Prevalence of hearing loss in 1598 adults with an intellectual disability: cross-sectional population based study’, *International journal of audiology*. Int J Audiol, 45(11), pp. 660–669. doi: 10.1080/14992020600920812.

Mijalkov, M. *et al.* (2021) ‘Dendritic spines are lost in clusters in Alzheimer’s disease’, *Scientific Reports 2021 11:1*. Nature Publishing Group, 11(1), pp. 1–11. doi: 10.1038/s41598-021-91726-x.

Miyoshi, E. *et al.* (2024) ‘Spatial and single-nucleus transcriptomic analysis of genetic and sporadic forms of Alzheimer’s disease’, *Nature Genetics 2024 56:12*. Nature Publishing Group, 56(12), pp. 2704–2717. doi: 10.1038/s41588-024-01961-x.

Mok, K. Y. *et al.* (2014) ‘Polymorphisms in BACE2 may affect the age of onset Alzheimer’s dementia in Down syndrome’, *Neurobiology of aging*. Neurobiol Aging, 35(6), pp. 1513.e1-1513.e5. doi: 10.1016/J.NEUROBIOLAGING.2013.12.022.

Moreno-Jiménez, E. P. *et al.* (2019) ‘Adult hippocampal neurogenesis is abundant in neurologically healthy subjects and drops sharply in patients with Alzheimer’s disease’, *Nature Medicine 2019 25:4*. Nature Publishing Group, 25(4), pp. 554–560. doi: 10.1038/s41591-019-0375-9.

Morris, J. K. and Alberman, E. (2009) ‘Trends in Down’s syndrome live births and antenatal diagnoses in England and Wales from 1989 to 2008: Analysis of data from the National Down Syndrome Cytogenetic Register’, *BMJ (Online)*. British Medical Journal Publishing Group, 339(7731), p. 1188. doi: 10.1136/bmj.b3794.

Motte, J. and Williams, R. S. (1989) ‘Age-related changes in the density and morphology of plaques and neurofibrillary tangles in Down syndrome brain’, *Acta neuropathologica*. Acta Neuropathol, 77(5), pp. 535–546. doi: 10.1007/BF00687256.

Mucke, L. *et al.* (2000) ‘High-level neuronal expression of abeta 1-42 in wild-type human amyloid protein precursor transgenic mice: synaptotoxicity without plaque formation’, *The Journal of neuroscience : the official journal of the Society for Neuroscience*. J Neurosci, 20(11), pp. 4050–4058. doi: 10.1523/JNEUROSCI.20-11-04050.2000.

Mullan, M. *et al.* (1992) ‘A pathogenic mutation for probable Alzheimer’s disease in the APP gene at the N-terminus of beta-amyloid’, *Nature genetics*. Nat Genet, 1(5), pp. 345–347. doi: 10.1038/NG0892-345.

Mumford, P. *et al.* (2022) ‘Genetic Mapping of APP and Amyloid-β Biology Modulation by Trisomy 21’, *Journal of Neuroscience*. Society for Neuroscience, 42(33), pp. 6453–6468. doi: 10.1523/JNEUROSCI.0521-22.2022.

Murrell, J. *et al.* (1991) ‘A mutation in the amyloid precursor protein associated with hereditary Alzheimer’s disease’, *Science (New York, N.Y.)*. Science, 254(5028), pp. 97–99. doi: 10.1126/SCIENCE.1925564.

Mutton, D., Alberman, E. and Hook, E. B. (1996) ‘Cytogenetic and epidemiological findings in Down syndrome, England and Wales 1989 to 1993. National Down Syndrome Cytogenetic Register and the Association of Clinical Cytogeneticists’, *Journal of medical genetics*. J Med Genet, 33(5), pp. 387–394. doi: 10.1136/JMG.33.5.387.

Nerelius, C. *et al.* (2009) ‘α-Helix targeting reduces amyloid-β peptide toxicity’, *Proceedings of the National Academy of Sciences of the United States of America*. National Academy of Sciences, 106(23), pp. 9191–9196. doi: 10.1073/PNAS.0810364106/SUPPL_FILE/SM1.AVI.

Niccoli, T. *et al.* (2016) ‘Increased Glucose Transport into Neurons Rescues Aβ Toxicity in Drosophila’, *Current biology : CB*. Curr Biol, 26(17), pp. 2291–2300. doi: 10.1016/J.CUB.2016.07.017.

Nichols, E. *et al.* (2022) ‘Estimation of the global prevalence of dementia in 2019 and forecasted prevalence in 2050: an analysis for the Global Burden of Disease Study 2019’, *The Lancet. Public health*. Lancet Public Health, 7(2), pp. e105–e125. doi: 10.1016/S2468-2667(21)00249-8.

Nordquist, S. K., Smith, S. R. and Pierce, J. T. (2018) ‘Systematic functional characterization of human 21st chromosome orthologs in Caenorhabditis elegans’, *G3: Genes, Genomes, Genetics*. Genetics Society of America, 8(3), pp. 967–979. doi: 10.1534/G3.118.200019/-/DC1.

O'Doherty, A. *et al.* (2005) 'Genetics: An aneuploid mouse strain carrying human chromosome 21 with Down syndrome phenotypes', *Science*, 309(5743), pp. 2033–2037. doi: 10.1126/science.1114535.

Oakley, H. *et al.* (2006) 'Intraneuronal beta-amyloid aggregates, neurodegeneration, and neuron loss in transgenic mice with five familial Alzheimer's disease mutations: potential factors in amyloid plaque formation', *The Journal of neuroscience : the official journal of the Society for Neuroscience*. J Neurosci, 26(40), pp. 10129–10140. doi: 10.1523/JNEUROSCI.1202-06.2006.

Ohtake, F. *et al.* (2018) 'K63 ubiquitylation triggers proteasomal degradation by seeding branched ubiquitin chains', *Proceedings of the National Academy of Sciences of the United States of America*. National Academy of Sciences, 115(7), pp. E1401–E1408. doi: 10.1073/PNAS.1716673115/SUPPL_FILE/PNAS.1716673115.SD02.XLSX.

Olabarria, M. *et al.* (2010) 'Concomitant astroglial atrophy and astrogliosis in a triple transgenic animal model of Alzheimer's disease', *Glia*. Glia, 58(7), pp. 831–838. doi: 10.1002/GLIA.20967.

Olmos-Serrano, J. L. *et al.* (2016) 'Down Syndrome Developmental Brain Transcriptome Reveals Defective Oligodendrocyte Differentiation and Myelination', *Neuron*. Neuron, 89(6), pp. 1208–1222. doi: 10.1016/J.NEURON.2016.01.042.

Ono, K. and Watanabe-Nakayama, T. (2021) 'Aggregation and structure of amyloid β-protein', *Neurochemistry International*. Pergamon, 151, p. 105208. doi: 10.1016/J.NEUINT.2021.105208.

Osterwalder, T. *et al.* (2001) 'A conditional tissue-specific transgene expression system using inducible GAL4', *Proceedings of the National Academy of Sciences*. National Academy of Sciences, 98(22), pp. 12596–12601. doi: 10.1073/PNAS.221303298.

Ovchinnikov, D. A. *et al.* (2018) 'The Impact of APP on Alzheimer-like Pathogenesis and Gene Expression in Down Syndrome iPSC-Derived Neurons', *Stem cell reports*. Stem Cell Reports, 11(1), pp. 32–42. doi: 10.1016/J.STEMCR.2018.05.004.

Palmer, C. R. *et al.* (2021) 'Altered cell and RNA isoform diversity in aging down syndrome brains', *Proceedings of the National Academy of Sciences of the United States of America*. National Academy of Sciences, 118(47), p. 2114326118. doi: 10.1073/PNAS.2114326118/-/DCSUPPLEMENTAL.

Palop, J. J. and Mucke, L. (2010) 'Amyloid-β Induced Neuronal Dysfunction in Alzheimer's Disease: From Synapses toward Neural Networks', *Nature neuroscience*. NIH Public Access, 13(7), p. 812. doi: 10.1038/NN.2583.

Pang, Z. P. *et al.* (2011) 'Induction of human neuronal cells by defined transcription factors', *Nature*. Nature, 476(7359), pp. 220–223. doi: 10.1038/NATURE10202.

Papavassiliou, P. *et al.* (2015) 'Mosaicism for trisomy 21: A review', *American Journal of Medical Genetics Part A*. John Wiley & Sons, Ltd, 167(1), pp. 26–39. doi: 10.1002/AJMG.A.36861.

Park, J. *et al.* (2010) 'Dyrk1A Phosphorylates p53 and Inhibits Proliferation of Embryonic Neuronal Cells', *Journal of Biological Chemistry*. Elsevier, 285(41), pp. 31895–31906. doi: 10.1074/JBC.M110.147520.

Patel, A. *et al.* (2015) 'RCAN1 links impaired neurotrophin trafficking to aberrant development of the sympathetic nervous system in Down syndrome', *Nature Communications 2015 6:1*. Nature Publishing Group, 6(1), pp. 1–17. doi: 10.1038/ncomms10119.

Pelleri, M. C. *et al.* (2019) 'Partial trisomy 21 map: Ten cases further supporting the highly restricted Down syndrome critical region (HR-DSCR) on human chromosome 21', *Molecular Genetics & Genomic Medicine*. Wiley-Blackwell, 7(8), p. e797. doi: 10.1002/MGG3.797.

Pelleri, M. C. *et al.* (2022) 'Partial trisomy 21 with or without highly restricted Down syndrome critical region (HR-DSCR): report of two new cases and reanalysis of the genotype–phenotype association', *BMC Medical Genomics*. BioMed Central Ltd, 15(1), pp. 1–12. doi: 10.1186/S12920-022-01422-6/FIGURES/4.

Piccoli, C. *et al.* (2013) 'Chronic pro-oxidative state and mitochondrial dysfunctions are more pronounced in fibroblasts from Down syndrome foeti with congenital heart defects', *Human molecular genetics*. Hum Mol Genet, 22(6), pp. 1218–1232. doi: 10.1093/HMG/DDS529.

Pickett, E. K. *et al.* (2018) 'Region-specific depletion of synaptic mitochondria in the brains of patients with Alzheimer's disease', *Acta Neuropathologica*. Springer Verlag, 136(5), p. 747. doi: 10.1007/S00401-018-1903-2.

Pinter, J. D. *et al.* (2001) 'Neuroanatomy of Down's syndrome: a high-resolution MRI study', *The American journal of psychiatry*. Am J Psychiatry, 158(10), pp. 1659–1665. doi: 10.1176/APPI.AJP.158.10.1659.

Pinto, B. *et al.* (2020) 'Rescuing Over-activated Microglia Restores Cognitive Performance in Juvenile Animals of the Dp(16) Mouse Model of Down Syndrome', *Neuron*. Cell Press, 108(5), pp. 887-904.e12. doi: 10.1016/J.NEURON.2020.09.010.

Piper, M. D. W. and Partridge, L. (2016) ‘Protocols to study aging in drosophila’, *Methods in Molecular Biology*. Humana Press Inc., 1478, pp. 291–302. doi: 10.1007/978-1-4939-6371-3_18/FIGURES/1.

Piper, M. D. W. and Partridge, L. (2018) ‘Drosophila as a model for ageing.’, *Biochimica et biophysica acta. Molecular basis of disease*, 1864(9 Pt A), pp. 2707–2717. doi: 10.1016/j.bbadis.2017.09.016.

Pizzano, S. *et al.* (2023) ‘The Drosophila homolog of APP promotes Dscam expression to drive axon terminal growth, revealing interaction between Down syndrome genes’, *DMM Disease Models and Mechanisms*. Company of Biologists Ltd, 16(9). doi: 10.1242/DMM.049725/328130.

Pooler, A. M. *et al.* (2015) ‘Amyloid accelerates tau propagation and toxicity in a model of early Alzheimer’s disease’, *Acta neuropathologica communications*. Acta Neuropathol Commun, 3, p. 14. doi: 10.1186/S40478-015-0199-X.

Potter, H., Granic, A. and Caneus, J. (2016) ‘Role of Trisomy 21 Mosaicism in Sporadic and Familial Alzheimer’s Disease’, *Current Alzheimer research*. Bentham Science Publishers Ltd., 13(1), p. 7. doi: 10.2174/1567205013011512071006 16.

Prandini, P. *et al.* (2007) ‘Natural Gene-Expression Variation in Down Syndrome Modulates the Outcome of Gene-Dosage Imbalance’, *American Journal of Human Genetics*. Elsevier, 81(2), p. 252. doi: 10.1086/519248.

Prasher, V. P. *et al.* (1998) ‘Molecular mapping of Alzheimer-type dementia in Down’s syndrome.’, *Annals of neurology*, 43(3), pp. 380–383. doi: 10.1002/ana.410430316.

Prüßing, K., Voigt, A. and Schulz, J. B. (2013) ‘Drosophila melanogaster as a model organism for Alzheimer’s disease’, *Molecular neurodegeneration*. Mol Neurodegener, 8(1). doi: 10.1186/1750-1326-8-35.

Qiu, J. J. *et al.* (2023) ‘Single-cell RNA sequencing of neural stem cells derived from human trisomic iPSCs reveals the abnormalities during neural differentiation of Down syndrome’, *Frontiers in molecular neuroscience*. Front Mol Neurosci, 16. doi: 10.3389/FNMOL.2023.1137123.

Qiu, W. Q. *et al.* (1998) ‘Insulin-degrading Enzyme Regulates Extracellular Levels of Amyloid β-Protein by Degradation’, *Journal of Biological Chemistry*. Elsevier, 273(49), pp. 32730–32738. doi: 10.1074/JBC.273.49.32730.

Quiroz, Y. T. *et al.* (2018) ‘Association Between Amyloid and Tau Accumulation in Young Adults With Autosomal Dominant Alzheimer Disease’, *JAMA neurology*. JAMA Neurol, 75(5), pp. 548–556. doi: 10.1001/JAMANEUROL.2017.4907.

Raser, J. M. and O’Shea, E. K. (2005) ‘Molecular biology - Noise in gene expression: Origins, consequences, and control’, *Science*. American Association for the Advancement of Science, 309(5743), pp. 2010–2013. doi: 10.1126/SCIENCE.1105891/SUPPL_FILE/RASER_SOM.PDF.

Raskin, J. *et al.* (2015) ‘Neurobiology of Alzheimer’s Disease: Integrated Molecular, Physiological, Anatomical, Biomarker, and Cognitive Dimensions’, *Current Alzheimer Research*. Bentham Science Publishers Ltd., 12(8), p. 712. doi: 10.2174/1567205012666150701103107.

Rastogi, M. *et al.* (2024) ‘Integrative multi-omic analysis reveals conserved cell-projection deficits in human Down syndrome brains’, *Neuron*. Cell Press. doi: 10.1016/J.NEURON.2024.05.002.

Ray, A., Speese, S. D. and Logan, M. A. (2017) ‘Glial Draper Rescues Aβ Toxicity in a Drosophila Model of Alzheimer’s Disease’, *The Journal of neuroscience : the official journal of the Society for Neuroscience*. J Neurosci, 37(49), pp. 11881–11893. doi: 10.1523/JNEUROSCI.0862-17.2017.

Real, R. *et al.* (2018) ‘In vivo modeling of human neuron dynamics and Down syndrome’, *Science (New York, N.Y.)*. Science, 362(6416). doi: 10.1126/SCIENCE.AAU1810.

Reeves, B. C. *et al.* (2020) ‘Glymphatic System Impairment in Alzheimer’s Disease and Idiopathic Normal Pressure Hydrocephalus’, *Trends in molecular medicine*. Trends Mol Med, 26(3), pp. 285–295. doi: 10.1016/J.MOLMED.2019.11.008.

Reeves, R. H. *et al.* (1995) ‘A mouse model for Down syndrome exhibits learning and behaviour deficits’, *Nature genetics*. Nat Genet, 11(2), pp. 177–184. doi: 10.1038/NG1095-177.

Regan, J. C. *et al.* (2016) ‘Sex difference in pathology of the ageing gut mediates the greater response of female lifespan to dietary restriction’, *eLife*. eLife Sciences Publications Ltd, 5(FEBRUARY2016). doi: 10.7554/ELIFE.10956.

Rhein, V. *et al.* (2009) ‘Amyloid-beta leads to impaired cellular respiration, energy production and mitochondrial electron chain complex activities in human neuroblastoma cells’, *Cellular and molecular neurobiology*. Cell Mol Neurobiol, 29(6–7), pp. 1063–1071. doi: 10.1007/S10571-009-9398-Y.

Rice, H. C. *et al.* (2019) ‘Secreted amyloid-β precursor protein functions as a GABABR1a ligand to modulate synaptic transmission’, *Science (New York, N.Y.)*. Science, 363(6423). doi: 10.1126/SCIENCE.AAO4827.

Rickle, A. *et al.* (2004) ‘Akt activity in Alzheimer’s disease and other neurodegenerative disorders’, *Neuroreport*. Neuroreport, 15(6), pp. 955–959. doi: 10.1097/00001756-200404290-00005.

Ries, M. and Sastre, M. (2016) ‘Mechanisms of Aβ clearance and degradation by glial cells’, *Frontiers in Aging Neuroscience*. Frontiers Media S.A., 8(JUN), p. 210313. doi: 10.3389/FNAGI.2016.00160/BIBTEX.

Ringman, J. M. *et al.* (2008) 'Mosaicism for trisomy 21 in a patient with young-onset dementia: a case report and brief literature review', *Archives of neurology*. Arch Neurol, 65(3), pp. 412–415. doi: 10.1001/ARCHNEUR.65.3.412.

Ripoli, C. *et al.* (2014) 'Intracellular accumulation of amyloid-β (Aβ) protein plays a major role in Aβ-induced alterations of glutamatergic synaptic transmission and plasticity', *The Journal of neuroscience : the official journal of the Society for Neuroscience*. J Neurosci, 34(38), pp. 12893–12903. doi: 10.1523/JNEUROSCI.1201-14.2014.

Rizzuto, R. *et al.* (2012) 'Mitochondria as sensors and regulators of calcium signalling', *Nature reviews. Molecular cell biology*. Nat Rev Mol Cell Biol, 13(9), pp. 566–578. doi: 10.1038/NRM3412.

Robinow, S. and White, K. (1988) 'The locus elav of Drosophila melanogaster is expressed in neurons at all developmental stages', *Developmental biology*. Dev Biol, 126(2), pp. 294–303. doi: 10.1016/0012-1606(88)90139-X.

Rogers, I. *et al.* (2012) 'Ageing Increases Vulnerability to Aβ42 Toxicity in Drosophila', *PLOS ONE*. Public Library of Science, 7(7), p. e40569. doi: 10.1371/JOURNAL.PONE.0040569.

Rørth, P. (1996) 'A modular misexpression screen in Drosophila detecting tissue-specific phenotypes', *Proceedings of the National Academy of Sciences of the United States of America*. Proc Natl Acad Sci U S A, 93(22), pp. 12418–12422. doi: 10.1073/PNAS.93.22.12418.

Rosen, D. R. *et al.* (1989) 'A Drosophila gene encoding a protein resembling the human beta-amyloid protein precursor', *Proceedings of the National Academy of Sciences of the United States of America*. Proc Natl Acad Sci U S A, 86(7), pp. 2478–2482. doi: 10.1073/PNAS.86.7.2478.

Rost, B. (1999) ‘Twilight zone of protein sequence alignments’, *Protein Engineering, Design and Selection*. Oxford Academic, 12(2), pp. 85–94. doi: 10.1093/PROTEIN/12.2.85.

Rovelet-Lecrux, A. *et al.* (2006) ‘APP locus duplication causes autosomal dominant early-onset Alzheimer disease with cerebral amyloid angiopathy.’, *Nature genetics*, 38(1), pp. 24–26. doi: 10.1038/ng1718.

Russo, M. L., Sousa, A. M. M. and Bhattacharyya, A. (2024) ‘Consequences of trisomy 21 for brain development in Down syndrome’, *Nature Reviews Neuroscience 2024 25:11*. Nature Publishing Group, 25(11), pp. 740–755. doi: 10.1038/s41583-024-00866-2.

Ryoo, S. R. *et al.* (2008) ‘Dual-specificity tyrosine(Y)-phosphorylation regulated kinase 1A-mediated phosphorylation of amyloid precursor protein: Evidence for a functional link between Down syndrome and Alzheimer’s disease’, *Journal of Neurochemistry*, 104(5), pp. 1333–1344. doi: 10.1111/J.1471-4159.2007.05075.X.

Ryu, Y. S. *et al.* (2010) ‘Dyrk1A-mediated phosphorylation of Presenilin 1: A functional link between Down syndrome and Alzheimer’s disease’, *Journal of Neurochemistry*, 115(3), pp. 574–584. doi: 10.1111/J.1471-4159.2010.06769.X.

Şahin, A. *et al.* (2017) ‘Human SOD1 ALS Mutations in a Drosophila Knock-In Model Cause Severe Phenotypes and Reveal Dosage-Sensitive Gain- and Loss-of-Function Components’, *Genetics*. Genetics, 205(2), pp. 707–723. doi: 10.1534/GENETICS.116.190850.

Saito, T. *et al.* (2014) ‘Single App knock-in mouse models of Alzheimer’s disease’, *Nature neuroscience*. Nat Neurosci, 17(5), pp. 661–663. doi: 10.1038/NN.3697.

Salemi, M. *et al.* (2013) ‘Pericentrin expression in Down’s syndrome’, *Neurological sciences : official journal of the Italian Neurological Society and of the Italian Society of Clinical Neurophysiology*. Neurol Sci, 34(11), pp. 2023–2025. doi: 10.1007/S10072-013-1529-Z.

Salemi, M. *et al.* (2021) ‘Role of long non-coding RNAs in Down syndrome patients: a transcriptome analysis study’, *Human cell*. Hum Cell, 34(6), pp. 1662–1670. doi: 10.1007/S13577-021-00602-3.

Sasaguri, H. *et al.* (2017) ‘APP mouse models for Alzheimer’s disease preclinical studies’, *The EMBO Journal*. Nature Publishing Group, 36(17), p. 2473. doi: 10.15252/EMBJ.201797397.

Savva, G. M. *et al.* (2006) ‘Maternal age-specific fetal loss rates in Down syndrome pregnancies’, *Prenatal Diagnosis*. Prenat Diagn, 26(6), pp. 499–504. doi: 10.1002/pd.1443.

Sawa, M. *et al.* (2021) ‘Impact of increased APP gene dose in Down syndrome and the Dp16 mouse model’, *Alzheimer’s & dementia : the journal of the Alzheimer’s Association*. Alzheimers Dement. doi: 10.1002/ALZ.12463.

Sawyer, E. M. *et al.* (2017) ‘Testis-specific ATP synthase peripheral stalk subunits required for tissue-specific mitochondrial morphogenesis in Drosophila’, *BMC Cell Biology*. BioMed Central Ltd., 18(1), pp. 1–15. doi: 10.1186/S12860-017-0132-1/FIGURES/7.

Schellenberg, G. D. *et al.* (1991) ‘Linkage analysis of familial Alzheimer disease, using chromosome 21 markers’, *American Journal of Human Genetics*. University of Chicago Press, 48(3), pp. 563–583.

Schelski, M. and Bradke, F. (2017) ‘Neuronal polarization: From spatiotemporal signaling to cytoskeletal dynamics’, *Molecular and Cellular Neuroscience*. Academic Press, 84, pp. 11–28. doi: 10.1016/J.MCN.2017.03.008.

Schlegel, P. *et al.* (2024) ‘Whole-brain annotation and multi-connectome cell typing of Drosophila’, *Nature 2024 634:8032*. Nature Publishing Group, 634(8032), pp. 139–152. doi: 10.1038/s41586-024-07686-5.

Schukken, K. M. and Sheltzer, J. M. (2022) ‘Extensive protein dosage compensation in aneuploid human cancers’, *Genome research*. NLM (Medline), 32(7), pp. 1254–1270. doi: 10.1101/GR.276378.121/-/DC1.

Schupf, N. *et al.* (1997) ‘Early menopause in women with Down’s syndrome’, *Journal of intellectual disability research : JIDR*. J Intellect Disabil Res, 41 (Pt 3)(3), pp. 264–267. doi: 10.1111/J.1365-2788.1997.TB00706.X.

Seol, S., Kwon, J. and Kang, H. J. (2023) ‘Cell type characterization of spatiotemporal gene co-expression modules in Down syndrome brain’, *iScience*. Elsevier, 26(1), p. 105884. doi: 10.1016/J.ISCI.2022.105884.

Shah, S. I. *et al.* (2019) ‘Mitochondrial fragmentation and network architecture in degenerative diseases’, *PLOS ONE*. Public Library of Science, 14(9), p. e0223014. doi: 10.1371/JOURNAL.PONE.0223014.

Shaposhnikov, M. *et al.* (2018) ‘Overexpression of CBS and CSE genes affects lifespan, stress resistance and locomotor activity in Drosophila melanogaster’, *Aging*. Aging (Albany NY), 10(11), pp. 3260–3272. doi: 10.18632/AGING.101630.

Sharma, A. *et al.* (2020) ‘Common genetic signatures of Alzheimer’s disease in Down Syndrome’, *F1000Research*. F1000Res, 9, p. 1299. doi: 10.12688/F1000RESEARCH.27096.2.

Shi, J. *et al.* (2015) 'Deubiquitinase USP47/UBP64E Regulates β-Catenin Ubiquitination and Degradation and Plays a Positive Role in Wnt Signaling', *Molecular and cellular biology*. Mol Cell Biol, 35(19), pp. 3301–3311. doi: 10.1128/MCB.00373-15.

Shi, W. L. *et al.* (2016) 'Integrated miRNA and mRNA expression profiling in fetal hippocampus with Down syndrome', *Journal of biomedical science*. J Biomed Sci, 23(1). doi: 10.1186/S12929-016-0265-0.

Shi, Y. *et al.* (2012) 'A human stem cell model of early Alzheimer's disease pathology in Down syndrome', *Science translational medicine*. Sci Transl Med, 4(124). doi: 10.1126/SCITRANSLMED.3003771.

Shimizu, E. *et al.* (2024) 'Symptoms and age of prodromal Alzheimer's disease in Down syndrome: a systematic review and meta-analysis', *Neurological Sciences*. Springer-Verlag Italia s.r.l., 45(6), pp. 2445–2460. doi: 10.1007/S10072-023-07292-9/FIGURES/3.

Sierksma, A. *et al.* (2020) 'Novel Alzheimer risk genes determine the microglia response to amyloid-β but not to TAU pathology', *EMBO Molecular Medicine*. Nature Publishing Group, 12(3). doi: 10.15252/EMMM.201910606.

Silverman, W. *et al.* (2023) 'Individualized estimated years from onset of Alzheimer's disease– related decline for adults with Down syndrome', *Alzheimer's & Dementia : Diagnosis, Assessment & Disease Monitoring*. John Wiley and Sons Inc, 15(2), p. e12444. doi: 10.1002/DAD2.12444.

Slanzi, A. *et al.* (2020) 'In vitro Models of Neurodegenerative Diseases', *Frontiers in Cell and Developmental Biology*. Frontiers Media S.A., 8, p. 534138. doi: 10.3389/FCELL.2020.00328/BIBTEX.

Sleegers, K. *et al.* (2006) ‘APP duplication is sufficient to cause early onset Alzheimer’s dementia with cerebral amyloid angiopathy.’, *Brain : a journal of neurology*, 129(Pt 11), pp. 2977–2983. doi: 10.1093/brain/awl203.

Söderberg, L. *et al.* (2024) ‘Amyloid-beta antibody binding to cerebral amyloid angiopathy fibrils and risk for amyloid-related imaging abnormalities’, *Scientific Reports 2024 14:1*. Nature Publishing Group, 14(1), pp. 1–15. doi: 10.1038/s41598-024-61691-2.

Sofola, O. *et al.* (2010) ‘Inhibition of GSK-3 Ameliorates Aβ Pathology in an Adult-Onset Drosophila Model of Alzheimer’s Disease’, *PLOS Genetics*. Public Library of Science, 6(9), p. e1001087. doi: 10.1371/JOURNAL.PGEN.1001087.

Song, Y. *et al.* (2017) ‘Single-Cell Alternative Splicing Analysis with Expedition Reveals Splicing Dynamics during Neuron Differentiation’, *Molecular cell*. Mol Cell, 67(1), pp. 148-161.e5. doi: 10.1016/J.MOLCEL.2017.06.003.

Spierer, A. N. *et al.* (2021) ‘FreeClimber: Automated quantification of climbing performance in Drosophila’, *Journal of Experimental Biology*. Company of Biologists Ltd, 224(2). doi: 10.1242/JEB.229377/267839/AM/FREECLIMBER-AUTOMATED-QUANTIFICATION-OF-CLIMBING.

Startin, C. M. *et al.* (2019) ‘Plasma biomarkers for amyloid, tau, and cytokines in Down syndrome and sporadic Alzheimer’s disease’, *Alzheimer’s Research and Therapy*. BioMed Central Ltd., 11(1). doi: 10.1186/s13195-019-0477-0.

Sullivan, S. E. and Young-Pearse, T. L. (2017) ‘Induced pluripotent stem cells as a discovery tool for Alzheimer’s disease’, *Brain research*. Brain Res, 1656, pp. 98–106. doi: 10.1016/J.BRAINRES.2015.10.005.

Sun, X. *et al.* (2011) 'Regulator of Calcineurin 1 (RCAN1) Facilitates Neuronal Apoptosis through Caspase-3 Activation', *Journal of Biological Chemistry*. Elsevier, 286(11), pp. 9049–9062. doi: 10.1074/JBC.M110.177519.

Sun, X. H. *et al.* (2019) 'MiR-155 mediates inflammatory injury of hippocampal neuronal cells via the activation of microglia', *Molecular Medicine Reports*.

Spandidos Publications, 19(4), pp. 2627–2635. doi: 10.3892/MMR.2019.9917/HTML.

Sun, X. Y. *et al.* (2022) 'Generation of Vascularized Brain Organoids to Study Neurovascular Interactions', *eLife*. eLife Sciences Publications Ltd, 11. doi: 10.7554/ELIFE.76707.

Sweeney, M. D., Sagare, A. P. and Zlokovic, B. V. (2018) 'Blood-brain barrier breakdown in Alzheimer disease and other neurodegenerative disorders', *Nature reviews. Neurology*. Nat Rev Neurol, 14(3), pp. 133–150. doi: 10.1038/NRNEUROL.2017.188.

Swerdlow, R. H., Burns, J. M. and Khan, S. M. (2014) 'The Alzheimer's disease mitochondrial cascade hypothesis: Progress and perspectives', *Biochimica et Biophysica Acta (BBA) - Molecular Basis of Disease*. Elsevier, 1842(8), pp. 1219–1231. doi: 10.1016/J.BBADIS.2013.09.010.

Swerdlow, R. H. and Khan, S. M. (2004) 'A "mitochondrial cascade hypothesis" for sporadic Alzheimer's disease', *Medical Hypotheses*. Churchill Livingstone, 63(1), pp. 8–20. doi: 10.1016/j.mehy.2003.12.045.

Sziraki, A. *et al.* (2023) 'A global view of aging and Alzheimer's pathogenesis-associated cell population dynamics and molecular signatures in human and mouse brains', *Nature genetics*. Nat Genet, 55(12), pp. 2104–2116. doi: 10.1038/S41588-023-01572-Y.

Tallino, S. *et al.* (2022) ‘Temporal and brain region-specific elevations of soluble Amyloid-β40-42 in the Ts65Dn mouse model of Down syndrome and Alzheimer’s disease’, *Aging cell*. Aging Cell, 21(4). doi: 10.1111/ACEL.13590.

Tan, F. H. P. *et al.* (2023) ‘Behavioural Effects and RNA-seq Analysis of Aβ42-Mediated Toxicity in a Drosophila Alzheimer’s Disease Model’, *Molecular Neurobiology*. Springer, 60(8), pp. 4716–4730. doi: 10.1007/S12035-023-03368-X/FIGURES/6.

Tan, K. L. *et al.* (2023) ‘Mitochondrial Dysfunction in Down Syndrome: From Pathology to Therapy’, *Neuroscience*. Elsevier Ltd, 511, pp. 1–12. doi: 10.1016/J.NEUROSCIENCE.2022.12.003/ASSET/3862D49F-0693-41B6-904E-1473627F0625/MAIN.ASSETS/GR3.SML.

Tan, L. *et al.* (2008) ‘The Toll-->NFkappaB signaling pathway mediates the neuropathological effects of the human Alzheimer’s Abeta42 polypeptide in Drosophila’, *PloS one*. PLoS One, 3(12). doi: 10.1371/JOURNAL.PONE.0003966.

Tcw, J. and Goate, A. M. (2017) ‘Genetics of β-Amyloid Precursor Protein in Alzheimer’s Disease’, *Cold Spring Harbor Perspectives in Medicine*, 7(6), p. a024539. doi: 10.1101/CSHPERSPECT.A024539.

Thibaudeau, T. A., Anderson, R. T. and Smith, D. M. (2018) ‘A common mechanism of proteasome impairment by neurodegenerative disease-associated oligomers’, *Nature Communications 2018 9:1*. Nature Publishing Group, 9(1), pp. 1–14. doi: 10.1038/s41467-018-03509-0.

de Toma, I., Sierra, C. and Dierssen, M. (2021) ‘Meta-analysis of transcriptomic data reveals clusters of consistently deregulated gene and disease ontologies in Down syndrome’, *PLOS Computational Biology*. Public Library of Science, 17(9), p. e1009317. doi: 10.1371/JOURNAL.PCBI.1009317.

Tosh, J. L. *et al.* (2021) 'Genetic dissection of down syndrome-associated alterations in APP/amyloid-β biology using mouse models', *Scientific Reports*. Nature Research, 11(1). doi: 10.1038/s41598-021-85062-3.

Troutwine, B. R. *et al.* (2022) 'Mitochondrial Function and Aβ in Alzheimer's Disease Postmortem Brain', *Neurobiology of disease*. Academic Press Inc., 171, p. 105781. doi: 10.1016/J.NBD.2022.105781.

Ugur, B., Chen, K. and Bellen, H. J. (2016) 'Drosophila tools and assays for the study of human diseases', *DMM Disease Models and Mechanisms*. Company of Biologists Ltd, 9(3), pp. 235–244. doi: 10.1242/DMM.023762.

Utagawa, E. C. *et al.* (2022) 'Neurogenesis and neuronal differentiation in the postnatal frontal cortex in Down syndrome', *Acta Neuropathologica Communications*. BioMed Central Ltd, 10(1), pp. 1–27. doi: 10.1186/S40478-022-01385-W/FIGURES/10.

Valenti, D. *et al.* (2010a) 'Impairment of F1F0-ATPase, adenine nucleotide translocator and adenylate kinase causes mitochondrial energy deficit in human skin fibroblasts with chromosome 21 trisomy', *The Biochemical journal*. Biochem J, 431(2), pp. 299–310. doi: 10.1042/BJ20100581.

Valenti, D. *et al.* (2010b) 'Impairment of F1F0-ATPase, adenine nucleotide translocator and adenylate kinase causes mitochondrial energy deficit in human skin fibroblasts with chromosome 21 trisomy', *Biochemical Journal*. Portland Press, 431(2), pp. 299–310. doi: 10.1042/BJ20100581.

Valero, R. *et al.* (2001) 'Characterization of alternatively spliced products and tissue-specific isoforms of USP28 and USP25', *Genome biology*. Genome Biol, 2(10). doi: 10.1186/GB-2001-2-10-RESEARCH0043.

Vanleeuwen, J. E. and Penzes, P. (2012) ‘Long-term perturbation of spine plasticity results in distinct impairments of cognitive function’, *Journal of neurochemistry*. J Neurochem, 123(5), pp. 781–789. doi: 10.1111/J.1471-4159.2012.07899.X.

Veitia, R. A. (2003) ‘Nonlinear effects in macromolecular assembly and dosage sensitivity’, *Journal of Theoretical Biology*. Academic Press, 220(1), pp. 19–25. doi: 10.1006/jtbi.2003.3105.

Veitia, R. A. and Birchler, J. A. (2015) ‘Models of buffering of dosage imbalances in protein complexes’, *Biology direct*. Biol Direct, 10(1). doi: 10.1186/S13062-015-0063-8.

Vermunt, L. *et al.* (2019) ‘Duration of preclinical, prodromal, and dementia stages of Alzheimer’s disease in relation to age, sex, and APOE genotype’, *Alzheimer’s & Dementia*. John Wiley & Sons, Ltd, 15(7), pp. 888–898. doi: 10.1016/J.JALZ.2019.04.001.

Videla, L. *et al.* (2022) ‘Longitudinal Clinical and Cognitive Changes Along the Alzheimer Disease Continuum in Down Syndrome’, *JAMA Network Open*. American Medical Association, 5(8), pp. e2225573–e2225573. doi: 10.1001/JAMANETWORKOPEN.2022.25573.

Vogel, J. W. *et al.* (2020) ‘Spread of pathological tau proteins through communicating neurons in human Alzheimer’s disease’, *Nature Communications 2020 11:1*. Nature Publishing Group, 11(1), pp. 1–15. doi: 10.1038/s41467-020-15701-2.

Wang, C. H. *et al.* (2017) ‘USP5/Leon deubiquitinase confines postsynaptic growth by maintaining ubiquitin homeostasis through Ubiquilin’, *eLife*. eLife Sciences Publications Ltd, 6, p. e26886. doi: 10.7554/ELIFE.26886.

Wang, E. T. *et al.* (2008) ‘Alternative isoform regulation in human tissue transcriptomes’, *Nature 2008 456:7221*. Nature Publishing Group, 456(7221), pp. 470–476. doi: 10.1038/nature07509.

Wang, G. *et al.* (2014) ‘Population-level expression variability of mitochondrial DNA-encoded genes in humans’, *European journal of human genetics : EJHG*. Eur J Hum Genet, 22(9), pp. 1093–1099. doi: 10.1038/EJHG.2013.293.

Wang, X. and Davis, R. L. (2021) ‘Early Mitochondrial Fragmentation and Dysfunction in a Drosophila Model for Alzheimer’s Disease’, *Molecular neurobiology*. Mol Neurobiol, 58(1), pp. 143–155. doi: 10.1007/S12035-020-02107-W.

Wang, Y. H. *et al.* (2023) ‘Identification of highly reliable risk genes for Alzheimer’s disease through joint-tissue integrative analysis’, *Frontiers in Aging Neuroscience*. Frontiers Media SA, 15, p. 1183119. doi: 10.3389/FNAGI.2023.1183119/BIBTEX.

Watson, L. A. and Meharena, H. S. (2023) ‘From neurodevelopment to neurodegeneration: utilizing human stem cell models to gain insight into Down syndrome’, *Frontiers in genetics*. Front Genet, 14. doi: 10.3389/FGENE.2023.1198129.

Wegiel, J. *et al.* (2004) ‘Cell type- and brain structure-specific patterns of distribution of minibrain kinase in human brain’, *Brain Research*. Elsevier, 1010(1–2), pp. 69–80. doi: 10.1016/J.BRAINRES.2004.03.008.

Wegiel, Jerzy *et al.* (2008) ‘The role of overexpressed DYRK1A protein in the early onset of neurofibrillary degeneration in Down syndrome’, *Acta Neuropathologica*. Springer, 116(4), pp. 391–407. doi: 10.1007/S00401-008-0419-6/FIGURES/7.

Wegiel, Jerzy *et al.* (2022) 'Developmental deficits and staging of dynamics of age associated Alzheimer's disease neurodegeneration and neuronal loss in subjects with Down syndrome', *Acta Neuropathologica Communications*. BioMed Central Ltd, 10(1), pp. 1–33. doi: 10.1186/S40478-021-01300-9/METRICS.

White, K. *et al.* (2018) 'Effect of Postmortem Interval and Years in Storage on RNA Quality of Tissue at a Repository of the NIH NeuroBioBank', *Biopreservation and biobanking*. Biopreserv Biobank, 16(2), pp. 148–157. doi: 10.1089/BIO.2017.0099.

WHO (2022) *A blueprint for dementia research*. Available at: https://www.who.int/publications/i/item/9789240058248 (Accessed: 9 December 2024).

Wilcock, D. M. *et al.* (2015) 'Down syndrome individuals with Alzheimer's disease have a distinct neuroinflammatory phenotype compared to sporadic Alzheimer's disease', *Neurobiology of aging*. Neurobiol Aging, 36(9), pp. 2468–2474. doi: 10.1016/J.NEUROBIOLAGING.2015.05.016.

Wilkins, H. M. *et al.* (2022) 'Mitochondrial Membrane Potential Influences Amyloid-β Protein Precursor Localization and Amyloid-β Secretion', *Journal of Alzheimer's disease : JAD*. J Alzheimers Dis, 85(1), pp. 381–394. doi: 10.3233/JAD-215280.

Wiseman, F. K. *et al.* (2015) 'A genetic cause of Alzheimer disease: mechanistic insights from Down syndrome.', *Nature reviews. Neuroscience*, 16(9), pp. 564–574. doi: 10.1038/nrn3983.

Wiseman, F. K. *et al.* (2018) 'Trisomy of human chromosome 21 enhances amyloid-b deposition independently of an extra copy of APP', *Brain*. Oxford University Press, 141(8), pp. 2457–2474. doi: 10.1093/brain/awy159.

Wisniewski, T. and Masurkar, A. V. (2023) ‘Gait dysfunction in Alzheimer disease’, *Handbook of Clinical Neurology*. Elsevier, 196, pp. 267–274. doi: 10.1016/B978-0-323-98817-9.00013-2.

Wolters, F. J. *et al.* (2020) ‘Twenty-seven-year time trends in dementia incidence in Europe and the United States: The Alzheimer Cohorts Consortium’, *Neurology*. Neurology, 95(5), pp. E519–E531. doi: 10.1212/WNL.0000000000010022.

Wright, C. J., Smith, C. W. J. and Jiggins, C. D. (2022) ‘Alternative splicing as a source of phenotypic diversity’, *Nature Reviews Genetics 2022 23:11*. Nature Publishing Group, 23(11), pp. 697–710. doi: 10.1038/s41576-022-00514-4.

Wu, C. I. *et al.* (2022) ‘APP and DYRK1A regulate axonal and synaptic vesicle protein networks and mediate Alzheimer’s pathology in trisomy 21 neurons’, *Molecular Psychiatry 2022 27:4*. Nature Publishing Group, 27(4), pp. 1970–1989. doi: 10.1038/s41380-022-01454-5.

Wu, Y. *et al.* (2016) ‘Regulation of global gene expression and cell proliferation by APP’, *Scientific Reports 2016 6:1*. Nature Publishing Group, 6(1), pp. 1–9. doi: 10.1038/srep22460.

Wu, Y. *et al.* (2021) ‘The effects of Cstb duplication on APP/amyloid-β pathology and cathepsin B activity in a mouse model’, *PloS one*. PLoS One, 16(7). doi: 10.1371/JOURNAL.PONE.0242236.

Wu, Y. *et al.* (2022) ‘Cell models for Down syndrome-Alzheimer’s disease research’, 6, p. 20210054. doi: 10.1042/NS20210054.

Wu, Y. *et al.* (2023) ‘Cathepsin B abundance, activity and microglial localisation in Alzheimer’s disease-Down syndrome and early onset Alzheimer’s disease; the role of elevated cystatin B’, *Acta neuropathologica communications*. Acta Neuropathol Commun, 11(1). doi: 10.1186/S40478-023-01632-8.

Wu, Y. T. *et al.* (2017) 'The changing prevalence and incidence of dementia over time - current evidence', *Nature reviews. Neurology*. Nat Rev Neurol, 13(6), pp. 327–339. doi: 10.1038/NRNEUROL.2017.63.

Xu, K. *et al.* (2022) 'Accelerated epigenetic aging in newborns with Down syndrome', *Aging Cell*. John Wiley & Sons, Ltd, 21(7), p. e13652. doi: 10.1111/ACEL.13652.

Xu, L. *et al.* (2021) 'Proteomic analysis of human frontal and temporal cortex using iTRAQ-based 2D LC-MS/MS', *Chinese Neurosurgical Journal*. BioMed Central Ltd, 7(1), p. 27. doi: 10.1186/S41016-021-00241-5.

Yabut, O. *et al.* (2010) 'Dyrk1A overexpression inhibits proliferation and induces premature neuronal differentiation of neural progenitor cells', *Soc Neuroscience.*

Yabut, J Domogauer, G D'Arcangelo. Journal of Neuroscience, 2010•Soc Neuroscience, 30(11), pp. 4004–4014. doi: 10.1523/JNEUROSCI.4711-09.2010.

Yagi, T. *et al.* (2011) 'Modeling familial Alzheimer's disease with induced pluripotent stem cells', *Human molecular genetics*. Hum Mol Genet, 20(23), pp. 4530–4539. doi: 10.1093/HMG/DDR394.

Yang, M. *et al.* (2023) 'Using Drosophila to identify naturally occurring genetic modifiers of amyloid beta 42- and tau-induced toxicity', *G3 (Bethesda, Md.)*. G3 (Bethesda), 13(9). doi: 10.1093/G3JOURNAL/JKAD132.

Yang, N. *et al.* (2011) 'Induced neuronal cells: how to make and define a neuron', *Cell stem cell*. Cell Stem Cell, 9(6), pp. 517–525. doi: 10.1016/J.STEM.2011.11.015.

Yin, X. *et al.* (2021) 'Dendritic/Post-synaptic Tau and Early Pathology of Alzheimer's Disease', *Frontiers in Molecular Neuroscience*. Frontiers Media S.A., 14, p. 671779. doi: 10.3389/FNMOL.2021.671779.

Yu, S. *et al.* (2022) 'Drosophila Innate Immunity Involves Multiple Signaling Pathways and Coordinated Communication Between Different Tissues', *Frontiers in Immunology*. Frontiers Media S.A., 13, p. 905370. doi: 10.3389/FIMMU.2022.905370.

Yu, T. *et al.* (2010) 'A mouse model of Down syndrome trisomic for all human chromosome 21 syntenic regions', *Human Molecular Genetics*. Oxford Academic, 19(14), pp. 2780–2791. doi: 10.1093/HMG/DDQ179.

Yu, Y. *et al.* (2020) 'PICALM rescues glutamatergic neurotransmission, behavioural function and survival in a Drosophila model of Aβ42 toxicity', *Human molecular genetics*. Hum Mol Genet, 29(14), pp. 2420–2434. doi: 10.1093/HMG/DDAA125.

Yun, H. J. *et al.* (2021) 'Regional Alterations in Cortical Sulcal Depth in Living Fetuses with Down Syndrome', *Cerebral cortex (New York, N.Y. : 1991)*. Cereb Cortex, 31(2), pp. 757–767. doi: 10.1093/CERCOR/BHAA255.

Zammit, M. D. *et al.* (2024) 'Characterizing the emergence of amyloid and tau burden in Down syndrome', *Alzheimer's & dementia : the journal of the Alzheimer's Association*. Alzheimers Dement, 20(1), pp. 388–398. doi: 10.1002/ALZ.13444.

Zamponi, E. and Helguera, P. R. (2019) 'The Shape of Mitochondrial Dysfunction in Down Syndrome', *Developmental neurobiology*. Dev Neurobiol, 79(7), pp. 613–621. doi: 10.1002/DNEU.22673.

Zdaniuk, G. *et al.* (2011) 'Astroglia disturbances during development of the central nervous system in fetuses with Down's syndrome', *Folia Neuropathologica*. Termedia, 49(2), pp. 109–114.

Zhang, H. *et al.* (2021) 'Possible Mechanisms of Tau Spread and Toxicity in Alzheimer's Disease', *Frontiers in cell and developmental biology*. Front Cell Dev Biol, 9. doi: 10.3389/FCELL.2021.707268.

Zhang, L. *et al.* (2013) 'Both K63 and K48 ubiquitin linkages signal lysosomal degradation of the LDL receptor', *Journal of Lipid Research*, 54(5), p. 1410. doi: 10.1194/JLR.M035774.

Zhang, R. *et al.* (2014) 'A circadian gene expression atlas in mammals: implications for biology and medicine', *Proceedings of the National Academy of Sciences of the United States of America*. Proc Natl Acad Sci U S A, 111(45), pp. 16219–16224. doi: 10.1073/PNAS.1408886111.

Zhang, X. *et al.* (2016) 'Cell-Type-Specific Alternative Splicing Governs Cell Fate in the Developing Cerebral Cortex', *Cell*. Cell, 166(5), pp. 1147-1162.e15. doi: 10.1016/J.CELL.2016.07.025.

Zhang, Y. *et al.* (2016a) 'Purification and Characterization of Progenitor and Mature Human Astrocytes Reveals Transcriptional and Functional Differences with Mouse', *Neuron*. Cell Press, 89(1), pp. 37–53. doi: 10.1016/J.NEURON.2015.11.013/ATTACHMENT/A14065F8-E9FD-4DF2-A3E8-44C20462ED4F/MMC6.PDF.

Zhang, Y. *et al.* (2016b) 'Purification and Characterization of Progenitor and Mature Human Astrocytes Reveals Transcriptional and Functional Differences with Mouse', *Neuron*. Cell Press, 89(1), pp. 37–53. doi: 10.1016/J.NEURON.2015.11.013/ATTACHMENT/A14065F8-E9FD-4DF2-A3E8-44C20462ED4F/MMC6.PDF.

Zhang, Y. *et al.* (2017) 'Aberrations in circulating inflammatory cytokine levels in patients with Down syndrome: a meta-analysis', *Oncotarget*. Oncotarget, 8(48), pp. 84489–84496. doi: 10.18632/ONCOTARGET.21060.

Zhao, B. *et al.* (2024) ‘In vivo RNAi screening identifies multiple deubiquitinases required for the maintenance of intestinal homeostasis in Drosophila’, *Insect Biochemistry and Molecular Biology*. Pergamon, 172, p. 104162. doi: 10.1016/J.IBMB.2024.104162.

Zhao, H. H. and Haddad, G. G. (2022) ‘Alzheimer’s disease like neuropathology in Down syndrome cortical organoids’, *Frontiers in Cellular Neuroscience*. Frontiers Media S.A., 16, p. 1050432. doi: 10.3389/FNCEL.2022.1050432/BIBTEX.

Zhao, R. *et al.* (2019) ‘Mitochondrial electron transport chain, ROS generation and uncoupling’, *International journal of molecular medicine*. doi: 10.3892/ijmm.2019.4188.

Zhao, Y. L. *et al.* (2021) ‘Environmental factors and risks of cognitive impairment and dementia: A systematic review and meta-analysis’, *Ageing Research Reviews*. Elsevier, 72, p. 101504. doi: 10.1016/J.ARR.2021.101504.

Zheng, Q. *et al.* (2021) ‘Trisomy 21–induced dysregulation of microglial homeostasis in Alzheimer’s brains is mediated by USP25’, *Science Advances*. American Association for the Advancement of Science, 7(1). doi: 10.1126/SCIADV.ABE1340/SUPPL_FILE/ABE1340_SM.PDF.

Zheng, Q. *et al.* (2022) ‘USP25 inhibition ameliorates Alzheimer’s pathology through the regulation of APP processing and Aβ generation’, *The Journal of Clinical Investigation*. American Society for Clinical Investigation, 132(5). doi: 10.1172/JCI152170.

Zhong, M. Z. *et al.* (2024) ‘Updates on mouse models of Alzheimer’s disease’, *Molecular Neurodegeneration 2024 19:1*. BioMed Central, 19(1), pp. 1–33. doi: 10.1186/S13024-024-00712-0.

Zhu, B., Parsons, T., Foley, C., *et al.* (2022) 'DYRK1A antagonists rescue degeneration and behavioural deficits of in vivo models based on amyloid-β, Tau and DYRK1A neurotoxicity', *Scientific Reports 2022 12:1*. Nature Publishing Group, 12(1), pp. 1–14. doi: 10.1038/s41598-022-19967-y.

Zhu, B., Parsons, T., Stensen, W., *et al.* (2022) 'DYRK1a Inhibitor Mediated Rescue of Drosophila Models of Alzheimer's Disease-Down Syndrome Phenotypes', *Frontiers in Pharmacology*. Frontiers Media S.A., 13, p. 881385. doi: 10.3389/FPHAR.2022.881385/BIBTEX.

Zhu, W. *et al.* (2021) 'Emerging Roles of Ubiquitin-Specific Protease 25 in Diseases', *Frontiers in Cell and Developmental Biology*. Frontiers Media S.A., 9, p. 1654. doi: 10.3389/FCELL.2021.698751/BIBTEX.

Zimbone, S. *et al.* (2018) 'Amyloid Beta monomers regulate cyclic adenosine monophosphate response element binding protein functions by activating type-1 insulin-like growth factor receptors in neuronal cells', *Aging Cell*. John Wiley & Sons, Ltd, 17(1), p. e12684. doi: 10.1111/ACEL.12684.

Zou, L. B. *et al.* (2006) 'Inhibition of Neprilysin by Infusion of Thiorphan into the Hippocampus Causes an Accumulation of Amyloid β and Impairment of Learning and Memory', *Journal of Pharmacology and Experimental Therapeutics*. American Society for Pharmacology and Experimental Therapeutics, 317(1), pp. 334–340. doi: 10.1124/JPET.105.095687.

Appendix

Table S3.1 Hsa21 genes not included in the *Drosophila* screen due to a lack of suitable orthologues or unavailability of overexpression lines.
Keratin-associated protein genes are highlighted in orange.

Hsa21 genes				
ABCC13	*COL6A2*	*KRTAP12-1*	*MCM3APAS*	*SH3BGR*
ADAMTS1	*CRYAA*	*KRTAP12-2*	*MIR125B2*	*SLC37A1*
ADAMTS5	*CSTB*	*KRTAP12-3*	*MIR155*	*SUMO3*
AIRE	*COL6A2*	*KRTAP12-4*	*MIR155HG*	*TFF2*
ANKRD30BP2	*CRYAA*	*KRTAP13-1*	*MIR3156-3*	*TFF3*
B3GALT5	*CSTB*	*KRTAP13-2*	*MIR3197*	*TIAM1*
BACE2	*CXADR*	*KRTAP13-3*	*MIR4327*	*TMPRSS3*
BACH1	*CYYR1*	*KRTAP13-4*	*MIR802*	*TTC3*
BRWD1	*DNMT3L*	*KRTAP15-1*	*MIR99A*	*U2AF1*
C21orf121	*DOPEY2*	*KRTAP19-1*	*MIRLET7C*	*UBASH3A*
C21orf122	*DSCR10*	*KRTAP19-2*	*MORC3*	*UBE2G2*
C21orf125	*DSCR3*	*KRTAP19-3*	*N6AMT1*	*UMODL1*
C21orf128	*DSCR4*	*KRTAP19-4*	*NCRNA00111*	*WRB*
C21orf129	*DSCR6*	*KRTAP19-5*	*NCRNA00112*	*ZNF295*
C21orf130	*DSCR8*	*KRTAP19-6*	*NCRNA00113*	
C21orf131	*DSCR9*	*KRTAP19-7*	*NCRNA00114*	
C21orf15	*ERG*	*KRTAP19-8*	*NCRNA00158*	
C21orf2	*FAM3B*	*KRTAP20-1*	*NCRNA00159*	
C21orf29	*FTCD*	*KRTAP20-2*	*NCRNA00161*	
C21orf33	*GRIK1AS*	*KRTAP20-3*	*NCRNA00162*	
C21orf56	*HMGN1*	*KRTAP20-4*	*NCRNA00163*	
C21orf57	*HSF2BP*	*KRTAP21-1*	*NCRNA00175*	
C21orf58	*HSPA13*	*KRTAP21-2*	*NCRNA00189*	
C21orf67	*HUNK*	*KRTAP21-3*	*NCRNA00257*	
C21orf7	*ICOSLG*	*KRTAP22-1*	*NCRNA00258*	
C21orf70	*IGSF5*	*KRTAP22-2*	*NRIP1*	
C21orf71	*JAM2*	*KRTAP23-1*	*PCP4*	
C21orf81	*KCNJ15*	*KRTAP24-1*	*PDE9A*	
C21orf84	*KCNJ6*	*KRTAP25-1*	*PDXK*	
C21orf88	*KRTAP10-1*	*KRTAP26-1*	*PIGP*	
C21orf90	*KRTAP10-10*	*KRTAP27-1*	*PLAC4*	
C21orf94	*KRTAP10-11*	*KRTAP6-1*	*POTED*	
C21orf96	*KRTAP10-12*	*KRTAP6-2*	*PRDM15*	
C2CD2	*KRTAP10-2*	*KRTAP6-3*	*PSMG1*	
CBR1	*KRTAP10-3*	*KRTAP7-1*	*PTTG1IP*	
CBR3	*KRTAP10-4*	*KRTAP8-1*	*RIPK4*	
CCT8	*KRTAP10-5*	*LCA5L*	*RRP1*	
CHAF1B	*KRTAP10-6*	*LOC100132288*	*RSPH1*	
CLDN14	*KRTAP10-7*	*LOC284837*	*RWDD2B*	

CLDN17	*KRTAP10-8*	*LOC642852*	*S100B*	
CLDN8	*KRTAP10-9*	*LSS*	*SETD4*	
COL6A1	*KRTAP11-1*	*MCM3AP*	*SFRS15*	

Table S3.2 (A-AC) Linear models of negative geotaxis assays for the non-significant interactions.
Significant interactions of interest between age and genotype in the -RU condition are highlighted in green.

A

achi				
Term	Estimate	Std Error	t Ratio	Prob>ltl
Induced (+RU)				
Age	-0.397253	0.033912	-11.714	<2e-16 ***
Genotype	-0.796622	0.733742	-1 .086	0.278
Age*Genotype	0.008819	0.045797	0.193	0.847
Uninduced (-RU)				
Age	-0.17874	0.06266	-2.853	0.00505 **
Genotype	-0.70748	1.87613	-0.377	0.70672
Age*Genotype	1.1239	0.8733	1.287	0.2

B

Agpat3				
Term	Estimate	Std Error	t Ratio	Prob>ltl
Induced (+RU)				
Age	-0.539972	0.024705	-21.857	<2e-16 ***
Genotype	-0.229481	0.676176	-0.339	0.734
Age*Genotype	-0.005319	0.036006	-0.148	0.883
Uninduced (-RU)				
Age*Genotype	0.05782	0.08578	0.674	0.50

C

Art8				
Term	Estimate	Std Error	t Ratio	Prob>ltl
Induced (+RU)				
Age	-0.38600	0.04631	-8.335	6.56e-16 ***
Genotype	0.86372	0.77566	1.114	0.266
Age*Genotype	-0.07366	0.06215	-1.185	0.236
Uninduced (-RU)				
Age	-0.32953	0.07997	-4.121	4.45e-05 ***
Genotype	-2.19410	1.17718	-1.864	0.063
Age*Genotype	0.14588	0.10747	1.357	0.175

D

Cbs				
Term	Estimate	Std Error	t Ratio	Prob>|t|
Induced (+RU)				
Age	-0.48586	0.03847	21.467	<2e-16 ***
Genotype	0.04745	0.83192	0.057	0.955
Age*Genotype	-0.04844	0.05500	-0.881	0.379
Uninduced (-RU)				
Age	-0.26727	0.05045	-5.298	1.76e-07 ***
Genotype	-3.10520	1.05028	-2.957	0.00326 **
Age*Genotype	0.22957	0.07073	3.246	0.00125 **

E

clumsy				
Term	Estimate	Std Error	t Ratio	Prob>|t|
Induced (+RU)				
Age	-0.83563	0.05648	-14.796	<2e-16 ***
Genotype	0.46766	1.49814	0.312	0.755
Age*Genotype	-0.09302	0.07899	-1.178	0.239
Uninduced (-RU)				
Age*Genotype	0.1775	0.2021	0.878	0.380

F

DIP1				
Term	Estimate	Std Error	t Ratio	Prob>|t|
Induced (+RU)				
Age	-0.38796	0.04731	-8.201	1.73e-15 ***
Genotype	-0.10110	0.81029	-0.125	0.901
Age*Genotype	-0.07170	0.06454	-1.111	0.267
Uninduced (-RU)				
Age	-0.28510	0.08426	-3.383	0.000772 ***
Genotype	-2.16634	1.27985	-1.693	0.091149
Age*Genotype	0.10145	0.11551	0.878	0.380219

G

Dscam4				
Term	Estimate	Std Error	t Ratio	Prob>|t|
Induced (+RU)				
Age	-0.531948	0.037192	-14.303	< 2e-16 ***
Genotype	-0.240957	0.802000	-0.300	0.764
Age*Genotype	-0.002355	0.053171	-0.044	0.965
Uninduced (-RU)				
Age	-0.10334	0.04673	-2.212	0.0275 *
Genotype	-1.29520	1.00432	-1.290	0.1978
Age*Genotype	0.06564	0.06647	0.987	0.3239

H

Ets97D				
Term	Estimate	Std Error	t Ratio	Prob>|t|
Induced (+RU)				
Age	-0.31531	0.03835	-8.223	1.51e-15 ***
Genotype	-0.73606	0.78517	-0.937	0.349
Age*Genotype	0.02804	0.05425	0.517	0.606
Uninduced (-RU)				
Age	0.03603	0.05631	0.640	0.523
Genotype	-0.19064	1.14289	-0.167	0.868
Age*Genotype	-0.02944	0.07542	-0.390	0.697

I

Ltn1				
Term	Estimate	Std Error	t Ratio	Prob>|t|
Induced (+RU)				
Age	-0.31324	0.02907	-10.774	< 2e-16 ***
Genotype	-0.05898	0.67446	-0.087	0.9304
Age*Genotype	-0.07520	0.04102	-1.833	0.0675
Uninduced (-RU)				
Age*Genotype				

N= too small

J

mRpL39				
Term	Estimate	Std Error	t Ratio	Prob>|t|
Induced (+RU)				
Age	-0.57727	0.03925	-14.706	< 2e-16 ***
Genotype	-0.85360	0.83116	-1.027	0.305
Age*Genotype	0.04297	0.05549	0.774	0.439
Uninduced (-RU)				
Age	-0.19761	0.05090	-3.882	0.000117 ***
Genotype	-2.63882	1.09325	-2.414	0.016137 *
Age*Genotype	0.15990	0.07346	2.177	0.029954 *

K

mys				
Term	Estimate	Std Error	t Ratio	Prob>|t|
Induced (+RU)				
Age	-0.51786	0.01818	-28.488	<2e-16 ***
Genotype	0.38787	0.50231	0.772	0.440
Age*Genotype	-0.03398	0.02537	-1.339	0.181
Uninduced (-RU)				
Age	-0.18052	0.02441	-7.394	2.38e-13 ***
Genotype	0.48995	0.67034	0.731	0.465
Age*Genotype	-0.03477	0.03405	-1.021	0.307

L

Nnp-1				
Term	Estimate	Std Error	t Ratio	Prob>|t|
Induced (+RU)				
Age	-0.64087	0.01959	-32.707	< 2e-16 ***
Genotype	-1.79401	0.50463	-3.555	0.000399 ***
Age*Genotype	0.04892	0.02635	1.857	0.063669
Uninduced (-RU)				
Age*Genotype	-0.06126	0.03733	-1.641	0.101

M

O-fut2				
Term	Estimate	Std Error	t Ratio	Prob>|t|
Induced (+RU)				
Age	-0.420845	0.028016	-15.022	< 2e-16 ***
Genotype	0.295828	0.634758	0.466	0.305
Age*Genotype	0.001829	0.040263	0.045	0.964
Uninduced (-RU)				
Age*Genotype	-0.01280	0.04636	-0.276	0.7826

N

Pfk				
Term	Estimate	Std Error	t Ratio	Prob>|t|
Induced (+RU)				
Age	-0.40046	0.02862	-13.995	< 2e-16 ***
Genotype	0.11094	0.64797	0.171	0.864
Age*Genotype	-0.02061	0.04063	-0.507	0.612
Uninduced (-RU)				
Age*Genotype	0.07773	0.04480	1.735	0.0831

O

Plp				
Term	Estimate	Std Error	t Ratio	Prob>|t|
Induced (+RU)				
Age	-0.42693	0.04137	-10.320	< 2e-16 ***
Genotype	1.75914	0.85270	2.063	0.0396 *
Age*Genotype	-0.10738	0.05768	-1.861	0.0632
Uninduced (-RU)				
Age	-0.15113	0.05161	-2.928	0.00357 **
Genotype	-1.30335	1.08818	-1.198	0.23161
Age*Genotype	0.11343	0.07253	1.564	0.11850

P

pnt				
Term	Estimate	Std Error	t Ratio	Prob>|t|
Induced (+RU)				
Age	-0.27691	0.03757	-7.370	6.11e-13 ***
Genotype	0.17276	0.80474	0.215	0.830
Age*Genotype	-0.02657	0.05347	-0.497	0.619
Uninduced (-RU)				
Age	-0.07716	0.04239	-1.820	0.0694
Genotype	0.54669	1.02412	0.534	0.5938
Age*Genotype	0.01465	0.06397	0.229	0.8190

Q

Pten				
Term	Estimate	Std Error	t Ratio	Prob>|t|
Induced (+RU)				
Age	-0.35029	0.04325	-8.100	3.5e-15 ***
Genotype	1.92898	0.80058	2.409	0.0163 *
Age*Genotype	-0.10937	0.06188	-1.768	0.0777
Uninduced (-RU)				
Age	-0.31560	0.07774	-4.060	5.66e-05 ***
Genotype	-1.41141	1.22583	-1.151	0.250
Age*Genotype	0.13195	0.11061	1.193	0.233

R

SIDL				
Term	Estimate	Std Error	t Ratio	Prob>|t|
Induced (+RU)				
Age	-0.590474	0.027995	-21.092	< 2e-16 ***
Genotype	-0.220222	0.566880	-0.388	0.698
Age*Genotype	0.007812	0.039309	0.199	0.843
Uninduced (-RU)				
Age*Genotype	0.07211	0.06707	1.075	0.283

S

sif				
Term	Estimate	Std Error	t Ratio	Prob>|t|
Induced (+RU)				
Age	-0.68376	0.07353	-9.299	< 2e-16 ***
Genotype	-1.91293	1.18654	-1.612	0.108
Age*Genotype	0.05672	0.10443	0.543	0.587
Uninduced (-RU)				
Age	-0.39113	0.07854	-4.980	9.06e-07 ***
Genotype	-3.48801	1.29802	-2.687	0.00747 **
Age*Genotype	0.16922	0.11565	1.463	0.14408

T

Sik2				
Term	Estimate	Std Error	t Ratio	Prob>|t|
Induced (+RU)				
Age	-0.83637	0.05481	-15.260	<2e-16 ***
Genotype	2.55398	1.47883	1.727	0.0847
Age*Genotype	-0.09228	0.07740	-1.192	0.2336
Uninduced (-RU)				
Age*Genotype	-0.01556	0.20073	-0.078	0.938

U

sim				
Term	Estimate	Std Error	t Ratio	Prob>|t|
Induced (+RU)				
Age	-0.69856	0.06840	-10.213	< 2e-16 ***
Genotype	-2.04957	1.10705	-1.851	0.0648
Age*Genotype	0.07151	0.09796	0.730	0.4657
Uninduced (-RU)				
Age	-0.12080	0.08963	-1.348	0.178
Genotype	1.13967	1.46968	0.775	0.438
Age*Genotype	-0.10110	0.13184	-0.767	0.444

V

Sod1				
Term	Estimate	Std Error	t Ratio	Prob>|t|
Induced (+RU)				
Age	-0.29627	0.05153	-5.749	1.62e-08 ***
Genotype	-1.06459	1.01481	-1.049	0.2947
Age*Genotype	0.13444	0.07316	1.838	0.0668
Uninduced (-RU)				
Age	0.02202	0.04668	0.472	0.6374
Genotype	2.52937	1.21781	2.077	0.0386 *
Age*Genotype	-0.03866	0.07516	-0.514	0.6073

W

Usp45-16				
Term	Estimate	Std Error	t Ratio	Prob>|t|
Induced (+RU)				
Age	-0.468068	0.046000	-10.175	3.71e-10 ***
Genotype	-0.578470	0.825502	-0.701	0.484
Age*Genotype	0.008408	0.064452	0.130	0.896
Uninduced (-RU)				
Age	-0.09668	0.08052	-1.201	0.230
Genotype	0.43424	1.23479	0.352	0.725
Age*Genotype	0.938	0.11122	-0.782	0.435

X

wuho				
Term	Estimate	Std Error	t Ratio	Prob>|t|
Induced (+RU)				
Age	-0.53430	0.03943	-13.550	< 2e-16 ***
Genotype	-1.00588	0.86851	-1.158	0.247
Age*Genotype	0.06406	0.05646	1.135	0.257
Uninduced (-RU)				
Age	-0.03770	0.05003	-0.754	0.452
Genotype	-1.22795	1.08420	-1.133	0.258
Age*Genotype	0.08713	0.07221	1.207	0.228

Y

CG11454				
Term	Estimate	Std Error	t Ratio	Prob>|t|
Induced (+RU)				
Age	-0.42909	0.04439	-9.666	< 2e-16 ***
Genotype	-0.54447	0.78239	-0.696	0.487
Age*Genotype	-0.03057	0.06081	-0.503	0.615
Uninduced (-RU)				
Age	-0.33557	0.08782	-3.821	0.000151 ***
Genotype	-2.75074	1.28964	-2.133	0.033462 *
Age*Genotype	0.15192	0.11603	1.309	0.191067

Z

CG12325				
Term	Estimate	Std Error	t Ratio	Prob>|t|
Induced (+RU)				
Age	-0.33557	0.08782	-3.821	0.000151 ***
Genotype	-2.75074	1.28964	-2.133	0.033462 *
Age*Genotype	0.15192	0.11603	1.309	0.191067
Uninduced (-RU)				
Age	-0.45785	0.02396	-19.111	< 2e-16 ***
Genotype	-2.77573	0.64909	-4.276	2.02e-05 ***
Age*Genotype	0.24256	0.03336	7.270	5.79e-13 ***

AA

CG17464				
Term	Estimate	Std Error	t Ratio	Prob>|t|
Induced (+RU)				
Age	-0.539505	0.036955	-14.599	< 2e-16 ***
Genotype	-0.031760	0.804283	-14.599	0.969
Age*Genotype	0.005202	0.053069	0.098	0.922
Uninduced (-RU)				
Age	-0.12752	0.05625	-2.267	0.0238 *
Genotype	-0.69977	1.16241	-0.602	0.5475

Age*Genotype	0.08982	0.07820	1.149	0.2513

AB

CG4266				
Term	Estimate	Std Error	t Ratio	Prob>|t|
Induced (+RU)				
Age	-0.42398	0.04944	-8.575	< 2e-16 ***
Genotype	-0.28336	0.84009	-0.337	0.736
Age*Genotype	-0.03568	0.06725	-0.531	0.596
Uninduced (-RU)				
Age	-0.23443	0.07996	-2.932	0.00351 **
Genotype	-0.92963	1.24845	-0.745	0.45683
Age*Genotype	0.05078	0.11333	0.448	0.65429

AC

CG42709				
Term	Estimate	Std Error	t Ratio	Prob>|t|
Induced (+RU)				
Age	-0.83653	0.06132	-13.642	< 2e-16 ***
Genotype	1.89404	1.58097	1.198	0.231
Age*Genotype	-0.09212	0.08341	-1.104	0.270
Uninduced (-RU)				
Age*Genotype	0.2726	0.2103	1.297	0.196

Table S3.3 Linear models of negative geotaxis assays for the significant interactions.
Significant interactions of interest are highlighted in green.

A

ATPsynCF6				
Term	Estimate	Std Error	t Ratio	Prob>|t|
Induced (+RU)				
Age	-0.52620	0.03098	-16.985	< 2e-16 ***
Genotype	-3.44234	0.70075	-4.912	1.3e-06 ***
Age*Genotype	0.13777	0.04352	3.165	0.00166 **
Uninduced (-RU)				
Age	-0.13452	0.04655	-2.890	0.00427 **
Genotype	-2.78210	1.78518	-1.558	0.12067
Age*Genotype	0.05538	0.19759	0.280	0.77955

B

Hcs				
Term	Estimate	Std Error	t Ratio	Prob>|t|
Induced (+RU)				
Age	-0.36992	0.07449	-4.966	9.9e-07 ***
Genotype	2.45144	1.20693	2.031	0.0429 *
Age*Genotype	-0.25713	0.10485	-2.452	0.0146 *
Uninduced (-RU)				
Age	0.10447	0.08624	1.211	0.226444
Genotype	5.29930	1.46428	3.619	0.000331 ***
Age*Genotype	-0.32637	0.12746	-2.561	0.010792 *
Effect of RU				
RU	-0.1014	0.4190	-0.242	0.808915
RU*Genotype	-1.9693	0.5867	-3.356	0.000824

C

mnb				
Term	Estimate	Std Error	t Ratio	Prob>|t|
Induced (+RU)				
Age	-0.29396	0.03131	-9.388	<2e-16 ***
Genotype	1.02424	0.73781	1.388	0.1657
Age*Genotype	-0.09357	0.04609	-2.030	0.0429 *
Uninduced (-RU)				
Age	0.3893	0.2080	1.872	0.0638
Genotype	-0.1000	4.4093	-0.023	0.9819
Age*Genotype	-0.1360	0.7836	-0.174	0.8625

D

Sb				
Term	Estimate	Std Error	t Ratio	Prob>|t|
Induced (+RU)				
Age	-0.29498	0.06985	-4.223	2.91e-05 ***
Genotype	2.77414	1.16608	2.379	0.01777 *
Age*Genotype	-0.33207	0.10153	-3.271	0.00115 **
Uninduced (-RU)				
Age	0.19897	0.07836	2.539	0.011454 *
Genotype	3.89838	1.32692	2.938	0.003475 **
Age*Genotype	-0.42087	0.11602	-3.628	0.000319 ***
Effect of RU				
RU	-2.077637	0.377121	-5.509	4.7e-08 ***
RU*Genotype	0.006998	0.542063	0.013	0.9897

E

SKIP				
Term	Estimate	Std Error	t Ratio	Prob>|t|
Induced (+RU)				
Age	-0.42318	0.06805	-6.219	1.13e-09 ***
Genotype	1.90231	1.12190	1.696	0.0906
Age*Genotype	-0.20386	0.09830	-2.074	0.0387 *
Uninduced (-RU)				
Age	-0.34003	0.09073	-3.748	0.000203 ***
Genotype	-0.90141	1.46361	-0.616	0.538296
Age*Genotype	0.11812	0.13038	0.906	0.365442

F

Usp47				
Term	Estimate	Std Error	t Ratio	Prob>|t|
Induced (+RU)				
Age	-0.42296	0.07006	-6.037	3.33e-09 ***
Genotype	0.92146	1.14770	0.803	0.4225
Age*Genotype	-0.20409	0.10045	-2.032	0.0428 *
Uninduced (-RU)				
Age	0.16927	0.08407	2.013	0.04471 *
Genotype	4.01378	1.39891	2.869	0.00432 **
Age*Genotype	-0.39117	0.12285	-3.184	0.00156 **
Effect of RU				
RU	-1.1184	0.3987	-2.805	0.00514 **
RU*Genotype	-0.9522	0.5632	-1.691	0.09127

Table S3.4 Repeats of climbing assays for *Hcs, mnb, Sb* and *SKIP* that showed significant interactions between age and genotype in the initial screen.
Significant interactions of interest are highlighted in green.

A

***Hcs* – repeat 2**				
Term	Estimate	Std Error	t Ratio	Prob>|t|
Induced (+RU)				
Age	-0.54831	0.01781	-30.787	< 2e-16 ***
Genotype	0.66710	0.42133	1.583	0.114
Age*Genotype	-0.01061	0.02468	-0.430	0.667
Uninduced (-RU)				
Age	-0.264754	0.026477	-9.999	< 2e-16 ***
Genotype	0.281534	0.608194	0.463	0.644
Age*Genotype	-0.002504	0.038358	-0.065	0.948
Effect of RU				
Intercept	12.2381	0.2418	50.604	< 2e-16 ***
RU	-4.2235	0.3379	-12.500	< 2e-16 ***
RU*Genotype	0.4220	0.4800	0.879	0.379

B

***mnb* – repeat 2**				
Term	Estimate	Std Error	t Ratio	Prob>|t|
Induced (+RU)				
Age	-0.48123	0.01785	-26.958	< 2e-16 ***
Genotype	0.63403	0.41690	1.521	0.1286
Age*Genotype	-0.05001	0.02472	-2.023	0.0433 *
Uninduced (-RU)				
Age	-0.18028	0.02557	-7.049	3.61e-12 ***
Genotype	-0.27048	0.57821	-0.468	0.6401
Age*Genotype	-0.08698	0.03650	-2.383	0.0174 *
Effect of RU				
RU	-5.1053	0.3325	-15.353	< 2e-16 ***
RU*Genotype	1.3037	0.4677	2.787	0.00537 **

***mnb* – repeat 3**				
Term	Estimate	Std Error	t Ratio	Prob>|t|
Induced (+RU)				
Age	-0.51760	0.03489	-14.835	< 2e-16 ***
Genotype	-1.62438	0.81818	-1.985	0.0476 *
Age*Genotype	0.08256	0.05200	1.588	0.1129

***mnb* - repeats combined**				
Repeat 1vs2				
Repeat 1vs3				
Age*Genotype	-0.006689	0.023235	-0.288	0.7735

C

Sb				
Term	Estimate	Std Error	t Ratio	Prob>ltl
Induced (+RU)				
Age	-0.47415	0.03468	-13.671	< 2e-16 ***
Genotype	-0.36736	0.72550	-0.506	0.613
Age*Genotype	0.07191	0.04708	1.527	0.127

D

SKIP				
Term	Estimate	Std Error	t Ratio	Prob>ltl
Induced (+RU)				
Age	-0.48576	0.01853	-26.219	< 2e-16 ***
Genotype	-0.40217	0.47648	-0.844	0.3988
Age*Genotype	0.04801	0.02886	1.663	0.0965
Uninduced (-RU)				
Age	-0.07043	0.02346	-3.001	0.00274 **
Genotype	0.79816	0.53861	1.482	0.13861
Age*Genotype	-0.03788	0.03341	-1.134	0.25708

Table S3.5 Log-rank test of lifespans of Hsa21 orthologue hits identified in the screen.
Significant interactions of interest are highlighted in green.

A *Hcs*

Log-rank test		
	n (dead/censored)	*p*-value
Hcs>elavGS Aβ42 +RU *w1118>elavGS Aβ42* +RU	130/4 145/0	0.025

B *mnb*

Log-rank test		
	n (dead/censored)	*p*-value
mnb>elavGS Aβ42 +RU *w1118>elavGS Aβ42* +RU	146/2 145/0	0.5123

mnb>elavGS Aβ42 vs w1118>elavGS Aβ42					
n (dead/censored)	293/4				
Cox proportional hazards					
	coef	exp(coef)	se(coef)	z	*p*-value
Genotype	0.2293	1.2578	0.1184	1.938	0.0527
RU	2.7964	16.3853	0.1657	16.881	< 2e-16
Genotype:RU	-0.2368	0.7892	0.1658	-1.428	0.1532

C *SKIP*

SKIP>elavGS Aβ42		
Log-rank test		
	n (dead/censored)	*p*-value
SKIP>elavGS Aβ42 +RU *w1118>elavGS* +RU	129/2 145/0	0.7405

Table S4.1 Repeats of climbing assays for *Usp47* that showed significant interactions between age and genotype in the initial screen.
Significant interactions of interest are highlighted in green.

Usp47 – repeat 2				
Term	Estimate	Std Error	t Ratio	Prob>|t|
Induced (+RU)				
Intercept	16.63222	0.32560	51.082	< 2e-16 ***
Age	-0.51128	0.01930	-26.486	< 2e-16 ***
Genotype	0.05314	0.44926	0.118	0.906
Age*Genotype	-0.03002	0.02656	-1.130	0.259
Uninduced (-RU)				
Age	-0.13464	0.02742	-4.911	1.08e-06 ***
Genotype	1.95493	0.61958	3.155	0.001659 **
Age*Genotype	14.16029	0.03891	-3.408	0.000685 ***
Effect of RU				
Intercept	12.3186	0.2544	48.428	< 2e-16 ***
RU	-3.2299	0.3500	-9.227	< 2e-16 ***
RU*Genotype	-0.5716	0.4880	-1.171	0.242

***Usp47* – repeat 3**				
Term	Estimate	Std Error	t Ratio	Prob>ltl
Induced (+RU)				
Age	-0.49591	0.03590	-13.815	< 2e-16 ***
Genotype	-1.25114	0.84359	-1.483	0.139
Age*Genotype	0.06088	0.05315	1.145	0.252

***Usp47* - repeats combined**				
Repeat 1vs2	1.385705	0.217450	6.373	2.29e-10 ***
Repeat 1vs3	0.562793	0.237828	2.366	0.0181 *
Age*Genotype	-0.006689	0.023235	-0.288	0.7735

Table S4.2 Log-rank and Cox proportional hazards tests for *Usp47* Aβ lifespans.
Significant interactions of interest are highlighted in green.

Usp47

Usp47>elavGS Aβ42 vs w1118>elavGS Aβ42		
Log-rank test		
	n (dead/censored)	*p*-value
Usp47>elavGS Aβ42 -RU *w1118>elavGS Aβ42* -RU	144/3 157/1	1.621e-06
Usp47>elavGS Aβ42 +RU *w1118>elavGS Aβ42* +RU	134/2 145/0	0.1866

Usp47>elavGS Aβ42 vs w1118>elavGS Aβ42					
n (dead/censored)	283/5				
Cox proportional hazards					
	coef	exp(coef)	se(coef)	z	*p*-value
Genotype	0.5226	1.6863	0.1175	4.446	8.73e-06
RU	3.4837	32.5787	0.1849	18.837	< 2e-16
Genotype:RU	-0.6128	0.5419	0.1676	-3.655	0.00026

Table S5.1 Repeats of climbing assays for *ATPsynCF6* that showed significant interactions between age and genotype in the initial screen.
Significant interactions of interest are highlighted in green.

A

***ATPsynCF6* – repeat 2**				
Term	Estimate	Std Error	t Ratio	Prob>|t|
Induced (+RU)				
Age	-0.53806	0.01781	-30.218	< 2e-16 ***
Genotype	1.13200	0.42709	2.651	0.00816 **
Age*Genotype	-0.02087	0.02495	-0.836	0.40307
Uninduced (-RU)				
Age	-0.13441	0.03251	-4.135	3.92e-05 ***
Genotype	0.86435	0.71251	1.213	0.22543
Age*Genotype	-0.13284	0.04254	-3.123	0.00186 **
Effect of RU				
Genotype				
RU	-5.8263	0.3290	-17.708	< 2e-16 ***
RU*Genotype	2.0247	0.4688	4.319	1.65e-05 ***

***ATPsynCF6* – repeat 3**				
Term	Estimate	Std Error	t Ratio	Prob>|t|
Induced (+RU)				
Age	-0.51716	0.03470	-14.906	< 2e-16 ***
Genotype	-0.65652	0.78125	-0.840	0.401
Age*Genotype	0.05997	0.04639	1.293	0.197

***ATPsynCF6* - repeats combined**				
Intercept	14.71648	0.29021	50.710	< 2e-16 ***
Repeat 1vs2	1.41785	0.20517	6.911	6.42e-12 ***
Repeat 1vs3	0.80963	0.22771	3.556	0.00039 ***
Age*Genotype	0.03661	0.02094	1.748	0.08064

Table S5.2 Log-rank and Cox proportional hazards tests for *ATPsynCF6* Aβ lifespans.
Significant interactions of interest are highlighted in green.

ATPsynCF6

Log-rank test		
	n (dead/censored)	*p*-value
ATPsynCF6>elavGS Aβ42 -RU *w1118>elavGS Aβ42* -RU	140/6 157/1	9.22068e-08
ATPsynCF6>elavGS Aβ42 +RU *w1118>elavGS Aβ42* +RU	146/8 147/0	0.0379

w1118>elavGS Aβ42 vs ATPsynCF6>elavGS Aβ42					
n (dead/censored)	286/14				
Cox proportional hazards					
	coef	exp(coef)	se(coef)	z	*p*-value
Genotype	0.5015	1.6511	0.1193	4.203	2.63e-05
RU	3.2423	25.5919	0.1647	19.680	< 2e-16
Genotype:RU	0.6049	0.5461	0.1672	-3.617	0.00030

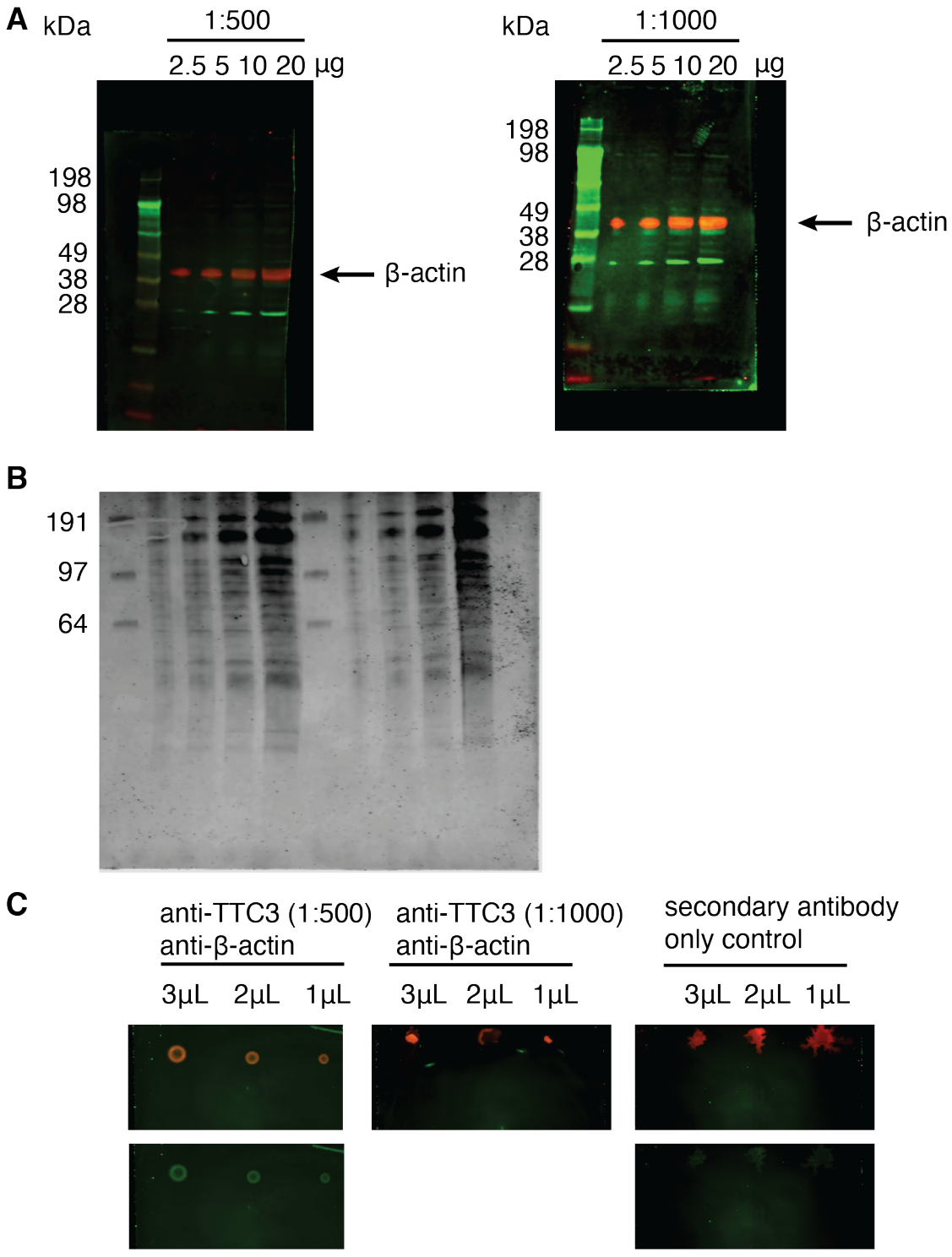

Figure S6.1 Work-up of TTC3 western blot.

(A) Western blot of HA human post-mortem brain tissue loading 2.5µg, 5µg, 10µg and 20µg probed with anti-TTC3 antibody ab80061 diluted at 1:500 and 1:1000. Anti-β-actin (A5441) was used as a loading control (red, 680nm). TTC3 could not be visualised at the expected 215 kDa (green, 800nm). A non-specific band was detected

around 28 kDa (green, 800nm). (B) Western blot with revert total protein stain to determine the range of protein sizes transferred to the membrane. (C) Dot blot of HA human post-mortem brain tissue added directly onto nitrocellulose membrane to determine whether TTC3 could be visualised using anti-TTC3 antibody ab80061 diluted at 1:500 and 1:1000 (green). Anti-β-actin (A5441) was used as a control (red). Secondary antibody only control to determine specificity of the anti-TTC3 antibody. Specificity could not be confirmed, as green dots were visible in the secondary antibody only control.

Table S6.1 Clustering and cell count of snRNA-seq dataset by *Farrell et al*.
Astro = astrocytes, excit = excitatory neurons, inhib = inhibitory neurons, fibro = fibroblasts, micro = microglia, olig = oligodendrocytes, OPC = oligodendrocyte progenitor cells, sm.mus = smooth muscle.

ID	astro_1	astro_2	astro_3	astro_4	endo	excit_1
cluster	4	11	22	28	7	0
CTRL	204	93	198	3	190	313
CTRL	221	49	954	1	118	123
CTRL	610	90	96	0	146	582
CTRL	17	160	0	388	99	30
EOAD	24	30	1	7	246	32
EOAD	59	350	8	234	526	113
EOAD	1307	183	34	1	164	64
EOAD	388	93	265	1	219	68
AD-DS	1	303	0	169	138	1106
AD-DS	268	228	315	27	691	929
AD-DS	704	112	12	1	455	318
AD-DS	54	196	0	9	247	51
AD-DS	19	112	3	124	112	436
AD-DS	4	991	0	4	185	249
AD-DS	343	166	1	0	128	757
AD-DS	7	245	0	86	167	303

excit_2	excit_3	excit_4	excit_5	excit_6	excit_7	excit_8	fibro	inhib_1	inhib_2	inhib_3	inhib_4
3	9	13	16	26	33	36	32	12	15	19	27
697	113	112	342	1	12	20	57	208	99	172	94
1131	206	6	883	0	0	74	6	493	216	384	161
370	94	74	115	0	1	5	27	278	321	98	71
4	158	204	3	5	159	11	39	125	172	67	53
0	7	152	2	115	0	0	33	44	29	13	17
16	47	133	4	594	6	21	35	135	21	68	62
932	187	27	604	0	1	44	18	170	94	347	130
372	49	24	249	0	0	6	109	123	35	62	56
0	87	377	0	403	1	10	38	91	50	58	86
324	252	191	176	17	2	13	95	298	188	176	76
341	178	107	184	0	0	22	20	272	165	220	110
4	539	591	4	2	396	27	93	394	478	232	171
8	472	504	1	19	72	6	33	66	176	135	52
11	260	101	4	46	4	3	24	146	316	49	41
36	775	115	13	0	3	0	22	118	153	166	71
0	85	307	0	186	23	3	43	170	143	96	70

micro_	micro_	olig_1	olig_10	olig_11	olig_12	olig_13	olig_2	olig_3	olig_4	olig_5	olig_6
2	10	1	29	31	35	37	6	8	14	17	20
528	107	81	1	284	0	0	23	24	47	2	0
128	22	2	6	4	0	0	3	1830	0	1	0
435	21	43	894	34	0	0	18	24	16	5	0
833	36	89	3	19	0	0	9	2	2515	0	0
80	89	0	1	2	338	0	0	0	2	1	2
181	207	6	5	51	1	0	19	27	0	2	0
297	181	4	5	7	0	0	34	1143	0	7	0
29	51	1	0	2	3	244	2	268	1	0	0
169	199	71	0	37	0	0	3473	7	2	7	1
492	107	32	45	152	0	0	66	37	11	16	2
266	324	95	21	40	0	0	58	141	2	609	5
90	877	2523	0	9	0	0	3	4	17	14	0
241	384	1677	2	1	0	0	52	14	87	16	0
203	384	35	0	22	0	0	52	2	2	30	1962
165	241	62	7	12	1	0	25	50	1	476	13
110	253	382	0	25	0	0	64	4	3	1253	4

olig_7	olig_8	olig_9	OPC_1	OPC_2	peri	sm.mus	T cells	Total cell
21	23	25	5	18	24	30	34	Overall total: 89649
5	0	1357	379	14	62	77	19	5938
8	0	0	750	7	59	3	11	7860
36	3	13	464	15	55	69	20	5143
1	0	1	16	391	53	31	33	5726
5	5	0	41	2	115	37	22	1494
452	1365	2	198	8	247	129	15	5347
34	7	12	506	4	88	45	2	6683
68	4	0	173	0	75	61	33	3134
2	0	8	6	280	45	10	18	7253
1212	387	6	564	8	283	160	42	7888
53	10	4	311	5	134	46	17	5362
0	0	1	67	536	72	58	98	7857
0	0	15	94	414	35	24	8	5414
3	0	0	58	408	83	36	12	5730
11	0	3	389	21	37	18	11	4410
3	0	0	18	251	57	26	23	4410